Synthesis and Evaluation of Desmethyl Azumamide Analogs

Maolanon, Alex

Publication date:
2014

Document Version
Peer reviewed version

Synthesis and Evaluation of Desmethyl Azumamide Analogs

Ph.D. Thesis

Alex R. Maolanon

February 2014

Department of Chemistry

Technical University of Denmark

Preface

The main work presented in this thesis was conducted at the Department of Chemistry, Technical University of Denmark (DTU) from November 2010 to February 2014 under the supervision of Associate Professor Christian A. Olsen. An external stay was held at the California Institute of Technology (CalTech) from January 2013 to July 2013 under the supervision of Professor Sarah E. Reisman.

The first chapter in the thesis describes the background of epigenetics and histone deacetylase (HDAC) enzymes. An overview of HDAC inhibitors is given, especially in relation to macrocyclic compounds. The second chapter describes the work on desmethyl azumamide analogs, their synthesis and biological evaluation and the third chapter focus on the project concerning azumamide analogs, possessing a thiol side chain functionality. Chapter four relates to the work performed at CalTech, primarily on the synthesis of pyrroloindolines.

First, I would like to thank my supervisor Christian A. Olsen for the three years in his research group. Christian has been an inspiring mentor and I am grateful that he has always taken the time to guide me, whenever I encountered difficulties in my work. I would also like to thank the rest of the research group for creating a great working environment and I would especially like to thank Jonas S. Laursen and Jesper S. Villadsen for scientific discussions and for proof reading my thesis. Regarding the work described in chapter two, I would like to thank Casper Hoeck, Charlotte H. Gotfredsen, Niels J. Christensen and Peter Fristrup for their contributions. I would also like to acknowledge all the technicians and the rest of the staff in building 201 for being great colleges. A special thanks to Sarah E. Reisman, who welcomed me to her research group, during my external stay.

My research at CalTech would not have been possible without the aid from Otto Mønsteds Fonden, Knud Højgaards Fond, Christian og Ottilia Brorsons Rejselegat for yngre videnskabsmænd og – kvinder, Oticon Fonden, Dansk Tennis Fond, and Kemisk forenings Rejsefond. I would also like to express my gratitude to the Lundbeck foundation for financing my Ph.D. studies at DTU.

I would like to thank my family and especially my brother Nicolai N. Maolanon for proof reading my thesis.

Lastly, I want to thank my wife Janne K. Nielsen for supporting me during the three years in my Ph.D. studies. I am thankful that Janne, Stewart, and Mingus joined me in the travels to USA. The experience would not have been the same without them.

Alex R. Maolanon

Kgs. Lyngby, February 2014.

Abstract

Histone deacetylases (HDACs) are a group of epigenetic modulators, which catalyze the removal of *ε-N*-acetylated lysine residues. Histones are the most studied targets, however, the acetylated state of a variety of other proteins are also modified by HDACs. Aberrant epigenetic processes have been associated with various types of cancer and HDACs have therefore been a target in the development of anticancer drugs. So far, two HDAC inhibitors have been approved by the food and drug administration (FDA) and several compounds are in clinical trials.

Macrocyclic HDAC inhibitors are interesting compounds, as they can interact with a variety of amino acids on the surface near the binding site; these interactions may be used to obtain selectivity for specific HDAC isozymes. The azumamides are potent HDAC inhibitors and since they possess a relatively weak zinc-binding group (ZBG), the activity must arise from interactions with the large cap group. The natural compounds have been used as an inspiration to synthesize new HDAC inhibitors.

A small structure activity relationship (SAR) study was conducted in collaboration with Jesper S. Villadsen. Aromatic substituents in the cyclic peptide were explored, while the primary modifications were done to the *β*-amino acid. Removal of the methyl group in the 2-position and changes to the unsaturation in the side at the 3-position, afforded six compounds. These were tested against HDAC enzymes from class I, IIb, and IV.

Minor changes in activity were observed among the azumamide analogs; however, removal of the methyl group had a significant impact relative to the natural products. To understand this effect, the NMR structure was solved with the assistance from Casper Hoeck and Charlotte H. Gotfredsen and docked conformations were obtained from Niels J. Christensen and Peter Fristrup. Compared to the natural compounds, the 3D-structure of the scaffold in the azumamide analogs were similar. Although a conclusion was not found, the preliminary docking results indicated favorable lipophilic interaction with the methyl group in the azumamides.

Largazole is another macrocylic natural product with HDAC inhibitory activity. The compound has a thioester functionality in the side chain, which is hydrolyzed before interaction with the enzymes. In the attempt to mimic the prodrug nature of largazole, compounds containing a thiol group were designed, as it was hypothesized that acylation with different lipids could generate compounds with improved cell penetrating properties. A desmethylated azumamide analog containing a thiol side chain was synthesized and tested against HDAC3. A low activity was observed, which was explained by the unfavorable linker length.

In the work performed at CalTech, five 2-*α*-phenylpyrroloindolines were synthesized; utilizing an NCS mediated cyclization as the key step. Chris Marotta and Christina McCleary Daeffler tested their effect against a variety of ligand-gated ion-channels. Among these, one compound proved to be an agonist for the $GABA_A$ receptor.

Resumé

Histone deacetylaser (HDACer) er en gruppe af enzymer, der regulerer epigenetiske ændringer ved at katalysere kløvning af acetylgrupper fra *ε-N*-acetylerede lysiner. Den mest undersøgte målgruppe er histonerne, men andre proteiner er dog også påvirket af HDACer. Der er fundet en sammenhæng mellem atypiske epigenetiske ændringer i forbindelse med forskellige typer af cancer. HDACerne har derfor været et mål i udviklingen af lægemidler til bekæmpelse af cancer. Indtil videre er to HDAC inhibitorer blevet godkendt af den amerikanske food and drug administration (FDA) og flere stoffer er i kliniske tests.

Makrocykliske HDAC inhibitorer er interessante stoffer, da de kan interagere med en stor del af aminosyrerne på overfladen tæt ved bindingslommen. Disse interaktioner kan muligvis blive brugt til at opnå selektivitet for specifikke HDAC isoenzymer. Azumamiderne er potente HDAC inhibitorer og eftersom de besidder en relativ svag zink bindende gruppe (ZBG), må aktiviteten opstå ved interaktioner med den store 'cap' gruppe. Naturstofferne er blevet brugt til inspiration for syntesen af nye HDAC inhibitorer.

Et mindre struktur-aktivitets studie (SAS) er blevet udført i samarbejde med Jesper S. Villadsen. Aromatiske substituenter i det cykliske peptid er blevet udforsket, dog er den primære modifikation udført på *ε*-aminosyren. Ved fjernelsen af methylgruppen fra 2-positionen og ændringer til den umættede del af sidekæden i 3-positionen, blev seks kemiske forbindelser dannet. Disse blev testet imod HDAC enzymer fra klasse I, IIb og IV.

En ubetydelig ændring i aktiviteten blev observeret iblandt azumamid analogerne, mens fjernelsen af methyl gruppen havde en betydelig effekt i forhold til naturstofferne. For at forstå denne effekt blev NMR strukturen opklaret med assistance fra Casper Hoeck og Charlotte H. Gotfredsen og docking strukturer blev dannet af Niels J. Christensen og Peter Fristrup. Sammenlignet med naturstofferne var 3D-strukturen af ringen i azumamid analogerne ens. Selvom der ikke kunne drages en endelig konklusion, indikerede de indledende docking resultater, at en favorabel lipofil interaktion kunne dannes med methyl gruppen i azumamiderne.

Largazol er et andet naturstof med HDAC inhibitorisk aktivitet. Strukturen har en thioester i sidekæden, der hydroliseres før interaktion med enzymet. I et forsøg på at efterligne dette naturlige 'prodrug', blev der designet strukturer med en thiol gruppe. Hypotesen var at strukturer med bedre celle penetrerende egenskaber kunne syntetiseres ved at acylere med forskellige typer fedtkæder. En desmethyl azumamid analog, indeholdende en thiol sidekæde, blev syntetiseret og testet imod HDAC3. En lav aktivitet blev observeret, hvilket blev forklaret af den ugunstige længde af linkeren.

I arbejdet foretaget på CalTech, blev fem 2-*α*-phenylpyrroloindoliner syntetiseret ved brug af en NCS medieret cyklisering. Deres aktivitet blev testet af Chris Marotta and Christina M. Daeffler imod forskellige typer ligandstyrede ionkanaler. Iblandt disse viste en af stofferne sig at være en agonist på $GABA_A$ receptoren.

Abbreviations

Amnaa	(*Z*)-(2*S*,3*R*)-3-amino-2-methyl-5-nonene-dioic acid, 9-amide
Amnda	(*Z*)-(2*S*,3*R*)-3-amino-2-methyl-5-nonenedioic acid
Aoda	(*S*)-2-amino-8-oxodecanoic acid
BAK	Bcl-2 homologous antagonist/killer
BAX	Bcl-2-associated X protein
BID	BH3 interacting-domain death agonist
Bcl-2	B-cell lymphoma-2
Boc	Tert-butyl carbamate
BOP	(Benzotriazol-1-yloxy)tris(dimethylamino)phosphonium hexafluorophosphate
CD95	Cluster of differentiation 95
CDK	Cyclin-dependent kinase
CaMK	$Ca2^{+}$/calmodulin-dependent kinase
CoA	Acetyl-co-enzyme A
Co-REST	Co-repressor of RE1-silencing transcription
CHAP	Cyclic hydroxamic-acid containing peptide
DBU	2,3,4,6,7,8,9,10-Octahydropyrimido[1,2-a]azepine
DIBAL-H	Diisobutylaluminum hydride
DNA	Deoxynucleic acid
DMAP	4-dimethylaminopyridine
DMF	N,N-Dimethylformamide
DMSO	Dimethyl sulfoxide
DPPA	Diphenylphosphorylazide
DR5	Death receptor 5
ee	Enantiomeric excess
EDC	1-Ethyl-3-(3-dimethylaminopropyl) carbodiimide hydrochloride
FDA	Food and drug administration
FDPP	Pentafluorophenyl diphenylphosphinate
Fmoc	9-Fluorenylmethoxycarbonyl
H4K16	Histone 4 lysine 16
HAT	Histone acetyl transferase
HDAC	Histone deacetylase
HDLP	Histone deacetylase-like protein
HIF-1α	Hypoxia-inducible factor 1α
HOBt	Hydroxybenzotriazole
HP1	Heterochromatin protein 1
HSP	Heat-shock protein
Ins(1,4,5,6)P_4	D-myo-inositol-(1,4,5,6)-tetrakisphosphate
MAC	Mitochondrial apoptosis-induced channel
MDR	Multidrug resistance
MEF2	Myocyte enhancement factor 2

NAD^+	Nicotineamide adenine dinucleotide
N-CoR	Nuclear receptor co-repressor
NuRD	Nucleosomes remodeling and decatylase
NCS	N-chlorosuccinimide
PCy3	Tricyclohexylphosphine
P-gp	P-glycoprotein
Red-Al	Sodium bis(2-methoxyethoxy)aluminumhydride
Runx2	Runt related transcription factor 2
SAHA	Suberoylanilide hydroxamic acid
SAR	Structure activity relationship
Sin3	Switch intensive 3
SMRT	Silencing mediator for retinoic acid and thyroid hormone receptors
TBS	Tert-butyldimethylsilyl ether
Tce	Trichloroethyl ester
Teoc	2-(Trimethylsilyl)ethoxycarbonyl
TFA	Trifluoroacetic acid
TRAIL	TNF-related apoptosis-inducing ligand
Red-Al	Sodium bis(2-methoxyethoxy)aluminumhydride
SAHA	Suberoylanilide hydroxamic acid
SPPS	Solid phase peptide synthesis
TSA	Trichostatin A
TrtSH	Triphenylmethanethiol
TMS	Trimethyl silane
TIPS	Triisopropylsilane
VEGF	Vascular endothelial growth factor
VHL	Von Hippel Lindau
VLC	Vacuum liquid chromatography
VPA	Valproic acid
ZBG	Zinc-binding group

Publications

Publications

Villadsen, J. S.; Stephansen, H. M.; Maolanon, A. R.; Harris, P.; Olsen, C. A., Total Synthesis and Full Histone Deacetylase Inhibitory Profiling of Azumamides A–E as Well as β^2- epi-Azumamide E and β^3-epi-Azumamide E. *Journal of Medicinal Chemistry* **2013,** *56* (16), 6512-6520

Publications in preparation

Maolanon, A. R.; Villadsen, J. S.; Hoeck, C.; Gotfredsen, C. H.; Harris, P.; Olsen, C. A., Structural editing of the azumamide scaffold: Synthesis and structure–activity relationships.

Contents

1 Introduction

1.1 Epigenetics

All genetic information of living organisms is stored in DNA. The same DNA is present in all cells; however, a variety of cell types exists, containing different gene expression profiles. These processes can be explained by epigenetic mechanisms, which is defined by changes in gene expression without altering the DNA sequence. DNA methylation and histone modifications are among the most studied epigenetic mechanisms.[1]

Long linear stretches of DNA coil around eight histone proteins consisting of two copies of H2A, H2B, H3, and H4. Linker DNA that wraps around histone H1 connects these units, known as nucleosomes.[2] The repeating nucleosome units, comprises the chromosome, which allows the DNA to be condensed into the small volume of the nucleus (Figure 1.1).

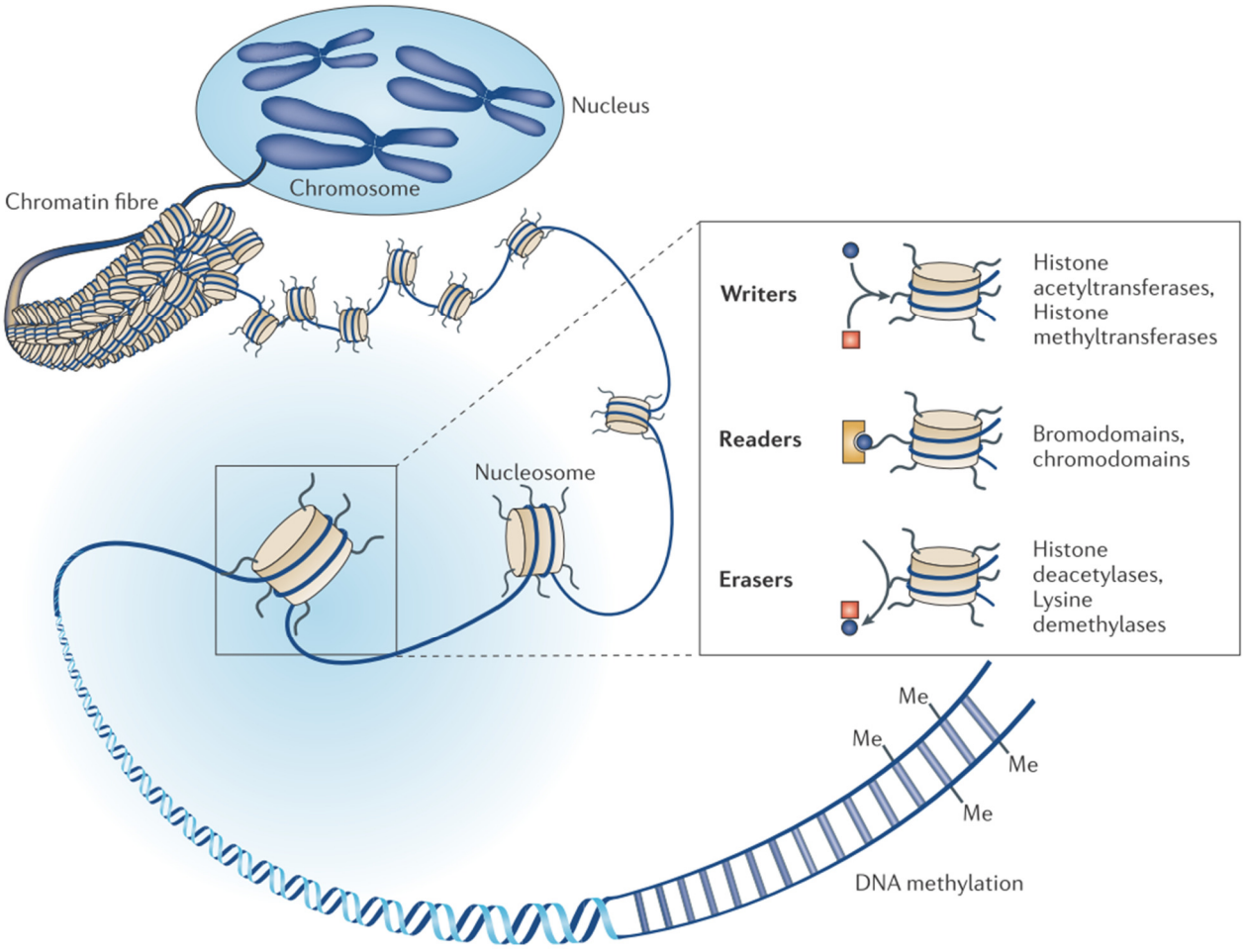

Figure 1.1 DNA wraps around histone proteins to form the nucleosome. These are compacted further into the chromosome, which can fit into the cell nucleus. Epigenetic alterations includes DNA methylation and modifications to the histone tails. Epigenetic modulators (writers) include histone acetyltransferases and histone methyltransferases. These alterations can be recognized by specific domains in proteins (readers), while other proteins including histone deacetylases and lysine demethylases, remove the modification (erasers). The figure was modified from ref [1].

The nucleosome plays a crucial role in transcription, as the packing prevents access of DNA-binding proteins to various loci.[2] The histones in each nucleosome are well defined, but the N-terminal tails that protrudes from the nucleosome are highly flexible. The tails contain a high proportion of conserved basic amino acids that can facilitate binding within the same nucleosome to stabilize contact to the DNA, as well as inter-nucleosomal interactions, which define the chromatin structure.[3] The strong stabilizing effects arise, in part, by interactions between the positive charge from the basic amino acids and the negatively charged phosphates in the backbone of DNA.

The histone tails are targets for posttranslational modifications at specific amino acid positions;[4] these include acetylation,[5] methylation,[6] phosphorylation,[7] and ubiquitylation.[8] Acetylation of lysine residues neutralize the positive charge, which leads to a weaker histone-DNA interaction. The structure of the chromatin will be less compact and become more accessible to various transcription factors. A specific acetylation on H4, lysine 16 (H4K16) is a crucial factor in shaping the dynamic chromatin structure.[9] Ubiquitylation of the C-terminal helix in H2B is another key site for posttranslational modifications, which has been shown to control the higher order structure of chromatin.[10] The ubiquitylated interference of the chromatin compaction proved to function in a cooperative fashion with acetylation at H4K16. While acetylated H4K16 affected the folding transition, ubiquitylated H2B was reported to occur at a later stage of the packing (Figure 1.2).

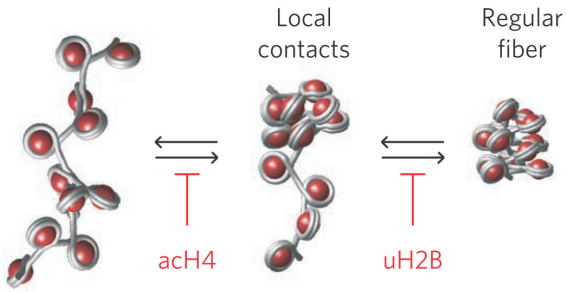

Figure 1.2 Acetylation and ubiquitylation interferes with the chromatin structure in a cooperative fashion. Lysine 16 on histone H4 and ubiquitylation of the C-terminal helix in H2B are key sites for the modifications. acH4: acetylated histone 4; uH2B: ubiquitylated H2B. The figure was obtained from ref [10].

In contrast to acetylation, histone methylation does not change the charged state of the amino acid residues. Different states of methylation can occur on the basic amino acids; lysine residues can be mono-, di-, or tri-methylated, while arginine residues can be mono- or di-methylated. Mono-methylated histidines have also been observed, but this rare alteration is not well characterized.[6] Kinases can phosphorylate serine, threonine, and tyrosine residues in the histone tails. In combination with the aforementioned alterations as well as other epigenetic modifications, a vast number of posttranslational combinations can be generated.

Even though the structural compaction gives a rational explanation of transcriptional control, the process is much more complex. The specific patterns of modified histone proteins establish a code that can be recognized by chromatin-associated proteins, to either initiate or suppress transcription. Furthermore, it has been proposed that the local concentration and combination of modified histones alter the chromatin structure, resulting in different epigenetic states, leading to silencing or activation of particular regions.[11]

Most of the enzymes that 'read' the histone code contain domains that recognize the specific alterations of the histones (Figure 1.1). This concept is demonstrated by heterochromatin protein 1 (HP1) that contains a chromo-domain, which is highly selective for methylated Lys9 in H3,[12] and by p300/CBP-associated factor (PCAF) containing a bromo-domain that targets acetylated Lys8 in H4 and Lys14 in H3.[13]

1.2 Histone transferases and histone deacetylases

The acetylated state of histone proteins is important for many cellular mechanisms. Acetylation of newly synthesized histone proteins is required for their assembly into the nucleosome[14] and modifications of lysine residues have a role in shaping the chromatin structure.[9] In agreement with the histone code model, deacetylation at certain sites are also key factors for regulating transcription.[15]

Two functional opposing enzymes, the histone acetyl transferases (HATs) and the histone deacetylases (HDACs) control the acetylation state of histone proteins. HATs catalyze acetylation of ε-amino groups of lysine residues using acetyl-coenzyme A (CoA) as a cofactor, while HDACs catalyze the reverse reaction.

The human HDACs are grouped into four classes based on their sequence similarity and domain organization (Figure 1.3). The "classical" mammalian HDACs, which can be divided into class I, IIa, IIb, and IV contain a zinc ion in the active site of the enzyme, while the sirtuins, belonging to class III HDACs, require NAD^+ as a cofactor. The sirtuins are structurally unrelated to the classical HDACs and will not be discussed further.

Acetyl removal from histone proteins are the most studied enzymatic function of HDACs. Certain HDACs can however catalyze deacetylation of cytoplasmic proteins and transcription factors. These epigenetic modifications may have many consequences. For example, acetylation and ubiquitinylation can occur on the same lysine residue in p53;[16] HDACs can therefore move the equilibrium towards ubiquitinylation, an alteration that may act as signal for degradation of the protein. Other processes that are regulated by acetylation/deacetylation are translocation and protein-protein interactions.[17]

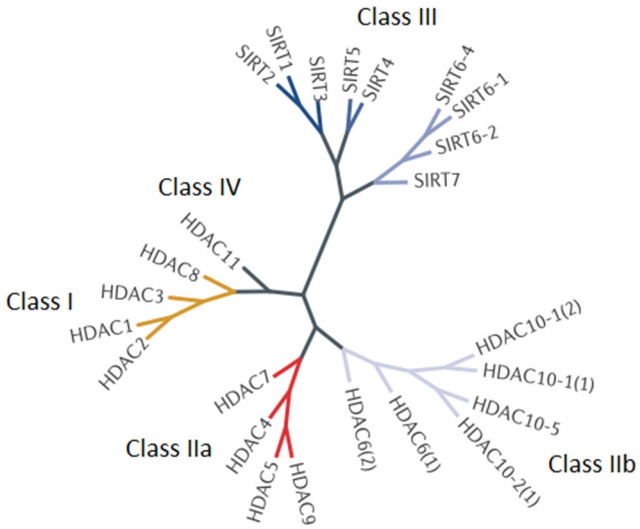

Figure 1.3. Phylogenetic tree of HDACs. The proteins on the branches are placed in accordance to their sequence similarity. The figure was modified from ref [1].

Class I HDACs

Class I HDACs are localized predominantly in the nucleus.[18] HDAC1 and 2 are closely related (Figure 1.3) and have a high sequence similarity (~82%).[5] They interact with each other in at least three multi-protein complexes; switch intensive 3- (Sin3), nucleosomes remodeling and decatylase- (NuRD), and the co-repressor of RE1-silencing transcription (Co-REST) complex, where they constitute the catalytic core (Figure 1.4).[19] The proteins in these complexes are necessary for deacetylase activity and for binding to DNA.[20] The function of HDAC1 and 2 is also regulated by kinases; hyperphosphorylation of the enzymes increase the deacetylase activity, but it also disrupts the complex formation. In parallel, hypophosphorylation decrease deacetylase

activity, while it promotes formation of the protein complex. These contradictory mechanisms are thought to maintain the HDACs activity at a certain optimal level.[21]

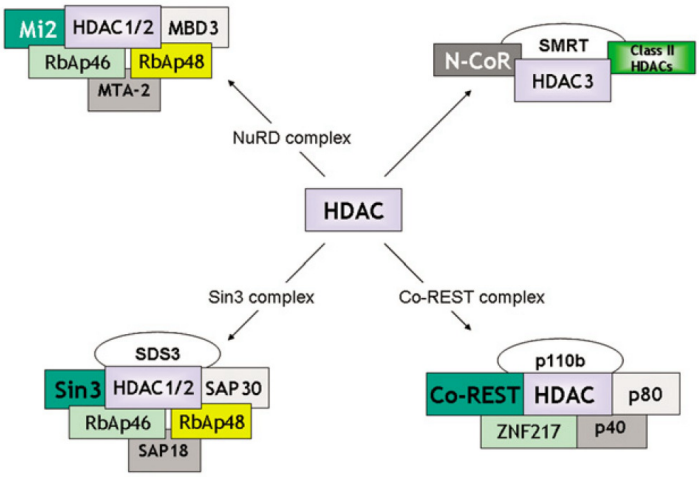

Figure 1.4 Composition of HDAC complexes. The figure was obtained from ref [22].

HDAC3 can be found in complex with nuclear receptor co-repressor (N-CoR) and silencing mediator for retinoic acid and thyroid hormone receptors (SMRT)[23] (Figure 1.4). Both N-CoR and SMRT contain a domain that activates HDAC3 for deacetylation.[24] Analysis of the HDAC3 crystal structure have identified a bound D-myo-inositol-(1,4,5,6)-tetrakisphosphate (Ins(1,4,5,6)P_4). Beside from functioning as a stabilizing link to connect HDAC3 and SMRT, Ins(1,4,5,6)P_4 was essential for HDAC activity. It has been proposed that the dynamics and conformation of HDAC3 change after binding to SMRT and Ins(1,4,5,6)P_4, which leads to a higher activity. Binding to Arg265 which is present in one of the loops surrounding the rim of the active site, seems to be particularly important, as the dynamic loop could facilitate access to the active site.[25] Recently, Ins(1,4,5,6)P_4 was also found to exert a regulatory role in HDAC1 with a protein from the NuRD-complex.[26]

Three crystal structures of HDAC2 exist, all of them co-crystalized with an inhibitor (PDB: 3MAX, 4XLZ, 4LY1). None of the crystal structures contain residues from the protein complex, but due to the high sequence similarity of the enzymes, in particular in the loop binding Ins(1,4,5,6)P_4, it is likely that inositol phosphate also have a role in regulating HDAC2.

In contrast to HDAC1–3, HDAC8 does not associate with any protein complexes.[19] By overlaying HDAC8 and HDAC3, a crucial difference is observed in the opening towards the active site. The important loop that is believed to facilitate ligand access in HDAC1 and 3, is much smaller in HDAC8. This crucial change could explain why HDAC8 is active as an uncomplexed enzyme.[25]

With regard to structure, HDAC8 is probably the most studied isozyme, with 21 published crystal structures to date, many of them co-crystalized with an inhibitor. Two sites for binding monovalent cations have been identified; one of which lies 7 Å from the divalent cation in the active site (site 1), while the second site is placed 21 Å away (site 2). It has been demonstrated that the occupation of one of the binding sites is crucial for HDAC activity, while occupation of both sites lowers activity of the enzyme.[27] It has therefore been suggested that intracellular monovalent cation concentration could be a regulating factor in HDAC8. The raised activity after binding one cation is thought to occur after occupying site 2, due to a stabilizing effect of the active conformation. Binding to site 1 is thought to lower the activity by decreasing pKa of the corresponding acid of His142 (Figure 1.5), which takes part in the deacetylation mechanism.

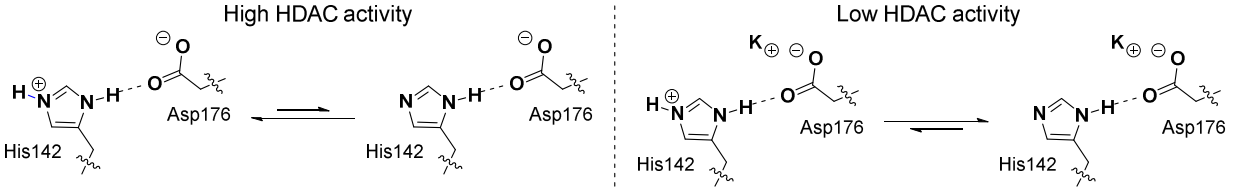

Figure 1.5 Effect on histidine protonation state by K^+ in HDAC8. Left: a protonated histidine is favored in the absence of K^+. Right: a deprotonated histidine is favored in the presence of K^+. The figure was modified from ref [27].

The functions of HDAC isozymes have been investigated in mice, by removing the gene that code for the specific HDAC. HDAC1 knockout mice have shown that the isozyme is crucial for embryonic development, as the mice die before embryonic day 10.5 (mouse stage E10.5). It was also shown that embryonic stem cells lacking HDAC1 had reduced proliferation rates, in accordance with an up-regulation of cyclin-dependent-kinase (CDK) inhibitor p21 and p27.[11] Deletion of HDAC1 or HDAC2 in cardiac tissue does not have any apparent effect on the development and function of the heart, but if both genes are knocked out simultaneously, newborn lethality is observed. This finding suggests that HDAC1 and 2 can uphold the same role in cardiac gene expression.[28]

The vital role of HDAC3 in embryonic development, has also been established from knockout mice, which showed an embryonic lethality by day 9.5 (mouse stage E9.5).[29] Deletion of HDAC3 in liver tissue has revealed a role in hepatic metabolism by disrupting lipid and cholesterol homeostasis,[30] and heart specific deletion has further revealed a role in regulating cardiac energy metabolism.[29] Deletion of HDAC3 in primary cells affect the S phase progression and cause DNA damage.[31]

Class IIa HDACs

Opposed to HDAC enzymes in class I, expression of class IIa HDACs are restricted to a certain number of cell types. A high expression of HDAC5 and 9 is seen in muscle-, heart-, and brain tissue; HDAC4 is highly expressed in the brain and growth platelets of the skeleton; while HDAC7 is highly expressed in endothelial cells and thymocytes.[18] All members of class IIa contain a large N-terminal domain that regulates transport between the nucleus and cytoplasm by binding to the protein 14-3-3. This binding is mediated by phosphorylation of conserved serine residues in the HDAC enzymes.[32]

Class IIa HDACs can be found in the SMRT-N-Cor-HDAC3 complex (Figure 1.4).[33] Association with this complex is crucial, as isolated class IIa enzymes do not show any HDAC activity. It has therefore been suggested that HDAC4, 5, and 7 might function as a link to recruit HDAC3 containing complexes.[33] Another proposed explanation is that class IIa enzymes is activated in the presence of HDAC3.[34] This suggestion is based on other possible HDAC-HDAC interactions, like HDAC1 and 2 that are found in the same complex.

HDAC4, 5, and 7 can all interact with myocyte enhancer factor 2 (MEF2). MEF2 has a significant regulatory role as a DNA transcription factor in muscle differentiation. When one of the HDACs associates with MEF2, the function is inhibited and muscle differentiation is blocked. Ca^{2+}/calmodulin dependent kinase (CaMK) can regain the activity by phosphorylating the HDACs, which leads to dissociation of the HDAC-MEF2 complex.[35]

During muscle differentiation, HDAC4, 5 and 7 are shuttled between the nucleus and the cytoplasm. The different localization in the various stages, suggests a specific role of gene regulation of each HDAC isoform during the cell differentiation.[5] HDAC4 knockout mice, show premature bone tissue formation as well as an early onset of chondrocyte hypertrophy. The regulatory role of HDAC4 arises from inhibition of transcription factor, runt related transcription factor 2 (Runx2).[36] HDAC9 can also interact with MEF2, CaMK and 14-3-3. This suggest a potential role in muscle differentiation as the other class IIa enzymes.[5]

Class IIb HDACs

HDAC6 is mainly localized in the cytoplasm, whereas HDAC10 resides in both cytoplasm and the nucleus.[37] HDAC6 possess two catalytic domains and a zinc finger – a structural motif that coordinates zinc ions.[38] Two catalytic domains are also found in HDAC10, but only the N-terminal catalytic domain is functional. HDAC10 is found in the liver, spleen, and kidney[5] and have been shown to bind to HDAC3 and SMRT.[39]

Aside from catalyzing deacetylation of histones, HDAC6 can also deacetylate α-tubulin[40], which regulates microtubule-dependent cell motility, and heat-shock protein (HSP) 90[41] which in the hyper-acetylated state loose chaperone activity.[41] Furthermore, the zinc finger domain is responsible for binding to ubiquitin. HDAC6 can thereby interfere with other biological mechanisms including aggresome function and degradation of misfolded proteins.[42]

HDAC6 knockout mice develop normally and even though the highest expression of the isozyme is found in the testis, normal function is retained as well. Hyperacetylated tubulin is observed, but without being vital for the mouse.[43]

Class IV HDAC

HDAC11 is the only isoform belonging to class IV. The enzyme is found in the brain, heart, muscle, kidney, and testes.[18] HDAC11 is not a part of any known complexes, so it might have a distinct function. The enzyme can repress expression of interleukin 10 (IL-10),[44] a cytokine which serve as a regulator of the immune response. The potential for HDAC11 as a therapeutic target was shown in rats after a liver transplantation, where silencing of HDAC11 genes proved superior relative to rats treated with an immunosuppressant.[45]

1.3 The role of histone deacetylases and histone deacetylase inhibitors in cancer

Each member of the HDAC family seems to have a specific function, as shown by the detrimental impact in HDAC knockout mice. Although histone modification is the most studied function of HDAC enzymes, a wide range of proteins are affected by the posttranslational modification. With the use of high-resolution mass spectrometry, 3600 lysine acetylation sites on 1750 proteins have been identified.[17] This vast amount of substrates that are affected, highlights the important role of HAT and HDACs as posttranslational modulators.

In addition to genetic defects, the onset and progression of cancer have been associated with aberrant epigenetic alterations.[46] One of the challenges in cancer therapy is to target malignant cells without affecting normal cells. It is therefore important to identify which type of HDAC enzymes that display abnormal activity in a given tumor type. An overview of HDAC expression related to cancer is shown in Table 1.1.

Table 1.1 HDAC expression in various cancer types.[a]

Class I HDACs	
1	Upregulated in gastric, colorectal, esophageal and pancreatic cancer.
2	Upregulated during early colorectal cancer at the polyb stage. Upregulated in cervical dysplasia and invasive carcinoma.
3	Upregulated in lung cancer, prostate and colon cancer.
8	Upregulated in neuroblastoma.
Class IIa HDACs	
4	Upregulated in breast cancer samples compared with renal, bladder and colorectal cancer.
5	Upregulated in colorectal cancer in contrast to renal, bladder and breast cancer.
7	Upregulated in colorectal cancer in contrast to bladder, renal and breast cancer.
9	Overexpressed in medulloblastoma/astrocytoma.
Class IIb HDACs	
6	High in oral squamous cell carcinoma.
10	Overexpressed in hepatocellular carcinoma.
Class IV HDACs	
11	Overexpressed in breast cancer.

[a] The table was modified from ref [47].

HDAC inhibitors have shown a great potential in cancer therapy, by exhibiting a high selectivity towards tumor cells.[48] In recent years, HDACs have therefore been a target in the development of new anticancer drugs. The majority of HDAC inhibitors up-regulate p21, which in turn can affect cyclin D and cyclin dependent kinase (CDK) 4 leading to cell cycle arrest and differentiation. Furthermore, HDAC inhibitors can induce apoptosis and inhibit angiogenesis (Figure 1.6).[49]

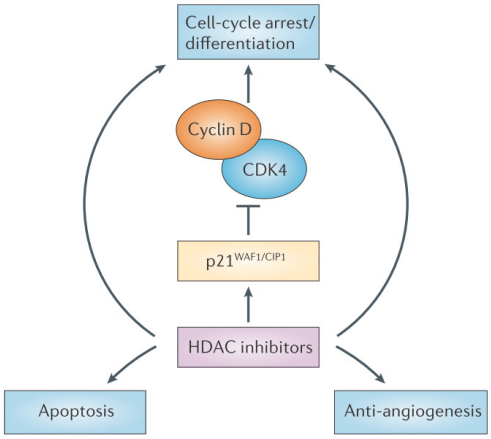

Figure 1.6 p21 is induced by the majority of HDAC inhibitors, leading to an inhibition of cyclin D and CDK4, which in turn promotes cell-cycle arrest and differentiation. HDAC inhibitors are also known to induce apoptosis and inhibit angiogenesis. The figure was obtained from ref [49].

HDAC inhibitors induces apoptosis

HDAC inhibitors have shown anticancer activity by selectively inducing the death receptors, cluster of differentiation 95 (CD95) and death receptor 5 (DR5), and their corresponding ligands, CD95L and TNF-related apoptosis-inducing ligand (TRAIL) respectively, in tumor cells (Figure 1.7).[50] Binding of CD95L to the death receptor, triggers adaptor proteins to bind which in turn recruits membrane-proximal activator

caspases (e.g. caspase-8 or -10). The activator caspase can then induce effector caspases (e.g. caspase-3 or -7), leading to apoptosis.[51]

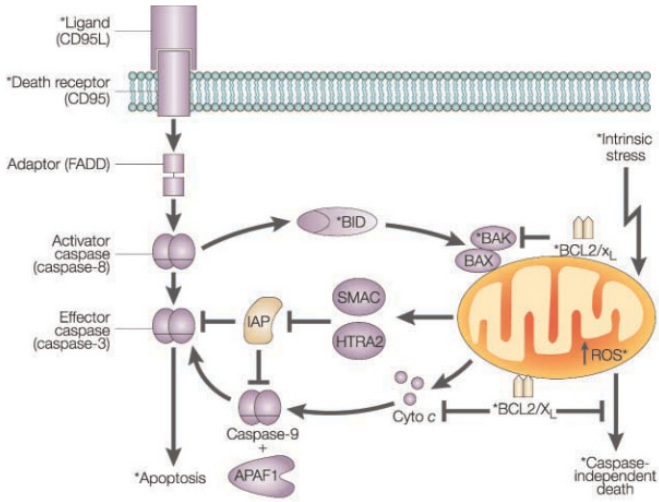

Figure 1.7 The death receptor pathway and the mitochondrial pathway. Activation of the death receptor induces a pathway involving caspases, which leads to apoptosis. In the mitochondrial pathway, an ion channel is formed in the mitochondria, which leads to release of cytochrome c along with proapoptotic proteins. The figure was obtained from ref [52].

Alternatively, the mitochondrial pathway can be activated by activator caspases, which cleave the proapoptotic protein, BH3 interacting-domain death agonist (BID). Truncated BID relocates and can induce formation of the mitochondrial apoptosis-induced channel (MAC), which is regulated by members of the B-cell lymphoma-2 (Bcl-2) family; the proapoptotic Bcl-2 homologous antagonist/killer (BAK) and Bcl-2-associated X protein (BAX) as well as the anti-apoptotic Bcl-2, Bcl-xL[53] (Figure 1.7). Formation of MAC triggers the release of cytochrome c along with other proapoptotic proteins, ultimately leading to apoptosis.

Multidrug resistance (MDR) is a complication that can arise in cancer treatment. A characteristic feature is the expression of the ABC-transporter P-glycoprotein (P-gp) that actively transports chemotoxins out of the cell. In addition, P-gp is able to inhibit caspase-3 activated apoptosis pathways.[54] The anticancer properties of the HDAC inhibitor, suberoylanilide hydroxamic acid (SAHA), has been investigated in a study of P-gp expressing MDR cancer cells. Even though the SAHA-induced caspase-3 pathway was inhibited by P-gp, SAHA proved effective against the cancer cells by inducing a caspase independent pathway, leading to cleavage of BID, which in turn lead to the release of cytochrome c and production of reactive oxygen species.[55]

In the non-acetylated form of Ku70 (a DNA-damage-response protein), the protein exists in a complex with BAX, suppressing apoptosis. When the cell is stressed, Ku70 is acetylated; the complex dissociates and BAX relocates to the mitochondria where apoptosis is induced.[56] HDAC6 has a role in this pathway, as the isozyme can interact with the Ku70-BAX complex.[57] Knocking out HDAC6 or using the HDAC6-specific inhibitor, tubacin, increased Ku70 acetylation which in turn triggered BAX-induced cell death.

Cell cycle arrest

A normal eukaryotic cell undergoes different phases before initiating cell division. Checkpoints in the cell cycle (G_1, G_2, M) ensure that the cell is healthy before proceeding to the next stage. A number of genes have important roles in these regulations; these include p53, Rb, and BRCA1, which are known as tumor suppressing genes. They can induce expression of cyclin-dependent kinase (CDK) inhibitors, which negatively

control cell cycle progression. Mutation or loss of these genes are common in many types of cancer, leading to uncontrolled cell growth.[58]

The critical role of HDAC1 and 2 in regulating the G1 checkpoint, has been demonstrated in fibroblasts.[59] Cells lacking both enzymes were retained in the G1 to S phase, due to an up-regulation of CDK inhibitors p21 and p57. p21 has generally been linked with cell arrest in the G_1 phase, however, HDAC inhibitor induced up-regulation of the CDK inhibitor has also shown to cause cell cycle arrest at the G_2-M checkpoint.[60]

HDAC inhibitors have also been implicated in blocking progression in the M phase. While many anticancer agents affect the formation of microtubules,[61] HDAC inhibitors have been shown to interfere with the kinetochore in two human cancer cell lines.[62]

Anti-angiogenesis

The progressive growth and metastasis of solid tumors rely on angiogenesis for supply of oxygen and nutrients, and for removal of CO_2 and waste products. One of the key elements for controlling angiogenesis is the hypoxia-inducible factor 1α (HIF-1α), which can stimulate the production of proangiogenic factors, such as the vascular endothelial growth factor (VEGF).[63]

Treatment with the HDAC inhibitor Trichostatin A (TSA), has shown an effect *in vitro* and *in vivo* by upregulating von Hippel Lindau (VHL) expression (promoting ubiquitination and degradation) and p53, while down-regulating HIF-1α and VEGF.[64] Others report that treatment with HDAC inhibitors induce degradation of HIF-1α, independent of VHL and p53.[65] An enhanced interaction between HIF-1α and HSP70 was observed and as the activity of HSP90 was known to be controlled by HDAC6,[41] the anti-angiogenic mechanism of HDAC inhibition was proposed to arise from an improper maturation of HIF-1α, leading to degradation.

1.4 Histone deacetylase inhibitors

As mentioned in the previous section, HDAC inhibitors have shown a potential in cancer treatment. Currently two HDAC inhibitors; SAHA (Figure 1.10) and romidepsin (Figure 1.29) have been approved by the food and drug administration (FDA) for treatment of cutaneous T-cell lymphoma,[66] and in 2011, romidepsin was also approved for treatment of peripheral T-cell lymphoma.[67] Several other HDAC inhibitors are at various stages in the drug development process.[68] SAHA and romidepsin are potent inhibitors, but they are not very selective for any particular HDAC isoform. The development of selective HDAC inhibitors could have a potential in drug development, as an activity for multiple targets usually accompanies a range of side effects. Selective HDAC inhibitors are also desired in a research perspective, as an increased knowledge of each HDAC isoform could be obtained.

Acyclic inhibitors

An enormous progress in understanding the binding of inhibitors to HDAC enzymes occurred when Pavletich and co-workers co-crystalized TSA and SAHA, separately bound to the histone deacetylase-like protein (HDLP). Even though the overall sequence similarity of the bacterial homologue to HDAC1 is only 35.2%, the active site of HDLP has a high resemblance.[69] The crystal structure highlighted important features of the active site; a surface binding domain, an ~11 Å deep narrow pocket leading to the catalytic zinc binding site, and a 14 Å internal cavity adjacent to the active site. (Figure 1.8).[69]

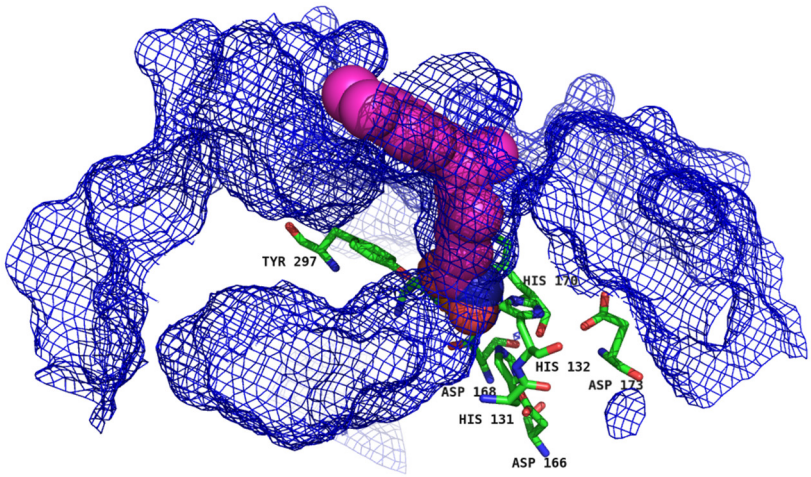

Figure 1.8 TSA (magenta, space filling model) bound to histone deacetylase-like protein (PDB: 1C3R). Amino acids involved in the deacetylation are shown as sticks.

The crystal structure also gave rise to a suggested deacetylation mechanism by the enzyme (Figure 1.9). A water molecule in the active site coordinates to Zn^{2+}. The zinc atom also coordinates the carbonyl oxygen from the acetylated lysine substrate, which will polarize the carbonyl, making it more susceptible to a nucleophilic attack. His131 activates the water molecule, which will react with the carbonyl group. A tetrahedral intermediate is formed, which is stabilized by Tyr297 and the zinc ion. Subsequent release of the acetate anion is assisted by His132 and Asp173.

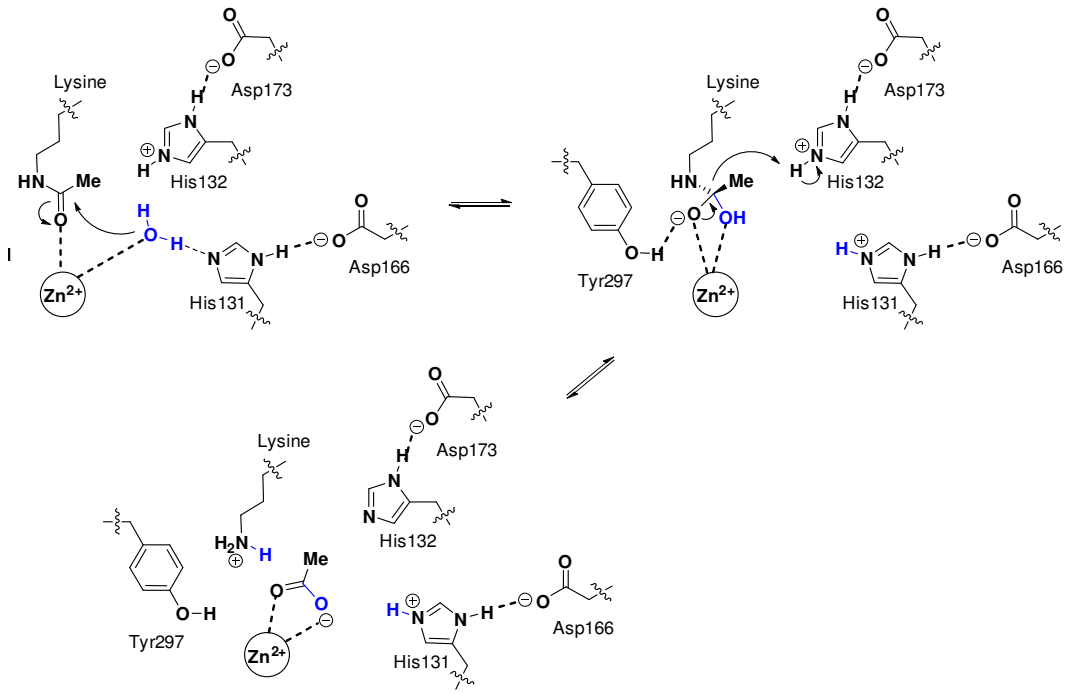

Figure 1.9 Deacetylation mechanism by HDACs, proposed by Pavletich and co-workers.[69] A water molecule reacts with the carbonyl group of an acetylated lysine residue, activated by Zn^{2+} and His131. The tetrahedral intermediate, stabilized by Zn^{2+} and Tyr297 collapses with the release of an acetate ion. The figure was modified from ref [70].

Alternatives to the deacetylation mechanism shown above, have been proposed by Zhang and co-workers suggesting that both His131 and His132 hydrogen bonds to the water molecule before the nucleophilic

attack,[71] and by Geerlings and co-workers, who suggested that a zinc-coordinated hydroxide, stabilized by Tyr297 would react with the acetylated lysine.[72]

Based on X-ray structures and the activity shown by various inhibitors, a pharmacophore has been generated for HDAC inhibitors (Figure 1.10, left). The model consists of a cap group that interacts with motifs on the surface of the protein, a linker region, and a zinc-binding group (ZBG) reaching into the active site.

In 1971, Breslow and co-workers observed that DMSO induced growth and differentiation in cancer cells. The attempt to understand this effect, lead to the discovery of the potent HDAC inhibitor, SAHA (Figure 1.10).[73] Another hydroxamic acid containing compound was discovered in 1975 when Koizumi and co-workers isolated TSA from strains of *Streptomyces hygroscopicus*.[74] However, the effect on mammalian HDACs were first discovered in 1990 (Figure 1.10).[75] Both TSA and SAHA are potent inhibitors of HDAC1, 2, 3, and 6.

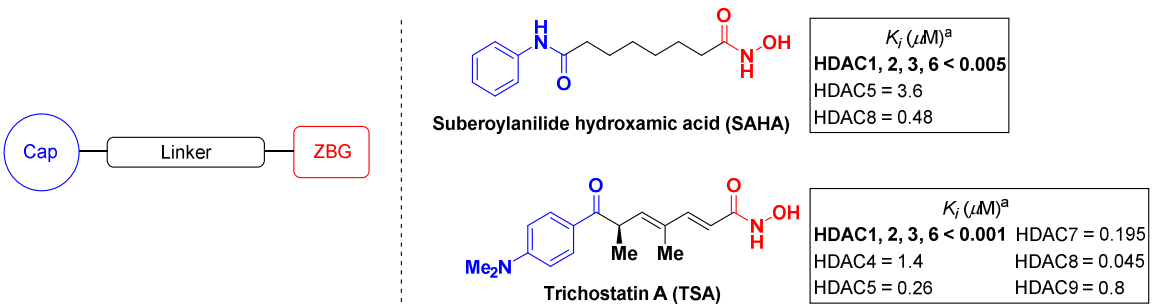

Figure 1.10 Hydroxamic acid containing HDAC inhibitors. [a] Data was obtained from ref [76].

The high potency of TSA and SAHA has been attributed their strong ZBG. Through the years, many compounds have emerged that have utilized the hydroxamic acid moiety; the compounds in Figure 1.11 are all at various stages in drug development.[1] Except for ACY-1215, the inhibitors are not selective towards a specific HDAC isozyme. This could be explained by the strong ZBG that might be too dominant a factor to convey selectivity. One could imagine that the hydroxamic acid interacts with other metalloproteins, which could lead to a range of side reactions. However, a recent investigation suggests that metalloenzyme inhibitors show minor off-target interactions.[77] SAHA was tested among these compounds, although off-target inhibition was observed, the effect was limited.

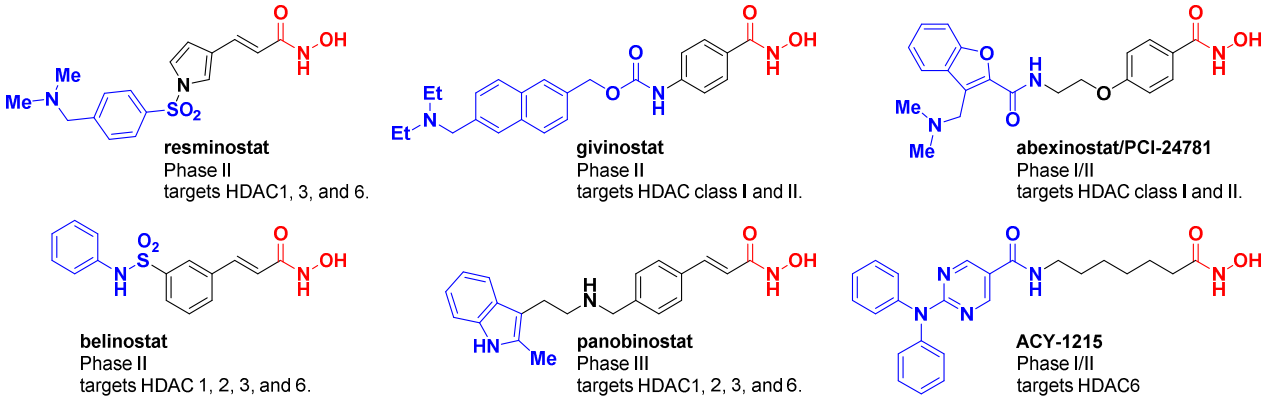

Figure 1.11 A selection of hydroxamic acid containing HDAC inhibitors that are in clinical trials.[1]

Another group of non-cyclic HDAC inhibitors contains an *ortho*-aminoanilide ZBG. Many of these compounds are linked to a phenyl group, which together with the ZBG comprise the benzamides. The compounds in this

group mainly inhibits class I HDAC enzymes, although they show a low activity towards HDAC8 (Figure 1.12). This selectivity within class I, has been explained by the presence of a specific amino acid near the binding site. In HDAC1, 2, and 3 a leucine is located close to the zinc-binding domain of the enzyme, while a tryptophan accommodates this position in HDAC8. Because of the tryptophan residue, the *ortho*-aminoanilide motif cannot chelate zinc with the optimal geometry and therefore becomes a weaker inhibitor.[78] While MS-275, MGCD-0103, and CI-994 are most potent towards HDAC1, an HDAC3 selective compound (MI-192) have been found by using a different cap group.[79]

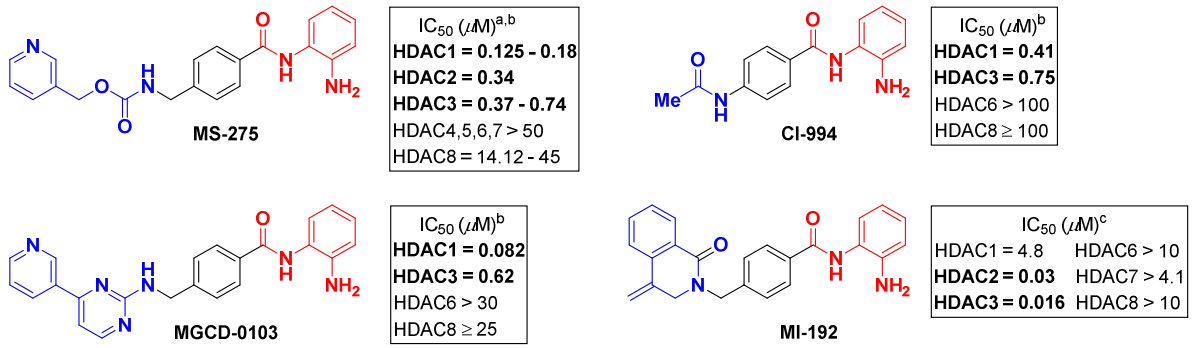

Figure 1.12 Benzamide containing HDAC inhibitors. [a] Data was obtained from ref [80]. [b] Data was obtained from ref [81]. [c] Data was obtained from ref [79].

The internal cavity present in HDLP (Figure 1.8), which has also been observed in other members of class I HDACs (HDAC1[26], 2,[82] 3,[25] and 8[83]) have been of interest in the design of new HDAC inhibitors. Both Moradei[84] and Witter[80] independently found an improved potency against HDAC1 and HDAC2, when a thienyl sustituent was added to the *para*-position of the aminoanilide motif in MS-275 (**1.1**, Figure 1.13). Interestingly, the new compound lost activity against HDAC3, while retaining potency for HDAC1 and 2.

A new class of compounds, containing an amino acid derived ZBG was found in a high throughput screening. One of the compounds (**1.2**) was confirmed by X-ray crystalography (PDB: 3SFH) to bind in the internal cavity as well.[83] The compound displayed a high selectivity towards HDAC8, being 19-fold more potent relative to HDAC1 and 43-fold more potent relative to HDAC2.

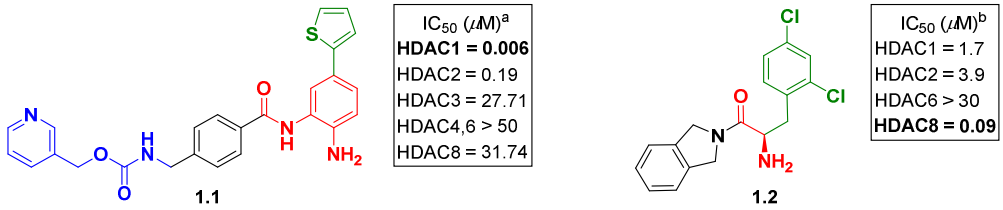

Figure 1.13 HDAC inhibitors, which utilizes binding to the internal cavity. [a] data was obtained from ref [80]. [b] data was obtained from ref [83].

Valproic acid (VPA), which has been prescribed for the treatment of bipolar disorder, major depression, and schizophrenia, is the only HDAC inhibitor that has been approved for neurological disorders.[85] VPA does not contain any cap group and possess a relative poor ZBG. These features might be the reason why VPA is not a potent inhibitor and does not show any particular selectivity, besides an even lower activity against HDAC6 and 10[86] (Figure 1.14). The therapeutic effect of VPA could be explained by a changed gene expression due to HDAC inhibition; however, VPA has been reported to influence a variety of biological pathways, so the direct contribution arising from HDAC inhibition is still unknown.[87]

Even though the majority of HDAC inhibitors fits the pharmacophore model, potent compounds that lack a cap group do exist. Even though the active site in the different HDAC isoforms has a high similarity, compound **1.3** and **1.4**, were shown to be selective inhibitors for HDAC8.[88] Remarkably, the small HDAC inhibitor BRD9757 have been shown to display selectivity towards HDAC6.[89]

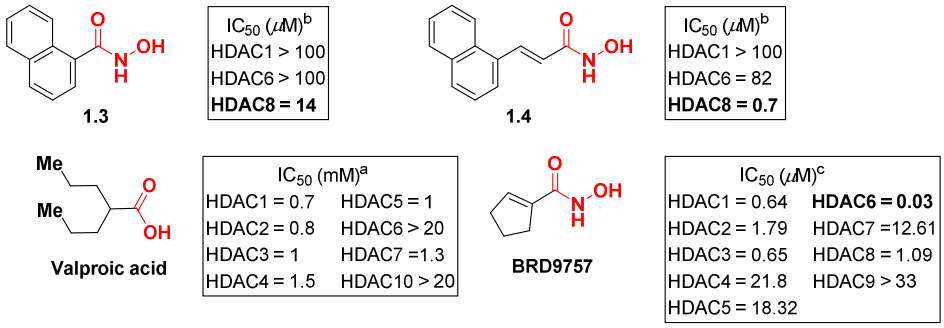

Figure 1.14 Small molecule HDAC inhibitors. [a] Data was obtained from ref [86]. [b] Data was obtained from ref [88]. [c] data was obtained from ref [89].

Isoform selective inhibitors have successfully been synthesized by changing the cap group, thereby exploiting the varying amino acid sequence on the surface in different isoforms. The high selectivity of tubacin for HDAC6 (Figure 1.15) has been explained by the narrow shape of the surface area, towards the active site in the enzyme. Docking experiments showed that the large surface binding domain of tubacin simultaneous made favorable lipophilic and polar interactions. A wider surface area towards the active site was observed in HDAC1 and HDAC8. Consequently, tubacin would only interact with one side of the surface areas and the binding affinity to these isoforms would therefore be lower. In comparison, the decreased selectivity of SAHA was explained by the deficiency to distinguish between any surface area in the different HDAC isozymes, due to the small cap group.[90]

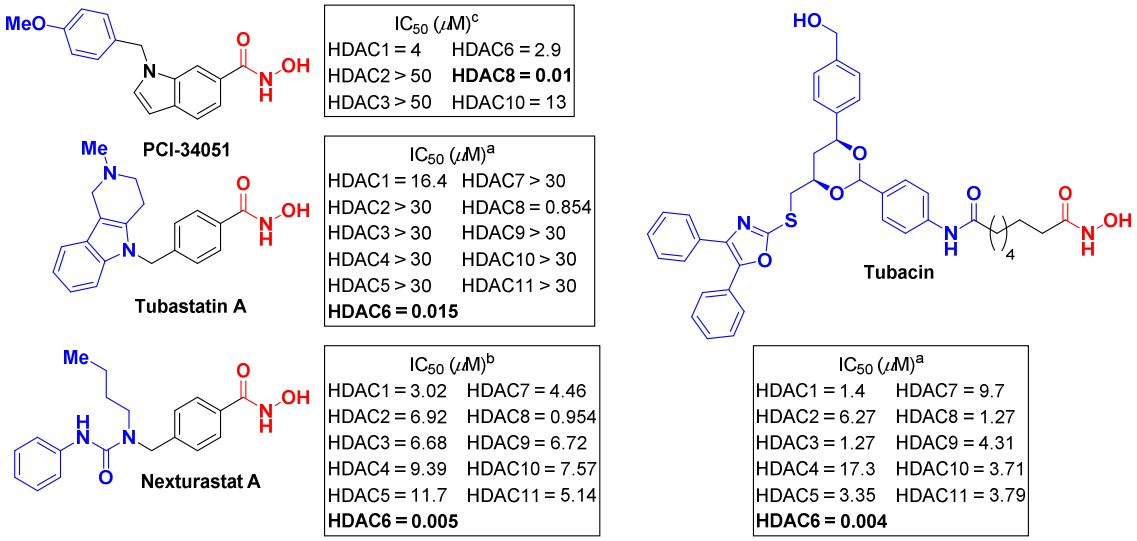

Figure 1.15 HDAC inhibitors utilizing cap group modifications. [a] Data was obtained from [91]. [b] Data was obtained from [92]. [c] Data was obtained from ref [93].

The varieties of inhibitors that have been co-crystalized with HDAC8 have assisted in elucidating unique features that have been used in the design of selective compounds. The crystal structures show a large difference in the binding site, depending on the inhibitor bound. In some cases, the ligand is bound through

a single narrow pocket to the active site (Figure 1.16, left), while a second pocket next to the binding site can be observed in others (Figure 1.16, middle). Access to the second pocket depends on the position of Phe152 and Tyr306, which are located between the two cavities. The binding site can even be seen as a single wide cavity after the movement of Phe152 (Figure 1.16, right). The selectivity observed for some inhibitors towards HDAC8, have been explained by the malleability of the enzyme.[94] Based on X-ray structures and molecular dynamics simulations, it has been suggested that the unbound enzyme exists as a wide cavity that will accommodate the ligand after coordination with zinc.[94]

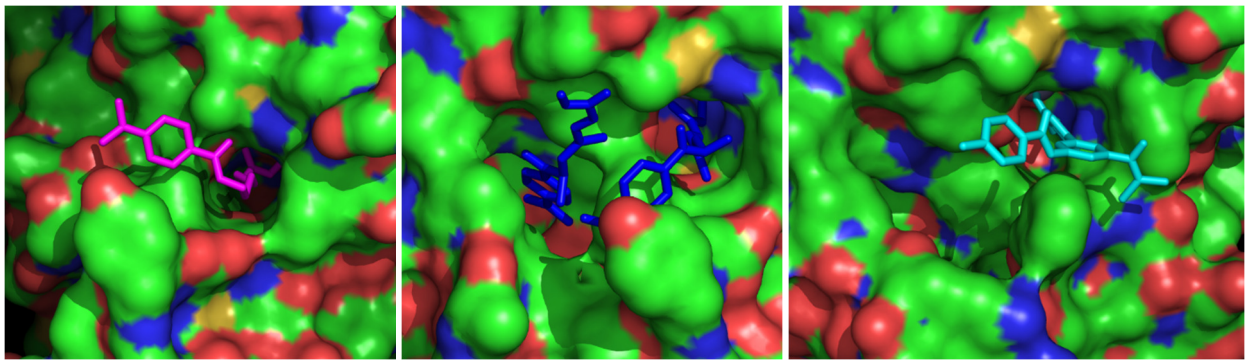

Figure 1.16 Binding of various inhibitors in HDAC8 demonstrates the malleability of the binding pocket. Left: single narrow pocket after binding of MS-344 (PDB: 1T67), middle: two pockets after binding with TSA (PDB: 1T64), right: wide cavity after binding of CRA-19156 (PDB: 1VKG).

Docking studies of PCI-34051 have shown that due to the short linker region, the inhibitor was able to trap the enzyme in the open cavity state, thereby taking advantage of the unique flexibility of the binding pocket in HDAC8. The low activity of SAHA was explained by loss of several hydrophobic interactions, as the cavity was changed to a single narrow pocket, when occupied by this ligand.[94] Several other HDAC8 selective inhibitors have used the distinctive secondary pocket found in HDAC8, by incorporating a *meta*-substituted pattern, which would direct the substituents to the minor cavity.[95]

Very few compounds show selectivity towards class IIa HDACs. However, in 2013 Nolan and co-workers reported a series of inhibitors containing a trifluoromethyloxadiazole ZBG (Figure 1.17).[96] The high selectivity of the compounds was explained by the bulky ZBG in combination with the U-shaped conformation that these inhibitors adapted after binding, which was unlikely to fit in other HDAC isozymes.

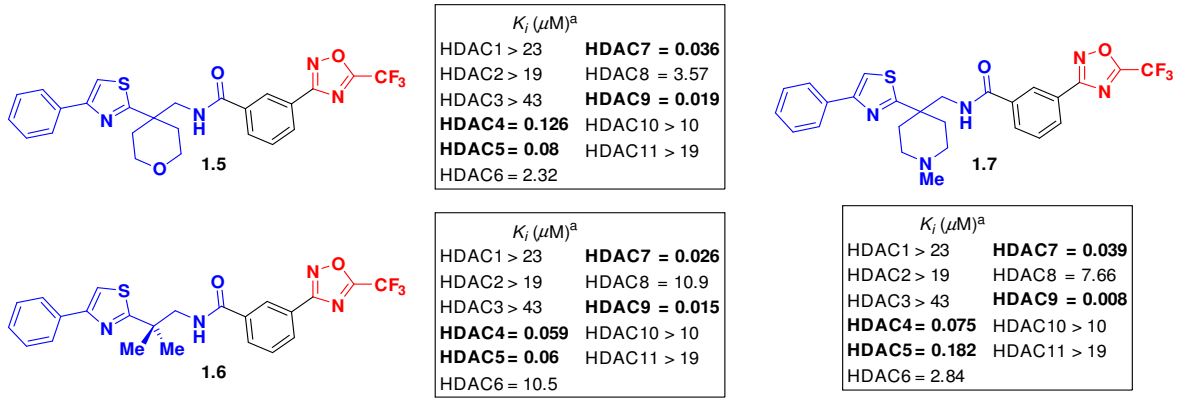

Figure 1.17 Class IIa selective HDAC inhibitors. [a] Data was obtained from ref [96].

Macrocyclic inhibitors

The macrocyclic inhibitors comprise both non-peptidic macrocycles as well as cyclic peptides and depsipeptides. The use of cyclic peptides in drug development could have improved features compared to their linear analogs. While linear peptides degrade readily *in vivo*, the cyclic peptides are stable towards exopeptidases. Endopeptidases usually require the peptide to adopt an extended conformation, small cyclic peptides will therefore also have a certain stability towards these enzymes.[97]

Macrocyclic inhibitors have been a key factor for understanding HDAC enzymes; a huge breakthrough occurred when Schreiber and co-workers used a modified cyclic peptide to isolate the first HDAC enzyme.[98] Macrocycles have also shown their potential in the pharmaceutical industry, with romidepsin on the market for treatment of cutaneous T-cell lymphoma and peripheral T-cell lymphoma.[66b, 67]

Most of the macrocyclic HDAC inhibitors are natural products or analogs based on these. However, a few non-natural compounds have been synthesized, which also show HDAC inhibitory activity. The wide range of macrocyclic HDAC inhibitors have expanded the knowledge regarding binding mode and selectivity.

α-Epoxy ketone containing cyclic peptides

Cyclic peptides containing an α-epoxy ketone as the ZBG includes WF-3161,[99] chlamydocin,[100] HC-toxin,[101] trapoxin A, B[102], and Cyl-1, 2[103] (Figure 1.18). All the peptides contain a proline or pipecolic acid next to the zinc-binding side chain and at least one D-amino acid.

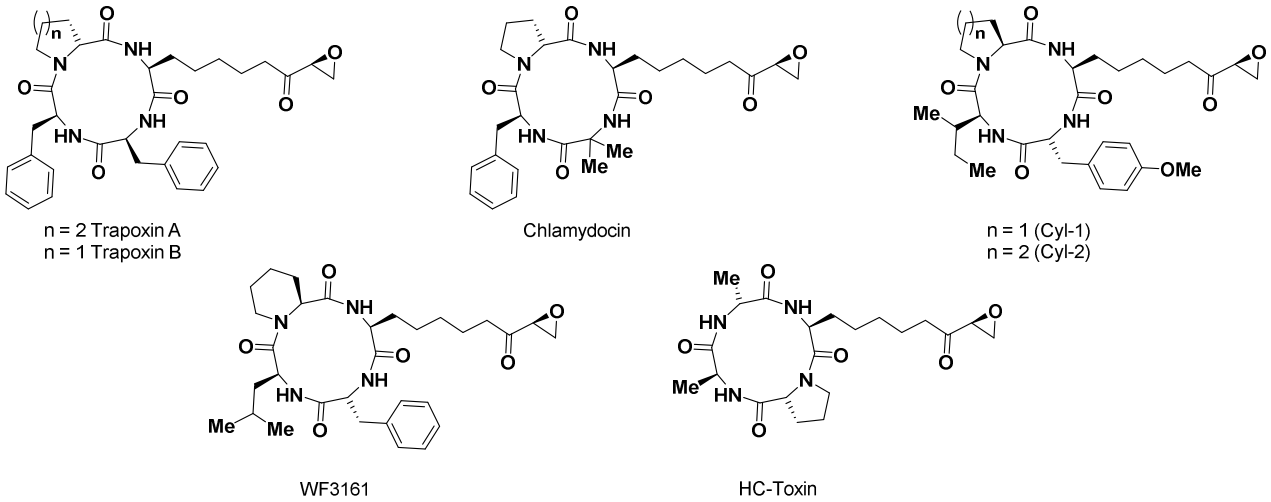

Figure 1.18 Cyclic peptides containing an *α*-epoxy ketone motif.

Trapoxin was isolated by Yoshida and co-workers in 1993 and tested *in vitro* on HDAC enzymes, partially purified from mice.[104] The natural compound was a potent inhibitor with an irreversible binding mode. Since very little was known about the HDAC enzymes, Schreiber and co-workers utilized the irreversible binding mode of trapoxin to investigate the enzymes. An affinity matrix was therefore constructed from an analog of trapoxin B (Scheme 1.1).[105]

The threitol-derived compound (**1.8**) was subjected to Swern oxidation, followed by a Wittig reaction to obtain **1.9**. Evans (*S*)-oxazolidinone was then added and the protected alcohol converted to the tosylate. Diastereoselective azidation afforded the (*S*)-azido imide, which was hydrolyzed to the free acid. Simultaneous hydrogenation of the alkene and azide afforded the amino acid, which was protected with a 9-fluorenylmethoxycarbonyl (Fmoc) group (**1.11**) and coupled to a tripeptide.

The cyclization was done by adding the peptide via syringe pump to a solution containing (benzotriazol-1-yloxy)tris(dimethylamino)phosphonium hexafluorophosphate (BOP), 4-dimethylaminopyridine (DMAP) and *N*,*N*-dimethylformamide (DMF). The slow addition minimized formation of dimers, which had been the main product in their total synthesis of trapoxin B. A protected lysine residue was incorporated as a replacement for one of the phenylalanines present in trapoxin B, so the cyclic peptide could be coupled to a solid support at a later stage (**1.13**). The acetonide was removed with aqueous HCl and the epoxide formation was facilitated by 2,3,4,6,7,8,9,10-octahydropyrimido[1,2-a]azepine (DBU). In the final step, an oxidation afforded the handle for the affinity matrix (K-trap), before attachment to the solid support. The phenylalanine to lysine substitution had little effect on HDAC binding *in vitro,* so by the use of [^{3}H]-trapoxin in combination with the affinity matrix, Schreiber and co-workers managed to isolate the first HDAC enzyme, which is now classified as HDAC1.[98, 105]

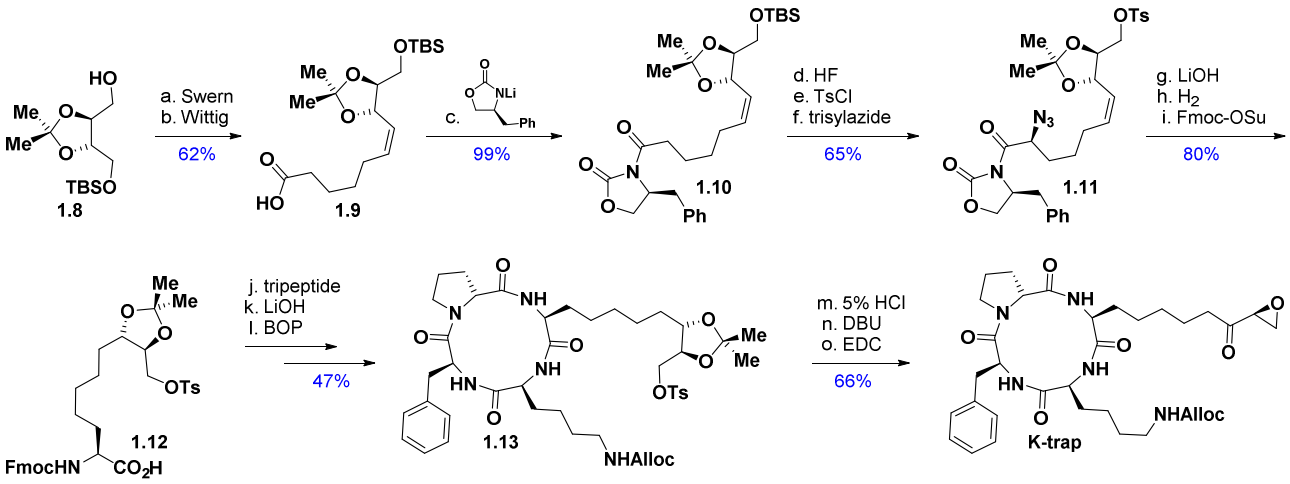

Scheme 1.1 (a) $(COCl)_2$, DMSO, Et_3N, CH_2Cl_2. (b) $LiO_2C(CH_2)_4CH{=}PPh_3$, THF. (c) Evans (*S*)-oxazolidinone, $(CH_3)_3CCOCl$, Et_3N. (d) HF, pyridine, THF. (e) TsCl, $^iPr_2NEt$, DMAP. (f) $KN(SiMe_3)_2$, THF, –78 °C, trisylazide, AcOH, 35 °C. (g) LiOH, THF, H_2O. (h) H_2, 10% Pd/C. (i) Fmoc-OSu, 2,6-lutidine, THF. (j) tripeptide, EDC, HOBt, NMM. (k) LiOH, THF, MeOH, H_2O. (l) BOP, DMAP, DMF. (m) 5% HCl, THF. (n) DBU, MeOH, 0 °C. (o) EDC, DMSO, Cl_2CHCO_2H.[105]

Chlamydocin, Cyl-2 and trapoxin A, B have been evaluated against a selection of HDACs (Table 1.2). All HDAC inhibitors showed selectivity towards HDAC1 compared to HDAC6, Table 1.2.[106] Cyl-2 proved to be particular selective with a 57,000 fold preference for HDAC1. In correlation with previous studies, an irreversible binding of trapoxin B was confirmed in the case of HDAC1, but for HDAC6 the inhibition proved to be reversible.

Table 1.2 HDAC inhibitory activity against HDAC1 and 6.

	IC_{50} (nM)		
Compound	HDAC1	HDAC6	HDAC6/HDAC1
Trapoxin A	0.82 ±0.29	524 ±240	640
Trapoxin B	0.11 ±0.01	360 ±160	3,300
Chlamydocin	0.15 ±0.03	1,100 ±430	7,300
Cyl-2	0.7 ±0.45	40,000 ±11,000	57,000

The data was obtained from ref [106].

A range of analogs, based on the scaffold of the natural compounds, was synthesized by substituting the α-epoxy ketone moiety with a hydroxamic acid (Figure 1.18, Table 1.3). These cyclic hydroxamic-acid containing peptides (CHAPs) showed increased activity for HDAC6. Although the selectivity was severely reduced, the analogs maintained a higher activity for HDAC1. This suggests that the large cap group of the natural compounds, at least to some degree, confer selectivity. Moreover, replacing the epoxy ketone of trapoxin B to the hydroxamic acid, converted the inhibitor to a reversible binder.

Table 1.3 HDAC inhibitory activity against HDAC1 and 6.

	IC_{50} (nM)		
Compound	HDAC1	HDAC6	HDAC6/HDAC1
CHAP (trapoxin A)	6.1 ±1.4 (7)	150 ±84 (4)	25
CHAP (trapoxin B)	1.9 ±0.5 (17)	19 ±3 (19)	10
CHAP (Cyl-2)	1.2 ±0.7 (2)	36 ±17 (>1000)	30
CHAP (Cyl-1)	4.4 ±1.8	110 ±84	25
CHAP (WF3161)	0.94 ±0.33	22 ±10	23
CHAP (chlamydocin)	0.44 ±0.23 (3)	38 ±12 (29)	86
CHAP (HC-toxin)	2.9 ±2.1	61 ±14	21

Potency relative to the natural compound is shown in parenthesis. Red: fold decrease, green: fold increase. The data was obtained from ref [106].

Even though the α-epoxy ketone containing compounds are potent inhibitors *in vitro*, only weak activity has been observed in animal models. This effect is thought to arise because of instability of the α-epoxy ketone moiety in the blood.[107] Whereas chlamydocin has a half-life of ~2.5 min in blood, CHAP based on Cyl-1 is more stable, with a half-life of ~50 min. This suggests that the therapeutic potential can be improved by changing the ZBG of the cyclic peptides.

CHAPs based on chlamydocin have been explored further by modifying the phenylalanine and the aminoisobutyric acid. An acetylated thiol was also explored as a ZBG in some of the analogs (Figure 1.19).[108] The biological data shows that modifications to the core structure are well tolerated at the indicated positions, whereas compound **1.19–1.21** are less potent inhibitors, especially against HDAC6 (Table 1.4).

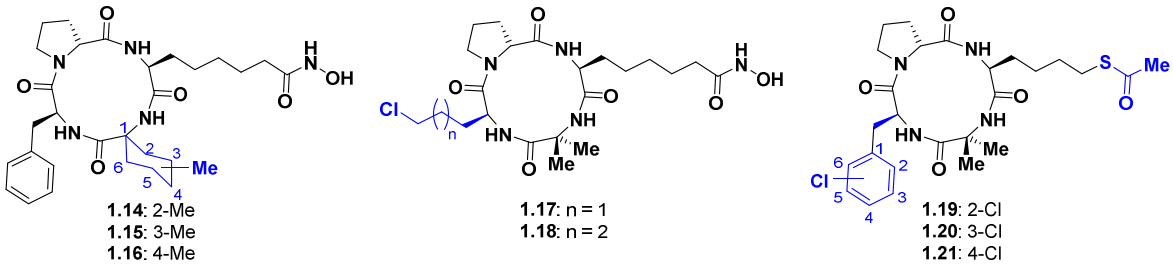

Figure 1.19 CHAP analogs based on chlamydocin.

Table 1.4 HDAC inhibitory activity against HDAC1, 4, and 6.

	IC_{50} (nM)						
Compound	HDAC1	HDAC4	HDAC6	Compound	HDAC1	HDAC4	HDAC6
TSA	23	34	65	**1.18**	10 (2)	15 (2)	96 (2)
1.14	10 (2)	6 (6)	130 (2)	**1.19**	27 (2)	nd	>1000 (>15)
1.15	15 (ep)	14(2)	160 (3)	**1.20**	28 (2)	nd	380 (6)
1.16	11 (2)	12(3)	170 (3)	**1.21**	38 (2)	nd	>1000 (>15)
1.17	14 (ep)	19(2)	110 (2)				

Potency relative to CHAP (chlamydocin) is shown in parantheses. Red: fold decrease, ep: equipotent, green: fold increase. Data was obtained from ref [108].

Apicidin

The fungal metabolites, apicidin and apicidin A (Table 1.5), were isolated in 1996 in a natural products screen against a broad range of parasites (apicomplexa). The anti-parasitic potency of apicidin is likely a consequence of its ability to inhibit apicomplexan HDACs with an IC_{50} of 1–2 nM.[109] The closely related analogs, apicidin B, C, D1, D2, and D3 (Table 1.5), were isolated in 2002,[110] and in 2010 variants E and F were discovered.[111]

Table 1.5 Known apicidin compounds.

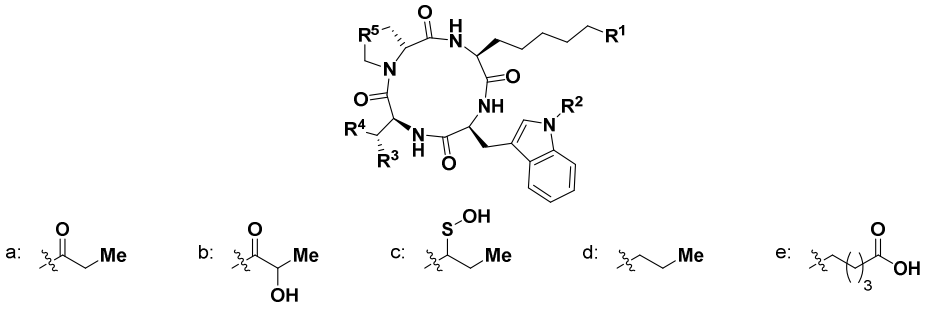

Name	R^1	R^2	R^3	R^4	R^5	HeLa NE[a]
Apicidin	a	OMe	Et	Me	CH_2CH_2	1
Apicidin A	a	H	Et	Me	CH_2CH_2	2
Apicidin B	a	OMe	Et	Me	CH_2	–
Apicidin C	a	OMe	Me	Me	CH_2CH_2	–
Apicidin D_1	b	OMe	Et	Me	CH_2CH_2	0.3
Apicidin D_2	c	OMe	Et	Me	CH_2CH_2	400
Apicidin D_3	b	OMe	Et	Me	CH_2CH_2	–
Apicidin E	d	OMe	Et	Me	CH_2CH_2	–
Apicidin F	e	OMe	Ph	H	CH_2CH_2	–

[a] Data was obtained from ref [110].

The first total synthesis of apicidin A was reported by Mou and Singh in 2001.[112] The side chain of apicidin was synthesized from L-glutamic acid to give the iodoamino ester **1.24**, and the key step in the strategy was a radical coupling of ethyl vinyl ketone to form the protected (S)-2-amino-8-oxodecanoic acid (**1.25**) (Scheme 1.2). The linear peptide was synthesized and activated as a pentafluorophenyl ester (**1.27**). Slow deprotection of the Cbz group afforded the cyclic peptide in 54% over 6 steps after deprotection of the indole.

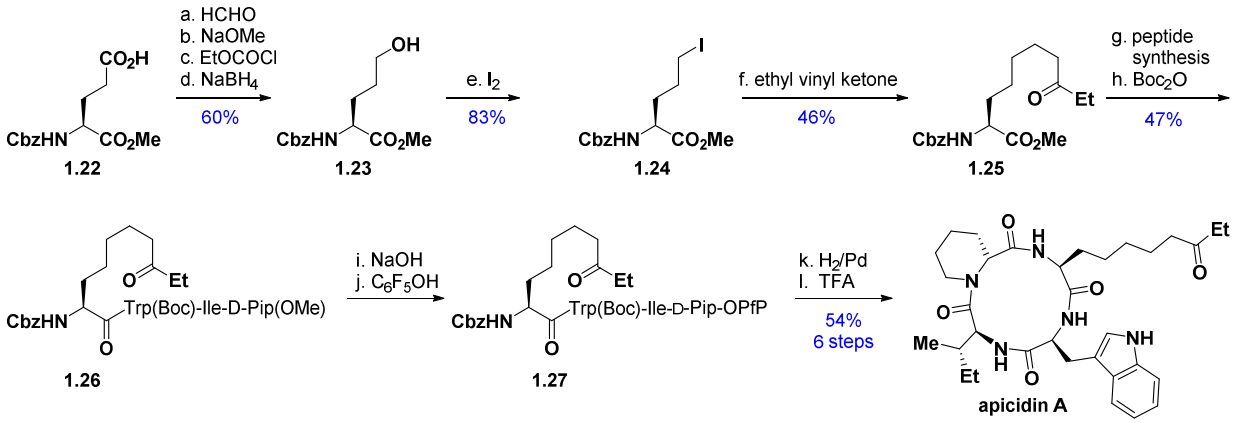

Scheme 1.2 The first total synthesis of apicidin A by Mou and Singh.[112] Reagents and conditions: (a) HCHO, cat. p-TSA. (b) NaOMe, MeOH. (c) EtOCOCl. (d) $NaBH_4$. (e) PPh_3, I_2, imidazole. (f) pent-1-en-3-one, n-Bu_3SnH, hv, Et_2O. (g) peptide synthesis. (h) Boc_2O, DMAP. (I) NaOH. (j) C_6F_5OH, EDAC/DMAP. (k) H_2/Pd, C_6H_{12}, dioxane.

Cyclization of tetrapeptides is known to be difficult because of the strained conformation that the linear peptides have to adopt; dimerization is a byproduct that is often observed.[113] In other total syntheses of apicidin and similar cyclic tetrapeptides, the site of cyclization between the C-terminal of proline and the N-terminal Aoda residue have been used.[105, 112, 114]

An extensive SAR study on the side chain of apicidin has been conducted;[115] a selection of these are presented in Table 1.6. The importance of the carbonyl functionality was evident, as activity was lost after reduction (entry 2, 3). The retained activity of the aldehyde (entry 18), support this fact. The space in the active site was explored by incorporating large substituents; *n*-propyl was well tolerated, while activity was lost when incorporating an isopropyl and a phenyl substituent. Exchanging the ketone for other known ZBGs (entry 15, 17) gave highly active compounds; in the case of the α-epoxy ketone moiety, substitution on C9 was better tolerated than on C7 (entry 15, 16). The optimal length of the side chain was found, in analogy to the length of an acetylated lysine, by having the carbonyl group at C8 (entry 8, 11). Interestingly, the acetylated thiols, which are hydrolyzed *in vitro*, showed the highest potency with the thiol at C7.

Table 1.6 Activity of apicidin analogs.

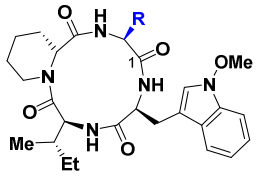

IC_{50} (nM)

Entry	R	HeLa	Entry	R	HeLa	Entry	R	HeLa
1	Apicidin	1	7	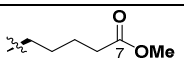	74	13[a]	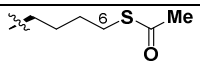	110
2	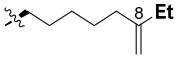	1450	8	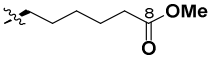	0.4	14[a]	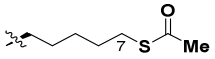	3
3	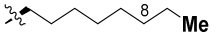	61	9	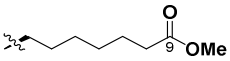	7	15	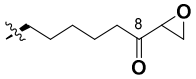	<0.1
4	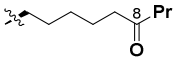	1	10	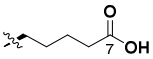	282	16	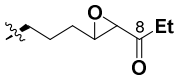	5
5	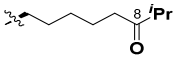	235	11	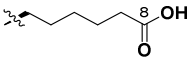	15	17	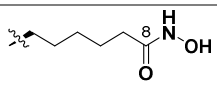	0.2
6	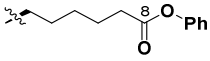	700	12	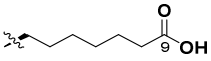	848	18	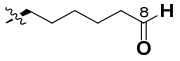	6

[a] thiol generated *in situ*. Data was obtained from ref [115].

While apicidin exists as the all *trans* conformation in [D_5]pyridine and CD_2Cl_2[116] three conformations have been observed in DMSO-d_6, in a ratio of approximately 80:15:5.[117] The major conformation was still the all *trans* (*t*-*t*-*t*-*t*), whereas a *cis* amide bond was observed between valine and pipecolic acid in the second most abundant structure. The *cis*-*trans*-*trans*-*trans* (*c*-*t*-*t*-*t*) conformation has also been observed in a crystal structure of apicidin,[116] but the biological active conformation of apicidin was still unknown. Ghadiri and co-workers therefore synthesized apicidin analogs containing 1,4-disubstituted 1,2,3-triazoles and 1,5-disubstituted 1,2,3-triazoles mimicking a *trans* amide- and a *cis* amide bond respectively (Figure 1.20).[117] Overlaying NMR structures of the *t*-*t*-*t*-*t* and *c*-*t*-*t*-*t* triazole analogs with their corresponding apicidin NMR structures showed a close similarity, confirming the use of the analogs as representatives in the biological testing. Similar to **1.28** and **1.29**, compound **1.30** displayed a single conformation (*c*-*t*-*c*-*t)* in NMR and was therefore evaluated in the HDAC assays as well.

1.30 showed decreased HDAC inhibitory activity against all isozymes compared to the other apicidin analogs. For **1.28** and **1.29** no significant change of activity was seen against HDAC3, however, for HDAC1 the all trans compound (**1.28**) lost ~8 fold potency, while **1.29** only displayed a minor change in IC_{50} value. Interestingly, **1.29** was more potent than apicidin for HDAC6 and especially against HDAC8 (Table 1.7).

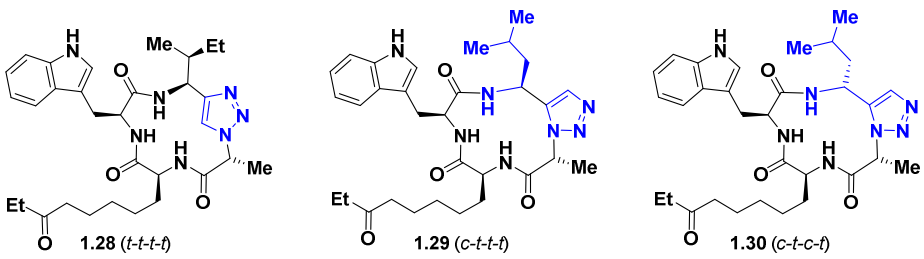

Figure 1.20 Conformational constrained apicidin analogs.

Table 1.7 HDAC inhibitory activity against HDAC1, 3, 6, and 8.

	IC_{50} (nM)			
Compound	HDAC1	HDAC3	HDAC6	HDAC8
Apicidin	3	11	>10,000	750
1.28 (*t-t-t-t*)	25 (8)	16 (2)	>10,000	nd[a]
1.29 (*c-t-t-t*)	7 (2)	9 (ep)	6100	105 (7)
1.30 (*c-t-c-t*)	75 (25)	119 (11)	>10,000	nd[a]

Potency relative to apicidin is shown in parantheses. Red: fold decrease, ep: equipotent, green: fold increase. nd: not determined. Data was obtained from ref [117].

Even though minor structural changes occur in the analogs, the altered HDAC activity was explained by the conformational change in the cyclic core. Apicidin exist primarily as the *t-t-t-t* conformation in most solvents,[109] however, the data suggests that apicidin interact with HDAC enzymes in the *c-t-t-t* conformation.

A significant change occurs in the backbone structure when the geometry of the peptide bond is altered, in particular the distance between Ile/Leu and Ala, but also the distance between Trp and the Aoda residue (Figure 1.21). The vector from C^{α} to C^{β} in the Aoda, Trp, and Ile/Leu side chains seems to lie in the plane of the ring structure in **1.30**, while it is projected above, in the biological active compounds **1.28** and **1.29**.

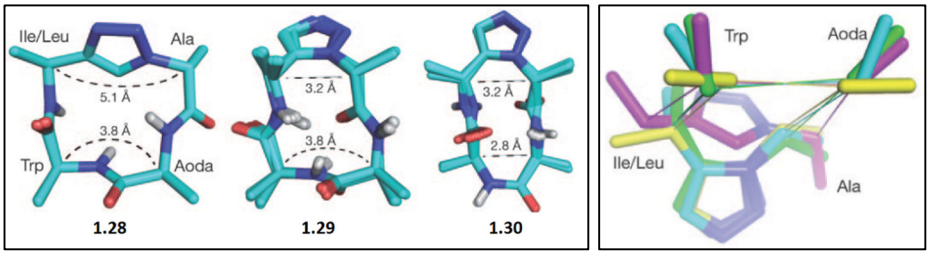

Figure 1.21 Changing the geometry of the amide bond alters the cyclic structure significantly. Left: **1.28**: (*t-t-t-t*), **1.29**: (*c-t-t-t*), **1.30**: (*c-t-c-t*). Right: The vector from C^{α} to C^{β} is projected above the plane in the biological active compounds. **1.28**: magenta, **1.29**: green and cyan, **1.30**: yellow. The figure was modified from ref [117].

Ghadiri and co-workers designed a range of analogs based on the scaffold of apicidin. By incorporating β-amino acids in the peptide backbone, a series of $\alpha_3\beta$ and $\alpha_2\beta_2$ cyclic peptides were constructed (Figure 1.22).[118]

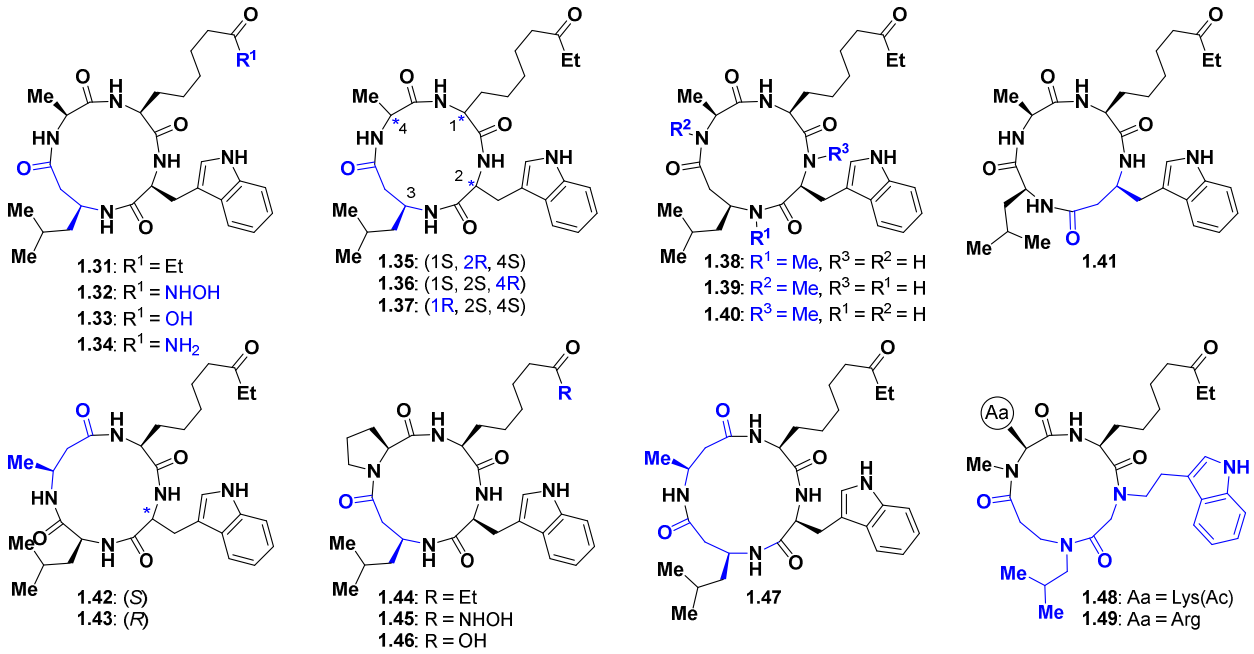

Figure 1.22 $\alpha_3\beta$ and $\alpha_2\beta_2$ cyclic peptides/peptoids based on apicidin.[118-119]

From HeLa cell nuclear extracts it was clear that compounds with a β-amino acid in the position of tryptophan or alanine (**1.41**, **1.42**, **1.43**) were less potent. No significant change was observed for compound **1.31** and **1.44**, so the analogs were further modified by altering the ZBG (**1.32**–**1.34**, **1.45**–**1.46**). Incorporating a hydroxamic acid increased the potency, while substituting for a carboxylic acid or an amide had a negative impact. The stereochemical requirements of the side chains were investigated by changing the chirality of individual residues (**1.35**-**1.37**). The tryptophan- and Aoda epimers showed a severe decrease in activity, while the change was modest when the alanine residue was modified. Analogs containing backbone methylated amides showed the same trend (**1.38**–**1.40**); while a modest decrease was observed for the alanine residue, changes to valine or tryptophan resulted in a significant loss of activity. The backbone scaffold was further investigated by incorporating an additional β-amino acid ($\alpha_2\beta_2$). Changing tryptophan and valine to β-amino acids resulted in more than 700-fold loss in potency (not shown), while the activity loss was lower when alanine and valine were changed to β-amino acids (**1.47**).

Recently, the **1.39** scaffold has been further investigated by substituting residues with peptoid units.[119] Although potency was decreased relative to apicidin (Table 1.8), compound **1.48** and **1.49** were potent inhibitors against HDAC1–3, with IC_{50} values ranging from 100–320 nM.

Table 1.8 HDAC inhibitory activity against HeLa NE.

			IC$_{50}$ (nM)		
Compound	HeLa NE	Compound	HeLa NE	Compound	HDAC1
1.31	19 (2)	**1.40**	> 1000 (>99)	**1.48**	180 (16)
1.32	<1 (>9)	**1.41**	480 (53)	**1.49**	200 (18)
1.33	300 (33)	**1.42**	200 (22)	Compound	HDAC2
1.34	2700 (>99)	**1.43**	>1000 (>99)	**1.48**	300 (9)
1.35	>1000 (>99)	**1.44**	9 (ep)	**1.49**	370 (5)
1.36	440 (49)	**1.45**	<1 (>9)	Compound	HDAC3
1.37	>1000 (>99)	**1.46**	250 (28)	**1.48**	100 (8)
1.38	2000 (>99)	**1.47**	250 (28)	**1.49**	320 (25)
1.39	40 (4)				

Potency relative to apicidin is shown in parenthesis. Red: fold decrease, ep: equipotent, green: fold increase. Data was obtain from ref [118-119]. NE: Nuclear extract.

Largazole

Largazole is a marine cyanobacterial secondary metabolite, isolated by Luesch and co-workers, from *Symploca sp*.[120] The natural compound consists of a long thioester side chain (the first known example produced by a cyanobacterium) and an unusual cyclic core containing a distinctive 4-methylthiazoline, linked to a thiazole (Figure 1.23).

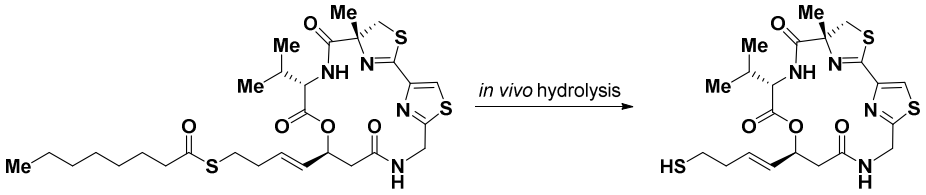

Figure 1.23 Largazole is a natural prodrug, which is hydrolized to its biological active form *in vivo*.

Largazole has attracted interest from a number of groups, demonstrated by at least 11 total syntheses. The first total synthesis was pulished by Luesch, Hong, and co-workers (Scheme 1.3).[121] Subunit **1.51** was made by condensation of **1.50** with H-(L)-Cys-CO_2Me. After TFA deprotection, the building block was coupled to **1.52**, which had been synthesized by a stereoselective syn-aldol reaction, using a chiral thiazolidinethione auxiliary.[122] The last amino acid was then attached and the depsipeptide was cyclized between valine and 4-methylthiazoline. The final compound was obtained by a cross metathesis with the thioester side chain using Grubbs 2nd generation catalyst. A high loading of the catalyst was needed (50 mol%), since the thioester coordinates to the ruthenium catalyst.

Both Cramer and co-workers[123] as well as Phillips and co-workers,[124] chose to attach the side chain in the final step via a cross metathesis, but instead of using a chiral auxiliary for synthesis of the β-hydroxyacyl subunit, the chirality was obtained by enzymatic resolution of a racemic β-hydroxyl ester.

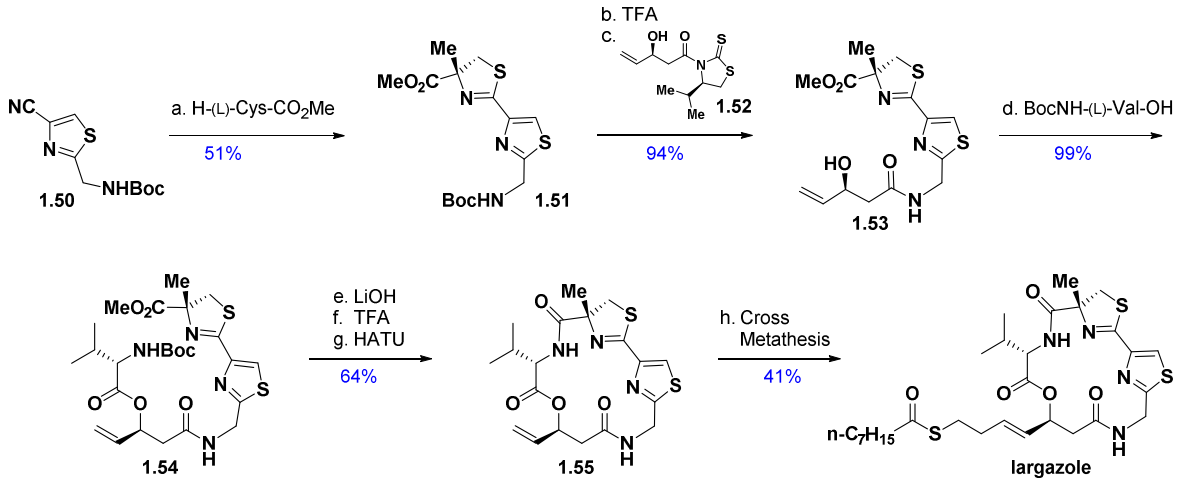

Scheme 1.3 Total synthesis of largazole by Luesch, Hong, and co-workers.[121] Reagents and conditions: (a) H-(L)-Cys-CO_2Me, Et_3N, EtOH, 50 °C, 72h. (b) TFA, CH_2Cl_2, 25 °C. (c) **1.52**, DMAP, CH_2Cl_2, 25 °C, 1h. (d) 2,4,6-trichlorobenzyl chloride, Et_3N, THF, 0 °C, then BocNH-(L)-Val-OH, DMAP, 25 °C, 10h. (e) 0.5 N LiOH, THF, H_2O, 0 °C, 3h. (f) TFA, CH_2Cl_2, 25 °C, 2h. (g) HATU, HOAt, $^iPr_2NEt$, CH_2Cl_2, 25 °C, 24h. (h) n-$C_7H_{15}COSCH_2CH_2CH{=}CH_2$.

The groups of Williams,[125] Ganesan,[126] and Xie[127] all chose to use a thiol protected β-hydroxy acid, in their total syntheses of largazole; Ganesans synthesis is shown in Scheme 1.4. Aldehyde **1.56** was obtained in two steps from acrolein and by using the same chiral auxiliary as in Luesch and Hong's total synthesis, the thiol protected β-hydroxy acid (**1.58**) was synthesized in good yield. Cyclization followed by trityl deprotection and acylation yielded the target compound.

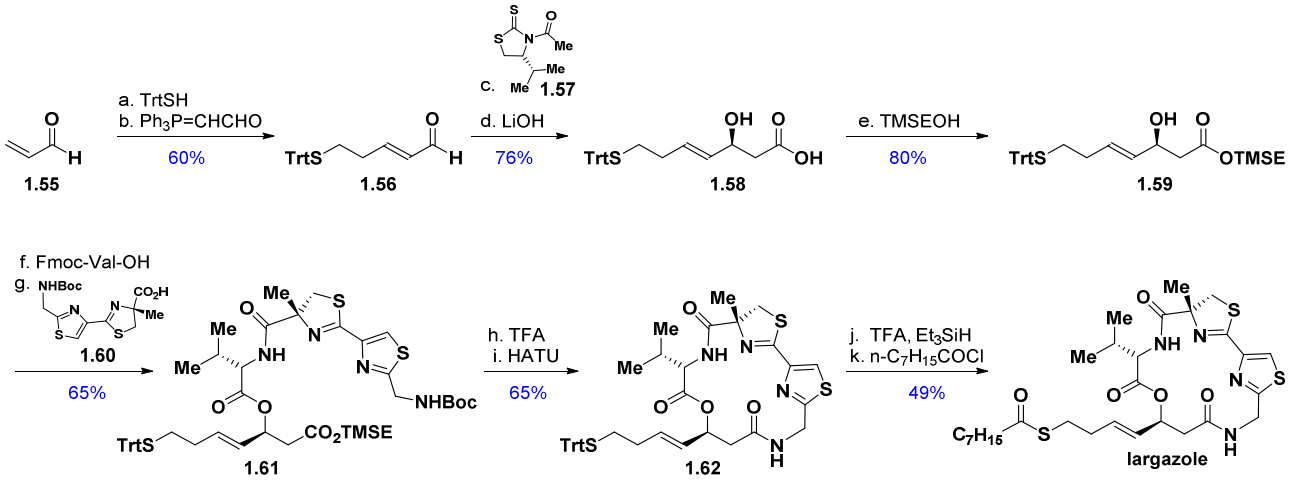

Scheme 1.4 Total synthesis of largazole by Ganesan and co-workers.[126] Reagents and conditions: (a) TrtSH, Et3N, CH_2Cl_2. (b) Ph_3P=CHCHO, benzene, reflux. (c) **1.57**, $TiCl_4$, *i*-Pr_2NEt, CH_2Cl_2. (d) LiOH, aq. THF. (e) TMSEOH, DCC, CH_2Cl_2. (f) Fmoc-Val-OH, DCC, CH_2Cl_2. (g) **1.60**, PyBOP, *i*-Pr_2NEt, CH_2Cl_2, overnight. (h) TFA, MeCN, overnight. (i) HATU, HOBt, *i*-Pr_2NEt, MeCN/CH_2Cl_2, overnight. (j) TFA, Et_3SiH, CH_2Cl_2, 0 °C to rt, 2h. (k) n-$C_7H_{15}COCl$, Et_3N, CH_2Cl_2, 0 °C to rt, 3h.

Jiang and co-workers published another interesting example, shown in Scheme 1.5. The stereochemistry of the *tert*-butyl-silyl (TBS) protected diol **1.65** was already set, as the commercially available (–)-malic acid was used as starting material. The methyl ester was saponified and protected with 2-(trimethylsilyl)ethanol, where after a selective deprotection of the primary alcohol afforded compound **1.67**. Swern oxidation to the aldehyde and Julia-Kocienski olefination afforded **1.69** favoring the *E* isomer (*E*/*Z*: 8/1). Selective removal of the primary alcohol, allowed insertion of a thioester using the Mitsunobu reaction and the final β-hydroxyacyl

building block was obtained by deprotecting the secondary alcohol. After connecting the subunits and cyclizing from the β-hydroxy acid to the thiazole subunit, the natural compound was obtained. Ghosh and co-workers chose to cyclize at the same position, but the β-hydroxy ester was obtained by enzymatic resolution followed by cross metathesis on the subunit.[128]

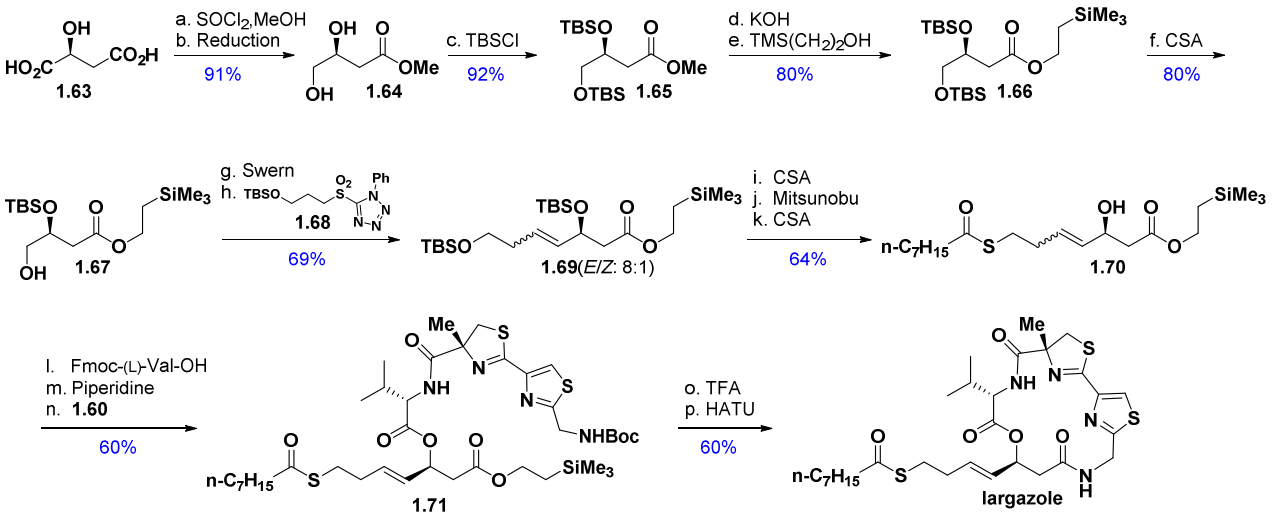

Scheme 1.5 Total synthesis of largazole by Jiang and co-workers.[129] Reagents and conditions: (a) $SOCl_2$, MeOH (b) BH_3, Me_2S, $NaBH_4$. (c) TBSCl, imidazole, DMF. (d) KOH, THF/H_2O. (e) DCC, $TMS(CH_2)_2OH$. (f) CSA, $CHCl_3$/MeOH. (4:1) (g) $(COCl)_2$, DMSO, Et_3N. (h) **1.68**, NaHMDS, THF. (i) CSA, $CHCl_3$/MeOH (9:1). (j) octanethioic acid, DEAD, Ph_3P, THF. (k) CSA, $CHCl_3$/MeOH (2:1). (l) Fmoc-(L)-Val-OH, EDCl, HOAt, DIPEA, CH_2Cl_2, rt. (m) piperidine, DMF, 20 min, rt. (n) **1.60**, EDC, HOAt, DIPEA, CH_2Cl_2, rt. (o) TFA, TES, CH_2Cl_2, 2h. (p) HATU, HOAt, DIPEA, CH_2Cl_2, 2 days, rt.

Most total syntheses of largazole have made disconnections as seen in Scheme 1.6. Various strategies have been used for incorporating the side chain; these include acylation after cyclizing the scaffold, or attachment via a cross metathesis. Cyclization with the thioester side chain has also been performed. In all the strategies, the core structure from three building blocks have been assembled from a β-hydroxy acid, valine and the 4-methylthiazoline linked thiazole. The stereochemistry for the β-hydroxy acid building block has primarily been obtained from an asymmetric aldol reaction or an enzymatic resolution.

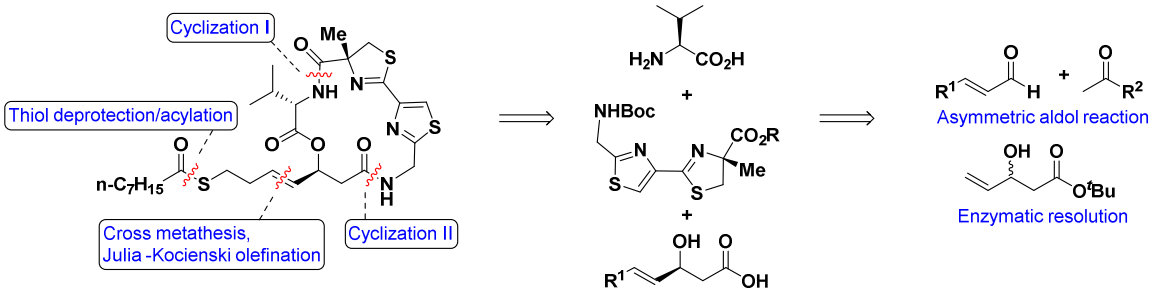

Scheme 1.6 **Cyclization I**: Luesch/Hong, Doi, Xie; **Cyclization II**: Williamms, Cramer, Phillips, Ghosh, Ye, Forsyth, Jiang, Ganesan; **Thiol deprotection/acylation**: Williams, Ye, Doi, Xie, Ganesan; **Cross metathesis**: Luesch/Hong, Cramer, Philips, Ghosh; **Julia-Kocienski olefination**: Jiang; **Asymmetric aldol reaction**: Luesch/Hong, Williams, Ye, Doi, Xie; **Enzymatic resolution**: Cramer, Philips, Ghosh. The figure was modified from ref [130].

Williams and co-workers demonstrated that largazole act as a prodrug and that the activity instead arises from its corresponding thiol.[125] This mode of action was discovered by testing largazole and its corresponding thiol against a number of HDAC isoforms. The data clearly showed the superior potency of largazole thiol, which was more than 250-fold more potent against HDAC1–3. When the inhibitory effect was

tested in a panel of melanoma cell lines, largazole was more potent (IC_{50} = 45–315 nM) compared to largazole thiol (IC_{50} = 360-2600 nM) emphasizing the prodrug nature. Largazole thiol has since been tested against the whole panel of HDAC enzymes (Table 1.9), showing high potency for HDAC1, 2, 3, 10, and 11, a decreased activity for HDAC6 and 8, while no inhibition is seen against class IIa.

Table 1.9 HDAC inhibitory activity against all HDACs.

	IC_{50} (nM)										
	Class I				Class IIa				Class IIb		Class IV
HDAC	1	2	3	8	4	5	7	9	6	10	11
Largazole thiol	0.4	0.9	0.7	102	IA[a]	IA	IA	IA	42	0.5	3

[a] IA: inactive below 1000 nM. The table was modified from ref [130].

In 2011, the binding mode of largazole as a thiol was further validated when the crystal structure of a HDAC8–largazole thiol complex was published.[131] When the crystal structure of largazole (uncomplexed) is compared with the binding mode in HDAC8,[123] minimal conformational changes are observed. In the HDAC8-largazole thiol complex, the rigid backbone is located on the surface of the protein. The thiol, which is most likely ionized, reaches the zinc ion through a narrow tunnel and obtains an ideal metal coordination geometry. The enzyme needs to modify its conformation to accommodate the ligand. Especially the orientation of Tyr100 and Asp101 in the L2 loop (Leu98-Phe109) is altered (highlighted in magenta, Figure 1.24).

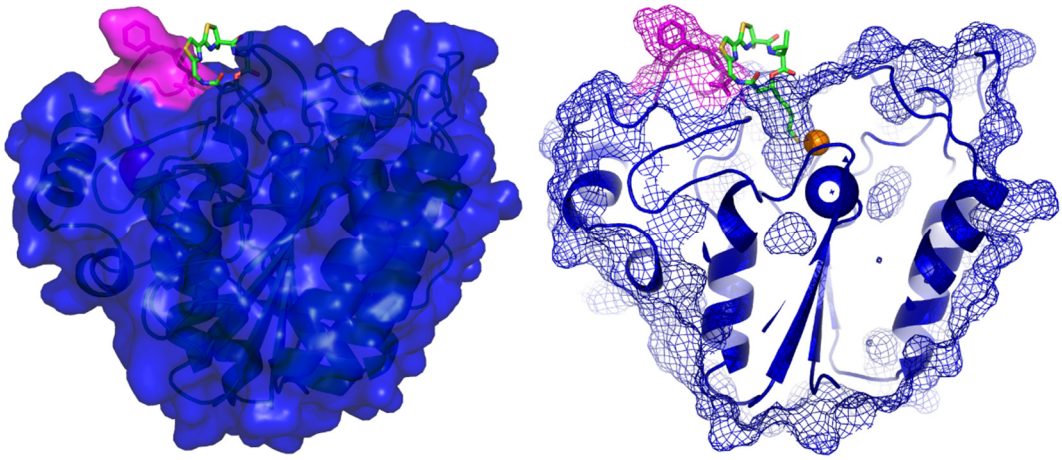

Figure 1.24. HDAC8–largazole thiol complex. Prominent conformational changes are colored magenta. Left: The large cap group of largazole-thiol interacts with amino acids on the surface of HDAC8. Right: The thiol side chain of hydrolyzed largazole reaches the zinc ion through a narrow binding pocket (PDB: 3RQD).[131]

Although differences exist between the HDAC isozymes, the crystal structure of HDAC8-largazole thiol provides a basis for understanding the biological results of other macrocycles that have been synthesized. In some cases, analogs of the thioester have been tested against the unhydrolyzed largazole.[132] Even though the active form of largazole is the free thiol, activity is still observed when the thioester is used on isolated HDAC enzymes *in vitro* (although with a much lower activity).

No improvement has been made when side chain modified analogs have been synthesized (Figure 1.25). The loss of activity, which is observed when altering the length of the linker (**1.77–1.79**), is in agreement with the crystal structure. If the length of the linker is too long, an unfavorable geometry in the zinc coordination is obtained, while removing a methylene results in the sulfur atom being unable to reach the zinc ion. The

low activity of **1.80** is not surprising, as the cap group of largazole would need to change its orientation dramatically in order for the side chain to reach the active site. The low potency of analogs with changed ZBG (**1.72**–**1.76**) is somewhat unexpected. However, activity might be regained if the length of the side chain was optimized further.

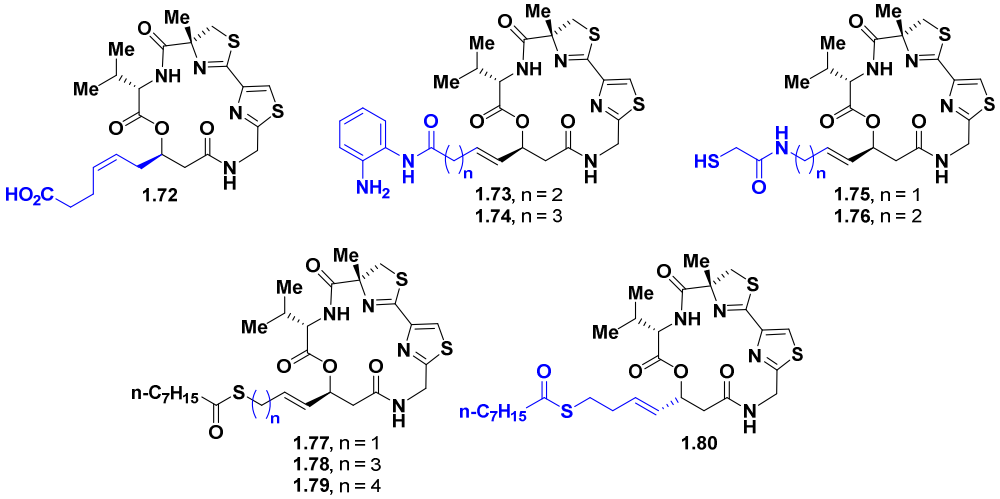

Figure 1.25 Largazole analogs containing a modified side chain.

Table 1.10 HDAC inhibitory activity against HDAC1, 2, 3, and 6.

	IC$_{50}$ (μM)			
Analogs	HDAC1	HDAC2	HDAC3	HDAC6
1.72[a]	>30 (>99)	>30 (>99)	>30 (>99)	>30 (>99)
1.73[a]	0.27 (>99)	4.1 (>99)	4.1 (>99)	>30 (>99)
1.74[a]	23 (>99)	29 (>99)	14 (>99)	>30 (>99)
1.75[a]	0.67 (>99)	1.6 (>99)	0.96 (>99)	0.7 (>99)
1.76[a]	1 (>99)	1.9 (>99)	1.5 (>99)	0.24 (6)

[a] Potency relative to largazole thiol is shown in parenthesis. Red: fold decrease. Data was obtained from ref [133].

Table 1.11 HDAC inhibitory activity against HDAC1 and 6.

	IC$_{50}$ (μM)		
Analogs	HeLa NE	HDAC1	HDAC6
1.77[a]	>20(>99)	–	–
1.78[a]	7.6 (>99)	0.69(91)	>10 (>5.5)
1.79[a]	4.1 (>99)	1.9(>99)	>10 (>5.5)
1.80[a]	>20(>99)	–	–

[a] Potency relative to largazole thiol is shown in parenthesis. Red: fold decrease. Data was obtained from ref [132a].

Modifications to the macrocycle in largazole seem to be better tolerated, although only a few analogs with an increased activity have been synthesized. Inconsistent results have been published regarding the activity of compound **1.81**. Nan and co-workers reported a 146-fold decrease in potency,[132b] while de Lera and co-workers described a 3-fold increased activity (Table 1.12).[132c] By evaluating the reduced potency of the similar compound **1.92**, (Table 1.12), a reduced activity seems to be most consistent. The thiazoline–thiazole subunit of largazole is pointed towards the solvent (Figure 1.26, right), the methyl group therefore does not seem to have any particular interaction. However, changing the subunit to a di-thiazole, will change the backbone structure, which could explain the lower potency. This explanation is in agreement with the equal activity of compound **1.84**. Since the thiazoline–thiazole subunit points toward the solvent, adding a hydrophobic ethyl group (**1.85**) would lead to unfavorable interactions, which also agrees with the observed activity. Adding a benzyl in the same position (**1.86**), surprisingly, increase the activity. This might be explained by π-π interactions between the benzyl group and either Phe100 or Tyr152, which are located in the vicinity (Figure 1.26).

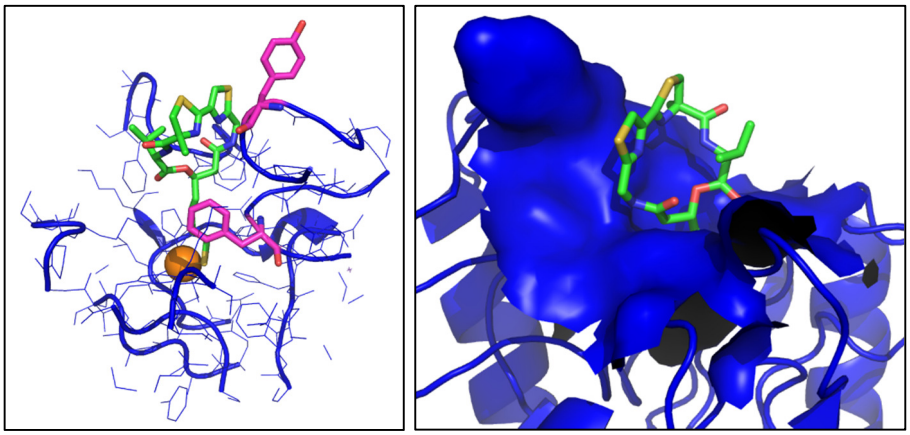

Figure 1.26 Largazole in HDAC8 (PDB:3RQD). Left: Phe100 and Tyr152 is located in the rim of the binding site and might interact with largazole analogs. Right: Surface view of largazole in HDAC8. The valine residue is exposed to the solvent.

The lower activity observed by substituting the lactone to a lactam (**1.95**), could be explained by an unfavorable change to the scaffold, resulting in a linker that is too short to reach the active site. When the thiol side chain has been incorporated in cyclic peptides, an extra methylene is usually needed to obtain the optimal length.[115, 134] It would therefore be interesting to see if the activity of **1.95** could be optimized by increasing the length of the linker as well.

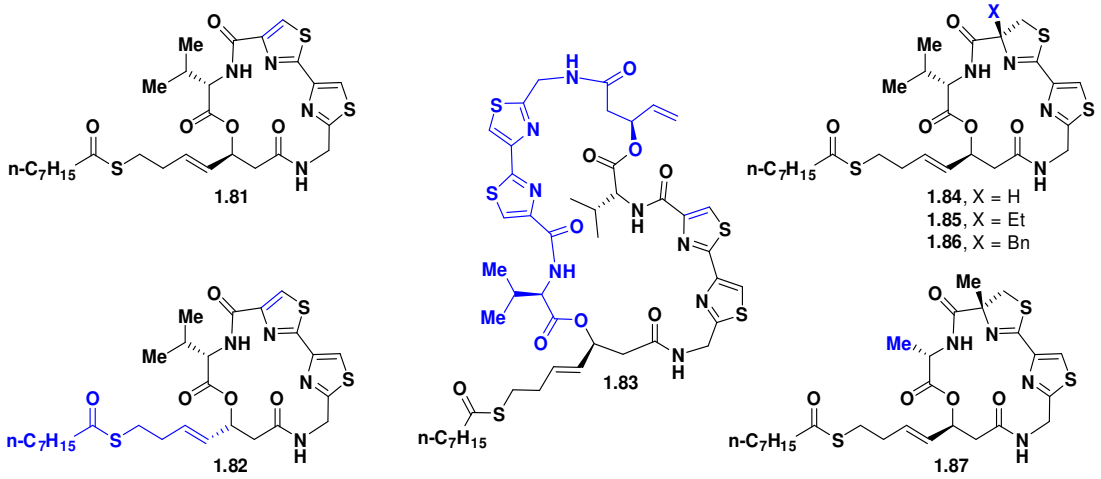

Figure 1.27 Largazole analogs with changes to the core structure.

Table 1.12 HDAC activity compared to largazole

	IC_{50} (μM)				
Analogs	HDAC1	HDAC2	HDAC3	HDAC4	HDAC6
1.81[a,b]	2 (146)[a]/0.0047 (3)[b]	18.5 (97)[a]	16.8 (69)[a]	3 (ep)[b]	14.7 (ep)[a]
1.82[a]	NA	NA	NA		NA
1.83[a]	NA	51.8 (>99)	22.6 (92)		NA
1.84[b]	0.0137 (ep)			7.5 (3)	
1.85[b]	0.161 (14)			4.9 (2)	
1.86[b]	0.0045 (3)			3 (ep)	
1.87[c]	0.044 (6)				3.3 (2)

Potency relative to the largazole is shown in parenthesis. Red: fold decrease, ep: equipotent green: fold increase. NA: Not active. [a] Data was obtained from ref [132b]. [b] Data was obtained from ref [132c]. [c] Data was obtained from ref [132a].

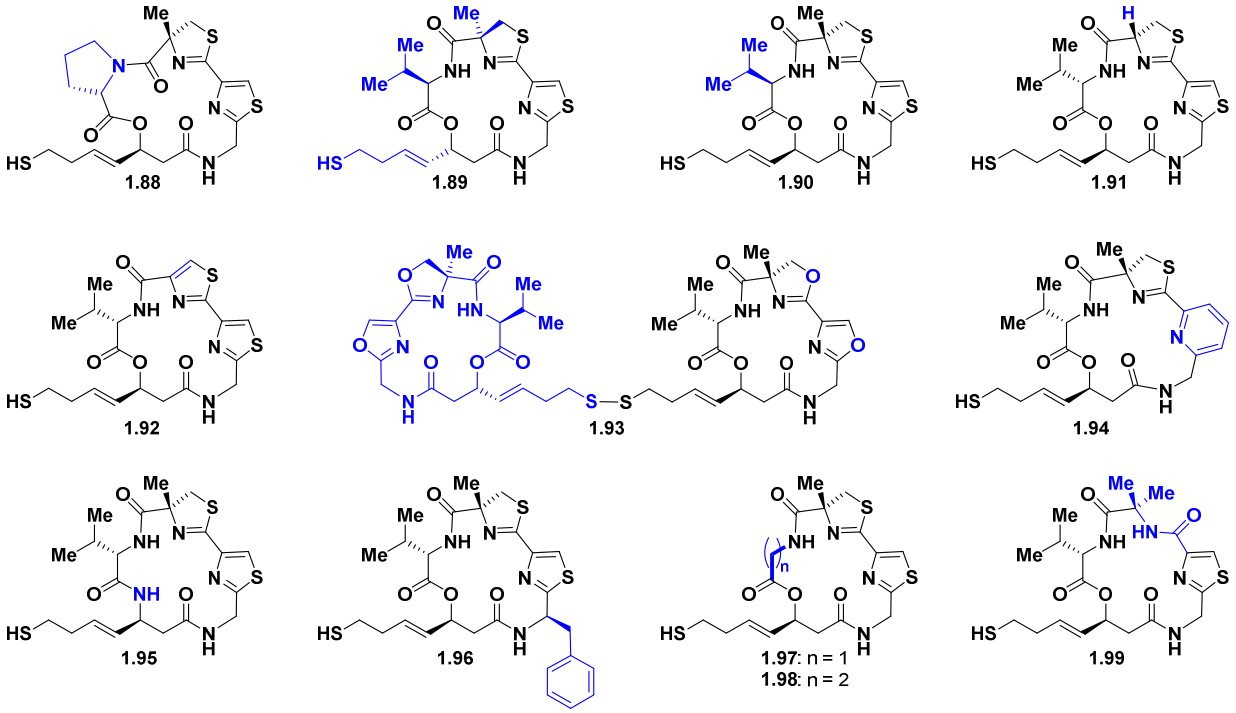

Figure 1.28 Largazole thiol analogs with changes to the core structure.

Table 1.13 HDAC activity against HDAC1, 2, 3, 6, and HeLa NE.

	IC_{50} (nM)					
Analogs	HDAC1	HDAC2	HDAC3	HDAC6	Analogs	HeLa NE
1.88[a]	0.11 (92)	0.8 (>99)	0.58 (>99)	13 (>99)	**1.96**[c]	17.2 (>99)
1.89[a]	1.2 (>99)	3.1 (>99)	1.9(>99)	2.2 (45)	**1.97**[c]	0.17 (4)
1.90[a]	0.03 (25)	0.082 (23)	0.084 (25)	0.68 (14)	**1.98**[c]	3.15 (73)
1.91[a]	0.002 (2)	0.005 (2)	0.004(ep)	0.13 (3)	**1.99**[c]	0.99 (23)
1.92[a]	0.077 (64)	0.12 (34)	0.085 (25)	>30 (>99)		
1.93[a]	0.0007 (2)	0.0017 (2)	0.0011 (2)	0.03 (ep)		
1.94[a]	0.0032 (4)	0.0008 (4)	0.0015 (3)	0.03 (ep)		
1.95[b]	0.0009 (9)	0.0004 (5)	0.0004 (4)	1.5 (38)		

Potency relative to the largazole thiol is shown in parenthesis. Red: fold decrease, green: fold increase, ep: equipotent.[a] Data was obtained from ref [133]. [b] Data was obtained from ref [135]. [c] Data was obtained from ref [126a]. NE: Nuclear extract.

Overall, it seems like changes to the backbone conformation of the cap group are not well tolerated. An alternative strategy for synthesizing new potent compounds involve changes to other features, such as the valine, which is exposed to the solvent (Figure 1.26). It might be possible to gain some activity by substituting with a hydrophilic residue. Even though HDAC8 belongs to class I, together with HDAC1–3, and the biological data in general can be explained from the co-crystalized structure of largazole thiol in HDAC8, the isozyme differs especially around the rim towards the active site. Thus, the rationale for constructing potent inhibitors for HDAC8 might therefore not be valid for all enzymes in class I.

Romidepsin and related compounds

The natural compound romidepsin was isolated from the Gram-negative bacterium *C. violaceum* in 1994, by Okuhara and co-workers in the search for compounds with antimicrobial and antitumor activities.[136] No significant effect was observed against microbes, but the natural compound showed potent activity against a variety of human carcinoma cell lines. Romidepsin is a 16-membered depsipeptide bridged by a disulfide. The compound is stable in serum and can readily penetrate the cell membrane. Once inside, the disulfide is reduced by glutathione reductase and the active structure is formed (Figure 1.29).[137] The free thiol most likely coordinates to the zinc ion in the active site, in a similar fashion as largazole (Figure 1.24). A docking structure of romidepsin in HDAC8 confirms a high similarity to the binding mode of largazole.[131]

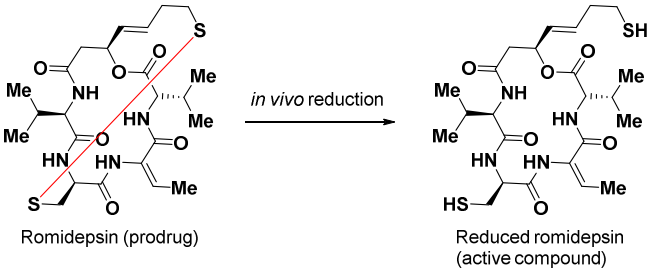

Figure 1.29 Romidepsin is a natural prodrug, which is reduced to its active form *in vivo*.

The first total synthesis was achieved by Simon and co-workers (Scheme 1.7).[138] Starting from methyl 2,4-pentadienoate a conjugate addition of triphenylmethanethiol (TrtSH) , followed by diisobutylaluminum hydride (DIBAL-H) reduction and Swern oxidation to the aldehyde afforded compound **1.56**. The thiol-containing β-hydroxy acid was then obtained, using Carreiras catalytic asymmetric aldol reaction. The enantiomer of **1.100** was originally synthesized in an effort to cyclize with an activated ester, but unacceptable low yields prompted a revised synthesis strategy. **1.101** was coupled to the tetrapeptide and cyclization was achieved using a Mitsunobu reaction to give the correct stereochemistry. A final oxidation with iodine in dilute MeOH afforded the natural product.

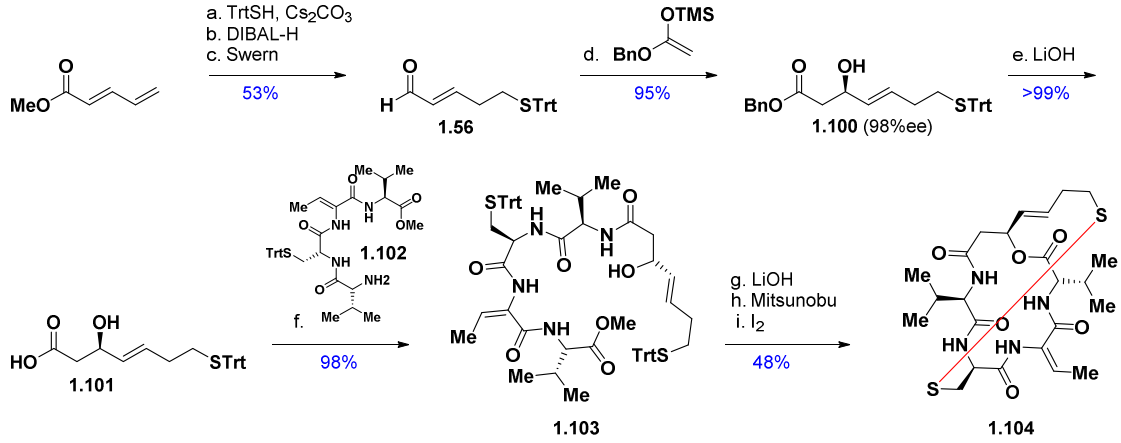

Scheme 1.7 Total synthesis of romidepsin by Simon and co-workers.[138] Reagents and conditions: (a) TrtSH, Cs_2CO_3. (b) DIBAL-H. (c) $(COCl)_2$, DMSO, Et_3N. (d) ((1-(benzyloxy)vinyl)oxy)trimethylsilane , Ti(IV) cat. (e) LiOH, MeOH. (f) **1.102**, BOP, *i*-Pr_2Et_3. (g) LiOH. (h) DIAD, PPh_3. (i) I_2.

The total synthesis of romidepsin has also been reported by Ganesan[126b] and Williams.[139] Due to difficulties in reproducing the enantioselectivity in Carreiras asymmetric aldol reaction, utilized by Simon and co-workers, both groups chose a different route for synthesizing the β-hydroxy acid.

Williams and co-workers initiated their synthesis from methyl 3,3-dimethoxypropionate to afford the propargylic ketone (**1.107**) in two steps via the Weinreb amide (**1.106**, Scheme 1.8). Noyori's asymmetric hydrogen transfer was then used to afford the *R*-propargylic alcohol in an enantiomeric excess (ee) of 98%, and the *trans* isomer (**1.108**) was obtained selectively using sodium bis(2-methoxyethoxy)aluminumhydride (Red-Al). Following selective tosylation of the primary alcohol, the dimethyl acetate was hydrolyzed with $LiBF_4$ and then oxidized to the carboxylic acid. The trityl-protected thiol was introduced at the last step, by replacing the tosylate. The final steps for obtaining romidepsin were done in analogy to Simon and co-workers, Scheme 1.7.

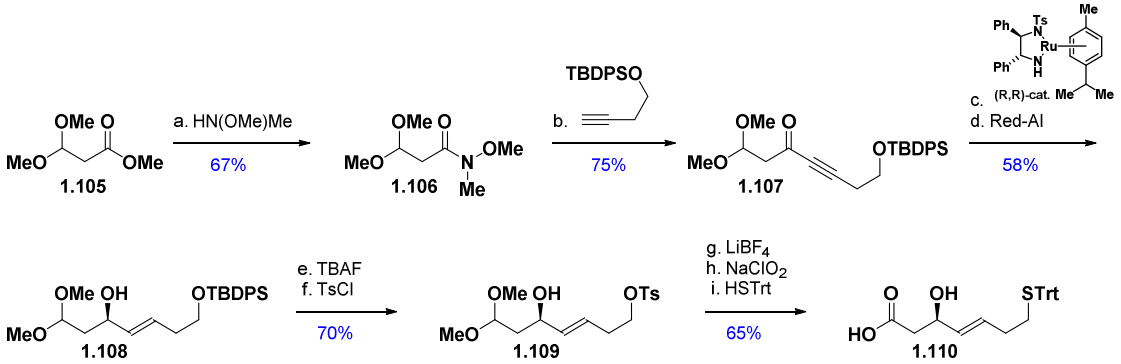

Scheme 1.8 Synthesis of the key intermediate by Williams and co-workers.[139] Reagents and conditions: (a) ^{i}PrMgCl, HN(OMe)Me, THF, 0 °C, 1.5h. (b) (but-3-yn-1-yloxy)(tert-butyl)diphenylsilane, n-BuLi, THF, –78 °C to 0 °C, 14h. (c) (*R*,*R*)-cat. (10mol%), ^{i}PrOH, 4d. (d) Red-Al, Et_2O, 0 °C to rt, 1h. (e) TBAF, THF, rt, 3.5h. (f) TsCl DMAP, CH_2Cl_2, rt, 2h. (g) $LiBF_4$, MeCN, H_2O, rt, 10d. (h) $NaClO_2$, NaH_2PO_4, 2-methyl-2-butene. (i) $HSCPh_3$, *t*-BuOK, THF, 0 °C, 3h.

Ganesan and co-workers already had a route for synthesis of the key intermediate (**1.58**), from their total synthesis of largazole, Scheme 1.4. Instead of a macrolactonization utilized by Simon and Williams, Ganesan chose a HATU mediated lactamization with D-Val on the N-terminal.[126b]

Romidepsin is one of the most potent HDAC inhibitor known, with IC_{50} values ~1 nM for HDAC1, 2, 3, 10, and 11 (Table 1.14). A cysteine residue near the active site is important for inhibition by romidepsin, as shown by an 8-fold decrease in potency after mutation of cysteine to serine. The cysteine residue (Cys151 in HDAC1) is conserved at least for HDAC1, 2, 3 and 8. The lower activity for HDAC8, must therefore be explained by other factors. At present, romidepsin is the only macrocyclic HDAC inhibitor that has been approved by the FDA.[66b]

Table 1.14 HDAC inhibitory activity against all HDACs.

	IC_{50} values (nM)										
	Class I				Class IIa				Class IIb		Class IV
HDAC	1	2	3	8	4	5	7	9	6	10	11
Romidepsin[a]	0.8	1	1.3	IA[b]	647	IA	IA	IA	226	0.9	0.3

[a] reduced romidepsin, [b] IA: inactive below 1000 nM. The table was modified from ref [130].

The spiruchostatis and thailandepsin A-F possess a very similar scaffold as romidepsin (Table 1.15). However, a γ-amino acid in these natural compounds exchanges the two α-amino acids next to the ester in romidepsin. The cyclic depsipeptides therefore consist of a 15-membered rings structure, relative to the 16-membered ring in romidepsin. All members of thailandepsin and spiruchostatins is thought to be natural prodrugs like romidepsin and largazole, as they show severely reduced activity when tested as the disulfide.[140]

Table 1.15 Related romidepsin compounds

Compound	R^1	R^2	IC_{50} (μM) HDAC1	HDAC4	HDAC6
Thailandepsin A[a]	b	f	0.00028 (ep)	37.22 (4)	0.83 (ep)
Thailandepsin B[a]	c	f	0.0012 (4)	57.44 (7)	1.19 (2)
Thailandepsin C[a]	b	e	0.0002 (ep)	38.04 (4)	0.78 (ep)
Thailandepsin D[a]	c	e	0.00048 (ep)	46.97 (5)	0.93 (ep)
Thailandepsin E[a]	b	g	0.00098 (3)	58.88 (7)	1.68 (3)
Thailandepsin F[a]	c	g	0.0026 (9)	132.5 (15)	1.92 (3)
Spiruchostatin A[b]	d	e	0.0033 (ep)	–	1.6 (4)
Spiruchostatin B[b]	d	f	0.0022 (ep)	–	1.4 (4)
Spiruchostatin C	a	f	–	–	–

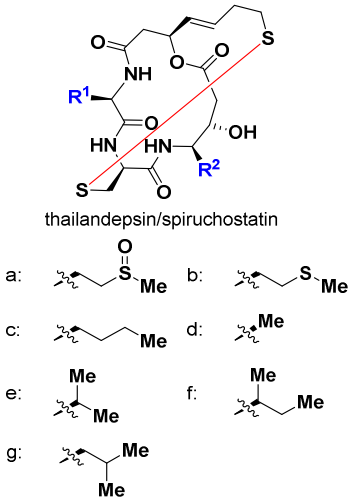

Potency relative to romidepsin is shown in parenthesis. Red: fold decrease, ep: equipotent. IC_{50} values are shown for the reduced form of the natural compound. [a] Data was obtained from ref [140a]. [b] Data was obtained from ref [140b].

Azumamide A–E

In the search for antitumor lead compounds, five cyclic tetrapeptides, azumamide A-E, were isolated from the marine sponge *Mycale izuensis* in 2006.[141] The Azumamides possess three D-amino acids and an unusual β-amino acid; [(Z)-(2*S*,3*R*)-3-amino-2-methyl-5-nonene-dioic acid, 9-amide] (Amnaa) in azumamide A, B, and D, while a [(Z)-(2*S*,3*R*)-3-amino-2-methyl-5-nonenedioic acid] (Amnda) is incorporated in azumamides C and E (Table 1.16). Compared to other cyclic HDAC inhibitors (e.g. trapoxin and apicidin) the azumamides display an inverse direction of the amide bonds and contain a β-amino acid in the cyclic scaffold.

Table 1.16 Azumamide A-E

Name	R^1	R^2	R^3
Azumamide A	NH_2	H	Me
Azumamide B	NH_2	OH	Me
Azumamide C	OH	OH	Me
Azumamide D	NH_2	H	H
Azumamide E	OH	H	Me

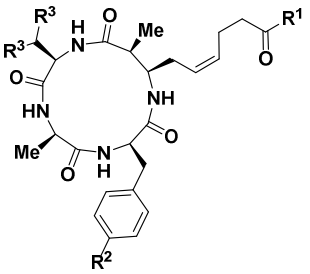

Since the discovery of the azumamides, different approaches to the total synthesis have been applied. Brown's crotylboration reaction[142] was utilized by De Riccardis and co-workers[143] in the synthesis of azumamide A and E, Scheme 1.9.

After oxidizing 3-benzyloxypropanol to aldehyde **1.112**, the key step provided a high diastereo- and enantioselective (d.r.> 99%; 98 % ee) transformation to intermediate **1.113**. Reductive ozonolysis followed by hydrolysis gave diol **1.114**, which was converted to the *tert*-butyl carbamate (Boc) protected amine **1.116**. Wittig reaction on aldehyde **1.117**, followed by oxidation of the unprotected alcohol gave the final building block **1.119**.

In the synthesis of azumamide A, macrolactamization did not work when the amide functionality was present. Different coupling reagents were explored (Pentafluorophenyl diphenylphosphinate (FDPP), diphenylphosphorylazide (DPPA), and 1-ethyl-3-(3-dimethylaminopropyl) carbodiimide hydrochloride (EDC)

with hydroxybenzotriazole (HOBt), but no trace of the product was observed. The β-amino acid was instead kept as the ethyl ester (**1.119**), coupled to a tripeptide and cyclized with phenylalanine on the C-terminal. FDPP mediated lactamization provided the cyclized peptide in 37% yield.

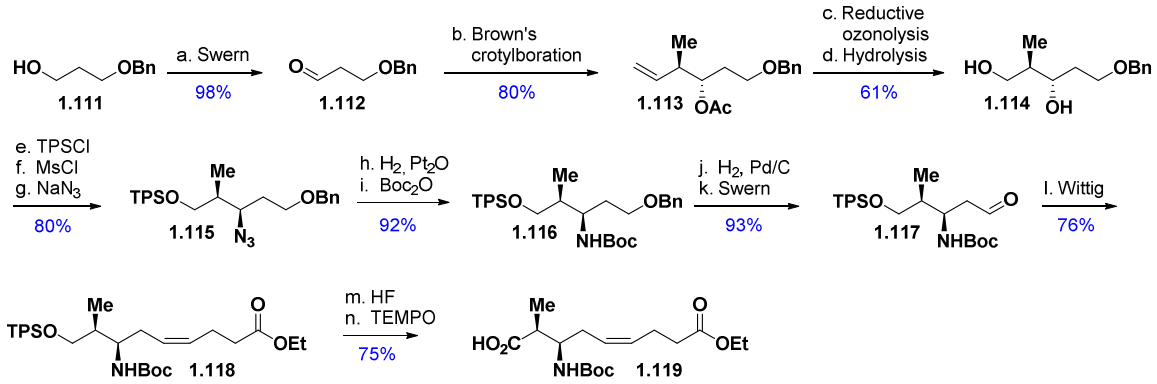

Scheme 1.9 Synthesis of the β-amino acid by De Riccardis and coworkers.[143] Reagents and conditions: (a) $(COCl)_2$, DMSO, Et_3N, CH_2Cl_2. (b) (*i*) (+)-Ipc_2BOMe, (*E*)-2-butene, *t*-BuOK, n-BuLi, $BF_3{\cdot}Et_2O$, THF, –78 °C; (*ii*) Ac_2O, py, CH_2Cl_2. (c) O_3; CH_2Cl_2, PPh_3, $NaBH_4$, EtOH. (d) K_2CO_3, MeOH. (e) TPSCl, DMAP, py, CH_2Cl_2. (f) MsCl, Et_3N, THF. (g) NaN_3, DMF, 60 °C. (h) H_2, Pt_2O, EtOAc. (i) Boc_2O, Et_3N, CH_2Cl_2. (j) H_2, Pd/C, EtOH. (k) oxalyl chloride, DMSO, Et_3N, CH_2Cl_2. (l) KHMDS, THF, $BrPPh_3(CH_2)_3CO_2Et$, –78 °C to rt. (m) HF/Py, py. (n) TEMPO, phosphate buffer, $NaClO_2$, NaClO, MeCN.

Ganesan and co-workers used a different strategy in their synthesis of azumamide A and E,[144] where Ellman's *tert*-butylsulfinyl auxiliary was used in the diastereoselective Mannich reaction, Scheme 1.10.[145] Introducing a trichloroethyl ester (Tce) (**1.121**) was nessesary, since alkaline hydrolysis of a benzyl ester protecting group was slow and caused epimerization of the β-amino acid. Dihydroxylation followed by hydrogenation and oxidative cleavage gave the β, γ-cis unsaturated aldehyde **1.122**. Using Ellman's chiral auxiliary in the Mannich reaction as the key step, the protected building block was obtained with high diasteroselectivity and a fair yield. Deprotection of the carboxylic acid gave **1.125**, with the auxiliary conveniently used as a protecting group in the peptide elongation. A phenylalanine to alanine cyclization was performed using HATU as coupling reagent, which provided the tetrapeptide in yields ranging from 55-85% in individual experiments.

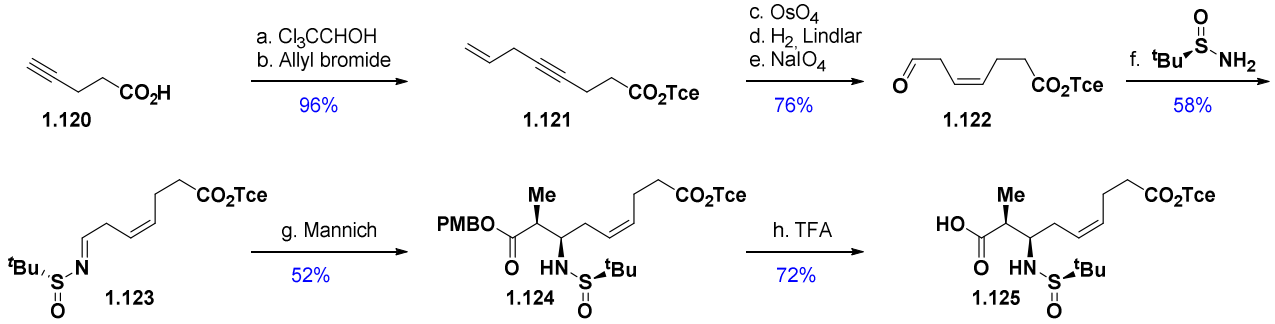

Scheme 1.10 Synthesis of the β-amino acid by Ganesan and co-workers.[144] Reagents and conditions: (a) 2,22-trichloroethanol, DIC, DMA, CH_2Cl_2. (b) allyl bromide, K_2CO_3, CuCl, DMF. (c) OsO_4, NMO, THF, H_2O (d) H_2, Lindlar cat., EtOAc. (e) $NaIO_4$, CH_2Cl_2. (f) $^tBuSONH_2$, $CuSO_4$, CH_2Cl_2. (g) $CH_3CH_2CO_2PMB$, LDA, $TiCl(O\text{-}iPr)_3$, THF. (h) TFA, anisole.

Chandrasekhar and co-workers initiated their synthesis by coupling a protected 4-pentyne-1-ol with chlorobutyne-1-ol to obtain **1.127**.[146] After selectively reducing one alkyne with $LiAlH_4$, the (2*S*, 3*R*) stereochemistry of the Amnda residue was introduced by a Katsuki-Sharpless asymmetric epoxidation followed by epoxide opening with methyl cuprate (Scheme 1.11, **1.129**, **1.131**). An EDCI/HOBt mediated cyclization between the β-amino acid and valine gave the cyclized peptide in 79% yield (Figure 1.31).

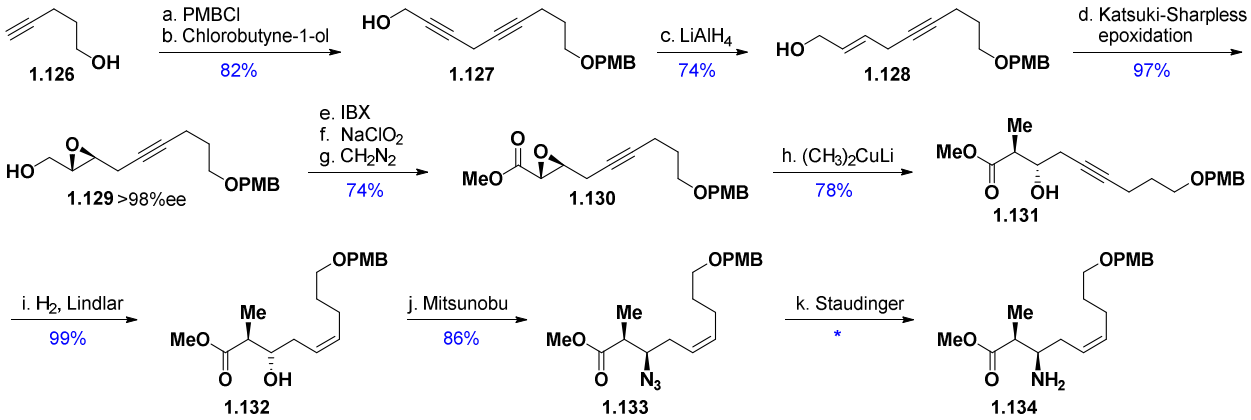

Scheme 1.11 Synthesis of the β-amino acid by Chandrasekhar and co-workers.[146] Reagents and conditions: (a) PMBCl, NaH, THF,(n-Bu)$_4$NI, 25 °C. (b) Chlorobutyne-1-ol, CuI, NaI, K_2CO_3. (c) $LiAlH_4$, Et_2O. (d) (+)-diethyl tartrate, Ti(O-^{i}Pr)$_4$ TBHP, CH_2Cl_2. (e) IBX (f) $NaClO_2$, NaH_2PO_4, 2-methyl-2-butene. (g) CH_2N_2. (h) $(CH_2)_2CuLi$, Et_2O. (i) H_2, Pd/$CuCO_3$, quinoline, benzene. (j) PPh_3, DIAD, DPPA, THF. (k) PPh_3, THF, H_2O. * Used without further purification.

Since no total synthesis of azumamides B-D existed and biological profiling had only been performed on azumamide E in HDAC1-9[147] Jesper S. Villadsen in our research group set out to synthesize all five azumamides.[148] The key step for synthesis of the Amnda and Amnaa side chains was an Ellman-type Mannich reaction (Scheme 1.12). The synthetic route also enabled synthesis of two analogs with an altered stereochemistry in the β^2- or β^3-position (**1.145**, **1.146**, Figure 1.31).

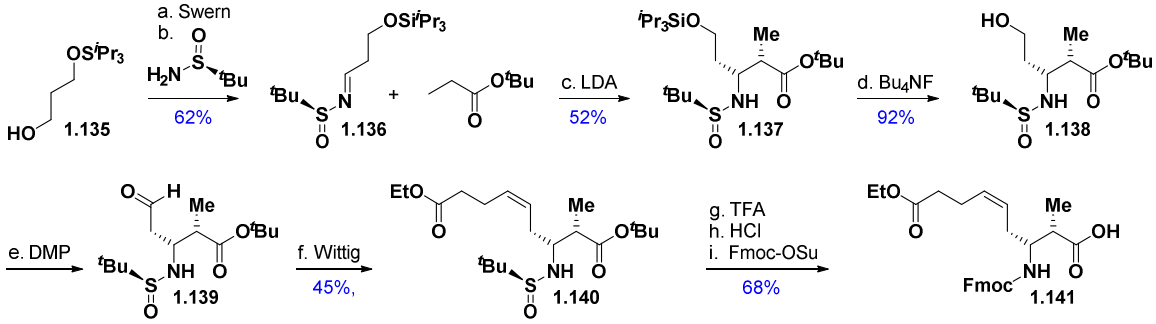

Scheme 1.12 Synthesis of the β-amino acid by Olsen and co-workers.[148] Reagents and conditions: (a) $(COCl)_2$, DMSO, Et_3N, CH_2Cl_2. (b) $CuSO_4$, (*S*)-(–)-2-methyl-2-propanesulfinamide, CH_2Cl_2. (c) HMPA, LDA, THF, –78 °C. (d) AcOH, Bu_4NF, THF 0 °C to rt, 1.5h. (e) $NaHCO_3$, DMP, CH_2Cl_2, 0 °C to rt, 1.5h. (f) $Ph_3PBr(CH_2)_3COOEt$, THF, –78 °C to rt, 18h. (g) TFA, CH_2Cl_2, 0 °C to rt 3h. (h) HCl, dioxane, 3h. (i) Fmoc-OSu, dioxane, H_2O, 0 °C to rt 2h.

Cyclization at three different positions in the total synthesis of azumamide E had been published and in each case, a different coupling reagent was used (Figure 1.30). Cyclization at different points in the scaffold, were therefore attempted.

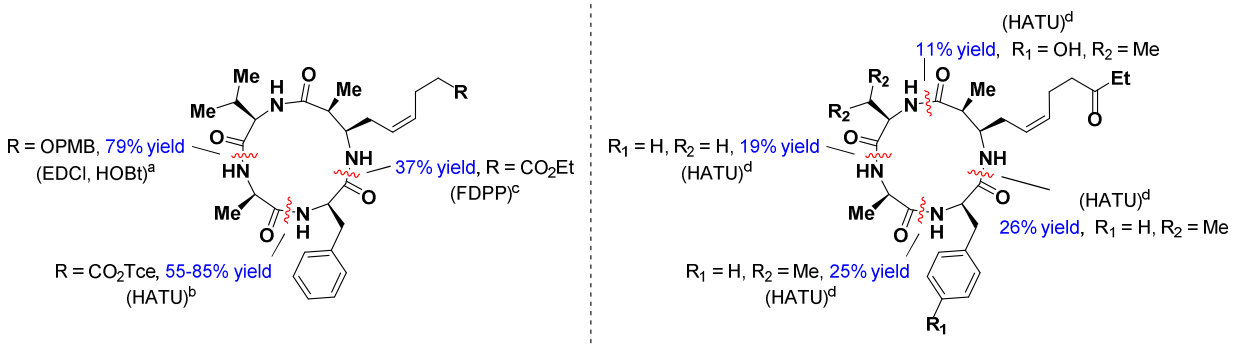

Figure 1.30 Left: Lactamization of azumamide E; [a] by Chandrasekhar and co-workers[146], [b] by Ganesan and co-workers[144], [c] by De Riccardis and co-workers.[143] Right: Lactamization of azumamide A-E; [d] by Olsen and co-workers[148]

Azumamide A-E as well as the β^2- and β^3 epimers, were profiled against the full panel of HDAC members, Table 1.17, Table 1.19. The data revealed that azumamide C and E were most active. This is consistent with the carboxylic acid being a better ZBG relative to the amide in azumamide A, B, and D. Additionally, in contrast to previous profiling on HeLa cell extracts,[147] azumamide C proved to be ~2-fold more active than azumamide C against most of the HDACs. Regarding the analogs, the potency of the azumamides was severely reduced when the stereochemistry in the β-amino acid was modified.

Table 1.17 HDAC inhibitory activity against all HDACs.

	K_i values (nM)										
	Class I				Class IIa				Class IIb		Class IV
HDAC	1	2	3	8	4	5	7	9	6	10	11
AzuA	>5000	>5000	3200	>5000	52%[a]	IA[b]	IA	IA	IA	IA	>5000
AzuB	5000	3000	3000	IA	IA	IA	IA	IA	IA	IA	>5000
AzuC	32±1	40±20	14±1	>5000	IA	IA	IA	IA	2000	10±4	35±3
AzuD	>5000	>5000	3700	IA	IA	IA	IA	IA	IA	IA	>5000
AzuE	67±7	50±30	25±5	4400	IA	IA	IA	IA	>5000	20±12	60±16

[a] Percent inhibition at 50 µM inhibitor concentration. [b] IA = inactive (<50% inhibition at 50 µM). Data was obtained from ref [148].

From the limited number of azumamide analogs that have been synthesized (Figure 1.31), two analogs have shown an increased activity. 48% inhibition in HeLa NE was observed when 10 μM of the sugar amino acid-containing analog (**1.147**) was applied, compared to 19% inhibition when the same amount of azumamide E was added (Table 1.18).[146] Changing the ZBG to a hydroxamic acid (**1.144**), showed a more dramatic effect (Table 1.19).[144] ~16-fold increase in potency was observed relative to azumamide E and more than 800-fold increase relative to azumamide A. These results show that the ZBG has an additive effect, which relates to the ability of the ZBG to coordinate zinc.

Table 1.18 % HDAC inhibition.

Compound	HeLa
Azumamide E (20 μM)	71
Azumamide E (10 μM)	19
1.147 (20 μM)	96
1.147 (10 μM)	48

Data was obtained from ref [146].

Modifications to the cyclic peptide core has resulted in a negative effect on binding to the HDAC enzymes.[147] In analog **1.143** the Amnda residue had been changed to a (2*R*, 3*S*) configuration, thereby changing the vector of the side chain, while all stereocenters are inverted in analog **1.142**. Since the azumamides display a reverse direction of the amide bonds, the enantiomer of azumamide E has a higher resemblance to other related cyclic peptides (e.g. trapoxin).

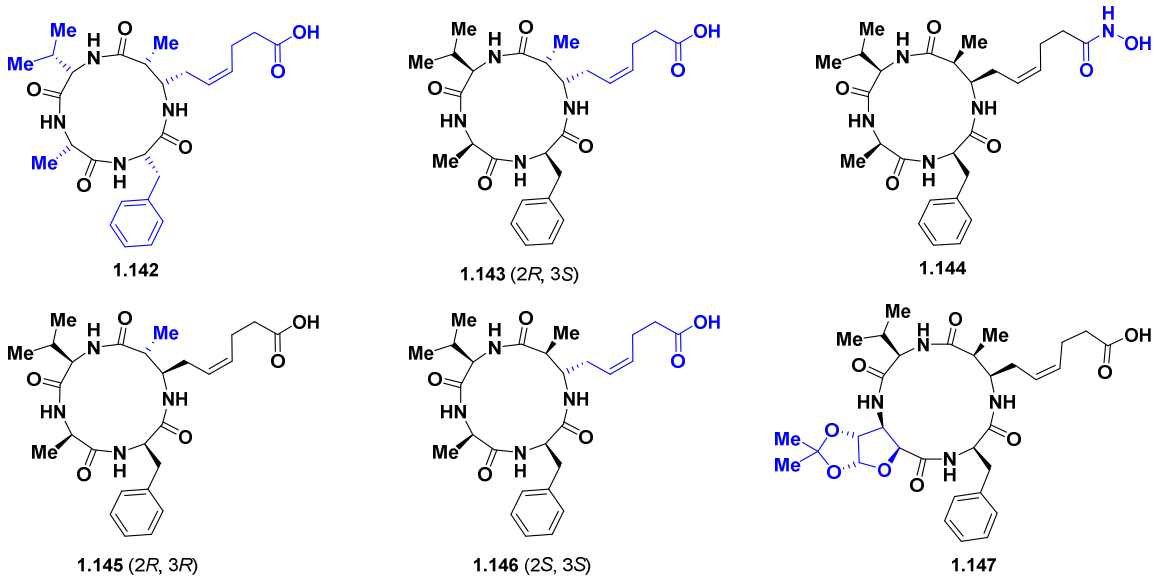

Figure 1.31 Azumamide analogs.

Table 1.19 HDAC inhibitory activity against HeLa and HDAC1-11.

	IC_{50} (μM)		
Compounds	HeLa NE	Compounds	HDAC1-11
1.142[b]	26 (>99)	**1.145** (2R,3R)[d]	NA[a]
1.143 (2R,3S)[b]	NA	**1.146** (2S,3S)[d]	NA[a]
1.144[c]	7 (16)		

Potency relative to romidepsin is shown in parenthesis. Red: fold decrease, ep: equipotent, green fold increase. NE: nuclear extract, [a] NA: no activity (<50% inhibition at 50 µM), [b] Data was obtained from ref [147]. [c] Data was obtained from ref [144]. [d] Data was obtained from ref [148].

The binding conformation of azumamide E has been investigated by docking studies in the crystal structure of histone deacetylase-like protein (HDLP).[69] Favorable hydrophobic interactions were observed between the Amnda side chain and the tunnel of HDLP leading to the active site, and the carboxylic acid formed favorable hydrogen bonds with two histidines and a tyrosine, besides from chelation with the zinc ion. The cyclic core of the peptide was placed in a shallow groove on the outside of the protein with the valine residue pointing towards the solvent and the phenylalanine positioned in a deep pocket of HDLP (Figure 1.32, left).

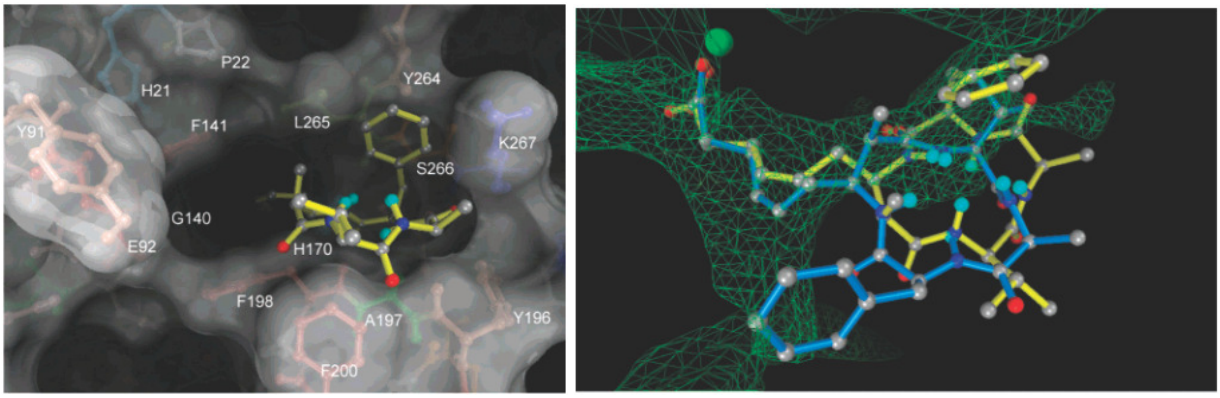

Figure 1.32 Left: Docking of Azumamide E in HDLP, Right: Docking of Azumamide E (yellow) and the enantiomer **1.142**, (blue).[147]

The lower activity of **1.142** and **1.143** was also examined in the docking study. Three binding modes were generated for **1.143**; none of these were found to be optimal, due to ineffective zinc coordination or loss of favorable interactions by valine and phenylalanine. Compound **1.143** retained HDAC activity, but compared to azumamide E it was reduced ~200-fold. Docking studies of this compound, showed interactions similar to azumamide E, but with the cyclic core inverted 180°, having L-Val of **1.143** occupying the space of D-Phe in

the natural compound (Figure 1.32, right). The loss of activity from analog **1.143** and **1.146** highlights the importance of the side chain positioning, while the amide bond direction seem to have a minor influence.

Compound **1.145** and **1.146** showed a low potency against all HDAC enzymes (Table 1.19). The lower activity of compound **1.146** is not surprising, as it would be unlikely that the Amnda residue and the cap group would maintain favorable interactions. However, the lower activity of analog **1.145** is unexpected. A possible explanation for this result could be a steric clash with residues in the binding pocket.

Miscellaneous cyclic inhibitors

The large cap group of macrocyclic inhibitors has the possibility of forming multiple interactions with residues in the rim of the active site in HDAC enzymes. The rigidity of the scaffold could also be favorable from an entropic perspective. Hanessian and co-workers synthesized a range of compounds based on **1.148**, which had shown to be a potent HDAC inhibitor.[149] The macrocycles that were generated utilized the rigid scaffold to probe the active conformation of the cap group, by simulating constrained analogs of the acyclic inhibitor (**1.148**).

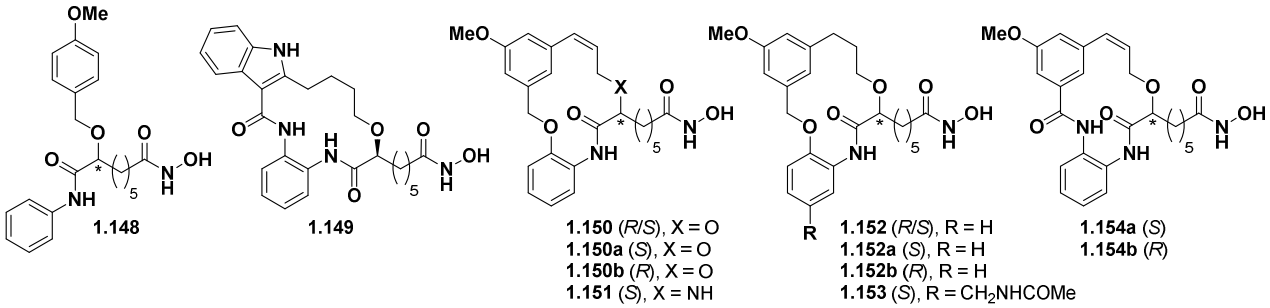

Figure 1.33 Macrocycles generated from lead compound **1.148**.

Cyclic compounds with only one aromatic substituent (not shown) lost activity relative to **1.148**, whereas the presence of a double bond (**1.150**) did not affect the overall HDAC inhibition (Table 1.20). Compounds containing the *S*-stereochemistry were in general (slightly) more potent.

Compound **1.151** with a nitrogen at the α-position of the suberoyl chain, and **1.153** containing an acetamido group on the anilide ring, were potent HDAC inhibitors with an improved activity towards HDAC8. The diamide based compounds (**1.149**, **1.154a**, and **1.154b**) showed an overall decreased activity, however, a high selectivity was observed towards HDAC6.

Table 1.20 HDAC inhibitory activity against all HDACs.

	IC_{50} (nM)										
	Class I				Class IIa				Class IIb		Class IV
HDAC	1	2	3	8	4	5	7	9	6	10	11
1.148	53.4	254	131	331	648	134	432	247	20.1	179	197
1.149	245	584	331	297	1690	496	2230	602	4.4	627	379
1.150	30.7	207	39.6	119	159	55.4	72.6	99.6	1.97	70.7	57.7
1.150a	31.7	158	55.7	198	79.4	62.2	27.8	60.6	0.84	62.5	22.9
1.150b	78.1	382	89	206	284	155	180	302	10.2	152	97.1
1.151	27.7	171	15.8	39.3	52.1	24.7	15.9	22.6	0.75	46.5	34.8
1.152	204	793	246	444	447	341	279	336	8.44	320	226
1.152a	72.2	268	93.6	136	118	109	61.2	123	3.43	190	103
1.152b	102	425	94.5	90.7	454	150	271	322	3.92	200	174
1.153	41.3	128	63.1	45.4	64.8	65.2	43.3	47.7	0.4	65.1	45.9
1.154a	864	3280	1114	534	5333	1660	4300	2020	59	2290	948
1.154b	1340	2530	885	682	3480	1340	2070	1140	75	1880	1110

Data was obtained from ref [149].

With the inspiration from macrolides that had been reported to function as peptide scaffold mimics,[150] Oyelere and coworkers incorporated the macrolide skeleton of TE-082 to mimic the prototypical peptidic macrocyclic cap group.[151]

Selectivity was observed for HeLa nuclear extract (consisting primarily of HDAC1 and 2),[151] relative to HDAC6 and 8. A linker dependence was also observed, with the optimal length of six methylenes (**1.155b**) between the triazole moiety and the ZBG.

Table 1.21 [a] measured from SAM-DI Mass spectrometry.[151]

	IC_{50} (nM)			K_i (nM)[a]
Compound	HeLa NE	HDAC8	HDAC6	HDAC8
1.155a	7.77	796.2	1180.1	1100
1.155b	1.03	544.6	728.7	210
1.155c	104.2	1909.3	1709.8	580
1.155d	163.6	2859.9	1916.9	620
1.155e	208.2	4557.8	3203.1	825

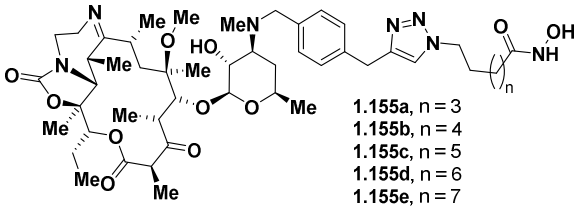

Etzkorn and co-workers have synthesized a macrocyclic inhibitor (**1.156**, Table 1.22), by combining the widely used hydroxamic acid head group with their previously synthesized peptide mimic.[152] **1.156** showed potent inhibition and ~4 fold selectivity towards HDAC1 relative to HDAC8. The advantage of using a rigid scaffold as cap group was shown by testing the corresponding linear compound (**1.157**), which lost ~3-fold activity.

Table 1.22 HDAC inhibitory activity against HeLa NE, HDAC1 and 8.

	IC_{50} (nM)		
Compound	HeLa NE	HDAC1	HDAC8
1.156	46±8	57±10	231±30
1.157	167±20	174±28	–

NE: Nuclear extract.

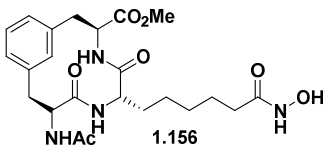

1.156

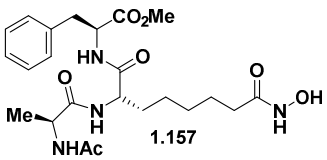

1.157

Marcaurelle and co-workers discovered potent HDAC inhibitors in a diversity-oriented synthesis strategy.[153] Medium to large macrocycles (8–14 membered rings) containing a variety of stereocenters were generated and screened in a high throughput coupled biochemical assay. 22,506 library compounds were tested as a single dose against HDAC2, and 32 of these were investigated in a dose–response assay. One compound was further studied in a stereo/structure activity relationship (Figure 1.34). BRD-4805 (Table 1.23) was discovered as the most potent compound, and BRD-8172 was found by modifying the side chain of BRD-4805. It is worth noticing that these inhibitors do not possess any ZBG, the potency must therefore arise from interactions in the opening of the HDAC binding site.

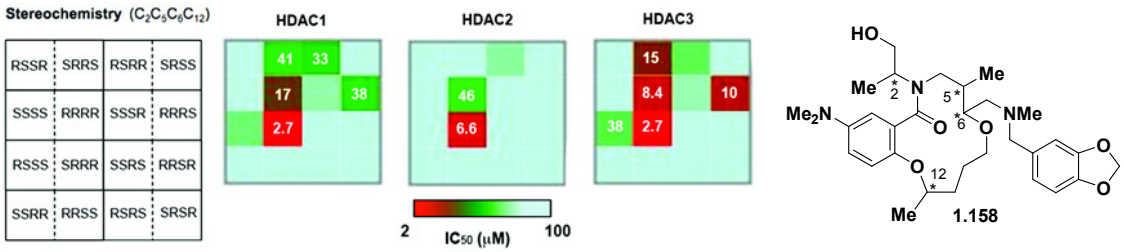

1.158

Figure 1.34 stereo/structure activity relationship study on selected compounds from a high throughput assay. The figure was modified from ref [153].

Table 1.23 HDAC inhibitory activity against HDAC1, 2, and 3.

	IC_{50} (μM)		
Compound	HDAC1	HDAC2	HDAC3
BRD-4805	2.7±0.3	6.6±0.4	2.7±0.2
BRD-8172	1.5±0.7	2.8±0.9	4.4±2.0

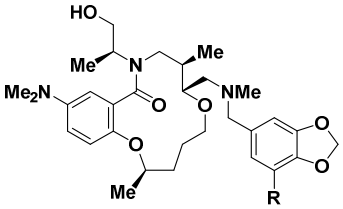

BRD-4805: R = H
BRD-8172: R = OMe

Ghadiri and co-workers, who recently published their work on cyclic $\alpha_3\beta$-tetrapeptides, also investigated compounds lacking a ZBG (Chart 1).[154] A SAR study was performed by altering the side chains of the α-amino acids in the scaffold. A propyl side chain at the position, which usually contained the ZBG, afforded the most potent inhibitor in the series; interestingly, incorporation of shorter or longer alkanes lowered the activity significantly. The R^3 side chain was sensitive to changes, but a potent compound was found by incorporating a substituted indole.

Chart 1 Structure activity relationship on cyclic peptides without a ZBG.

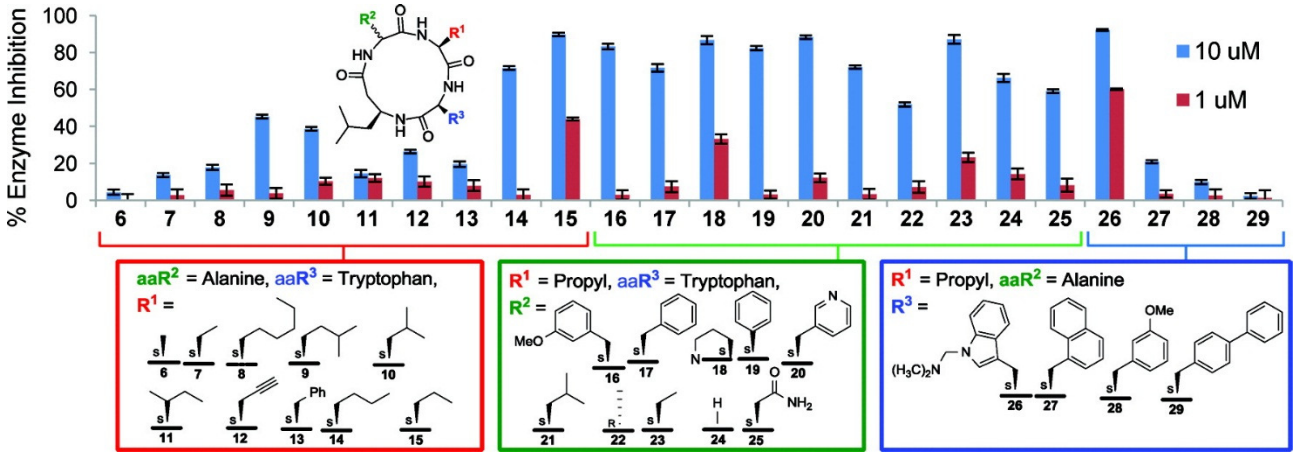

Table 1.24 HDAC inhibitory activity against HDAC1, 2, 3, and 6.

	IC_{50} (μM)			
Compound	HDAC1	HDAC2	HDAC3	HDAC6
1.159	0.98	1.5	1.4	>20[a]
1.160	0.68	1.4	0.8	>20[b]

[a] 37% inhibition at 20 μM. [b] 46% inhibition at 20 μM. Data was obtained from ref [154].

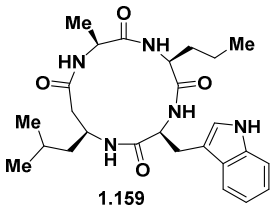

1.159

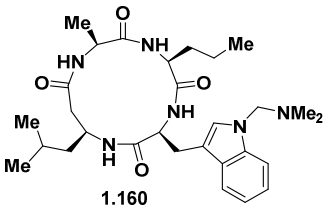

1.160

1.5 Summary

Epigenetic mechanisms play a crucial role in a variety of cellular processes. Two functional opposing epigenetic modulators, HATs and HDACs, control the acetylation state of the histone proteins. These modifications can lead to a change in the chromatin structure, which regulates access for DNA-binding proteins. In combination with other posttranslational modifiers, the HATs/HDACs generate patterns that forms a 'histone code'. These specific alterations that are recognized by proteins, forms the basis of a complex control of gene expression.

An aberrant HDAC expression have been associated with various types of cancer, HDAC inhibitors have therefore been a promising strategy in drug development. Two HDAC inhibitors (SAHA and romidepsin) have been approved by the FDA and several compounds are in clinical trials. SAHA and romidepsin are unselective HDAC inhibitors, whether or not this property is beneficial for anti-cancer treatment is still unknown. A lot of effort has been focused on synthesizing selective HDAC inhibitors, these compounds could be used as a tool for investigating the effect of each HDAC isozyme.

A pharmacophore, consisting of a ZBG, a linker, and a cap group, describes the majority of HDAC inhibitors. Among these are the macrocyclic HDAC inhibitor, which possess the most complex cap group. Due to their potential for interacting with less conserved amino acids on the rim towards the active site, a higher potential for HDAC inhibitory selectivity has been suggested.

A large number of macrocyclic natural products have exhibited inhibitory effects against HDACs. A range of these compounds has been utilized as lead structures in the search for higher activity or selectivity. These analogs have all aided in understanding the requirements for a potent inhibitor.

2 Desmethyl Azumamide Analogs

SAR studies of desmethylated azumamide compounds were conducted in collaboration with Jesper S. Villadsen. Jesper has synthesized desmethylated analogs, as well as dimethylated compounds, both containing a side chain in the 3-position with a *cis* double bond. Jesper and I have tested the compounds in HDAC assays, to obtain duplicate measurements.

Casper Hoeck and Charlotte H. Gotfredsen have been a great help for obtaining 800 MHz NMR data from the Carlsberg laboratory. They also performed most of the work regarding the 3D-structure elucidation. Niels J. Christensen and Peter Fristrup have been conducting the docking studies.

2.1 Introduction

The azumamides are interesting compounds as they retain high activity as HDAC inhibitors, even though they have relatively poor ZBGs. The potency of the macrocyclic HDAC inhibitors may therefore be ascribed to the multiple interactions between the cyclic peptide core and the opening towards the active site in the HDAC enzymes. Macrocycles have been proposed to possess a scaffold with a higher potential for HDAC inhibitory selectivity.[155] This suggestion has been based on less conserved amino acids in the rim of the active site, across the HDAC isozymes.[156] The combination of a large cap group and a poor ZBG, could be an advantage for obtaining selective HDAC inhibitors, as a strong ZBG might be too dominant an interaction to confer high selectivity.

An overview of the amino acid variability of the solvent exposed area, was obtained by aligning class I HDACs using the program 'Pymol' (Figure 2.1). The greatest differences between the HDAC isozymes are observed in three areas on the surface near the binding pocket, these prominent residues are shown in Table 2.1. HDAC1 and 2 are most similar, which is also evident from the sequence alignment. Glu98 and Asp99 are found near the opening in HDAC1; these amino acids are conserved in HDAC2, but in HDAC3 and 8, Glu98 (in HDAC1) has been changed to an aspartic acid and a tyrosine respectively. HDAC8 is less similar to the other HDAC isozymes, few amino acids are conserved in the sequence alignment and from Figure 2.1 the area near the pocket is wider, especially at the two locations that are circled in HDAC8. Areas near the binding site in HDAC1, 2 and 3 also seem to vary depending on the position of the carboxylic acid residues. However, it is important to emphasize that the crystal structures are only a representation of one conformation of a dynamic enzyme. In addition, each enzyme is crystalized differently. HDAC1 is co-crystalized with a protein domain from the NuRD-complex, HDAC2 and 8 are co-crystalized with an inhibitor, and HDAC3 is co-crystalized with a co-repressor. The orientation of the amino acid residues might therefore be involved in other interactions in each circumstance.

Table 2.1 Sequence comparison of amino acids from class I HDACs, near the opening towards the active site.

	97	98	99	100	101	201	202	203		204	205		206	269	270	271
HDAC1	G	**E**	**D**	C	P	Y	G	**E**	-	**Y**	F	-	P	D	R	**L**
HDAC2	G	**E**	**D**	C	P	Y	G	**E**	-	**Y**	F	-	P	D	R	**L**
HDAC3	G	**D**	**D**	C	P	Y	G	**N**	-	**Y**	F	F	P	D	R	**L**
HDAC8	G	**Y**	**D**	C	P	F	S	**P**	G	**F**	F	-	P	D	P	**M**

The numbering is based on the HDAC1 sequence

Overall, it seems plausible that interactions from a complex cap group could exploit differences further away from the binding site. However, introducing higher selectivity for either HDAC1 or 2 based on differences near the binding cavity would be a challenge.

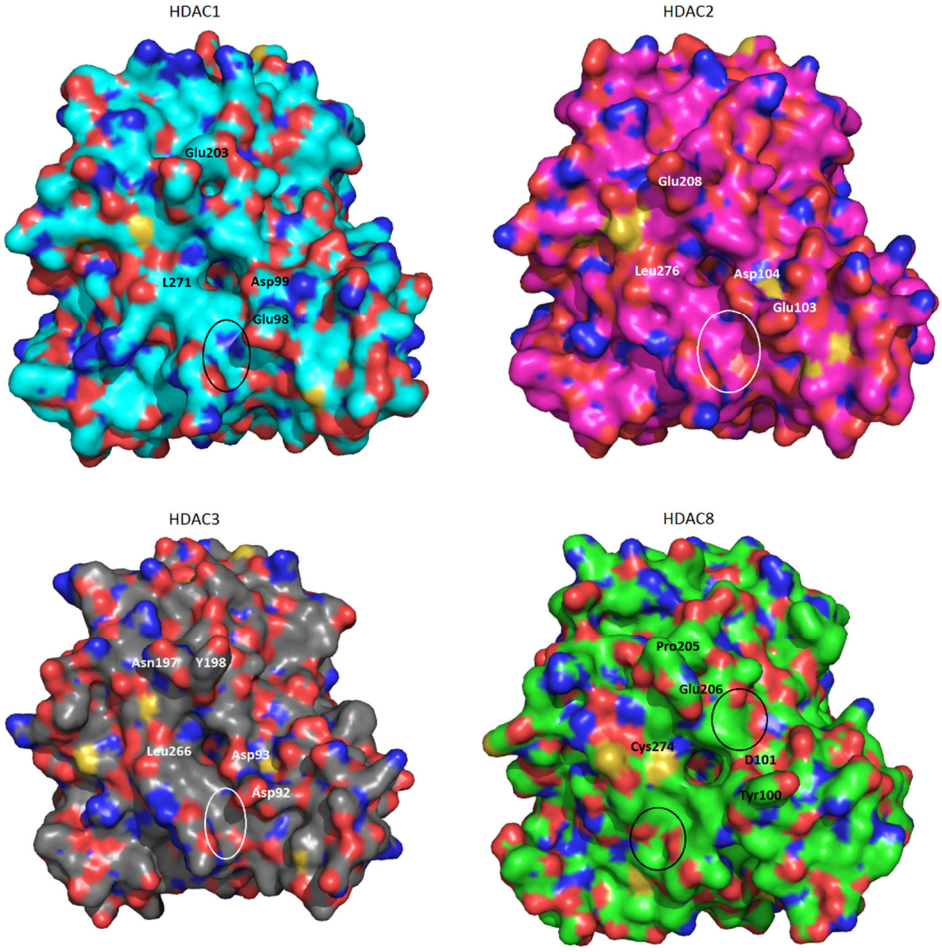

Figure 2.1 Comparison of the surface area on class I HDACs. Cyan: HDAC1 (PDB:4BKX), magenta: HDAC2 (PDB:4LY1), grey: HDAC3 (PDB:4A69), green: HDAC8 (PDB: 3RQD). The structures were aligned in pymol.

Jesper Villadsen in our research group completed the total synthesis of the azumamides.[148] The synthetic strategy enabled preparation of two azumamide analogs (**1.145** and **1.146**) with an altered stereochemistry in the β-amino acid residue; these compounds were also evaluated for HDAC inhibitory activity. The significant change in potency of the analog containing an inverted methyl group in the β^2-position, encouraged us to conduct a SAR study; hence dimethylated analogs as well as desmethyl compounds were designed. For the desmethylated compounds, the significance of the olefin in the side chain was also investigated. This was done by changing the olefin to a *trans* double bond at a position similar to largazole and romidepsin. An analog containing a saturated side chain (similar to apicidin) was also synthesized.

Docking studies of azuamide E in HDLP, shows stabilizing hydrophobic interactions between phenylalanine and a pocket in the enzyme (Figure 1.32).[147] The presence of an aromatic amino acid residue in many other macrocyclic inhibitors (e.g. apicidin A and trapoxin) suggests that this residue is important for HDAC inhibitory activity. Beside from phenylalanine and tyrosine, which is present in the azumamides, a tryptophan residue was also incorporated in the analogs (Figure 2.2).

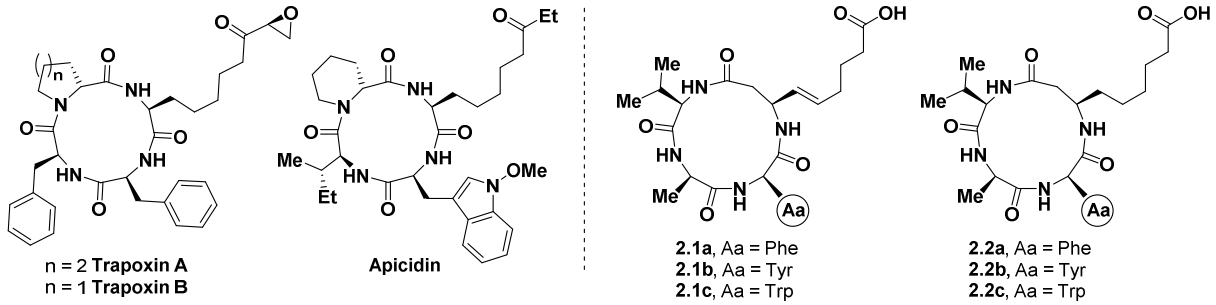

Figure 2.2 Left: trapoxin A, B, and apicidin possess an aromatic amino acid next to the side chain. Right: azumamide analogs for the SAR study.

2.2 1st strategy

Our first approach for synthesizing desmethylated azumamide analogs relied on the preparation of cyclic peptides containing a vinyl substituent. The side chain could thereafter be attached by cross metathesis; an approach previously reported by Bruno and co-workers, in their syntheses of FR235222 analogs,[157] and by Luesch, Hong, and co-workers in the total synthesis of largazole (Scheme 1.3).[121] From the vinyl cyclic tetrapeptides, a variety of compounds containing different ZBG's could be accessed through cross metathesis. Since the methyl substituent had been removed from the β-amino acid, formation of the building block could be obtained from readily available L-aspartic acid (Scheme 2.1).

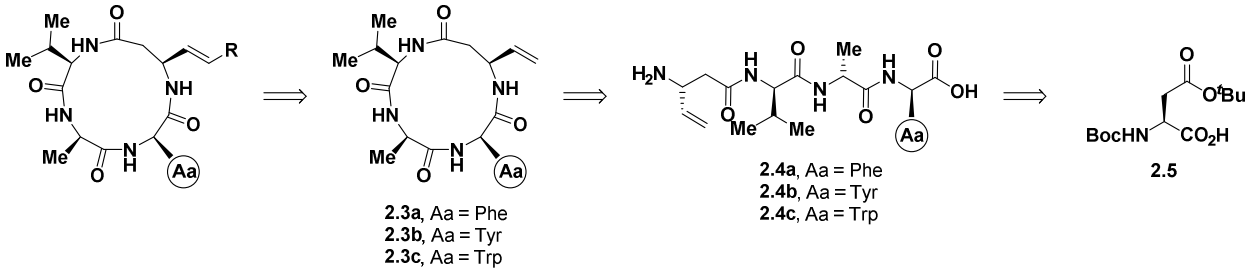

Scheme 2.1 Retrosynthetic analysis of the azumamide analogs.

Background; cross metathesis

The metathesis reactions includes ring closing metathesis (RCM),[158] ring opening metathesis (ROM),[159] and cross metathesis (CM).[160] Some of the widely used catalysts for the olefin metathesis are shown in Figure 2.3, developed by, Hoveyda, Grubbs, and Schrock.[161]

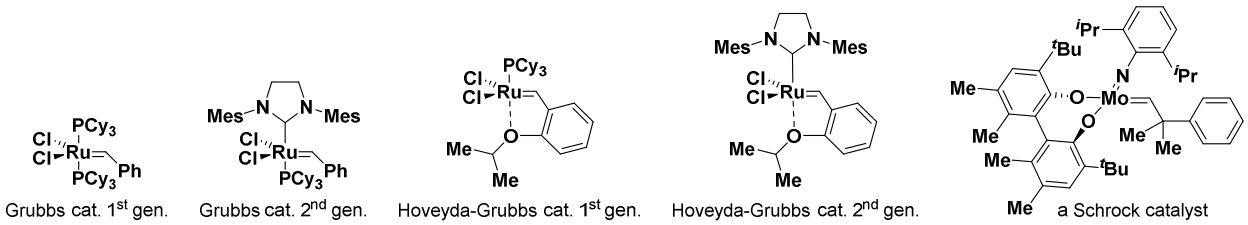

Figure 2.3 widely used commercial available catalysts for olefin metatheses.

Hérisson and Chauvin described the well-established mechanism for olefin metathesis in 1971,[162] illustrated in Scheme 2.2 for two terminal olefins, using Grubbs catalyst 1st generation. The catalytic activity arises when tricyclohexylphosphine (PCy_3) dissociates, as a 14 electron species is generated. Although Grubbs catalyst 1st generation readily releases PCy_3 (large k_1) to form the reactive adduct, PCy_3 quickly coordinates back to

ruthenium (K_{-1}/K_2>>1). In contrast, the dissociation of PCy_3 from Grubbs 2nd generation catalyst is inefficient, but coordinates better with the olefin once PCy_3 is lost (k_{-1}/k_2 ~1).[163] **A** coordinates to the metal catalyst and makes a [2+2] cycloaddition, to form a metallocyclobutane intermediate **B**,[164] which rearranges to produce **C**. **E** can then coordinate to **D**, where after ethene is released. Coordination of **I** to **H**, will generate the desired cross metathesis product and a new catalytic cycle begins from **D**.

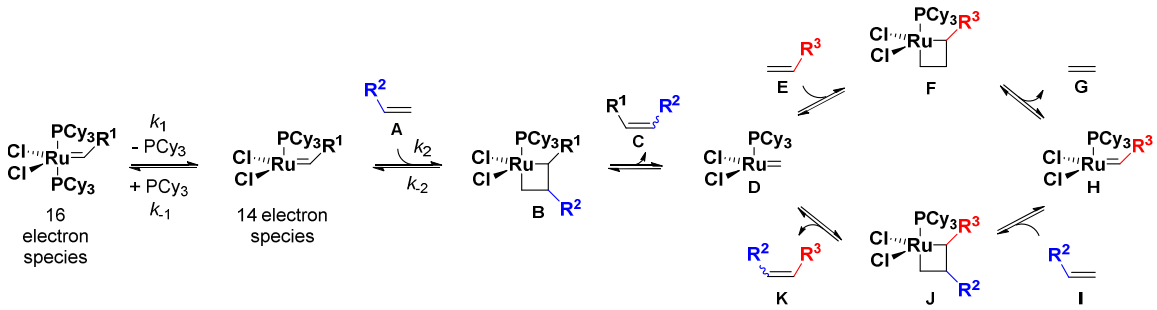

Scheme 2.2 Mechanism of the cross metathesis.[162, 164] Grubbs catalyst 1st generation is activated after PCy_3 dissociates. The catalytic cycle begins with a coordination of **E** to **D**, which ultimately forms the desired product **K**. The scheme was modified from ref [165] and [166].

The optimal pathway for the cross metathesis is shown in Scheme 2.2; however, each olefin can also form homodimers. This lack of selectivity have been addressed by Grubbs and co-workers, who created a model based on olefin reactivity to aid the prediction of selective and non-selective cross metathesis reactions.[167] The olefins were categorized in four classes, based on their ability to homodimerize and the ability to re-enter the catalytic cycle after dimerization, (Table 2.2).

Table 2.2 Categorization of olefins of type I–IV.

Type I	Rapid homodimerization, homodimers consumable
Type II	Slow homodimerization, homodimers sparingly consumable
Type III	No homodimerization
Type IV	Olefins inert to CM, but do not deactivate the catalyst

The table was modified from ref [167].

The reactivity are highest in type I compounds, consisting of electron rich olefins and decreases to the least active olefins for type IV compounds, comprising sterically hindered or electron poor olefins. The most reactive type I olefins undergo rapid homodimerization; however, the dimer is still able to undergo a secondary metathesis by re-entering the catalytic cycle. To avoid a statistical mixture of homodimers and cross metathesis product, 10 equivalents of one of the olefins are necessary to obtain >90% selectivity of the desired compound. Olefins belonging to type II does not undergo homodimerization as fast as type I, but do not react as readily after formation of the homodimer either. Similar to type I compounds, combining two olefins from type II will result in a statistical mixture, but with lower yields as the olefins are less reactive. Type III compounds do not undergo homodimerization but can still react with olefins from type I or II. Type IV olefins do not undergo cross metathesis at all, but also do not inactivate the catalyst.

Combining olefins of different types can effectively generate selective CM products. If a type I olefin is reacted to a type II or III, homodimers of type I olefins will initially form. However, as the homodimers readily undergo secondary metathesis, reaction to type II or III olefins will also occur. As ethylene is released from the system (Scheme 2.2), the product distribution is driven towards the CM product.

Building block synthesis

The building block was prepared using a similar procedure from Bradner, Williams, and co-workers,[135] by reducing BocNH-L-Asp-(O^{t}Bu)-OH to the corresponding alcohol via an isobutyl anhydride intermediate (Scheme 2.3). A two-step procedure; oxidation immediately followed by a Wittig reaction, was crucial as the aldehyde was prone to epimerization. The vinyl building block was obtained, but the yield was unacceptable due to incomplete oxidation of the alcohol in the Swern reaction (entry 1, Table 2.3).

Table 2.3 Optimization of the oxidation.

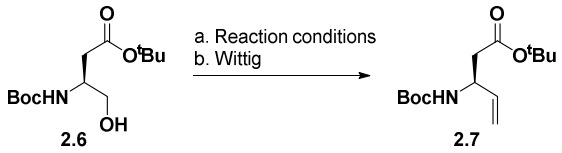

Entry	Reaction conditions	Yield (%)
1	DMSO, oxalylchloride, ^{i}Pr$_2$EtN.	37
2	DMP (1.3 + 0.6 equiv), CH_2Cl_2.	nd[a]
3	DMSO, oxalylchloride, Et_3N.	85

[a] nd: not determined, incomplete oxidation. DMP: Dess-Martin periodinane.

Since Dess-Martin oxidation did not give a complete reaction either (entry 2), the conditions in the Swern oxidation were reevaluated. Hünig's base, which was used in Bradners procedure,[135] has been used when compounds were prone to epimerize. However, since repeating attempts using Hünigs base did not give a complete reaction, the base was changed to triethylamine. This modification gave consistent results and afforded the alkene in 85% yield over two steps. The desired building block was obtained after removing the *tert*-butyl group with LiOH in quantitative yield (Scheme 2.3).

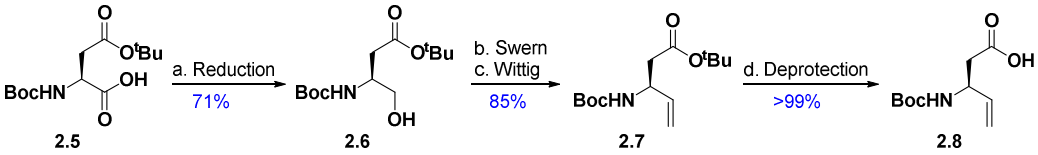

Scheme 2.3 Reagents and conditions: (a) NMM, ^{i}BuOCOCl, $NaBH_4$, MeOH, THF, –30 °C to rt, 3h. (b) $(COCl)_2$, DMSO, Et_3N, CH_2Cl_2, –78 °C to –40 °C to rt, 2h. (c) PPh_3CH_3Br, KHMDS (0.5 M in toluene), THF, –78 °C to rt, 4 h. (d) LiOH, MeOH, THF.

Solid-phase peptide synthesis and cyclization

The linear peptide was prepared by solid-phase peptide synthesis (SPPS), using a 2-chlorotrityl resin. A sequence consisting of coupling and deprotecting Fmoc-amino acids was performed, until the desired peptide length was obtained (Scheme 2.4). **2.8** was added as the final amino acid, where after the peptide was cleaved from the solid support, at the same time removing the Boc group on the building block. Impurities were removed by triturating in Et_2O, and the crude peptide was then cyclized under highly diluted reaction conditions, to avoid dimerization. Cross metathesis was attempted on the cyclized peptide; however, the compound was insoluble in solvents normally used in cross metatheses. Incorporation of a Boc protected tryptophan in the cyclic peptide overcame the solubility issue. However, no product was observed after refluxing in dichloromethane and attempts using microwave did not produce better results.

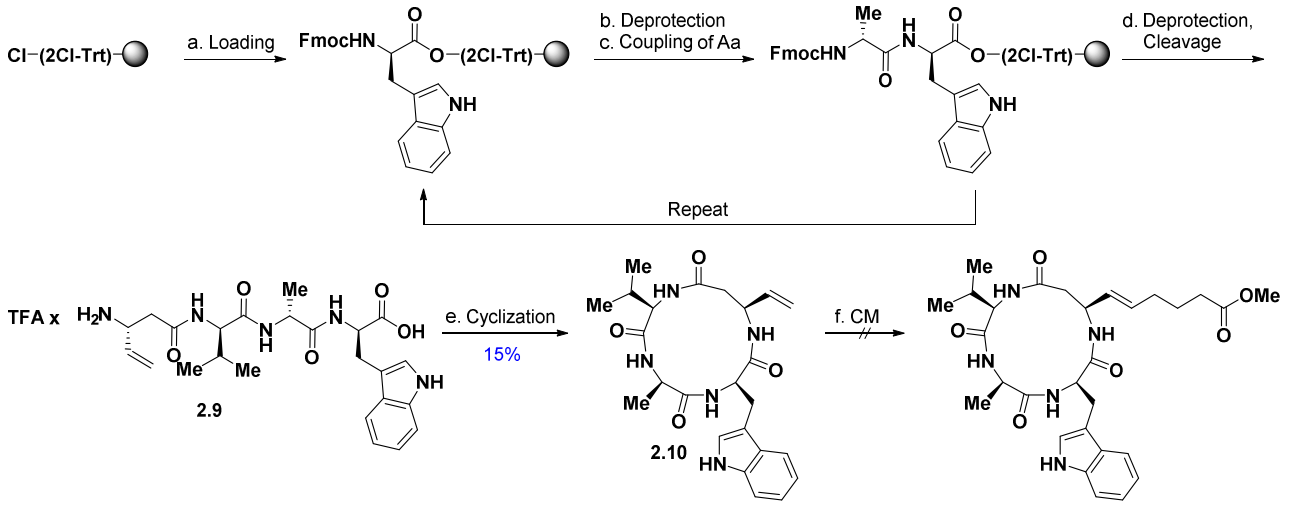

Scheme 2.4 Reagents and conditions: (a) Fmoc-D-Trp-OH, $^{i}Pr_2EtN$; CH_2Cl_2. (b) 20% piperidine in DMF, DBU:piperidine:DMF (2:2:96). (c) HATU, 2,6-lutidine, Aa (Fmoc-D-Ala-OH, Fmoc-D-Val-OH, **2.8**), DMF. (d) 20% piperidine in DMF, DBU:piperidine:DMF (2:2:96), 50% TFA in CH_2Cl_2. (e) HATU, $^{i}Pr_2EtN$, DMF. (f) *i*. 5-hexenoic acid methyl ester, Hoveyda–Grubbs 2nd gen. cat., CH_2Cl_2, reflux. *ii*. 5-hexenoic acid methyl ester, Hoveyda–Grubbs 2nd gen. cat., CH_2Cl_2, μW.

2.3 2nd Strategy

Optimizing the Cross Metathesis

To overcome complications with the vinyl containing cyclic peptide, another route was designed using building block **2.7** for the cross metathesis instead. The reaction was optimized by screening different catalysts. Besides the well-known Grubbs and Hoveyda-Grubbs catalysts (Figure 2.3), two catalysts containing an electron withdrawing group on the isopropoxybenzylidene ligand were also examined (Figure 2.4).

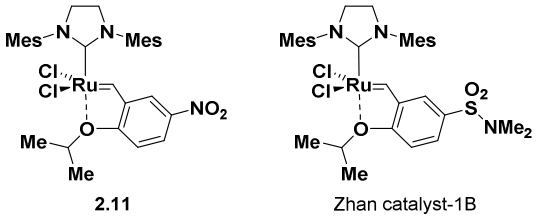

Figure 2.4 Catalysts containing an electron-withdrawing group.

The electron-withdrawing group have been shown to increase the activity of the catalyst, as the ether-ruthenium bond is weakened.[168] Zhan catalyst-1B was commercially available, while **2.11** was synthesized using procedures from Grela and co-workers.[168b] Starting from commercially available 2-hydroxy-5-nitrobenzaldehyde catalyst (**2.11**) was synthesized in three steps (Scheme 2.5). Purification of the final product was achieved by column chromatography, as the catalyst has an improved stability relative to the Grubbs catalysts (**2.11** can be stored in air at 4 °C for more than 4 weeks without decomposition or loss of activity).[168b]

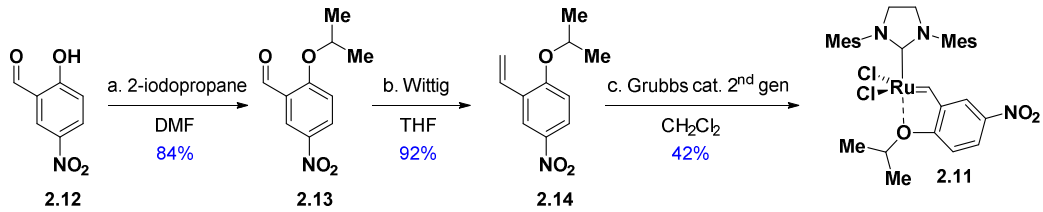

Scheme 2.5. Reagents and conditions: (a) 2-iodopropane, K_2CO_3, Cs_2CO_3, DMF. (b) Ph_3PCH_3Br, KHMDS (0.5m M in toluene), THF. (c) Grubbs cat. 2nd gen., CuCl, CH_2Cl_2.

Both Grubbs and Hoveyda-Grubbs 1st generation catalysts (entry 1, 4; Table 2.4) gave poor yields in the reaction. Even though a significant improvement was observed for Zhan catalyst-1B and **2.11** (entry 6, 7), the activity was not improved relative to Grubbs and Hoveyda-Grubbs 2nd generation catalysts (entry 3, 5). The best conditions were found using 10% Hoveyda-Grubbs catalyst 2nd generation to give a 67% yield (entry 5).

Table 2.4. Catalyst screening for the cross metathesis.

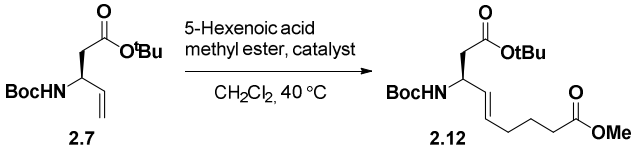

entry	catalyst	yield (%)[a]
1	Grubbs cat. 1st gen., 0.1 equiv	11
2	Grubbs cat. 2nd gen., 0.05 equiv	54
3	Grubbs cat. 2nd gen., 0.1 equiv	62
4	Hoveyda-Grubbs cat. 1st gen., 0.1 equiv	12
5	Hoveyda-Grubbs cat. 2nd gen., 0.1 equiv	67
6	Zhan catalyst 1B, 0.1 equiv	62
7	**2.11**, 0.1 equiv	52

[a] isolated trans isomer.

The free carboxylic acid, needed for the peptide synthesis was obtained in two steps by deprotecting with TFA, followed by re-protecting the amine functionality with Boc_2O. The masked carboxylic acid in the side chain would hereby remain unaffected. The second building block, containing the saturated linker, could easily be obtained by reducing the double bond of **2.13**, Scheme 2.6.

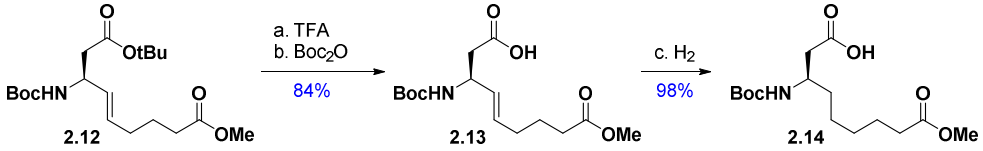

Scheme 2.6. Reagents and conditions: (a) TFA, CH_2Cl_2, 2h. (b) Boc_2O, $^iPr_2EtN$, CH_2Cl_2, 19h. (c) H_2, Pd/C (10 wt %), 17h.

Synthesis of desmethyl azumamide analogs

The two building blocks were coupled to tripeptides on solid support containing D-Phe, D-Tyr or D-Trp at the C-terminal. After cleavage from the resin, the linear peptides were triturated and cyclized. The crude compounds were saponified with LiOH and then purified by preparative HPLC (Scheme 2.7).

All the synthesized azumamide analogs were obtained in poor yields. The Trp analogs proved particular challenging; the synthesis of **2.2c** was unsuccessful and only 3% yield was obtained for **2.1c**. The low yields

could in part be explained by the low solubility of the products, as it was suspected that the cyclic peptides were precipitating on the column in the preparative HPLC runs. Purifying the compounds by column chromatography gave better yields; however, it was not possible to isolate the products in the desired purity.

The difficulties observed with the Trp containing analogs, might be due to unwanted side reactions from the indole. This problem could easily be evaded by using a Boc-protected indole in the solid phase peptide synthesis (SPPS). Since trityl resins are highly labile to acids, the peptide can be cleaved in mild conditions without affecting the Boc group.

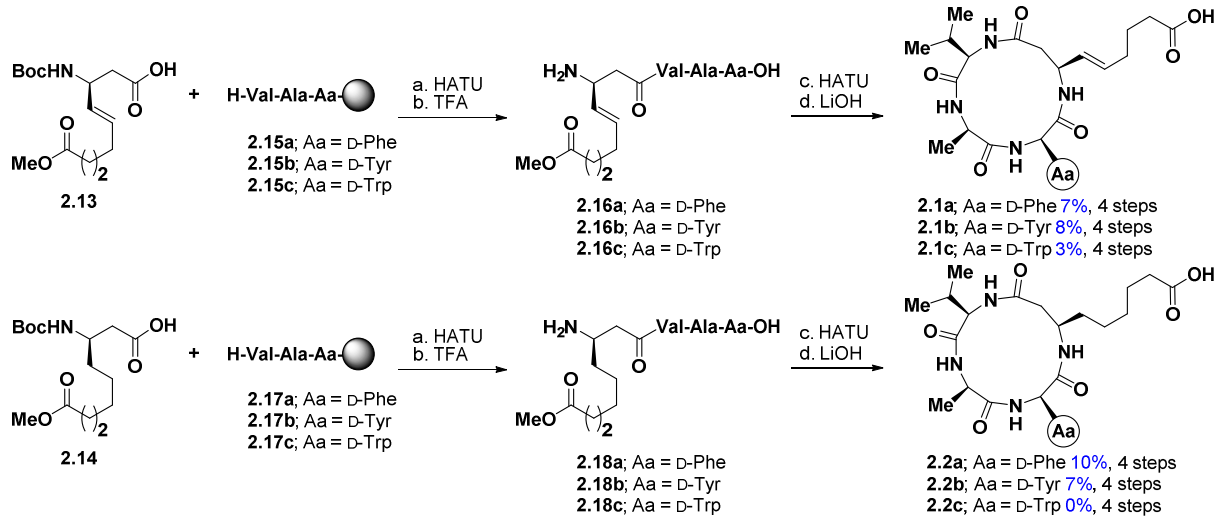

Scheme 2.7. Reagents and conditions: Synthesis of desmethylated azumamide analogs. Reagents and conditions: (a) HATU, 2,6-lutidine, DMF, 18h. (b) 50% TFA in CH_2Cl_2, 2x 30 min. (c) HATU, $^iPr_2EtN$, 17h–65h. (d) LiOH, THF, H_2O.

The position of the peptide cyclization could also have an effect on the yield. In total syntheses of the azumamides, researchers have utilized varying synthetic routes and chosen to cyclize at different positions, with yields ranging from 11% to 85% (Figure 1.30). Since a direct comparison of the yields is difficult due to the different coupling reagents used, a cyclization study was initialized.

Cyclization Experiments

Cyclization experiments were conducted on four linear simplified tetra peptide sequences, consisting of a vinyl β-amino acid, (D)-Val, (D)-Ala and (D)-Trp, each with a different amino acid on the C-terminal, Table 2.5. As standard reaction conditions, 1-[Bis(dimethylamino)methylene]-1H-1,2,3-triazolo[4,5-b]pyridinium 3-oxid hexafluorophosphate (HATU) was used as coupling reagent with addition of Hünig's base and the linear peptide was diluted to 0.5 mM in DMF, to lower the risk of dimerization.

Cyclizing at position A and C afforded the product with minimal degrees of byproducts (entry 1 and 4), while an N-terminal guanidinylated compound was observed when cyclization was attempted between D-Val and D-Ala (entry 2). To overcome this side reaction, a non-guanidino based coupling reagent, (benzotriazol-1-yloxy)tripyrrolidinophosphonium hexafluorophosphate (PyBOP)), was examined. However, dimerization and epimerization of both the linear and cyclic peptide was observed (entry 3). Exchanging Hünigs base for 2,6-lutidine gave a very slow reaction and an epimerized product was observed (entry 5). Even though all cyclization experiments were highly diluted, a large amount of dimerization was observed when cyclizing between D-Trp and the β-amino acid (entry 6). Since this was the same position that was used to synthesize compound **2.1a–c, 2.2a–c**, we were confident that the yields could be optimized by changing the point of cyclization.

Table 2.5 Cyclization experiments on a simplified peptide.

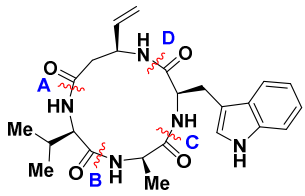

entry	position	conditions	side reactions	isolated yield[a]
1	A	HATU, DIEA, DMF, 1.5 h.	Minimal degree of side reaction.	42%
2	B	HATU, DIEA, DMF, 26 h.	N-terminal guanidinylation.	22%
3	B	PyBOP, DIEA, DMF, 3 h.	Racemization, dimerization, incomplete cyclization.	18%
4	C	HATU, DIEA, DMF, 26 h.	Minimal degree of side reaction.	39%
5	C	HATU, 2,6-lutidine, DMF, 69 h.	Racemization.	16%
6	D	HATU, DIEA, DMF, 26 h.	Dimerization.	15%

[a]Isolated yield from HPLC

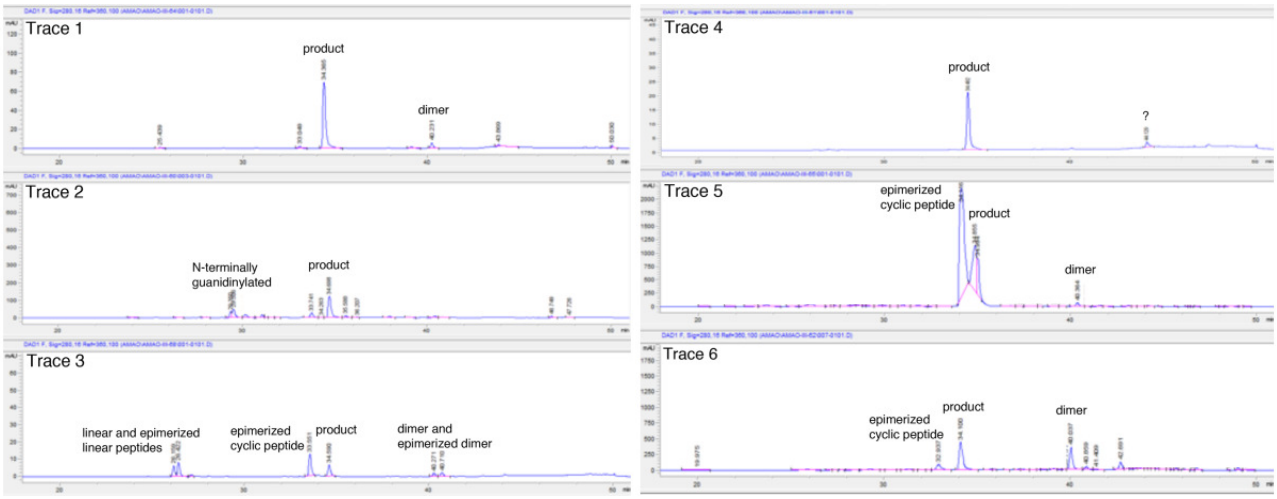

Synthesis of compound 2.2c

Two positions were found from the cyclization experiments, which gave equally high yielding reactions. The position with the β-amino acid as C-terminal residue was chosen, since any unreacted starting material could be easily isolated after loading to the resin.

The N-terminal Boc protecting group of **2.14** was changed to the base labile Fmoc group, so the building block was compatible with the trityl resin. To avoid possible side reactions in the cyclization, a Boc-protected Trp was used in the peptide elongation. The protecting group was kept on the Trp, by changing the cleavage procedure, using 2,2,2-trifluoroethanol and acetic acid instead of TFA. After cyclizing the peptide and cleaving the protecting groups, compound **2.2c** was obtained in a 48% yield over 12 steps, Scheme 2.8.

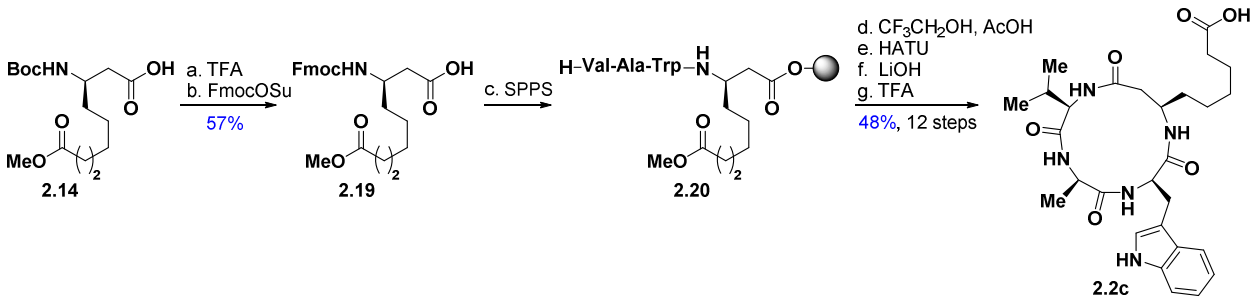

Scheme 2.8. Reagents and conditions: (a) 20% TFA in CH_2Cl_2, 4.5h. (b) FmocOSu, K_2CO_3, H_2O, dioxane, 0 °C to rt, 2.5h. (c) Aa (Fmoc-D-Trp-OH, Fmoc-D-Ala-OH, Fmoc-D-Val-OH), HATU, 2,6-lutidine, DMF; 20% piperidine in DMF, DBU:piperidine:DMF (2:2:96). (d) CF_3CH_2OH, AcOH, CH_2Cl_2. (e) HATU, $^iPr_2EtN$, DMF. (f) LiOH, THF, H_2O. (g) 50% TFA in H_2O.

2.4 Biochemical testing

Background; HDAC assays

A biochemical assay for evaluating the potency of HDAC inhibitors has been developed by Bradner and co-workers.[125, 169] Compound **2.21** (Figure 2.5) was used as substrate to evaluate the activity of HDAC1, 2, 3, and 6, but since a low catalytic turnover was observed for HDAC8 and class IIa HDACs, the acetyl group was replaced by the more labile trifluoroacetyl group (**2.22**).

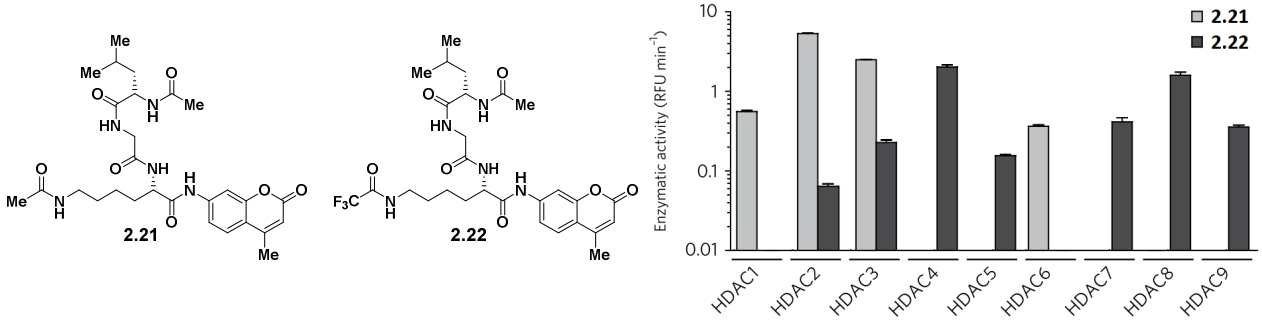

Figure 2.5 Left: Substrate **2.21** is used for analyzing HDAC1, 2, 3, and 6. Substrate **2.22** is used for analyzing HDAC 4, 7, 8, and 9. Right: Enzyme activity on substrate **2.21** and **2.22** using different HDAC isozymes. The figure was modified from ref [169].

The substrate is a tripeptide with an acetylated/trifluoroacetylated lysine residue and a fluorophore (7-amino-4-methylcoumarin) on the C-terminus. The HDAC inhibitory activity of a compound is based on fluorescence, as this property is correlated with the substrate turnover.

After addition of an HDAC enzyme, the positively charged lysine residue on the peptide substrate is exposed. Trypsin, which is added subsequently, recognizes the positively charged lysine and cleaves the amide bond connecting the fluorophore. When 7-amino-4-methylcoumarin is amidated, the fluorescent properties are quenched, but after cleavage by trypsin, the coumarin compound becomes highly flouresent. If an inhibitor is added along with the HDAC enzyme, an amount of substrate will not be deacylated. Trypsin will not be able to recognize the substrate and a low fluorescence is observed (Scheme 2.9).

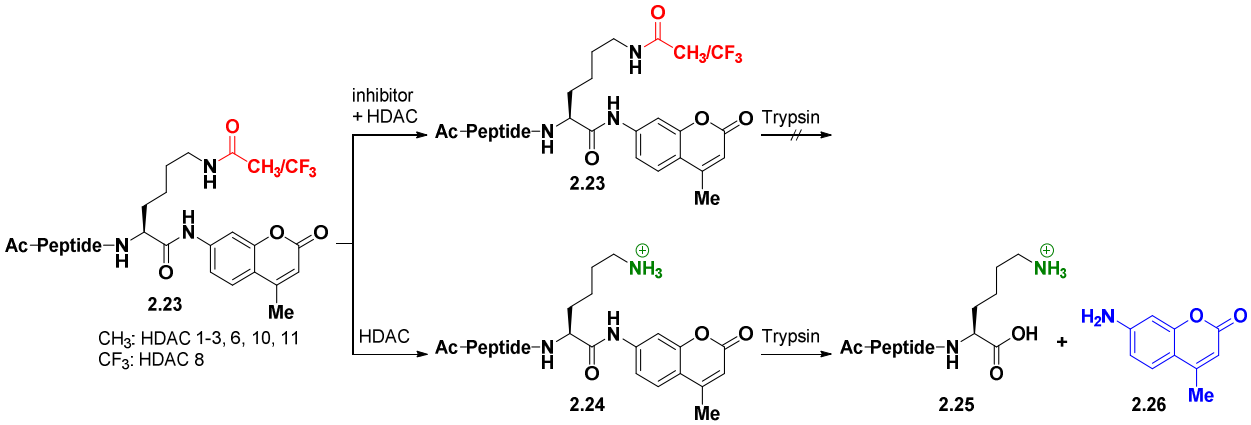

Scheme 2.9 Principles of the HDAC assays. If the HDAC enzyme is inhibited, trypsin will not cleave the amide bond connecting lysine and the fluorophore. Without inhibitor, HDAC enzymes will deacylate the lysine residue. The positively charged amine is recognized by trypsin that will release the fluorophore.

Biochemical profiling

The six cyclic peptides (**2.1a–c** and **2.2a–c**) were tested in HDAC assays, along with desmethyl and dimethyl analogs containing a *cis* olefin (**2.27a–c** and **2.28a–c**). An initial screen against HDAC4 and 7 indicated that the analogs were poor inhibitors of class IIa. The compounds were therefore only evaluated in class I, class IIb, and class IV (Table 2.6). IC_{50} values were converted to K_i values, using Cheng-Prusoff's equation [$K_i = IC_{50}/(1 + [S]/K_m]$[170] assuming a fast-on–fast-off mechanism.

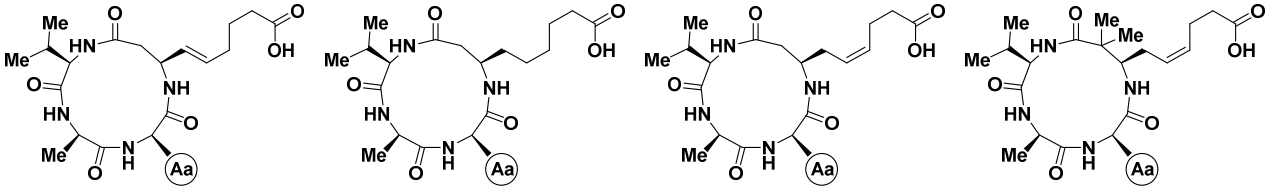

2.1a; Aa = D-Phe
2.1b; Aa = D-Tyr
2.1c; Aa = D-Trp

2.2a; Aa = D-Phe
2.2b; Aa = D-Tyr
2.2c; Aa = D-Trp

2.27a[a]; Aa = D-Phe
2.27b[a]; Aa = D-Tyr
2.27c[a]; Aa = D-Trp

2.28a[a]; Aa = D-Phe
2.28b[a]; Aa = D-Tyr
2.28c[a]; Aa = D-Trp

Figure 2.6 Compounds that were evaluated in the HDAC assay. [a] Compounds that were synthesized by Jesper S. Villadsen.

Table 2.6 HDAC inhibitory activity against HDACs from class I, IIb, and IV.

	K_i (μM)						
	Class I				Class IIb		Class IV
Compound	HDAC1	HDAC2	HDAC3	HDAC8	HDAC6	HDAC10	HDAC11
2.1a	1.41±0.37	1.86±0.04	1.62±0.31	8.57±3.61	IA[a]	IA	3.60±0.61
2.1b	0.83±0.26	0.66±0.28	0.55±0.26	IA	2.60±0.96	0.30±0.004	1.43±0.42
2.1c	0.57±0.08	0.45±0.31	0.65±0.44	3.35±2.06	4.44±0.36	0.26±0.005	1.24±0.61
2.2a	1.02±0.39	0.85±0.11	0.78±0.23	IA	IA	0.53±0.163	2.43±1.27
2.2b	0.78±0.68	0.32±0.20	0.26±0.16	IA	3.96±2.24	0.15±0.074	0.98±0.82
2.2c[b]	1.15±0.13	1.58±0.38	2.35±0.91	12.17±0.77	IA	0.38±0.068	3.20±1.80
2.27a	0.65±0.26	0.98±0.14	0.91±0.16	IA	IA	0.27±0.034	1.72±0.26
2.27b	0.34±0.23	0.21±0.07	0.37±0.29	IA	7.08±0.72	0.15±0.007	0.87±0.40
2.27c	0.23±0.13	0.17±0.01	0.57±0.16	5.93±0.71	IA	0.13±0.036	0.95±0.71

[a] IA: inactive (IC_{50} > 20 µM), [b] The data will be reevaluated in the near future.

When the K_i values were analyzed, it became apparent that the results from **2.2c** were outliers compared to the general trend. An analysis of the DMSO stock used in the enzyme assays showed a minor impurity, but it could not be determined if the impurity had also been present in the enzyme assays. A reevaluation of compound **2.2c** will be performed in the near future.

The azumamide analogs showed the highest activity against HDAC10, followed by HDAC1-3. Activity was also found against HDAC11, while poor inhibition was observed against HDAC6 and 8. All desmethylated compounds were more potent against the isozymes relative to azumamide A, B, and D. The higher activity of the analogs is most likely due to the carboxylic acid moiety, which coordinates zinc better than the amide functionality.

Table 2.7 gives an overview of the tyrosine containing compounds, compared with azumamide C while the phenylalanine containing analogs are compared with azumamide E in (Table 2.8). The only difference between compound **2.27a** and azumamide E, as well as **2.27b** and azumamide C, is the methyl group in the β^2-position; the direct influence of removing the methyl group can therefore be evaluated from these compounds.

Compared to HDAC6 and 8, removal of the methyl group seem to have a minor effect. However, azumamide C and E are relatively weak inhibitors of these isozymes, so the small difference is also an expression of the general poor activity against the enzymes. When the other HDAC isoforms are compared, it is evident that the methyl group has an important function, as **2.27a** and **2.27b** show a 5 to 36-fold decrease in potency.

Table 2.7 Potency of the tyrosine containing azumamide analogs.

	K_i (μM)						
	Class I				Class IIb		Class IV
Compound	HDAC1	HDAC2	HDAC3	HDAC8	HDAC6	HDAC10	HDAC11
2.1b	0.83 (26)	0.66 (17)	0.55 (39)	IA	2.6 (ep)	0.3 (30)	1.43 (41)
2.2b	0.78 (24)	0.32 (8)	0.26 (19)	IA	3.69 (2)	0.15 (15)	0.98 (28)
2.27b	0.34 (11)	0.21 (5)	0.37 (26)	IA	7.08 (4)	0.15 (15)	0.87 (25)

Potency relative to azumamide C is shown in parenthesis. Red: decreased potency, ep: equipotent.

Table 2.8 Potency of the phenyl containing azumamide analogs.

	K_i (μM)						
	Class I				Class IIb		Class IV
Compound	HDAC1	HDAC2	HDAC3	HDAC8	HDAC6	HDAC10	HDAC11
2.1a	1.14 (17)	1.86 (37)	1.62 (64)	8.57 (2)	IA	IA	3.6 (30)
2.2a	1.02 (15)	0.85 (17)	0.78 (31)	IA	IA	0.53 (27)	2.43 (41)
2.27a	0.65 (10)	0.98 (20)	0.91 (36)	IA	IA	0.27 (14)	1.72 (29)

Potency relative to azumamide E is shown in parenthesis. Red: decreased potency, ep: equipotent.

Compounds with a *trans* olefin in the side chain shows the weakest inhibitory activity, while analogs containing a *cis* olefin and a saturated side chain are equally potent. Regarding the aromatic residue, phenylalanine-containing compounds are the weakest inhibitors, while differences between compounds containing a tyrosine relative to a tryptophane is insignificant. These data are in agreement with the activity of azumamide C, which is the most potent inhibitor for all HDAC enzymes. The negative effect of

incorporating a phenylalanine and a *trans* olefin is evident from compound **2.1a**, which portray the weakest inhibition for HDAC1–3, 10 and 11.

Table 2.9 HDAC inhibitory activity against HDACs from class I, IIb, and IV.

	% Enzyme inhibtion						
	Class I				Class IIb		Class IV
Compound	HDAC1	HDAC2	HDAC3	HDAC8	HDAC6	HDAC10	HDAC11
2.28a (20μM)	16±9	8±4	8±8	IA[a]	IA	IA	IA
2.28a (10μM)	10±8	4±2	5±1	IA	IA	IA	IA
2.28b (20μM)	15±16	11±3	8±1	IA	IA	IA	IA
2.28b (10μM)	11±6	8±2	7±1	IA	IA	IA	IA
2.28c (20μM)	65±16	68±9	62±7	14±6	40±33	7±7	26±9
2.28c (10μM)	54±8	53±25	47±21	6±1	17±23	IA	22±20

[a] IA: inactive (IC_{50} > 20 µM)

A low activity was observed for the dimethylated compounds in preliminary tests, the analogs were therefore only tested at two doses. **2.28a** and **2.28b** showed minor activity against the HDAC enzymes, with a maximum inhibition of ~16% against HDAC1 at 20 μM. **2.28c** displayed a higher activity with IC_{50} values ~10 μM against HDAC1–3.

2.5 Conformational analysis

We were interested in solving the three dimensional structure of the desmethylated azumamide analogs, as the decreased activity might be explained by a conformational change in the core structure of the cyclic peptide. Casper Hoeck and Charlotte Held Gotfredsen did the primary work in elucidating the NMR structure.

All amide bonds in azumamide A-E exhibit *trans* conformations,[147] we therefore analyzed the NMR spectra of the azumamide analogs, to see if any *cis* amides were present. NOESY/ROESY interactions between H^{α} on adjacent amino acids would indicate a *cis* amide, but no correlations were found. The ^{1}H-NMR of the desmethyl analogs indicated a second conformation, illustrated by peaks with intensities <10% of the major structure. A *cis* peptide bond was observed in this conformation, between the aromatic amino acid substituent and alanine. However, the ^{1}H-NMR of azumamide A–E, also show a second conformation in similar proportions, so it seems unlikely that the loss of activity could be explained from this structure.

Even though the major conformation of the desmethylated analogs does not contain *cis* peptide bonds, an altered three-dimensional structure would still be a possible explanation for the lower activity. The identity of the side chains in small ring sized peptides have in particular been shown to alter the overall structure.[171] We therefore set out to solve the conformation of the desmethyl azumamide analogs in solution, with the use of NMR and modelling. Using a known distance as reference, the integrals of the ROESY correlations can be used to measure intramolecular distances. It is essential that the distance between the protons remain fixed on the NMR time scale and the number of ROESY signals that could be used, were further limited by scalar couplings. The challenges were partly overcome when the samples were recorded on an 800 MHz NMR machine from the Carlsberg laboratory.

We hoped to solve the solution structure in water, as this conformation would resemble the assay conditions best. Unfortunately, the azumamide analogs were insoluble, up to 15% H_2O in DMSO-d_6 was

added, but an insufficient amount of compound was dissolved to obtain a useful NMR spectrum. All samples were therefore analyzed in DMSO- d_6.

Two computational methods were utilized for solving the three-dimensional structure. In the first method, the program 'Maestro' was used to simulate the lowest energy conformation in water. 200 structures from the ensample of generated conformations for **2.27b** and azumamide A respectively (the functional group was removed in the calculations) were then correlated with the *J*-coupling and the NOESY/ROESY signals from the NMR data. A structure from each, which correlated best with the NMR data, were then overlaid for comparison (Figure 2.7).

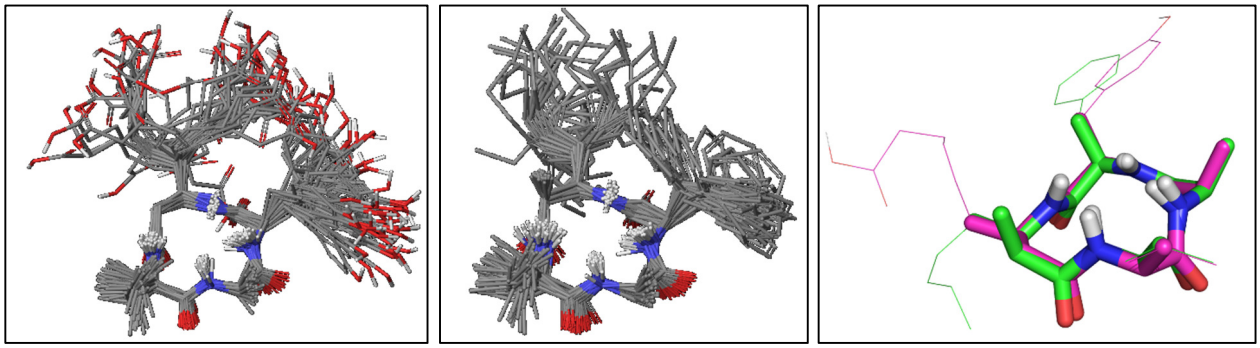

Figure 2.7 left: 50 conformations of **2.27b** from the energy minimization in water. Middle: 50 conformations of azumamide A (functional group removed for the calculations) from the energy minimization in water. Right: an overlay of a representative structure from the energy minimization, which correlates best with the NMR data. Green: Azumamide E, Magenta: **2.27b**.

In the second method, NOESY/ROESY data were used to set constraints to the cyclic structure when the simulations were performed. This was done by adding a penalty to the system if the distance between two protons changed more than 20%, compared to the data from the NMR spectra. The 100 structures with the lowest energy is shown for **2.27b** and azumamide A in Figure 2.8, (left, middle). A compound from each ensample is compared in Figure 2.8, right.

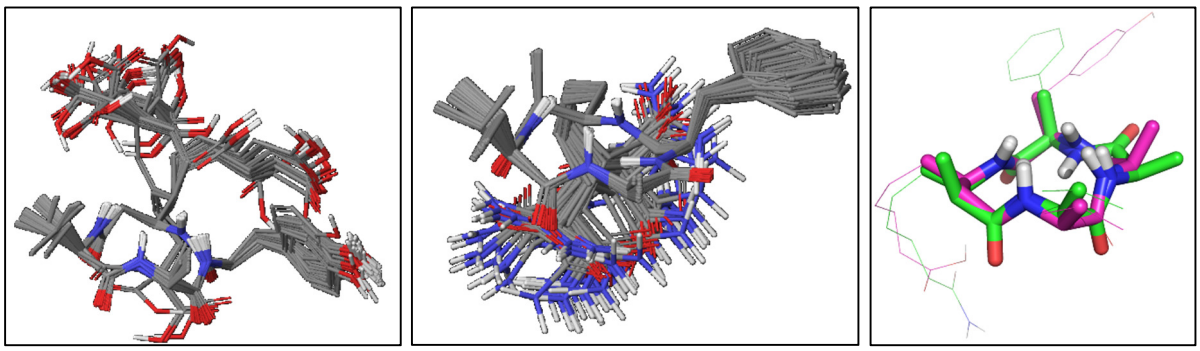

Figure 2.8 Left: The 100 lowest energy conformations simulated with constraints for **2.27b**. Middle: The 100 lowest energy conformations simulated with constraints for azumamide A. Right: overlay of a structure from each ensample. Green: azumamide E, magenta: **2.27b**.

The results from each method show that the difference in the core structure of the compounds do not vary significant. The greatest difference is seen in the second method, where an amide NH between the aromatic residue and alanine from the natural compound points to the middle of the structure. This conformation originates from the NOESY correlation between the NH and H^{α}-Ala. However, in this conformation, the distance between the NH and the methyl group in alanine does not correlate with the NMR data; so even though the cyclic peptide can be viewed as a rigid structure, the 3-D conformation is an ensample of closely

related structures with a certain flexibility. Overall, the structural difference in the backbone between the azumamides and the des-methylated compounds were small. Similar NOESY/ROESY correlations were found and the *J*-couplings were comparable.

Since the core structure of the desmethyl analogs did not change significantly relative to the azumamides, we speculated that the difference in HDAC inhibitory activity might arise from a preferred orientation of the side chain. The steric bulk from the methyl group in the azumamides might direct the side chain to a favorable position relative to the binding pocket. Since the azumamide analogs do not possess this group, a wider degree of freedom could be imagined, which would lead to a greater loss of entropy after binding.

Azumamide E and a desmethylated analog were simulated in water, using the same method as previously described for the energy minimization. 200 structures were obtained from the simulation, which each represented one conformation of the compounds after a given time period. The torsion angles between C^{γ} and H^{α} were then analyzed and plotted against the number of structures with the given angle (Figure 2.9). A positive angle denotes a direction pointing away from the methyl group, while a negative angle indicates a direction towards the methyl group.

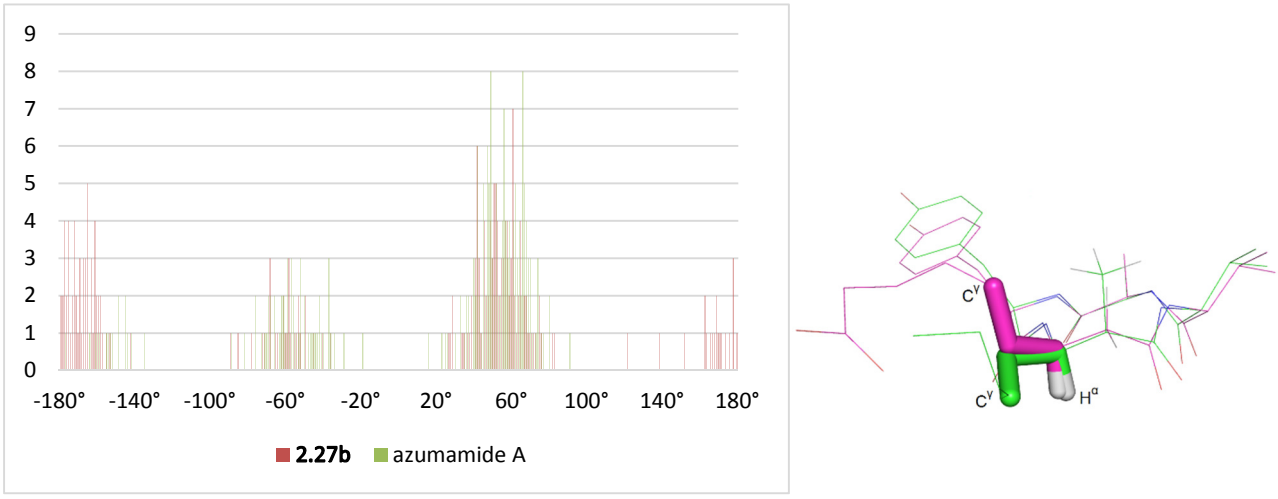

Figure 2.9 The number of generated structures from the energy minimization are shown as a function of the torsion angle between C^{γ} and H^{α}.

The desmethyl analog are found in clusters around -60°, 60°, and 180° in accordance to lowest energy of a staggered conformation (Figure 2.7). Azumamide E primarily possess an angle at 60°, some around -60°, and very few close to 180°. These data shows that the natural compounds may have a favorable predefined conformation of the side chain, which could be an important factor in the enzyme interaction.

2.6 Docking studies

The increased potency of the natural compounds could arise from favorable hydrophobic interactions between the binding pocket and the methyl group. Docking investigations could give us insight into this aspect.

The docking simulations on **2.1a–c, 2.2a–c** were performed in HDAC3 (PDB: 4A69)[25] by Niels J. Christensen and Peter Fristrup. The enzyme is crystalized as a dimer with SMRT and inositol phosphate; these co-factors were kept in the docking simulations (Figure 2.10, left). Although chain A and B are very similar, initial dockings showed slightly better results for chain B and this chain was chosen for further work. It should be noted that these preliminary docking results were performed on a rigid enzyme and thus neglects

potential induced fit effects. Optimized structures will be obtained by allowing the enzyme to minimize after the docking.

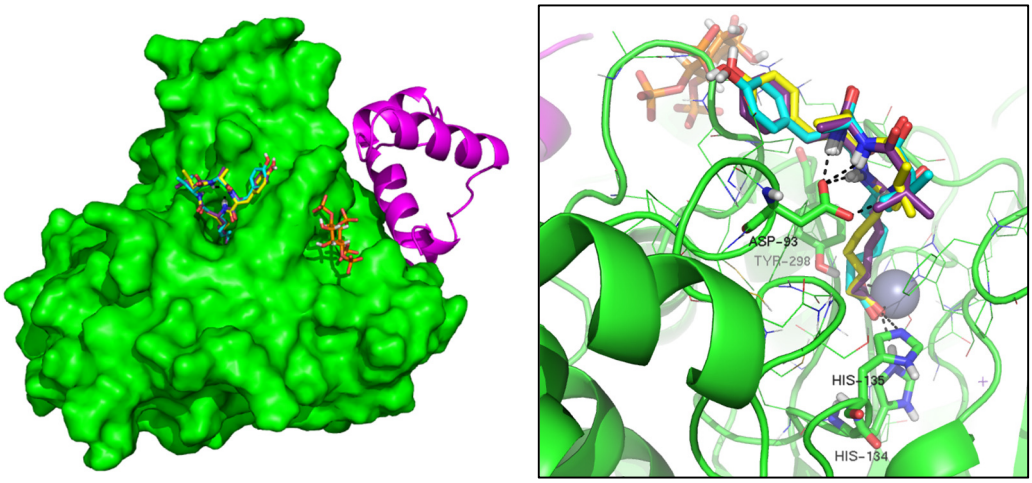

Figure 2.10 Docking poses of **2.1b**, **2.2b**, and **2.27b** in HDAC3. Left: Surface view of the docked structures in HDAC3. Right: Asp93 coordinates to all amide nitrogens in the cyclic scaffold. Green: HDAC3, magenta: SMRT, orange: inositol phosphate, purple: **2.1b**, yellow: **2.2b**, cyan: **2.27b**.

Each analog bind in a similar fashion to HDAC3, compound **2.1b**, **2.2b**, and **2.27b** is shown as representative examples in Figure 2.10. Asp93 has a particularly important interaction by coordinating with all the amide nitrogens in the cyclic core. Besides from coordination with the zinc atom, the carboxylic acid ZBG forms favorable interactions with His 134, His135, and Tyr298 (Figure 2.11). It is not clear from the docking results why the natural products possess a higher HDAC inhibitory activity relative to the analogs. However, favorable lipophilic interactions could occur between Phe200 and the methyl group in the azumamides.

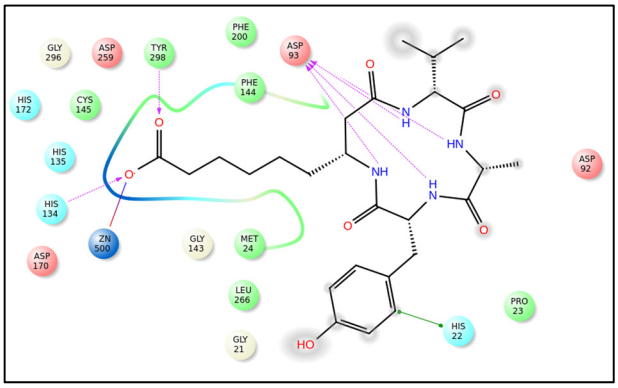

Figure 2.11 Binding interactions of **2.2b** docked in HDAC3.

The phenylalanine containing compounds (including azumamide E), show a lower activity towards HDAC1–3. Since tyrosine and tryptophan can form hydrogen bonds, these interactions would be an obvious explanation for the higher activity. However, the phenylalanine containing compounds are only ~2-fold less potent. The change in activity might therefore be a combination of the negative effect from removing a water molecule from the binding site and the positive effect from obtaining favorable hydrogen bond interactions. No hydrophilic interactions can be seen from the docking results, but since a rigid enzyme has been used for the simulations, amino acids near the cavity might move to interact with the ligand. His22 and Asp92 are located close to the aromatic substituent and might have a role in the binding.

2.7 Summary

The complex cap group, which is present in macrocyclic HDAC inhibitors, can interact with a range of residues in the rim towards the active site. Since the amino acids in this area are less conserved across the HDAC enzymes, there is a higher potential for macrocycles to selectively inhibit specific isoforms.

Even though the azumamides possess a relatively weak ZBG, they are potent HDAC inhibitors. The activity must therefore arise from interactions with the cyclic peptide. This cyclic scaffold was investigated by removing the methyl group from the β-amino acid. In addition, changes to the side chain were made, by incorporating a *trans* olefin- and a saturated side chain. A tryptophan residue was also integrated in these analogs.

The first strategy relied on synthesis of a cyclic peptide containing a vinyl substituent. A cross metathesis would then generate the target compound. Different reaction conditions were explored, but no product was observed. In the second strategy, the cross metathesis was performed on the amino acid building block instead. Incorporation in the linear peptide followed by a cyclization reaction afforded the desired compounds. The best yield was obtained by cyclizing between the β-amino acid residue and D-valine.

The desmethyl azumamide analogs were tested against HDAC enzymes in class I, IIb, and IV. The compounds had a decreased potency against all HDAC isozymes. However, the loss of activity towards HDAC1 relative to azumamide E, and HDAC1 and 2 relative to azumamide C, was not significant. The compounds with a phenylalanine as the aromatic substituent and a *trans* olefin in the side chain were the weakest HDAC inhibitors.

Casper Hoeck and Charlotte Held Gotfredsen performed conformational studies of the azumamide analogs, to find that the cyclic core of the scaffold was similar to the natural compounds. Regarding the side chain of the azumamide analogs, a higher flexibility was observed relative to the natural compounds.

Docking studies performed in HDAC3 by Niels J. Christensen and Peter Fristrup, showed a binding mode similar to the natural products. An important interaction was seen between Asp93 and all the NH-amides in the scaffold. A lipophilic interaction between Phe200 and the methyl group in azumamide C/E, could be determining for an altered activity, but the predefined orientation of the side chain in the natural products could also be a factor. His22 is located close to the aromatic amino acid in the ligand. This might explain the higher activity for compounds containing a tyrosine or a tryptophan.

3 Desmethylated thioester compounds

3.1 Introduction

The masked thiol of largazole facilitates transport across the cell membrane. Once inside, the natural product is activated after hydrolysis of the side chain. The ability of the azumamides to cross cell membranes might be improved in a similar fashion. We hypothesized that the potency of our desmethylated compounds could be increased, by changing the weak carboxylic acid ZBG to the more potent thiol. With this compound in hand, we could explore different motifs that would facilitate cell permeation. Interestingly, macrocyclic analogs with an incorporated thiol linker have an optimal length that differs from largazole and romidepsin (Figure 3.1).[115, 134]

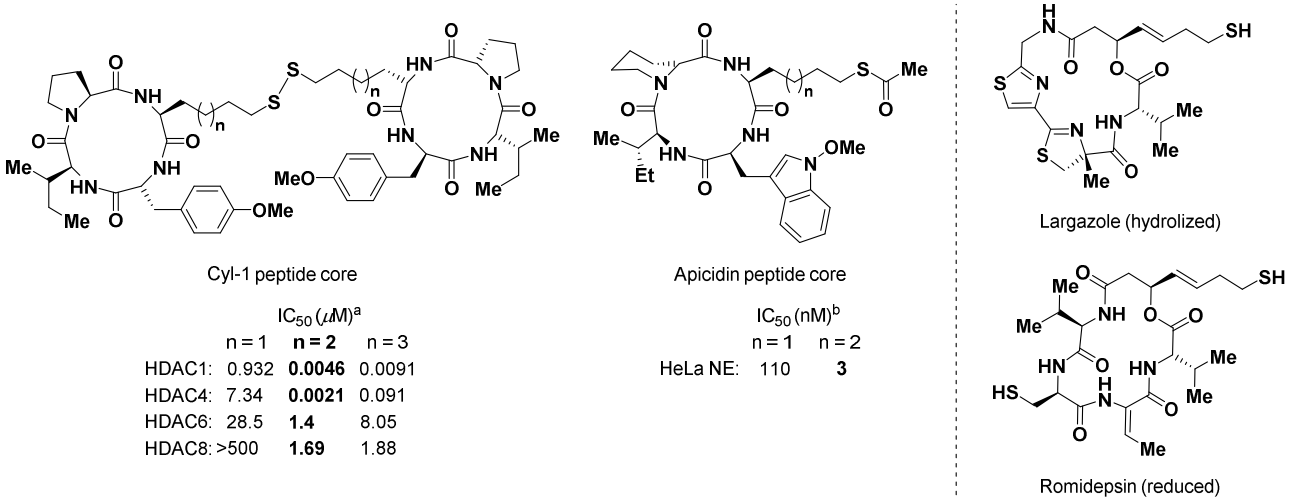

Figure 3.1 Left: Cyclic peptides containing a thiol side chain. [a] The disulfide was reduced in the assay.[134] [b] The thiol was generated in situ.[115] Right: active structure of largazole and romidepsin.

We suspected that a chain consisting of five methylenes would have the optimal length, as the desmethylated azumamide core bears a higher resemblance to Cyl-1 and apicidin, than for largazole or romidepsin. Niels J. Christensen performed docking studies of analogs containing 4, 5, and 6 methylenes as the linker length of the thiol side chain in HDAC8, to see if a length of four methylenes would be able to reach the zinc atom (Figure 3.2). Since largazole is co-crystalized in HDAC8, a direct comparison of the linker length could be made when this isozyme was used.

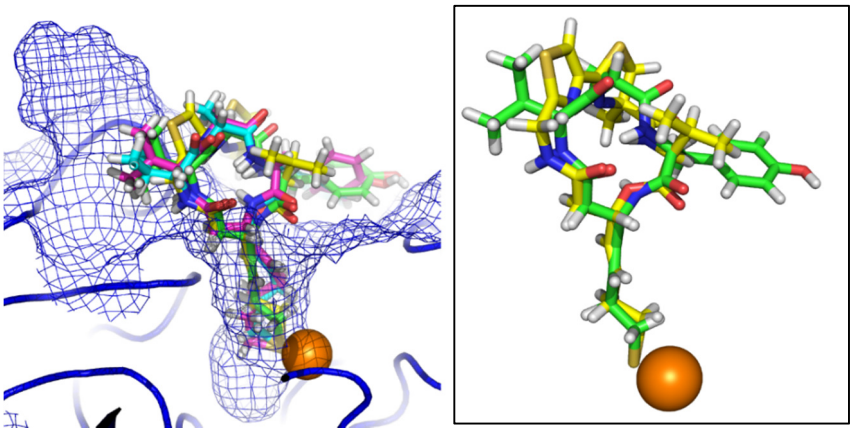

Figure 3.2 Left: Desmethyl azumamide analogs docked in HDAC3 (PDB: 3RQD). Right: comparison of largazole and an azumamide analog with 4 methylenes (**3.1a**). Green: **3.1a** (4 methylenes), cyan: **3.1b** (5 methylenes), magenta: **3.1c** (6 methylenes), yellow: largazole (from the crystal structure).

From the docking poses it seems likely that all the compounds are able to reach the zinc ion. In addition, the compound with a linker of 4 methylenes had a docking pose very similar to largazole (Figure 3.2, right).

Since the backbone of the desmethylated azumamides differs from Cyl-1 and apicidin, and the docking poses suggested that all compounds were able to reach the zinc atom, we planned to synthesize and test analogs containing a thiol linker with 4, 5, and 6 methylenes (Figure 3.3, left).

Largazole is a natural pro-drug that penetrates the cell membrane, facilitated by the octanoyl side chain. Inside the cell, the thioester is hydrolyzed to generate the active compound.[125] We were curious to know if the membrane penetration could be enhanced in our analogs, by incorporating the octanoyl moiety from largazole. We were especially interested to know if the permeation could be optimized further by using a different type of thioester. Using lipoproteins as inspiration, the surface of which is covered by phospholipids, we envisioned the synthesis of **3.2a–3.2c** (Figure 3.3).

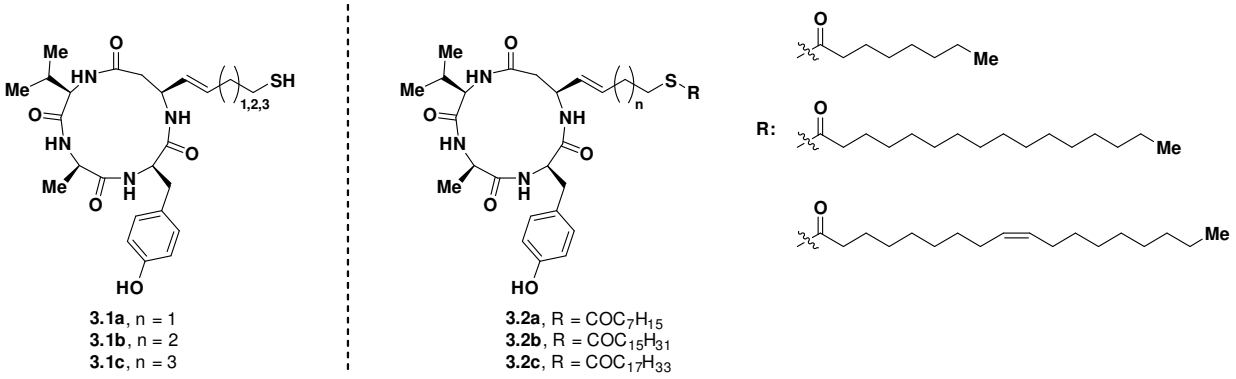

Figure 3.3 Target compounds. Left: Thiol linker with different length. Right: Interesting thioesters for evaluation in cell membrane penetration studies.

3.2 1st Strategy

In the first strategy towards synthesis of thioester containing cyclic peptides, the focus was turned towards a side chain similar to the one found in largazole, Scheme 3.1. It was hypotesized that the thioester building block could be obtained by a cross metathesis, in a similar approach as in the syntheses of **2.1abc–2.2abc**. Incorporation of the building block into a linear peptide followed by cyclization would give the azumamide-largazole hybrid (**3.2a**), while **3.1a** could be obtained by hydrolyzing the thioester.

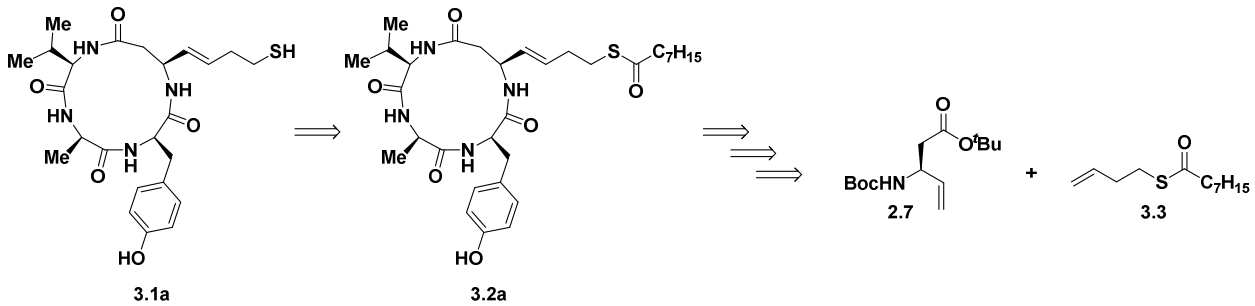

Scheme 3.1 Retrosynthetic analysis of compound **3.1a**.

The thioester ligand for the cross metathesis was prepared by a three step procedure starting from octanoyl chloride. **3.4** was first generated via hydrolysis of a 1-(acylthio)ethaniminium chloride intermediate. The crude thioacid was then converted to the ligand by reaction with 4-bromo-1-butene, Scheme 3.2.[172]

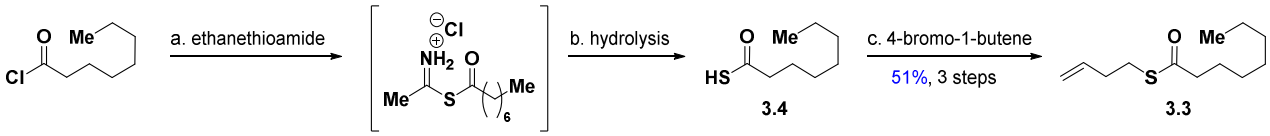

Scheme 3.2. Reagents and conditions: (a) ethanethioamide, 30 °C, 42h. (b) NaOH, 30 min. (c) 4-bromo-1-butene, K_2CO_3, 18h.

The reaction conditions for the cross metathesis were optimized by changing the catalyst and evaluating different solvents (Table 3.1). Grubbs 2nd generation catalyst and the catalysts containing the electron withdrawing groups, gave the best results (entry 1, 4, 5). However, it was not possible to isolate a pure product. Even though the building block differed significantly from the starting material, both compounds had a similar retention time, making isolation difficult. The mixture of **2.7** and **3.5** (~1:1) was therefore carried through to the next step in the synthesis.

Table 3.1 Catalyst screening for the cross metathesis.

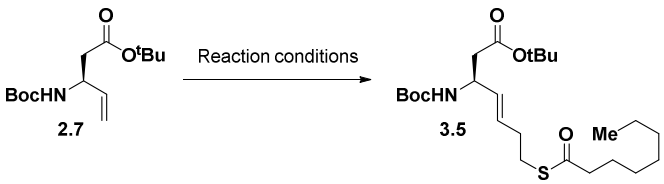

entry	Reaction conditions	yield (%)[a]
1	Grubbs cat. 2nd gen., 0.2 equiv, toluene, 60 °C.	38%, 60% BRSM
2	Hoveyda-Grubbs cat. 2nd gen., toluene, 60 °C.	26%, 47% BRSM
3	Hoveyda-Grubbs cat. 2nd gen., 0.2 equiv, DCM, 40°C	15%, 33% BRSM
4	Zhan catalyst 1B, 0.2 equiv, toluene, 60 °C.	42%
5	**2.11**, 0.2 equiv, toluene, 60 °C.	43%, 66% BRSM
6	**2.11**, 0.1 equiv + 0.05 equiv, $C_2H_4Cl_2$, 90°C.	11%

[a] trans isomer calculated by NMR.

The deprotected building block (**3.6**) was unstable during column chromatography; the mixture was therefore used directly in the peptide synthesis.*

* The synthesis was done before the optimized position in the peptide cyclization was evaluated.

The linear thioester tetrapeptide was isolated from the vinyl byproduct by preparative HPLC after cleavage from the resin (Scheme 3.2). Due to the small amount of linear peptide that was isolated, everything was used for the following cyclization reaction. Unfortunately no product was obtained from the reaction, this could be explained by an aminolysis. However, only one small peak appeared in the preparative HPLC run, which could not confirm the suggested byproduct.

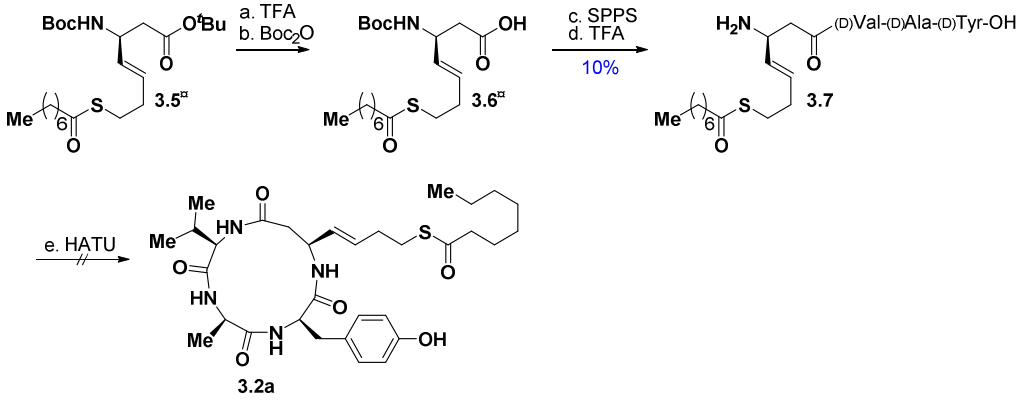

Scheme 3.3. Reagents and conditions: (a) TFA, CH_2Cl_2, 2h. (b) Boc_2O, $^iPr_2EtN$, 24h. (c) H-D-Val-D-Ala-D-Tyr-(2-Cl-Trt-resin), HATU, 2,6-lutidine, DMF, 15h. (d) 50% TFA in CH_2Cl_2, 2x 30 min. (e) HATU, $^iPr_2EtN$, 18h. ¤ ~ 1:1 mixure with **2.7**.

3.3 2nd Strategy

In Bradner and co-workers total synthesis of largazole, compound **3.8** was synthesized (Scheme 3.4).[135] The thiolprotected building block was obtained by cross metathesis of a free alcohol, followed by substitution with triphenylmethanethiol.

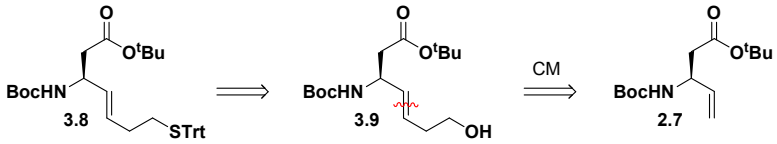

Scheme 3.4 Synthetic strategy utilized by Bradner and co-workers.[135]

The reported procedure could conveniently be used in the synthesis of **3.2a**. However, the reaction proved difficult to reproduce; less than 21% yield of an impure product was isolated from the cross metathesis (Table 3.2, entry 1) and substituting the catalyst or changing the solvent, did not improve the yield (entry 2, 3). Since the unprotected hydroxyl group might coordinate too strongly with the catalyst, the alcohol was triisopropylsilane (TIPS) protected. Unfortunately, this modification did not improve the yield either (entry 4). An attempt to obtain the protected thiol directly (entry 5) did not produce any product, only the thiolprotected homodimer was observed.

Table 3.2 Catalyst screening for the cross metathesis.

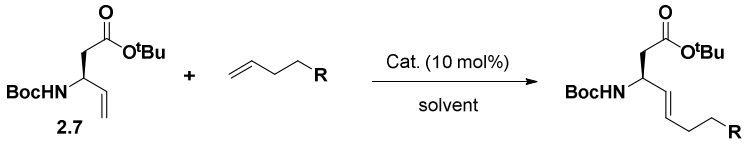

Entry	R	reaction conditions	Yield (%)
1	OH	Grubbs 2nd gen, CH_2Cl_2	~21, impure
2	OH	Hoveyda-Grubbs 2nd gen, CH_2Cl_2	LCMS: almost no product
3	OH	Grubbs 2nd gen, toluene	LCMS: almost no product
4	OTIPS	Hoveyda-Grubbs 2nd gen, CH_2Cl_2	10%, impure
5	STrt	Hoveyda-Grubbs 2nd gen, CH_2Cl_2	No product (dimer byproduct)

The ring closing metathesis (RCM) generally produce better yields, so it was envisioned that the building block could be set up for a RCM reaction, followed by hydrolytic ring opening to afford the product (Scheme 3.5). **2.8** was reacted with 3-butene-1-yl bromide, to form the diene **3.11**. The metathesis proceeded to form an impure product. Judged by NMR, a mixture of *cis* and *trans* isomers was obtained, with the *cis* isomer as the dominant compound (approximately 20% *trans* isomer). Because of the modest yield and the mixture of isomers, this strategy was abandonned.

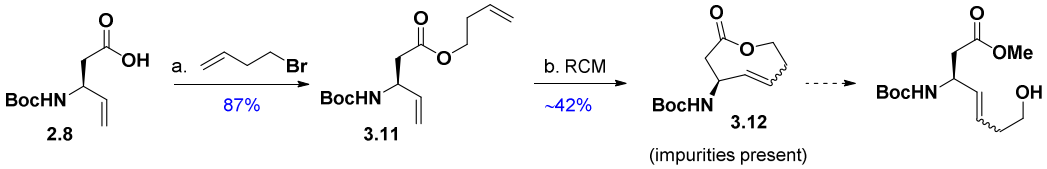

Scheme 3.5: Reagents and conditions: (a) 4-bromo-1-butene, K_2CO_3, DMF, 3h. (b) Grubbs 2nd gen. cat., CH_2Cl_2, 18h.

3.4 3rd Strategy

The new strategy involved oxidation of alcohol **2.6** to an aldehyde, which could be subjected to a Julia-Kocienski olefination (Scheme 3.6). Substitution with triphenylmethanethiol would subsequently give the target building block.

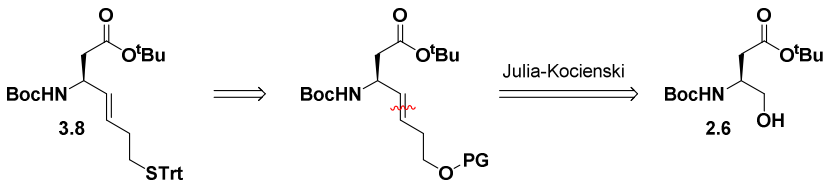

Scheme 3.6 Retrosynthetic analysis of the thiolprotected building block.

Background; the Julia-Kocienski reaction

The Julia-Kocienski reaction has been utilized in the total synthesis of many natural compounds,[173] among these are Jiang and co-workers total synthesis of Largazole.[129] The Julia-Kocienski reaction involves the reaction between an aldehyde and an α-metalated sulfone.[174] After addition of a strong base, an *anti*- (B) or a *syn* alkoxide (**G**) is formed, which subsequently undergoes a Smiles rearrangement[175] through a spirocyclic intermediate (Scheme 3.7). Due to steric interactions between R_1 and R_2, the intermediate of the *anti*-conformation is higher in energy (**D**). If the Smiles rearrangement is the rate determining step, it is most

likely that a *cis* alkene will form, as the *anti*-alkoxide will rearrange slower than the *syn*-alkoxide ($k_3 < k_4$). The olefin is obtained after another rotational change, to facilitate elimination of sulfur dioxide and the heterocycle.[174, 176]

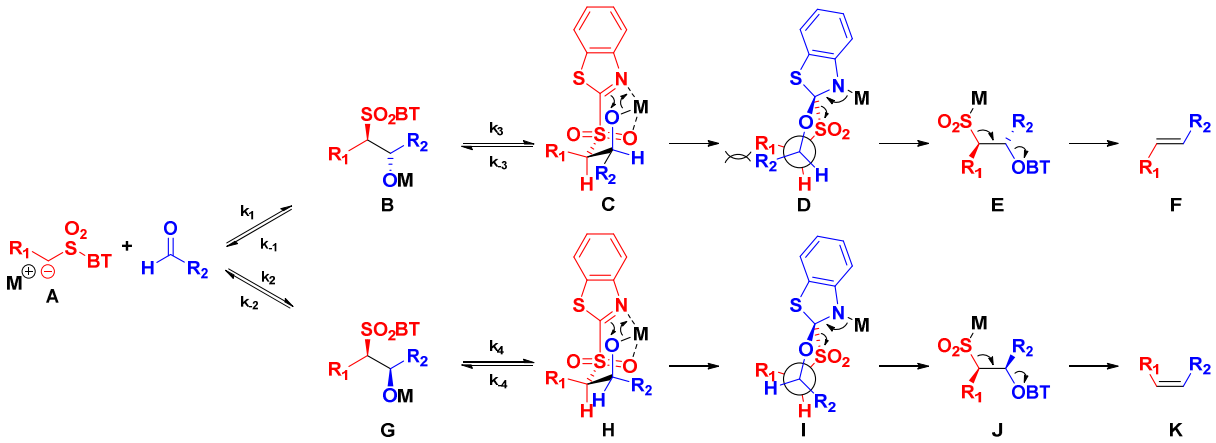

Scheme 3.7 Mechanism of the Julia-Kocienski reaction. The scheme was modified from ref [176b].

Kocienski optimized the one-pot procedure further, by introducing 1-phenyl-1H-tetrazol-5-yl sulfones (PT)[177] and 1-*tert*-butyl-1H-tetrazol-5-yl sulfones (TBT)[178] which are less prone to self-condensation, presumably because of the bulky substituent which shields a nucleophilic attack. The modified Julia reaction is therefore also known as the Julia-Kocienski reaction.

Use of aliphatic PT sulfones have indicated an irreversible reaction with aldehydes.[176b] The relative reaction rate to form the alkoxides (k_1, k_2) will therefore dictate the selectivity of the reaction. Kocienski and co-workers demonstrated that PT sulfones provided a high ratio of *trans* alkenes in the absence of electronic and steric factors, in contrast to the Julia-Lythgoe reaction. The base counter ion increased *trans* selectivity in the series $Li^+ < Na^+ < K^+$ and the stereoselectivity could be further improved by using a polar solvent such as THF and DME.[177]

Synthesis

The ligand for the Julia-Kocienski olefination was prepared from a mono protected 1,3-propanediol, which was subjected to a Mitsunobu reaction followed by oxidation to produce **3.15a**/**3.15b**, Scheme 3.8.

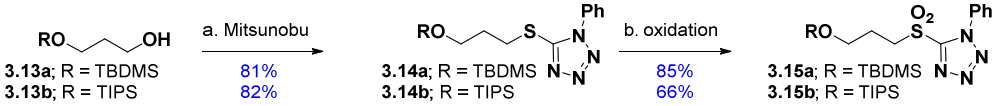

Scheme 3.8 Reagents and conditions: (a) PPh_3, DIAD, THF, 1-phenyl-1H-tetrazole-5-thiol, 0 °C, 4h to rt, 1h. (b) $NaHCO_3$, m-CPBA, 3h.

KHMDS was chosen as base, because of the *trans* selectivity that has shown to increase with the size of the counter ion.[177] Less than 10% of impure product was isolated (Scheme 3.9), and substituting the TBDMS protecting group to the more stable TIPS, did not produce a better result.

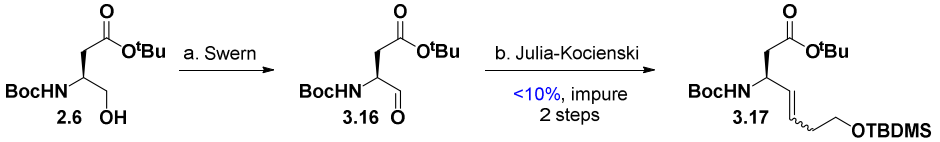

Scheme 3.9 Reagents and conditions: (a) $(COCl)_2$, DMSO, Et_3N, CH_2Cl_2, –78 °C to –40 °C to rt, 2h. (b) **3.15a**, KHMDS (0.5 M in toluene), THF, –78 °C, 3h.

We speculated that the low yields might be a consequence of the α-metalated PT withdrawing a proton from the Boc-protected amine, instead of making the nucleophilic attack. To test this hypothesis, the olefination was attempted on a purified aldehyde. Adding one equivalent KHMDS, did not produce any compound, but when a second equivalent of KHMDS was added, the starting material was consumed and the product could be isolated in 29% yield (Scheme 3.10). Although the simple test was not conclusive, the higher yield in the reaction supported the hypothesis that the NH in the *tert*-butyl carbamate would release a proton.

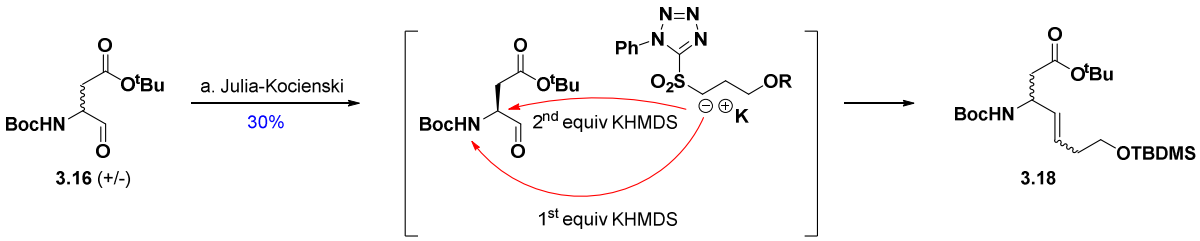

Scheme 3.10 Proposed explanation of the low yielding Julia-Kocienski reaction.

Since aldehyde **3.16** is prone to racemization, adding more than one equivalent of base would not be a viable strategy. However, if the amino acid was di-Boc-protected, the Julia-Kocienski olefination would still be possible.

The di-Boc-protected aspartic acid was synthesized in excellent yields over three steps from Boc-L-Asp(tBu)-OH. However, reducing the carboxylic acid resulted in a low yield, and the Swern oxidation did not produce any desired product, Scheme 3.11. Instead of exploring different oxidation methods, we decided to try a different strategy, since both the Julia-Kocienski reaction as well as the reduction needed to be optimized.

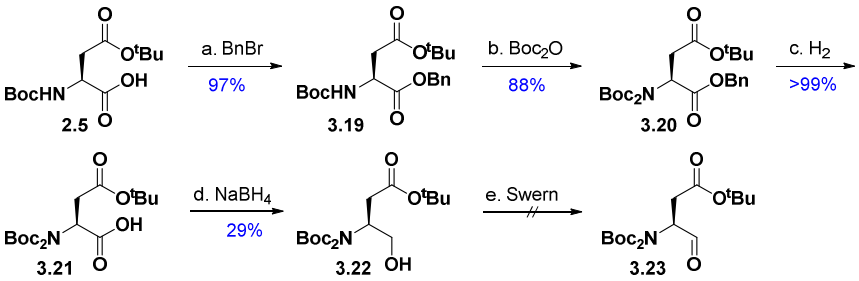

Scheme 3.11 (a) BnBr, K_2CO_3, DMF, 2h. (b) Boc_2O, DMAP, MeCN, 20h. (c) H_2, Pd/C (10%), MeOH, 24h. (d) $NaBH_4$, NMM, ^{i}BuOCl, THF, –25 °C to –10 °C to rt, 2h. (e) oxalyl chloride, DMSO, Et_3N, CH_2Cl_2, –78 °C to –40 °C to rt.

3.5 4th Strategy

The biological tests of the desmethyl azumamide analogs, showed that activity was decreased when a *trans* alkene was introduced. This activity could be regained to some extent by reducing the side chain (Table 2.6). We therefore decided to focus on the saturated thioester. This way, the side chain could be attached using a Wittig reaction, without considering *cis-trans* selectivity, as the double bond would be reduced in the following step, Scheme 3.12.

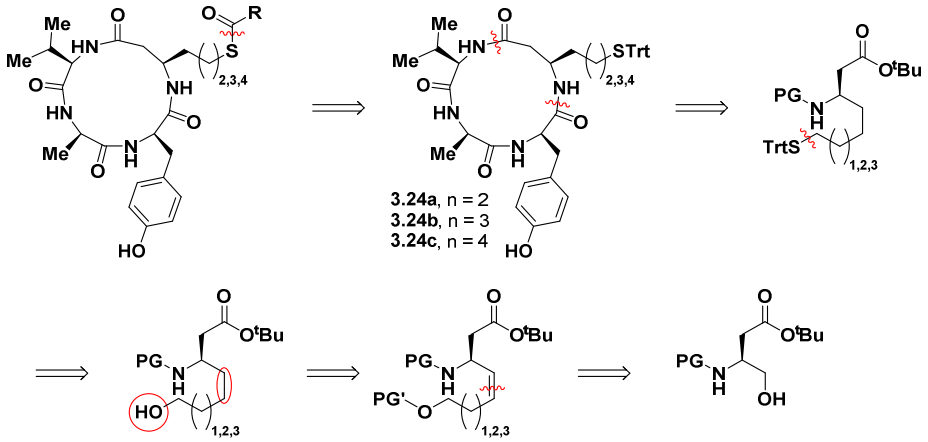

Scheme 3.12 Retrosynthetic analysis for thioester containing analogs.

Background; the Wittig reaction

The use of the Wittig reaction has been extensively reported in the literature and is one of the most effective ways of forming the carbon–carbon bond. Since Geissler and Wittig reported the reaction between methylenetriphenylphosphorane and benzophenone in 1953,[179] the Wittig reaction has evolved into variants including the Horner-Wadsworth-Emmons reaction,[180] and the Schlosser modification.[181]

The Wittig reaction usually proceeds by generating a reactive phosphonium ylide, followed by addition of an aldehyde or ketone. Ylides can be categorized according to their relative stability, which depends on the substituent attached to the *α*-carbon (Scheme 3.13). Non-stabilized ylides will predominantly form *cis* alkenes, although a high *trans* selectivity can be obtained with certain phosphonium species.[182] For non-stabilized- and semi-stabilized ylides, the highest *cis* selectivity occur for tertiary aldehydes, while reactions with primary aldehydes will favor *trans* selectivity.[183] Stabilized ylides generally show high *trans* selectivity in polar aprotic solvents.[184]

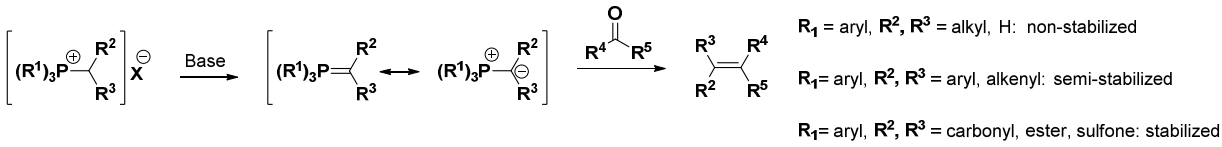

Scheme 3.13 Classification of ylides. The figure was modified from ref [185].

Synthesis of thiol containing cyclic peptide

A TIPS protected Wittig reagent was synthesized in two steps from 3-bromo-1-propanol in satisfying yields (**3.26**, Scheme 3.14). After addition of KHMDS, the ylide was reacted with aldehyde **3.16** to give the *cis* olefin, Scheme 3.14.

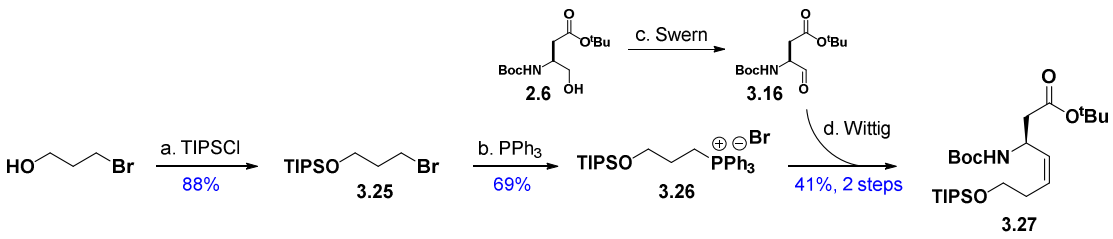

Scheme 3.14 Reagents and conditions: (a) imidazole, 2-bromopropanol, TIPSCl, CH_2Cl_2. (b) PPh_3, toluene, reflux, 4d. (c) $(COCl)_2$, DMSO, Et_3N, CH_2Cl_2, –78 °C to –40 °C to rt, 2h. (d) KHMDS (0.5 M in toluene), **3.16**, THF, –78 °C to rt, 15h.

The alkene was reduced with H_2 using Pd/C (10%) as catalyst. In addition to the desired compound, two byproducts had formed. The first byproduct had lost the TIPS protecting group (**3.28**), while the TIPSO had been cleaved in the other byproduct (**3.29**), Table 3.3. Since a free hydroxyl group was needed for the next steps, the TIPS removal was not an issue. However, to avoid byproduct **3.29**, a small catalyst screen was performed, Table 3.3.

Table 3.3 Catalyst screening for reduction of the olefin.

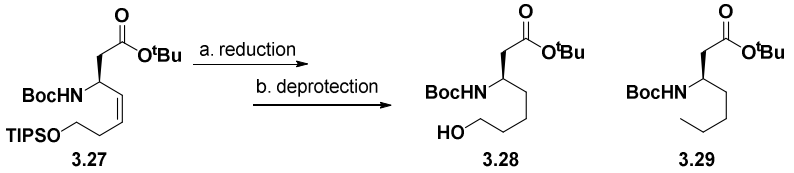

entry	catalyst[a]	Yield (%)	
		3.28	**3.29**
1	10% Pd/C	48	16
2	20% $Pd(OH)_2/C$	nd[b]	nd[b]
3	10% Pt/C	87	0

[a]General reaction conditions: (a) H_2, **catalyst**, MeOH, 24h; (b) TBAF, AcOH, THF. [b] nd: no data, poor reaction judged by TLC.

Changing the catalyst to $Pd(OH)_2/C$ gave multiple spots on TLC (entry 2), thus the catalyst was changed to Pt/C instead (entry 3). This change gave a quantitative yield of the reduced product, and **3.28** could be isolated in 87% yield over two steps.

The protected thiol was introduced by tosylating the hydroxyl group followed by an S_N2 reaction with triphenylmethanethiol. The cyclization experiments on the simplified peptide had shown that a higher yield was obtained with the β-amino acid on the C-terminal. The Boc protecting group was therefore exchanged to an Fmoc protecting group. After peptide elongation and cyclization, removal of protecting groups afforded the target compound (**3.35**), Scheme 3.15.

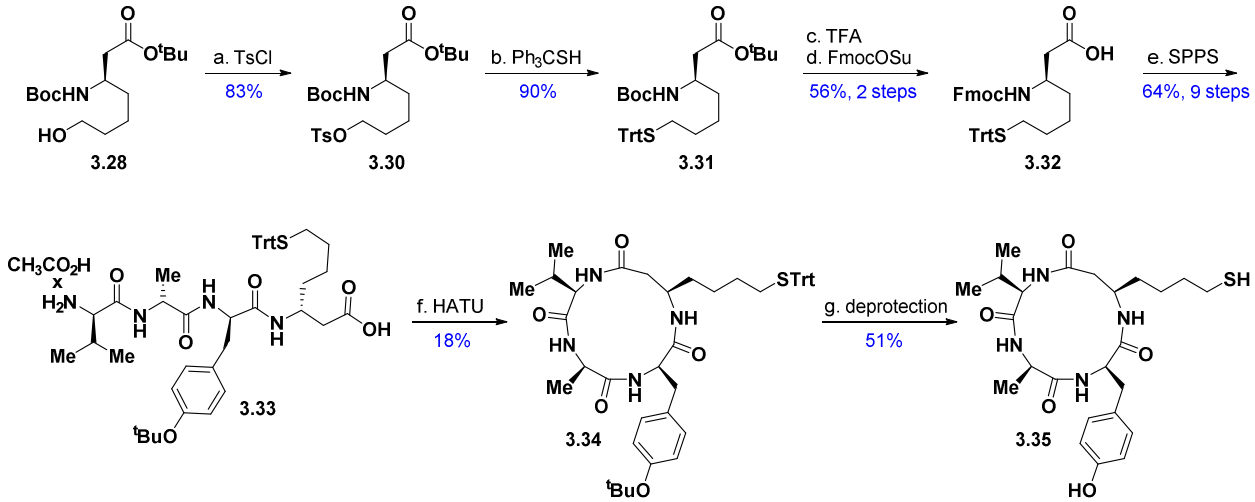

Scheme 3.15 Reagents and conditions: (a) TsCl, DMAP, Et_3N, 5h. (b) Ph_3CSH, KO^{t}Bu, THF, 0 °C to rt, 4h. (c) TFA, CH_2Cl_2, 0 °C, 4h. (d) FmocOSu, K_2CO_3, H_2O, DMF, 3h. (e) *i*. Cl-(2-Cl-Trt)-resin, $^i Pr_2EtN$, CH_2Cl_2. *ii*. 20% piperidine in DMF, DBU:piperidine:DMF (2:2:96). *iii*. HATU, 2,6-lutidine, Aa (Fmoc-D-Tyr-OH, Fmoc-D-Ala-OH, Fmoc-D-Val-OH), DMF. *iv*. 20% piperidine in DMF, DBU:piperidine:DMF (2:2:96). *v*. 50% TFA in CH_2Cl_2. (f) HATU, $^i Pr_2EtN$, DMF, 19h. (g) TFA, $^i Pr_3SiH$, 0 °C to rt, 2h.

Synthesis of C5 and C6 thiol side chains

After synthesizing the first thiol containing cyclic peptide (**3.35**), a modified route was chosen to circumvent the Boc to Fmoc manipulation. An orthogonal protecting group strategy was devised, involving a 2-(trimethylsilyl)ethoxycarbonyl (Teoc) protected amine, which is stable to the alkaline conditions in the Wittig reaction and still compatible with the trityl resin in the SPPS. The alcohol was protected with a benzyl group that could be removed in the same step as the alkene reduction (Scheme 3.16).

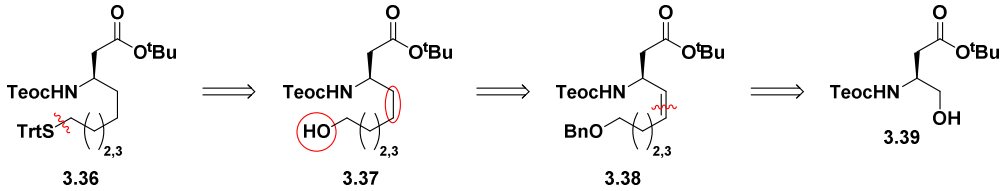

Scheme 3.16 Retrosynthetic analysis of protected thiol building block.

The Teoc-protected alcohol was obtained in good yield starting from H-Asp(O^{t}Bu)-OH (Scheme 3.17).

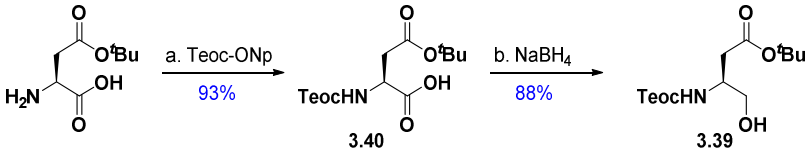

Scheme 3.17 (a) Teoc-ONp, Et_3N, H_2O, dioxane, 24h. (b) ^{i}BuOCOCl, NMM, 1,2-dimethoxyethane, $NaBH_4$, H_2O, 40 min.

The Wittig reagent was prepared by monoprotecting a diol, followed by an Appel reaction to convert the unprotected alcohol to a bromide (**3.42a**, **3.42b**, Scheme 3.18). Triphenylphosphine was added in the last step, and the reaction was refluxed in toluene for 3 days.

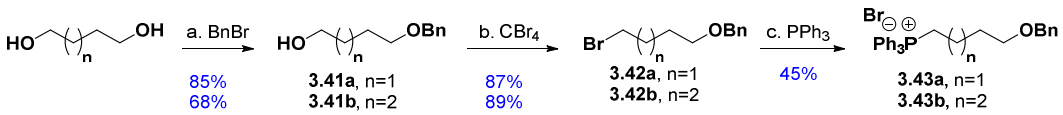

Scheme 3.18 (a) NaH, BnBr, THF, reflux, 18h. (b) PPh_3, CBr_4, Et_2O, reflux, 2h. (c) PPh_3, toluene, reflux, 24h.

The standard procedure of precipitating the Wittig reagent in an apolar solvent, proved difficult for **3.43b** compared to **3.43a**. The presence of an extra methylene in combination with the benzyl ether resulted in a lipophilic compound that formed an oil when trituration was attempted.

Inconsistent results were observed in the synthesis of the phosphonium bromide (**3.43a**). In the first attempt, am impurity was observed in the ^{1}H-NMR, while a clean product was isolated in the second attempt, albeit in a significant lower yield. By further examination, the byproduct from the first reaction was found to be benzyltriphenylphosphonium bromide. After searching the literature for similar side reactions, it was uncovered that Keller and co-workers had seen a similar byproduct when they synthesized the same Wittig reagent.[186] They were able to optimize the reaction by exchanging the bromide to an iodide, lowering the reaction temperature (80°C) and allowing longer reaction time (158h). Although complications arose in the syntheses towards **3.1b** and **3.1c**, a viable strategy was found. We expect to synthesize the final compounds in the near future.

3.6 Biochemical data

As a preliminary study, **3.1a** was tested against HDAC3 using the same assay conditions as previously described (section 2.4). However, to avoid disulfide formation, tris(2-carboxyethyl)phosphine (TCEP) was added to the buffer solution.

Even though the carboxylic acid in the desmethyl azumamide scaffold was substituted for a potent ZBG, the analog exhibited poor inhibition against HDAC3, with an IC_{50} of ~20 μM (Table 3.4). These data suggest that the linker length is not optimal for HDAC inhibition.

Table 3.4 Potency of **3.1b** against HDAC3

Compound	concentration	% Enzyme inhibition
3.35	20 μM	52
3.35	5 μM	20
3.35	1.25 μM	0

3.7 Summary

The side chain of largazole is an octanoyl thioester, which upon entry to the cell is hydrolyzed to the thiol. This natural prodrug was used as inspiration in the design of cyclic peptides containing the desmethyl azumamide scaffold.

To obtain the optimal length for binding in the HDAC enzymes, thiol side chains consisting of four, five, or six methylenes were designed. Different approaches for synthesizing these thiol-containing azumamides have been investigated.

In the first strategy, synthesis of a thioester building block via cross metathesis was accomplished in moderate yields. Although difficulties arose in the purification, a linear peptide was obtained. However, attempts on cyclizing the peptide did not provide the target compound. In the second strategy, different ligands were investigated in a cross metathesis with a vinyl building block to obtain a trityl protected thiol. However, the reaction was unsuccessful and exploring a ring closing metathesis strategy, did not provide the product in the desired yields either. In the third strategy, the Julia-Kociensky reaction was explored. The Boc-protected amine functionality proved to be insufficient for the reaction conditions and complications emerged in attempts to prepare a new building block.

The Wittig reaction was successfully applied in the synthesis of a cyclic peptide containing a thiol side chain with a length of four methylenes. The compound, which was tested against HDAC3 proved to be a poor inhibitor. Optimization of the protection group strategy gave complications in the preparation of Wittig reagents. However, new reaction conditions have been found and synthesis of the final compounds will be completed in the near future.

4 Work performed at California Institute of Technology

Part of the Ph.D. studies at the Technical University of Denmark involves an external stay. Sarah E. Reisman was kind to welcome me into her research group at California Institute of Technology. During the six month, I worked on two projects. Synthesis of pyrroloindolines with Dr. Lindsay Repka, and total synthesis of SCH 64877.

4.1 Synthesis of 2α-phenylpyrroloindolines for biological evaluation

Dr. Lindsay Repka, a former graduate student in Sarah E. Reisman's research group, initiated the project concerning synthesis of 2α-phenylpyrrolindolines. The biological evaluation was conducted by Chris Marotta and Christina McCleary Daeffler from Dennis Dougherty's research group at California Institute of Technology.

Introduction

The pyrroloindoline scaffold is present in many natural products and a broad range of biological properties are associated with these compounds. For example, the epidithiodioxopiperazine compounds, bionectin A and B exhibit antibacterial activity,[187] asperazine has shown selective cytotoxicity against leukemia,[188] and physostigmine is a cholinesterase inhibitor[189] (Figure 4.1).

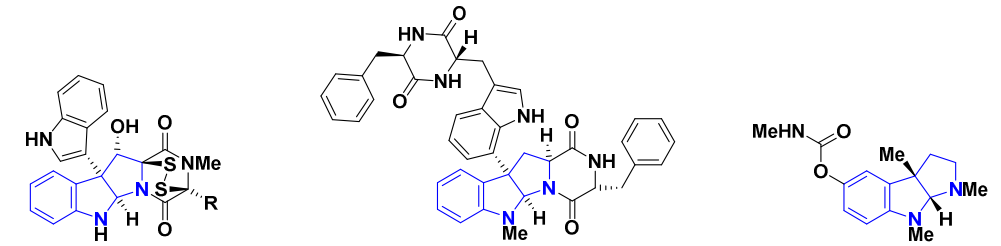

Figure 4.1 Pyrroloindoline natural products. Bionection A and B exhibit antibacterial activity, asperazine show anticancer activity and physostigmine is a cholinesterase inhibitor.

Methods for synthesizing enantioenriched pyrroloindolines, within the context of natural product synthesis, have been investigated in the Reisman research group. Lindsay M. Repka and Jane Ni have synthesized a range of pyrroloindolines, starting from C(3)-substituted indoles. The reaction proceeds by a [3+2] cycloaddition, catalyzed by an (*R*)-BINOL·$SnCl_4$ complex[190] (Scheme 4.1).

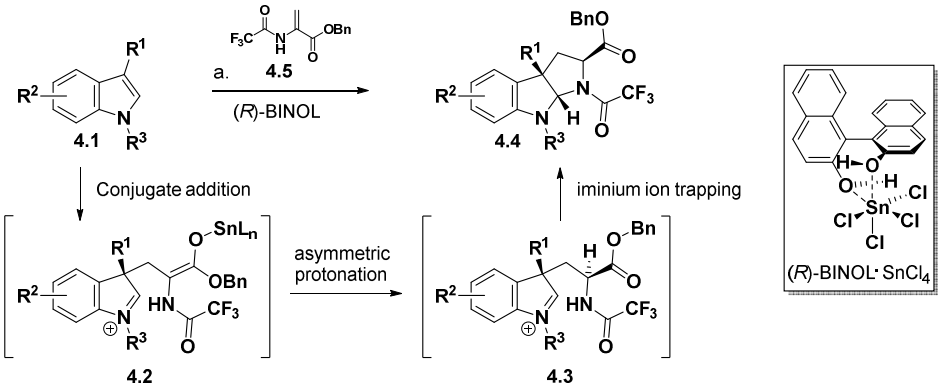

Scheme 4.1 Proposed mechanism for the [3+2] cycloaddition. Reagents and conditions: (a) (R)-BINOL, $SnCl_4$, CH_2Cl_2, 23 °C.

A stepwise mechanism was proposed; after a conjugate addition of the indole to the acrylate, a catalyst-controlled protonation afforded **4.3**, which was subsequently cyclized onto the iminium ion.[191] The enantio- and diastereoselectivity was found to be dependent on the type of acrylate that was used; the best results was obtained by using **4.5** as shown in Scheme 4.1.

Preparation of 1st generation pyrroloindolines

When the same conditions were applied for the synthesis of tryptophan derivatives using 2-phenylindole as starting material, a low yield and poor ee was obtained. However, the reactivity was significantly improved when a methyl 2-acetamidoacrylate was used.[191]

Lindsay Repka used these conditions to synthesize a carboxylic acid containing hydroxy pyrroloindoline (**4.10**, Scheme 4.2). After the Friedel–Craft conjugate addition to afford **4.8**, the amide was methylated using NaH as base. Compound **4.9** was obtained in good yields, but with a substantially reduced ee. By *in situ* formation of HCl, the acetamide was hydrolyzed, although the reaction was slow and low yielding. **4.10** was cyclized using *N*-chlorosuccinimide (NCS), and the hydroxy pyrroloindoline was obtained after quenching with NH_4OH and stirring in SiO_2. The *exo* and the *endo* compounds were obtained in a dr of 64:36, and could be isolated by preparative HPLC, although in less than 90% purity.

Saponification of the *exo* compound (**4.11**) using LiOH, gave the corresponding carboxylic acid, but only 11% of the product was obtained. Crude NMR following saponification of the *endo* product, suggested formation of the corresponding carboxylic acid, but after preparative HPLC, the *exo* product (**4.12**) was obtained in 1% yield. The data suggested that decomposition and isomerization could be a factor.[192]

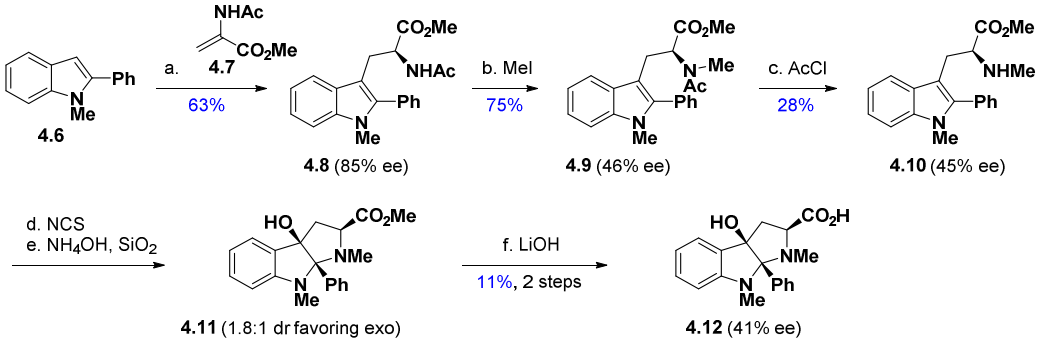

Scheme 4.2 Synthesis of carboxylic acid containing 2-α-phenylpyrroloindoline, conducted by Lindsay Repka. Reagents and conditions: (a) **4.7**, (*R*)-3,3'-dibromo-BINOL, CH_2Cl_2. (b) NaH, MeI, DMF, 0 °C. (c) AcCl (32 equiv), MeOH, 60 °C, 76h. (d) NCS, MeCN. (e) NH_4OH, SiO_2, MeCN, H_2O. (f) LiOH >25 equiv, THF/H_2O (1:1).

Electrophysiological experiments on compound **4.12** (41% ee)

Ion channels can be activated by changes in the potential near the channels (voltage gated ion channels) or by interaction with specific chemicals (ligand gated ion channels). Voltage clamp techniques, make it possible to distinguish between these effects.[193]

The two-electrode voltage clamp method is an electrophysiological technique that utilizes two intracellular electrodes to set the membrane potential at a fixed value. One electrode is used as a voltage sensor (e_v), while the other electrode can inject current (e_i) (Scheme 4.2). If ions cross the cell membrane, the potential is measured by e_v, and e_i injects a current equal to the change, thereby stabilizing the potential at a fixed value. Specific ion channels can be investigated by injecting RNA into frog oocytes, which will express the specific proteins on the membrane surface.[194]

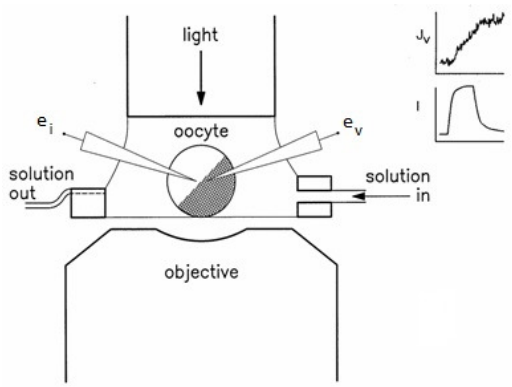

Figure 4.2 Two-electrode voltage clamp method. The electrode e_i can inject current to stabilize the membrane potential, which is measured by e_v.

The biological investigation of compound **4.12** was conducted on oocytes expressing a variety of different ligand-gated ion channel receptors (Table 4.1). A minor selectivity was observed, with no significant inhibition of the GlyR, $GluR2_A$, and $5HT3_A$ receptors.

Table 4.1 Preliminary results of compound **4.12** (41%ee), tested against I variety of ligand gated ion channels.

Entry	Receptor	% current reduction
1	$(\alpha 1)_2(\beta 1\text{-L9'A})\delta\gamma$ mouse muscle	21 ± 1
2	$(\alpha 4)_2(\beta 2)_3$ nAChR	20 ± 1
3	$\alpha 7$-T6'S nAChR	67 ± 1
4	$5HT3_AR$	3 ± 1
5	$(\alpha 1)_2(\beta 2)_2\gamma 2$ $GABA_AR$	27 ± 4
6	GlurR2	6 ± 1
7	GlyR2	6 ± 1

Ligands can inhibit the ion channels by binding at the primary binding site, at an allosteric binding site, or by functioning as a channel blocker. To get a better understanding of the binding mode, new target compounds were designed (Figure 4.3). In contrast to the zwitterionic nature of **4.13** and **4.14** compound **4.15**, **4.16**, and **4.17** are believed to be positively charged at physiological pH. It should be possible to determine if these compounds bind as channel blockers, by switching to a positively current in the two-electrode voltage clamp experiments. If they bind in the ion channel, the positive charged compounds should be released quickly.

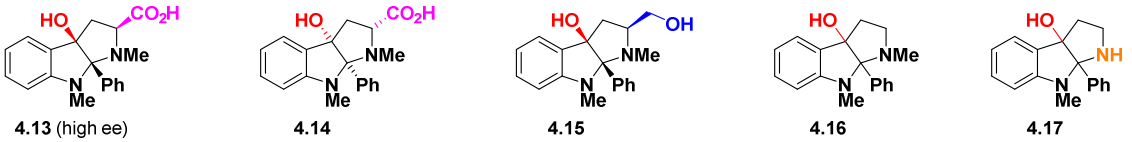

Figure 4.3 Target compounds for further biological investigations.

When I joined the Reisman research group, I continued the project initiated by Lindsay Repka. Besides from synthesizing **4.15**–**4.17**, a new strategy for the synthesis of compound **4.13** was going to be attempted, so the ee could be optimized (Figure 4.3)

Synthesis of pyrroloindoline **4.16**

Synthesis of **4.22** was commenced from tryptamine, which was Cbz protected followed by methylation of the protected amine and the indole nitrogen. Arylation of the indole was conducted using procedures from Albericio, Lavilla and co-workers (Scheme 4.3).[195]

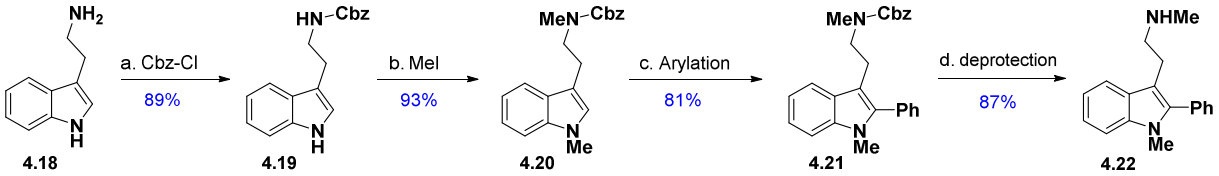

Scheme 4.3 Reagents and conditions: (a) $NaHCO_3$, Cbz-Cl, H_2O, CH_2Cl_2, 40 min. (b) NaH, MeI, THF, 0 °C to rt, 2h. (c) 2-NO_2Bz, $AgBF_4$, $Pd_2(OAc)_2$, DMF, PhI, rt, 30 min, then μW 150 °C 4 min. (d) Et_3SiH, Et_3N, $Pd_2(dba)_3{\cdot}CHCl_3$, CH_2Cl_2, 16h.

After deprotecting the amine functionality, the oxidative cyclization proved to be a challenge. Previous cyclization attempts by Lindsay Repka had indicated an optimal reaction time of 90 min as the product decomposed over time.

In contrast to the former observation, the product did not decompose, when I reproduced the reaction conditions. The starting material had been consumed after 4h, without decomposition of the product (entry 1, Table 4.2). Unfortunately, the reaction could not be reproduced, so different reaction conditions were investigated.

NCS is unstable in light, so it was crucial that the reaction was kept in the dark. Adding an additional equivalent of NCS caused the product to decompose (entry 3, 4). Furthermore, if NCS and **4.22** were mixed before adding the solvent, the reaction would usually not succeed (entry 5). The most consistent results were obtained when recrystallized NCS was dissolved in MeCN and added dropwise to **4.22** in MeCN. 4Å molsieves were added and the reaction was kept under argon, while keeping the reaction in the dark (entry 6, 7).

Table 4.2 Exploration of the NCS mediated oxidative cyclization.

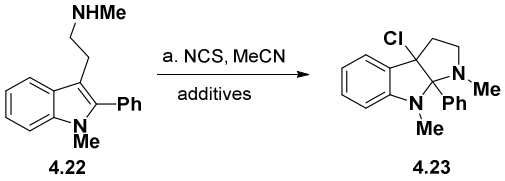

4.22 4.23

Entry	Additive	NCS method of addition (equiv)	Scale (µmol); Conc. (mM)	Time (h)	Result [a]
1	–	solution (1.0)	50; 33	4	**4.23**
2	4Å MS	neat[b] (0.83)	20; 20	1	**4.23**
3	4Å MS	neat[b] (1.1)	20; nd	4	nr[c]
4	–	Solution[b] (1.0 + 1.0)	50; 50	7	nr
5	–	neat[b] (1.0)	50; 33	6.5	nr
6	4Å MS	solution[b] (1.0)	50; 50	2	**4.23**
7	4Å MS	solution[b] (1.0)	140; 56	2	**4.23**

[a] Reactions were conducted under an argon atmosphere in the dark. Conversion to **4.23** was monitored by LCMS. [b] NCS was recrystallized from toluene. nd: not determined. [c] nr: no reaction.

In the procedure for synthesizing **4.12** (Scheme 4.2), Lindsay Repka reported the use of NH_4OH for quenching the reaction, followed by stirring in SiO_2. When the same conditions were used for the synthesis of **4.22**, a peak could be detected on LCMS (M+H =280.2 g/mol), with one mass unit less than the target compound. The new product turned out to be **4.24** (Scheme 4.4) due to a substitution by NH_3. **4.16** was instead obtained by quenching with aqueous $Na_2S_2O_4$ followed by stirring in H_2O/MeCN with SiO_2. The unstable chloride intermediate would thereby be converted to a hydroxy containing pyrroloindoline. A lower yield was obtained for **4.16** compared to **4.24**. The cyclization conditions were similar for both compounds, so the difference in yields might be explained by the stability of the compounds under the different workup conditions.

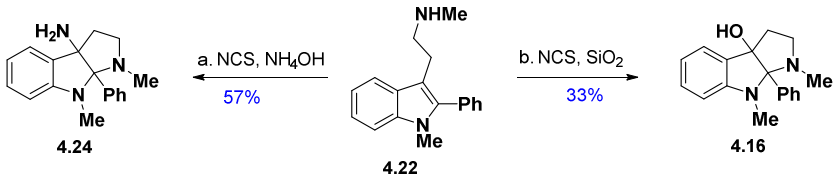

4.24 4.22 4.16

Scheme 4.4 Reagents and conditions: (a) *i.* NCS, MeCN, 4Å molsieves. *ii.* NH_4OH, 3h. (b) *i.*NCS, MeCN, 4Å molsieves, 1.5h. *ii.*SiO_2, H_2O, MeCN.

Synthesis of pyrroloindoline 4.17

The Cbz protected tryptamine could be selectively methylated on the indole nitrogen using MeI and KOH. The following arylation succeeded in satisfactory yield and the oxidative cyclization was also performed without any difficulties to get the N-protected pyrroloindoline intermediate. It was decided to include **4.27** in the biological testing, as the large Cbz protecting group most likely had an impact on activity, which could aid in elucidating the binding mode of these types of compounds. Minor impurities were observed after column chromatography of **4.27**, a small amount was therefore purified by HPLC to obtain the purity needed for the biological testing. Removal of the Cbz group was achieved using Et_3SiH as the H_2 donor, but besides

the desired product, a silyl carbamate had formed. This intermediate could easily be cleaved by stirring the compound in a solution of $NaHCO_3$ in THF.

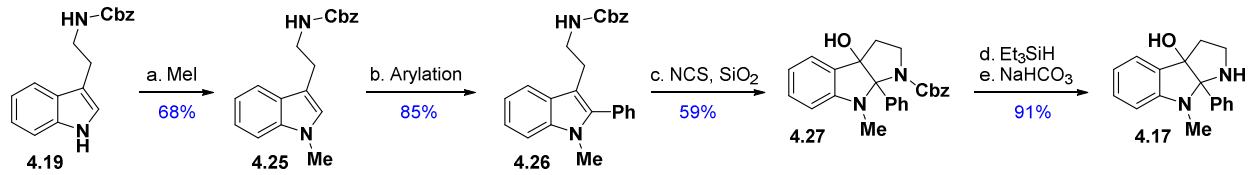

Scheme 4.5 Reagents and conditions: (a) MeI, KOH, Acetone, 1h. (b) PhI, 2-NO_2Bz, $AgBF_4$, $Pd_2(OAc)_2$, DMF, rt, 30 min then μW 150 °C 4 min (c) *i*. NCS, MeCN, 4Å molsieves, 6h. *ii*. MeCN, H_2O, SiO_2 (d) $Pd_2(dba)_3 \cdot CHCl_3$, Et_3SiH, Et_3N, THF, 19h. (e) $NaHCO_3$, THF, H_2O, 5h.

Synthesis of pyrroloindoline 4.13

The original procedure for preparation of **4.13** had some synthetic challenges. Racemization was observed under the methylation conditions and a poor yield was obtained when hydrolyzing the acetamide. Furthermore, a lot of compound was lost upon saponification of the methyl ester. We therefore sought a new route for synthesizing the carboxylic acid containing pyrroloindoline.

Racemization of the compound could be avoided by starting with a carboxylic acid instead of the methyl ester from the original strategy. (L)-Trp was therefore Cbz protected followed by addition of MeI. Arylation of the indole gave compound **4.31** in fair yields. Gratifyingly, with minor loss of enantiomeric purity.

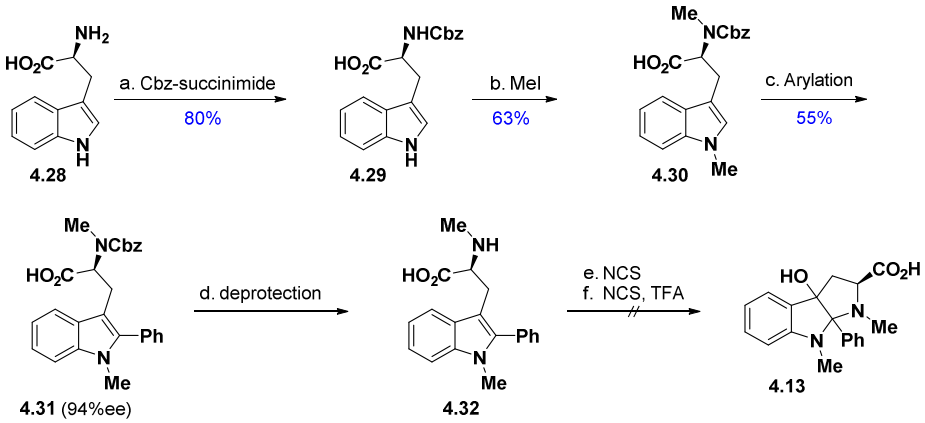

Scheme 4.6 Reagents and conditions: (a) Cbz-succinimide, K_2CO_3, H2O, DMF, 0 °C to rt, 40 min. (b) MeI, NaH, THF, 0 °C to rt, 29h. (c) PhI, 2-NO_2Bz, $AgBF_4$, $Pd_2(OAc)_2$, DMF, rt 30 min, then μW 150 °C 4 min. (d) $Pd_2dba_3 \cdot CHCl_3$, Et_3SiH, Et_3N, CH_2Cl_2, 29h. (e) NCS, MeCN, SiO_2. (f) NCS, MeCN, TFA additive, SiO_2.

Purification of **4.32** proved to be challenging due to the low solubility of the compound. By combining fractions from several reactions, it was possible to obtain pure material for the indole cyclization. Different solvents were attempted as well as multiple oxidation reagents, but no successful cyclization was observed. The carboxylic acid was therefore protected as the methyl ester, where after the Cbz protecting group was removed (Scheme 4.7). The unprotected compound once again proved troublesome to purify, which was reflected in the low yield. Cyclization of the pyrroloindoline protected methyl ester, afforded a mixture of two diastereomers (**4.35**, **4.36**) that could not be separated by column chromatography. Both compounds were therefore carried through to the next step. Saponification of the methyl ester, using LiOH at room temperature, was monitored on LCMS. While the *endo* compound reacted slowly, the *exo* compound was saponified readily. Purification by column chromatography afforded **4.13** as a pure compound in 33% yield, while the *endo* product could not be isolated.

The saponification was repeated, but with the temperature kept at 0 °C. When the *exo*-compound **4.36** was consumed, the reaction was quenched and purified to afford 47% of **4.13** and a 50% recovery of **4.35**.

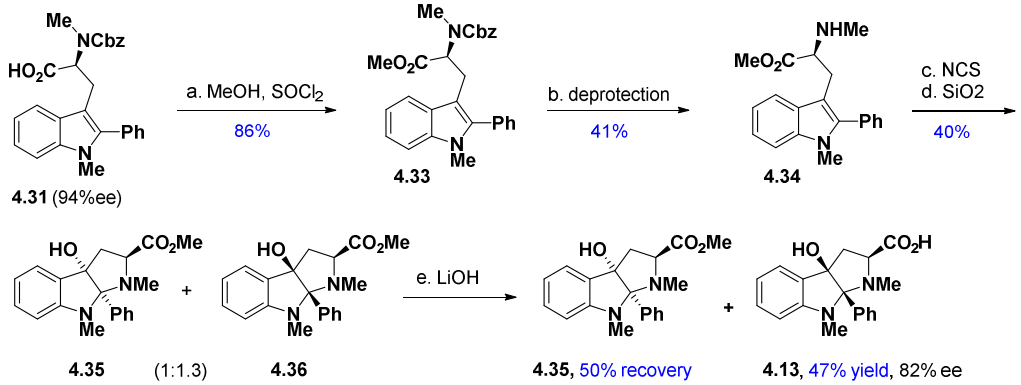

Scheme 4.7 Reagents and conditions: (a) $SOCl_2$, MeOH, 40 °C, 5h. (b) Et_3SiH, Et_3N, $Pd_2(dba)_3$, CH_2Cl_2, 20h. (c) NCS, MeCN, 4Å molsieves, 5.5h. (d) SiO_2, MeCN, H_2O, 30 min. (e) LiOH, THF, H_2O, 0 °C, 2.5h.

Synthesis of pyrroloindoline 4.15

The hydroxy pyrroloindoline **4.15**, could be elaborated from **4.31** by converting the carboxylic acid to the anhydride followed by $NaBH_4$ mediated reduction. After removal of the Cbz protection group, the oxidative cyclization was attempted. Unfortunately, the reaction did not proceed while having a free hydroxy group present.

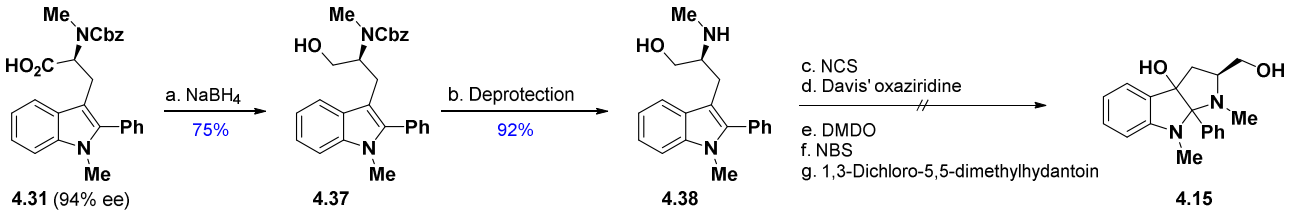

Scheme 4.8 Reagents and conditions: (a) NMM, MeOCOCl, $NaBH_4$, THF, –30 °C to –20 °C, 1.5h. (b) $Pd_2dba_3 \cdot CHCl_3$, Et_3SiH, Et_3N, CH_2Cl_2, 18h. (c) NCS, MeCN. (d) Davis' oxaziridine, CH_2Cl_2. (e) DMDO, acetone, CH_2Cl_2. (f) NBS, MeCN. (g) 1,3-Dichloro-5,5-dimethylhydantoin, MeCN.

4.38 was protected with TESCl, but due to time limitations, synthesis of compound **4.40** and **4.15** was not completed.

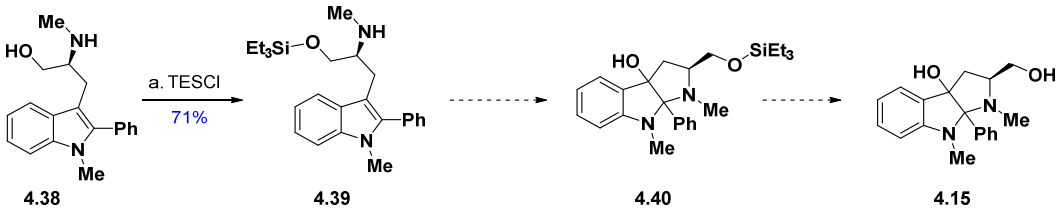

Scheme 4.9 Reagents and conditions: (a) TESCl, Et_3N, DMAP, THF, 0 °C to rt, 3h.

Biochemical testing

Chris Marotta and Christina McCleary Daeffler tested the five 2-α-phenyl pyrroloindolies (Figure 4.4) on oocytes expressing a variety of ion channels (Table 4.3). The effect of the compounds were tested along with

an agonist for the particular receptor, so the antagonistic effect could be measured. A fixed concentration of the pyrroloindolines were used in combination with the EC_{50} concentration of the agonist.

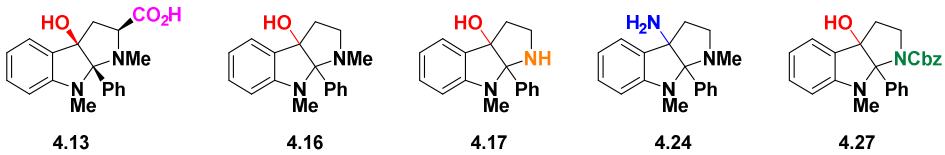

Figure 4.4

Enantioenriched **4.13** did not change the antagonistic activity compared to the previous data (Table 4.1). Compound **4.16**, **4.17**, **4.24**, and **4.27** exhibited a similar low activity against $GluR2_A$, GlyR, and $5HT3_AR$, while almost all compounds were antagonists to the nicotine acetylcholine receptors. The antagonistic effect from the structural diverse pyrroloindolines indicated that a specific binding interaction does not occur. The effects could instead arise from blocking the ion channel; however, a positive current was not used in the preliminary testing to verify the binding mode.

Interestingly, **4.16** potentiates the effect of GABA on the $GABA_A$ receptor by 52%. Furthermore, **4.16** is also able to activate the $GABA_A$ receptor without addition of GABA, generating ~10% current relative to the isolated GABA induced signal (Figure 4.5). 40 µM of **4.16** and 11 µM GABA (=IC_{50}) was used in both experiments.

Table 4.3 Be sure that 20a is enantio enriched compound.

	% Change in current				
Receptor	**4.13**	**4.16**[b]	**4.24**	**4.17**	**4.27**
$(\alpha 1)_2(\beta 1\text{-L9'S})\delta\gamma$mouse muscle	-21 ±1	- 53 ±3	- 81 ±6	- 7 ±3	- 29 ±3
$\alpha 7$-T6'S nAChR	-67 ±1	- 92 ±4	- 96 ±3	- 57 ±10	- 68 ±7
$(\alpha 4\text{-L9'A})_2(\beta 2)_3$ nAChR	-20 ±1	- 29 ±6	- 44 ±2	- 11 ±2	- 47 ±4
$(\alpha 1)_2(\beta 2)_2\gamma 2$ $GABA_AR$	-27 ±4	+ 52 ±10	+ 10 ±5	- 27 ±21	- 27 ±11
$(\alpha 1)_2(\beta 2)_2$ $GABA_AR$	nd	+15 ±1	nd	nd	nd
$GluR2_A$	-6 ±1	- 9 ±6	- 12 ±5	- 11 ±5	0 ±2
GlyR	-6 ±1	+3 ±7	- 16 ±6	+ 18 ±10	- 9 ±9
$5HT3_AR$	-3 ±1	- 3 ±5	- 11 ±8	+ 3 ±12	-23 ±4

20 μM concentration of the pyrroloindolines and EC_{50} concentrations of the agonists were used. Standard deviations are based on the average of three to four experiments. [b] Run with a 40 µM concentration of **4.16**. nd: not determined.

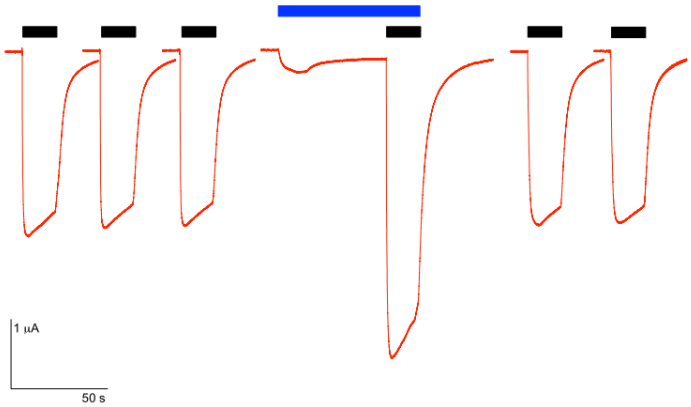

Figure 4.5 Current trace: blue: 40 μM **4.16**, 11 μM GABA (=IC_{50})

4.2 Side chain preparation towards the epidithiodiketopiperazine SCH 64877

Dr. Jay Codelli, a former graduate student in Sarah E. Reisman's research group was working on total synthesis of the natural compound SCH 64877. When I joined the group, I assisted Jay in synthesizing the side chain of the compound.

Introduction

The epipolythiodioxopiperazines (ETP) are secondary metabolites from fungi, characterized by a bridged disulfide or polysulfide on a diketopiperazine. Compounds belonging to this group have shown a variety of biological activities, such as antitumor, antimicrobial, antiviral, immunosuppressive, and inhibitory activities on various enzymes. The biological activity has been assigned the disulfide/polysulfide moiety, as reduction of the functionality has typically led to complete loss of activity.[196]

Three thiodiketopiperazine metabolites SCH 64874, SCH 64875, and SCH 64877 (Figure 4.6) was isolated in 1997 from an unidentified fungus.[197] The compounds showed antagonistic activity for the epidermal growth factor (EGF) receptor, with IC_{50} values of 1.0, 1.0, 1.25 µg/mL respectively. Compounds with a similar scaffold have been isolated from the fungi *Arachniotus aureus* (aranotin, acetylaranotin),[198] *Aspergillus terreus* (acetylaranotin),[199] and *Emericella heterothallica* (emathallicin C) (Figure 4.6).[200]

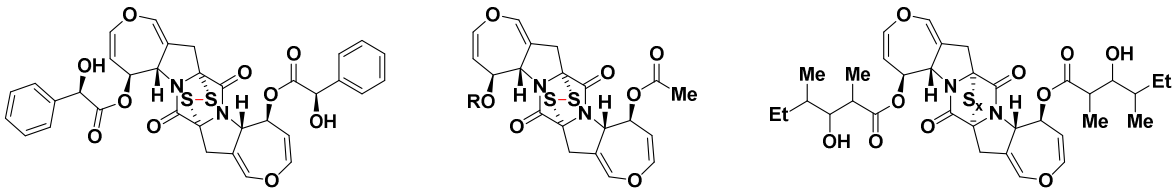

Figure 4.6 SCH 64877 and related compounds.

Towards the total synthesis of SCH 64877

The total synthesis of acetylaranotin was completed in the Reisman research group in 2011.[201] The strategy opened up the possibility for accessing additional members of the ETP family. The natural compound SCH 64877, containing four sulfur atoms bridging a diketopipeazine (Figure 4.6), could be obtained directly by elaborating on an intermediate from the total synthesis. The stereochemistry of the two β-hydroxyester side

chains are unknown; however, the exact structure of SCH 64877 could be elucidated if the total synthesis succeeded.

Nelson and co-workers have showed that *cis* β-lactones can be synthesized with high enantio- and diastereoselection, using trimethyl silane (TMS) protected quinine (TMSq) or quinidine (TMSQ) as catalyst (Scheme 4.10).[202]

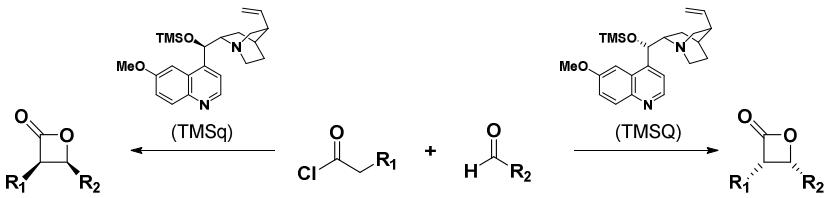

Scheme 4.10 *Cis-*β–lactones can be generated by a ketene-aldehyde cycloaddition using TMS protected quinine (TMSq) or TMS protected quinidine (TMSQ) as catalyst.[202]

Using these reaction procedures, Jay Codelli initiated synthesis of the side chains. Starting from propanoyl chloride and 2-methylbutyraldehyde he achieved to synthesize the side chain with the (2*R*, 3*S*, 4*S*) stereochemistry (Scheme 4.11). However, comparing the spectral data with the published spectra for SCH 64877, the synthesized compound did not turn out to be the natural compound.

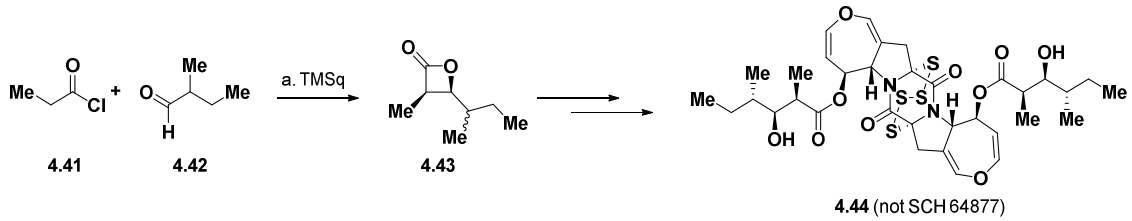

Scheme 4.11 Incorporation of a side chain with the (2*R*, 3*S*, 4*S*) stereochemistry, was not the natural product, SCH 64877.

When I joined the project, the focus was set on synthesizing the (2*S*, 3*R*, 4*R*) diastereomer. Jay Codelli had used a procedure, where the *cis-*β-lactone **4.43**, could be obtained by a [2+2] cycloaddition using TMSQ as catalyst. The *trans* isomer could be formed by exposing **4.43** to alkaline conditions (Scheme 4.12). The *cis-* and *trans-*β-lactones could easily be separated by column chromatography, while the diastereomeric benzyl esters was separated using an automated flash chromatography system.

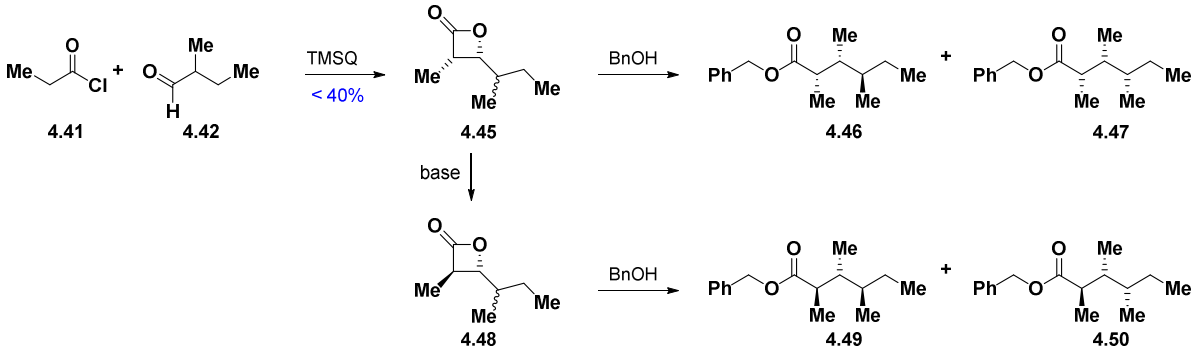

Scheme 4.12 Initial syntheses by Jay Codelli. The *trans-*β-lactone could be formed by addition of a base and the benzyl-protected diastereoisomers (**4.46**, **4.47**, **4.49**, and **4.50**) could be isolated.

1st strategy

The proposed mechanism of the [2+2] cycloaddition (Scheme 4.13) starts from the ketene, which is generated *in situ* from the acid chloride. TMS protected quinine or quinidine adds to form an enolate, stabilized by the Lewis acid. A six membered transition state forms, which collapses to the *cis*-β-lactone.

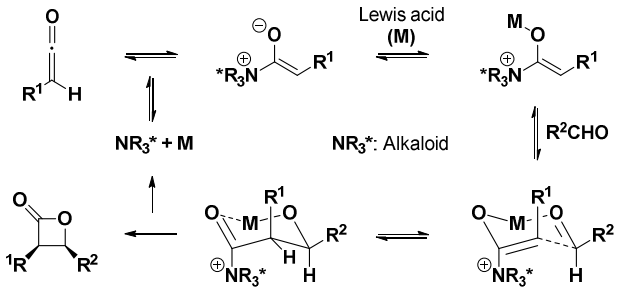

Scheme 4.13 Postulated mechanism for the [2+2] cycloaddition. Redrawn from ref [202].

The optimal reaction procedure employed by Nelson and co-workers[202] included dissolution of the protected quinine/quinidine and $LiClO_4$ in Et_2O, followed by addition of CH_2Cl_2 (Et_2O was necessary to dissolve $LiClO_4$). For challenging substrates, the amount of Lewis acid could be raised to increase the yields. After cooling the reaction to –40 °C or –78 °C, $^{i}Pr_2NEt$ was added followed by addition of the aldehyde. Dropwise addition of the acid chloride in CH_2Cl_2 (4 M) over 1–4 h ensured a slow conversion of the ketene. The reaction was run between 7–16 h before the reaction was quenched.

The reaction conditions used by Jay in the first attempts in the [2+2] cycloaddition, were based on the original procedure in the formation of an α-substituted aldehyde. The best yields were obtained by raising the amount of Lewis acid to 3.3 equiv, but the product was still obtained in less than 40% yield. I therefore attempted to optimize the reaction by changing different parameters, Table 4.4.

Dimerization of the ketene is a known byproduct, so by using a higher concentration of the aldehyde, formation of the byproduct might be lowered. Unfortunately, the product was obtained in a very low yield. Exchanging the acid chloride for an acid bromide did not change the outcome of the reaction and substituting $^{i}Pr_2NEt$, with an inorganic base did not provide any compound at all. A higher amount of the Lewis acid was added, but this attempt was also unsuccessful. Since a larger volume of Et_2O was needed to dissolve the $LiClO_4$, the solvent might destabilize the transition state, resulting in lower yield. All the reactions had been performed at –40 °C. With the known risk of obtaining a mixture of diastereomers, the temperature was raised to 0 °C. However, only 10% yield was obtained from this reaction.

The best result was obtained by increasing the amount of acid chloride, indicating that this starting material was consumed before reacting with the aldehyde, probably by dimer formation. The acid chloride was therefore diluted to a larger volume of CH_2Cl_2 before addition to the reaction mixture, hoping that an even lower concentration of the acid chloride would eliminate dimerization. As the yield did not improve, it was hypothesized that the lower ratio of Et_2O present in the reaction mixture might be too low, leading to precipitation of the Lewis acid. The acid chloride was therefore dissolved in the same Et_2O–CH_2Cl_2 ratio before addition. However, this change did not improve formation of the β-lactone.

Table 4.4 Exploration of different reaction conditions in the [2+2]-cycloaddition.

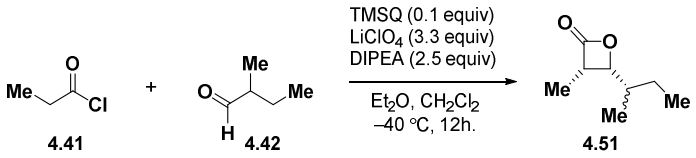

4.41 4.42 4.51

Entry	Changes to reaction conditions	Yield
1	Higher conc. of aldehyde	13%
2	Diluted acid chloride (DCM)	29%
3	Diluted acid chloride (Et_2O/DCM 1:2)	31%
4	Acid bromide	27%
5	Temp.: 0°C	10%
6	8 equiv. acid chloride	40%
7	$LiCO_3$ instead of $^iPr_2NEt$	0%
8	10 equiv. $LiClO_4$	nd[a]

[a] nd: not determined, low yield judged by crude NMR.

The low yields in the reaction, can most likely be explained by the hindered aldehyde being too unreactive. A screen of different Lewis acids was planned, as activation of the aldehyde might afford the product in a better yield. Before a significant improvement to the reaction conditions was fund, it was uncovered that the reaction gave a low ee of **4.46**, which was the target molecule. The synthetic strategy was therefore revised.

2nd strategy

For synthesis of the side chain, diastereoselectivity was a high priority. We envisioned that **4.53** and **4.57** could be synthesized by a directed hydrogenation, while **4.54** and **4.58** could be obtained using Evans aldol reaction (Scheme 4.14). Beside the diastereomers shown, the enantiomers could be synthesized, starting from the *R*-oxazolidinone auxiliary.

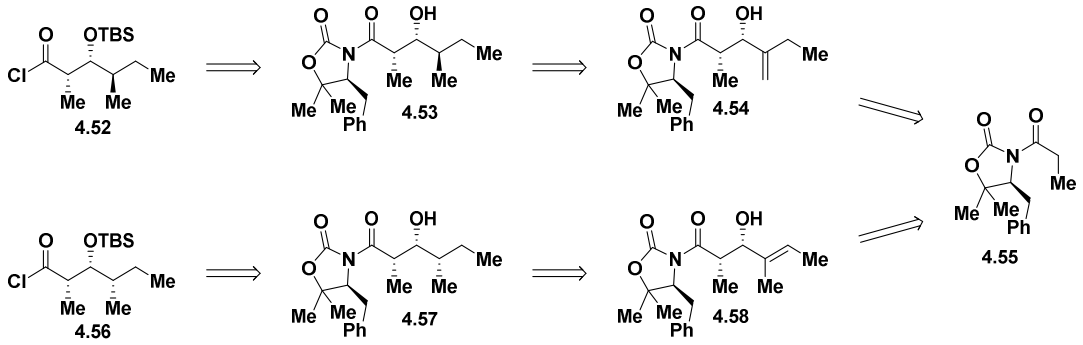

Scheme 4.14 Retrosynthetic analysis of side chains towards SCH-64877.

Synthesis of the side chain for SCH 46877

Evans auxiliary was prepared from the methyl ester of phenylalanine. After Boc protecting the amine functionality, a Grignard reaction afforded compound **4.61**. Cyclization after addition of ^{t}BuOK, provided the auxiliary in good yields over three steps (Scheme 4.15).

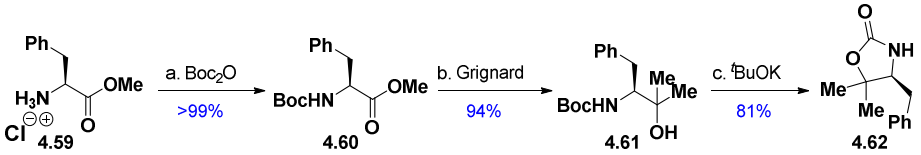

Scheme 4.15 Reagents and conditions: (a) Boc_2O, $^{i}Pr_2EtN$, CH_2Cl_2, 12h. (b) MeMgBr, THF, Et_2O, 0 °C, 12h. (c) ^{t}BuOK, THF, 0 °C, 30 min.

Propionyl chloride was added to auxiliary **4.62** to afford **4.55** in good yield. Evans aldol reaction was thereafter applied, which provided **4.54** in a diastereomeric ratio (dr) of 94:6, calculated by NMR. **4.65** was obtained in a similar fashion, by using the *R*-auxiliary (**4.63**).

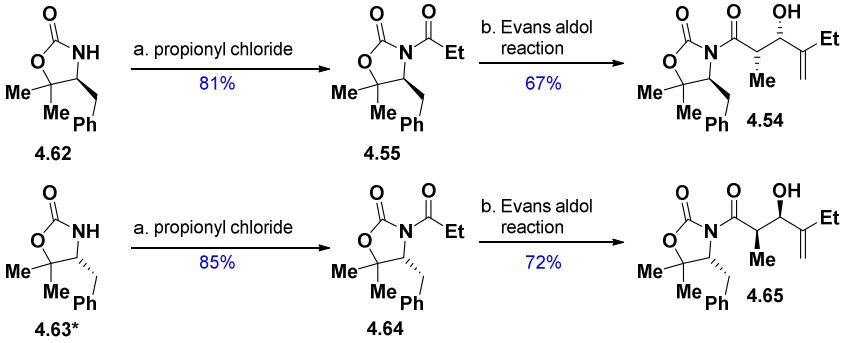

Scheme 4.16 Reagents and conditions: (a) propionyl chloride, n-BuLi, THF, –78 °C to rt, 3h. (b) 2-ethyl acrolein, Bu_2BOTf, DIPEA, CH_2Cl_2, 0 °C to –78 °C to rt, 12h. ***4.63** was obtained from the chemical storage room at CalTech.

The final stereocenter was set by a directed hydrogenation, using [Rh(NBD)(DIPHOS-4)BF_4] as catalyst. High pressure was necessary for obtaining high ee.[203] The reaction was therefore performed in an autoclave reactor, which was assembled in a glove box, since the catalyst was unstable in the presence of oxygen and H_2O.

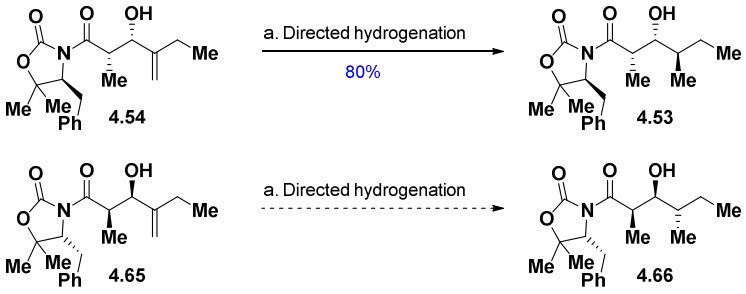

Scheme 4.17 Reagents and conditions: (a) H_2, [Rh(NBD)(DIPHOS-4)]BF_4], CH_2Cl_2, 460 psi, 1h.

The crude compound was filtrated and judged by NMR, a dr of 83:11:6 was calculated. Due to time limitations, the last steps in the syntheses were not performed.

Summary

2-α-phenyl pyrroloindolines were succefully synthesized to investigate the activity in ligand-gated ion channel receptors. An improved synthetic strategy afforded **4.13** in a high ee, and in the synthesis of

compound **4.16**, a minor alterations in the workup conditions provided compound **4.24**. The bulky Cbz protection group in **4.27** was included in the biological tests and **4.17** was obtained in one step from this compound.

From the electrophysiological experiments, compound **4.16** was found to potentiate the effect of GABA on the $GABA_A$ receptor. In addition, **4.16** was also able to activate the $GABA_A$ receptor without addition of an agonist.

Towards the synthesis of SCH 46877, different reaction conditions were investigated in a [2+2] cycloaddition reaction. However, the yields were not improved and a low ee was obtained. Evans aldol reaction was successfully applied and a directed hydrogenation provided **4.53**, which after few modifications can be incorporated in the core structure of SCH 46877.

5 Conclusion and perspectives

In recent years, there has been a huge progress in the field of HDACs and their epigenetic mechanisms. HDAC assays have been developed[169] and recombinant HDAC isozymes can be readily tested. A number of HDAC X-ray structures have been reported and many of these are co-crystalized with an inhibitor. These structures have in particular guided the design of new potent and selective compounds.

Six azumamide analogs have been synthesized, all with the methyl group removed from the 2-position of the β-amino acid. Different amino acids were investigated as well as modifications to the unsaturation in the side chain. The key step in the synthetic route was a cross metathesis on a vinyl amino acid building block, which could be obtained readily from commercially available L-aspartic acid. An optimized position for the cyclization was found, which lead to a significant improved yield.

The azumamide analogs were tested against HDACs from class I, IIb, and IV. The effect of removing the methyl group was clear as all the analogs had a substantial loss of activity. Compounds containing a phenylalanine and a *trans* olefin in the side chain, were slightly less potent.

The effect of removing the methyl group was further investigated by solving the NMR structure and analyzing the docking poses in the crystal structure of HDAC3. Although a minor conformational change in backbone of the desmethylated compounds was observed, the methyl group may have an effect by minimizing movement of the side chain. Docking poses of the analogs showed a similar binding mode as the natural compounds, but a lipophilic interaction with the methyl group in the azumamides might be an important factor.

With the knowledge from the biological activity as well as the NMR structure and docking conformations, it would be interesting to elaborate on azumamide modifications. Incorporation of a larger substituent in the β^2-position (an ethyl, isopropyl, or *tert*-butyl) could provide valuable information of a possible hydrophobic interaction with the enzymes. The direction of the side chain is known to be important for activity; another possible modification could therefore be to constrain the direction of the side chain.

In a related project, azumamide analogs containing a thioester side chain were designed with the focus on obtaining compounds with better cell penetrating capabilities. Using the Wittig reaction, a desmethylated azumamide analog containing a thiol side chain was synthesized and tested against HDAC3. The low HDAC inhibitory activity that was observed was most likely due to an unfavorable length of the side chain. With the establishment of a successful route, syntheses of compounds with an altered length will be readily accessible. Different thioesters can then be explored in relation to cell permeability.

6 Experimental

Experimentals for Chapter 2

General

All chemicals and solvents were analytical grade and used without further purification. Vacuum liquid chromatography (VLC) was performed on silica gel 60 (particle size 0.015−0.040 μm). UPLC−MS analyses were performed on a Waters Acquity ultra high-performance liquid chromatography system. A gradient with eluent I (0.1% HCOOH in water) and eluent II (0.1% HCOOH in acetonitrile) rising linearly from 0% to 95% of II during t = 0.00–2.50 min was applied at a flow rate of 1 mL/min (gradient A) or during t = 0.00–5.20 min (gradient B). Analytical HPLC was performed on a [150 mm × 4.6 mm, C_{18} Phenomenex Luna column (3 μm)] using an Agilent 1100 LC system equipped with a UV detector. A gradient with eluent III (95:5:0.1, water−MeCN−TFA) and eluent IV (0.1% TFA in acetonitrile) rising linearly from 0% to 95% of IV during t = 2−20 min was applied at a flow rate of 1 mL/min (gradient C). Preparative reversed-phase HPLC was performed on a [250 mm × 20 mm, C_{18} Phenomenex Luna column (5 μm, 100 Å)] using an Agilent 1260 LC system equipped with a diode array UV detector and an evaporative light scattering detector (ELSD). A gradient C with eluent III and eluent IV rising linearly from 0% to 95% of IV during t = 5−45 min was applied at a flow rate of 20 mL/min. 1D and 2D NMR spectra were recorded on a Varian Mercury 300 instrument or a Varian INOVA 500 MHz instrument. All spectra were recorded at 298 K. Correlation spectroscopy (COSY) spectra were recorded with a relaxation delay of 1.5 sec before each scan, a spectral width of 6k × 6k, collecting 8 FIDs and 1k × 512 data points. Heteronuclear single quantum coherence (HSQC) spectra were recorded with a relaxation delay of 1.5 sec before each scan, a spectral width of 6k × 25k, collecting 16 FIDs and 1k × 128 datapoints. Heteronuclear 2-bond correlation (H2BC) spectra were recorded with a relaxation delay of 1.5 sec before each scan, a spectral width of 4k × 35k, collecting 16 FIDs at 295 K and 1k × 256 datapoints. Heteronuclear multiple-bond correlation (HMBC) spectra were recorded with a relaxation delay of 1.5 sec before each scan, a spectral width of 6k × 35 k, collecting 32 FIDs and 1k × 256 datapoints. Chemical shifts are reported in ppm relative to deuterated solvent peaks as internal standards (δH, DMSO-d_6 2.50 ppm; δC, DMSO-d_6 39.52 ppm, δH, CD_3OH 3.30 ppm, δH, $CDCl_3$ 7.26 ppm; δC, $CDCl_3$ 77.16 ppm). Coupling constants (J) are given in hertz (Hz). Multiplicities of ^{1}H NMR signals are reported as follows: s, singlet; d, doublet; t, triplet; q, quartet; m, multiplet.

(S)-tert-butyl 3-((tert-butoxycarbonyl)amino)-4-hydroxybutanoate (2.6).[135]

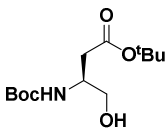

To a solution of Boc-(L)-Asp(^{t}Bu)-OH (15.3 g, 53 mmol) in THF (260 mL) at –30 °C was added N-methylmorpholine (6 mL, 54 mmol) followed by dropwise addition of ^{i}BuOCOCl (7 mL, 54 mmol). The reaction was warmed to –10 °C and stirred for 30 min, then cooled to –30°C where after $NaBH_4$ (7.19 g, 190 mmol) was added in one portion, followed by dropwise addition of MeOH (53 mL). The reaction was stirred at room temperature for 2h, then quenched with sat. aq. NH_4Cl (50 mL). The aqueous phase was extracted with Et_2O (3 × 100 mL) and the combined organic phases were washed with 1M HCl (2 × 100 mL) and brine (2 × 100 mL), dried (Na_2SO_4), filtered, and concentrated. Purification by VLC (0–50% AcOEt in heptane) afforded the desired alcohol **2.6** (10.3 g, 71%) as white crystals. ^{1}H NMR (300 MHz, $CDCl_3$) δ 5.23 (s, 1H), 4.05 – 3.83 (m, 1H), 3.65 (d, J = 4.8 Hz, 2H), 2.87 (brs, 1H), 2.53 (dd,

J = 15.3, 6.2 Hz, 1H), 2.47 (dd, *J* = 15.4, 6.2 Hz, 1H), 1.43 (s, 9H), 1.42 (s, 9H). ^{13}C NMR (75 MHz, $CDCl_3$) *δ* 171.3, 156.0, 81.4, 79.8, 64.9, 49.7, 37.6; $[\alpha]^{25}_D$ = 6°; Mp = 39–42°C.

(S)-tert-butyl 3-((tert-butoxycarbonyl)amino)pent-4-enoate (**2.7**).[135]

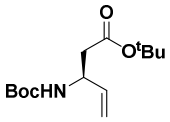

To a solution of oxalyl chloride (0.53 mL, 6.1 mmol) in anhydrous CH_2Cl_2 (25 mL) at –78°C was added DMSO (0.87 mL, 12.2 mmol) in anhydrous CH_2Cl_2 (4 mL) dropwise. After 20 min, **2.6** (954 mg, 3.5 mmol) in anhydrous CH_2Cl_2 (4 mL) was added dropwise and the reaction mixture was stirred for another 20 min followed by dropwise addition of Et_3N (2.6 mL) in anhydrous CH_2Cl_2 (9 mL). The reaction was then warmed to –40°C and stirred for 1 h. The solution was poured onto a mixture of Et_2O/1 M $KHSO_4$ (1:1, 120 mL) where after the organic phase was washed with $KHSO_4$ (1 M, 60 mL). The aqueous phases were then extracted with Et_2O (75 mL) and the combined organic phases were washed with sat. $NaHCO_3$ (2 × 100 mL) and brine (2 × 100 mL), dried ($MgSO_4$, Na_2SO_4), filtered, and concentrated. The crude product was dried under high vacuum for 15 min and used without further purification. ^{1}H NMR (300 MHz, $CDCl_3$) δ 9.64 (s, 1 H), 5.6 (d, 1 H, J = 8.35 Hz), 4.32 (m, 1 H), 2.91 (dd, 1 H, J = 4.84, 17.14 Hz), 2.73 (dd, 1 H, J = 4.98, 17.14 Hz), 1.46 (s, 9 H), 1.43 (s, 9 H).

KHMDS (0.5 M in toluene, 14.1 mL, 7.05 mmol) was added dropwise to a stirred solution of PPh_3CH_3Br (2.63 g, 7.36 mmol) in anhydrous THF (40 mL) at room temperature. After 1h the reaction was cooled to –78 °C and crude the crude aldehyde in anhydrous THF (5 mL) was added dropwise. The reaction was warmed to room temperature over 1h, then stirred for an additional hour. The reaction was quenched with sat. aq. NH_4Cl (25 mL) and extracted with Et_2O (50 mL). The combined organic phases were washed with 1M HCl (2 × 50 mL), sat $NaHCO_3$ (2 × 50 mL), and brine (2 × 50 mL), dried ($MgSO_4$), filtered, and concentrated. Purification by VLC (0–6% AcOEt in heptane) afforded the product (796 mg, 85% 2 steps) as white crystals. ^{1}H NMR (300 MHz, $CDCl_3$) δ 5.81 (ddd, 1 H, *J* = 5.2, 10.4, 17.2 Hz), 5.19 (brs, 1 H), 5.18 (ddd, 1 H, *J* = 1.1, 1.7, 17.2 Hz), 5.11 (ddd, 1 H, *J* = 1.1, 1.6, 10.4 Hz), 4.45 (brs, 1 H), 2.51 (dd, 1 H, *J* = 5.9, 15.3 Hz), 2.45(dd, 1 H, 6, 15.3 Hz), 1.42 (s, 18 H)); ^{13}C NMR (75 MHz, CDCl3) δ 170.6, 155.2, 137.5, 115.2, 81.3, 79.5, 49.6, 40.5, 28.5, 28.2; $[\alpha]^{25}_D$ = 21.5°; Mp = 37–39°C.

(S)-3-((tert-butoxycarbonyl)amino)pent-4-enoic acid (**2.8**).[135]

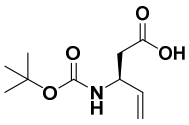

To **2.7** (432.9 mg, 1.6 mmol) in THF (10 mL) and MeOH (10 mL) was added 1 M LiOH (10 mL). The reaction was stirred at 50°C for 7 h, and then quenched with 1M HCl (10 mL). The aqueous phase was extracted with Et_2O (3 x 40 mL) and concentration to give the carboxylic acid (313 mg, 91%) as yellow crystals. ^{1}H NMR (300 MHz, $CDCl_3$) δ 5.86 (ddd, 1 H, *J* = 5.4, 10.4, 17.2 Hz), 5.22 (ddd, 1 H, *J* = 0.9, 1.6, 17.2 Hz), 5.18 - 5.13 (m, 1 H), 5.16 (brs, 1 H), 4.51 (brs, 1 H), 2.66 (d, 1 H, *J* = 4.7 Hz), 1. 45 (s, 9 H); ^{13}C NMR (300 MHz, $CDCl_3$) δ 176.3, 155.4, 137, 115.7, 80, 49.2, 39.1, 28.4. ; $[\alpha]^{25}_D$ = +19°; Mp = 58–61°C.

((R)-3-aminopent-4-enoyl)-D-valine-D-alanine-D-tryptophan (**2.9**).

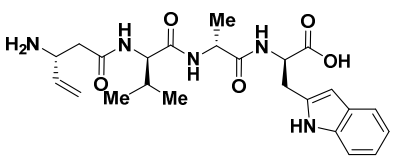

To a polystyrene 2-chlorotrityl resin in a fritted syringe, was added Fmoc-D-Trp-OH (2 equiv) and ^{i}Pr$_2$EtN (4 equiv) in anhydrous CH_2Cl_2. The reaction was put on a tilting table for 1h, then washed with CH_2Cl_2 (x3). The resin was capped with a mixture of CH_2Cl_2:MeOH: ^{i}Pr$_2$EtN (4:1:0.5) for 20 min then was washed with DMF (x3), MeOH (x3), and CH_2Cl_2 (x3). The Fmoc group was removed with 20% piperidine in DMF (2x 30 min), then with DBU:piperidine:DMF (2:2:96) (15

min), and finally washed with DMF (x3), MeOH (x3), and CH_2Cl_2 (x3). Fmoc-D-Ala-OH (3 equiv) was preactivated with HATU (3 equiv) and 2,6-lutidine (6 equiv) in DMF for 5 min, then added to the resin. The reaction was put on a tilting table for 4h, then washed with DMF (x3), MeOH (x3), and CH_2Cl_2 (x3). The cycle was repeated with Fmoc-D-Val-OH, and **2.8**. Cleavage of the tetrapeptide was done with 50% TFA in CH_2Cl_2 (2x 30 min). The solvent was evaporated until a small volume was left, then triturated with Et_2O. The peptide was used without further purification. ^{1}H NMR (300 MHz, DMSO-D_6) δ 10.86 (s, 1H), 8.34 – 7.94 (m, 6H), 7.52 (d, *J* = 7.6 Hz, 1H), 7.33 (d, *J* = 8.0 Hz, 1H), 7.15 (d, *J* = 2.2 Hz, 1H), 7.06 (t, *J* = 8.0 Hz, 1H), 6.97 (t, *J* = 7.4 Hz, 1H), 5.79 (ddd, *J* = 17.3, 10.6, 6.7 Hz, 1H), 5.31 (t, *J* = 14.5 Hz, 2H), 4.56 – 4.40 (m, 1H), 4.40 – 4.27 (m, 1H), 4.27 – 4.14 (m, 1H), 3.99 (brs, 1H), 3.09 (ddd, *J* = 22.3, 14.7, 6.5 Hz, 2H), 2.76 – 2.53 (m, 2H), 1.93 (d, *J* = 6.6 Hz, 1H), 1.20 (d, *J* = 7.0 Hz, 3H), 0.93 – 0.64 (m, 6H).

(3R,6R,9R,13S)-3-((1H-indol-2-yl)methyl)-9-isopropyl-6-methyl-13-vinyl-1,4,7,10-tetraazacyclotridecane-2,5,8,11-tetraone (**2.10**)

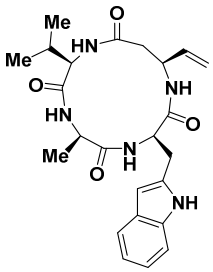

To **2.9** (20.8 mg, 0.044 mmol) in DMF (87 mL) was added ^{i}Pr$_2$EtN (60.9 µL, 0.35 mmol) followed by HATU (33.5 mg, 0.088 mmol). The reaction was stirred at room temperature for 15h and the solvent was then evaporated. Purification by preparative HPLC gave the desired product as white needle crystals (2.9 mg, 15%). ^{1}H NMR (500 MHz, DMSO) δ 10.88 (s, 14H), 7.90 (d, 1H, *J* = 7.8 Hz), 7.84 (d, 16H, *J* = 6.5 Hz), 7.68 (d, *J* = 11.2 Hz, 1H), 7.60 – 7.45 (m, 34H), 7.36 (dt, *J* = 28.4, 8.0 Hz, 50H), 7.24 (d, *J* = 9.8 Hz, 2H), 7.13 – 7.02 (m, 34H), 7.02 – 6.92 (m, 18H), 5.93 (s, 1H), 5.84 (ddd, *J* = 17.2, 10.4, 4.6 Hz, 15H), 5.13 – 4.99 (m, 34H), 4.40 (s, 32H), 4.32 (dq, *J* = 14.7, 7.3 Hz, 16H), 4.09 (d, *J* = 5.3 Hz, 9H), 3.97 – 3.93 (m, 1H), 3.82 (s, 16H), 3.32 (s, 26H), 3.17 (d, *J* = 5.2 Hz, 32H), 3.06 (d, *J* = 2.5 Hz, 33H), 2.55 – 2.46 (m, 159H), 1.96 (d, *J* = 6.6 Hz, 16H), 1.17 (d, *J* = 7.4 Hz, 46H), 0.92 (s, 89H), 0.81 (d, *J* = 6.8 Hz, 7H), 0.65 (d, *J* = 6.3 Hz, 3H). HRMS calc'd for $C_{29}H_{39}N_5O_6H^+$ [M+H$^+$] = 554.2973, found 554.2977.

2-isopropoxy-5-nitrobenzaldehyde (**2.13**).[204]

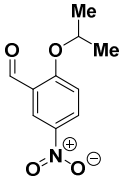

2-Iodopropane (0.59 mL, 5.91 mmol) was added to 2-hydroxy-5-nitro-benzaldehyde (494.2 mg, 2.96 mmol), K_2CO_3 (1.64 g, 11.84 mmol), and Cs_2CO_3 (386 mg, 1.19 mmol) in DMF (10 mL). The reaction was heated to 60°C and stirred for 24 h. The reaction was diluted with AcOEt (10 mL), washed with 1M HCl (2 x 20 mL), $NaHCO_3$ (2 x 20 mL) and brine (2 x 20 mL), dried (Na_2SO_4), filtered and concentrated. Purification by VLC (0–15% AcOEt in heptane) gave the product (520 mg, 84%) as a white solid. ^{1}H NMR (300 MHz, $CDCl_3$): δ 10.46 (s, 1 H), 8.7 (d, 1 H, *J* = 2.9 Hz), 8.4 (dd, 1 H, *J* = 2.9, 9.2 Hz), 7.09 (d, 1 H, *J* = 9.3 Hz), 4.84 (h, 1 H, *J* = 6.1 Hz), 1.48 (d, 6 H, *J* = 6.1 Hz); ^{13}C NMR (300 MHz, $CDCl_3$) δ 188, 164.5, 141.1, 130.6, 125.1, 124.7, 113.8, 72.8, 21.9.

1-isopropoxy-4-nitro-2-vinylbenzene (**2.14**).[204]

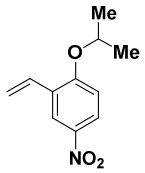

To Ph_3PCH_3Br (1.04 g, 2.9 mmol) in anhydrous THF (20 mL) was added 0.5 M KHMDS in toluene (5.5 mL, 2.74 mmol) dropwise. The reaction was cooled to -78°C and **2.13** in anhydrous THF (2.5 mL) was added dropwise. The reaction was warmed to room temperature over 30 min and quenched with NH_4Cl (20 mL). The aqueous phase was extracted with Et_2O (2 x 25 mL), washed with $NaHCO_3$ (2 x 20 mL) and brine (2 x 20 mL), dried (Na_2SO_4), filtered and concentrated. Purification by VLC (0–15% AcOEt in heptane) gave the desired product (276 mg, 92%) as orange crystals. ^{1}H NMR (300 MHz, $CDCl_3$): δ 8.35 (d, 1 H, *J* = 2.8 Hz), 8.1 (dd, 1 H, *J* = 2.8, 9.1 Hz), 6.99 (dd, 1 H, 11.2, 17.8 Hz),

6.9 (d, 1 H, *J* = 9.2 Hz), 5.86 (dd, 1 H, 1.1, 17.7 Hz), 5.39 (dd, 1 H, 1.1, 11.2 Hz), 4.7 (h, 1 H, 6 Hz), 1.41 (d, 6 H, 6.1 Hz); ^{13}C NMR (300 MHz, $CDCl_3$) δ 160.1, 141.1, 130.2, 128.2, 124.7, 122.5, 116.9, 112.3, 71.6, 22.0; Mp = 31°C - 33°C.

(1,3-dimesitylimidazolidin-2-yl)(2-isopropoxy-5-nitrobenzylidene)ruthenium(V) chloride (**2.11**).[204]

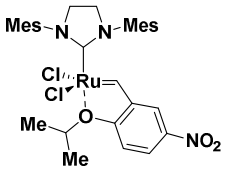

Grubbs catalyst 2nd generation (148 mg, 0.17 mmol) and CuCl (18.4 mg, 0.17 mmol) in anhydrous CH_2Cl_2 (9 mL) were transfered to a schlenk tube and degassed with Ar. **2.14** in anhydrous CH_2Cl_2 (4 mL) was added and the reaction stirred at 30°C for 24 h. Purification by VLC (0–25%) gave the desired product (48.5 mg, 42%) as a green solid. ^1H NMR (300 MHz, $CDCl_3$) δ 16.47 (s, 1H), 8.42 (dd, 1H, *J* = 9.1, 2.7 Hz), 7.82 (d, 1H, *J* = 2.7 Hz), 7.1 (s, 4H), 6.89 (d, 1H, *J* = 9.0 Hz), 4.98 (sept, 1H, *J* = 6.21 Hz), 4.21 (s, 4H), 2.46 (s, 9H), 2.44 (s, 9H), 1.30 (d, *J* = 6.1 Hz, 6H).

(S,E)-1-tert-butyl 9-methyl 3-((tert-butoxycarbonyl)amino)non-4-enedioate (**2.12**)

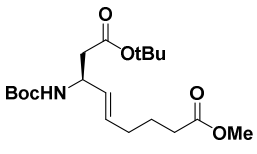

General methods for the cross methatesis.

To **2.7** in degassed, anhydrous CH_2Cl_2 was added methyl 5-hexenoate (3 equiv), followed by a catalyst. The reaction was heated to reflux 17-20h, evaporated on silica and purified by VLC (0–40% AcOEt in heptane) to obtain the product (12-67%) as a brown oil.

Entry 1

The compound was synthesized according to the general procedure, using Grubbs catalyst 1st generation (0.1 equiv) as the catalyst. Yield: 18 mg, 11%.

Entry 2

The compound was synthesized according to the general procedure, using Grubbs catalyst 2nd generation (0.05 equiv) as the catalyst. Yield: 79 mg, 54%.

Entry 3

The compound was synthesized according to the general procedure, using Grubbs catalyst 2nd generation (0.1 equiv) as the catalyst. Yield: 89 mg, 62%.

Entry 4

The compound was synthesized according to the general procedure, using Hoveyda Grubbs catalyst 1st generation (0.1 equiv) as the catalyst. Yield: 17 mg, 12%.

Entry 5

The compound was synthesized according to the general procedure, using Hoveyda Grubbs catalyst 2nd generation (0.1 equiv) as the catalyst. Yield: 225 mg, 67%.

Entry 6

The compound was synthesized according to the general procedure, using Zhan catalyst 1B (0.1 equiv) as the catalyst. Yield: 92 mg, 62%.

Entry 7

The compound was synthesized according to the general procedure, using **2.11** (0.1 equiv) as the catalyst. Yield: 135 mg, 52%.

^{1}H NMR (300 MHz, CDCl3) δ 5.58 (dtd, *J* = 13.6, 6.3, 0.8 Hz, 1H), 5.43 (dd, *J* = 15.5, 5.7 Hz, 1H), 5.14 (brs, 1H), 4.41 (brs, 1H), 3.66 (s, 3H), 2.47 (d, *J* = 5.9 Hz, 2H), 2.29 (t, *J* = 7.5 Hz, 2H), 2.05 (q, *J* = 7.2 Hz, 2H), 1.69 (p, *J* = 7.4 Hz, 2H), 1.43 (s, 18H). ^{13}C NMR (300 MHz, $CDCl_3$) δ 173.9, 170.5, 155, 130.4, 130.2, 81, 79.3, 51.5, 49.1, 40.8, 33.2, 31.4, 28.4, 28, 24.2; HRMS calc'd for $C_{19}H_{33}NO_6H^+$ [M+H$^+$] 372.2381, found 372.2379; $[\alpha]^{25}_D$ = –1.1°.

(S,E)-3-((tert-butoxycarbonyl)amino)-9-methoxy-9-oxonon-4-enoic acid (2.13).

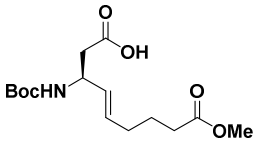

To **2.12** (212 mg, 0.57 mmol) in CH_2Cl_2 (20 mL) was added TFA (6 mL, 78.2 mmol). The reaction was stirred at room temperature for 2h and the solvent was then evaporated to give the crude product as an orange oil. ^{1}H NMR (300 MHz, $CDCl_3$) δ 7.87 (brs, 3H), 6.85 (brs, 1H), 6.07 – 5.74 (m, 1H), 5.51 (dd, *J* = 15.3, 7.6 Hz, 1H), 4.06 (s, 1H), 3.65 (s, 3H), 3.02 – 2.56 (m, 2H), 2.30 (t, *J* = 7.4 qHz, 2H), 2.19 – 1.94 (m, 2H), 1.85 – 1.60 (m, 2H).

To the crude amino acid (176 mg, 0.53 mmol) and ^{i}Pr$_2$NEt (0.24 mL, 1.38 mmol) in CH_2Cl_2 (2 mL) was added di-tert-butyl dicarbonate (159 μL, 69 mmol) dropwise. The reaction was stirred at room temperature for 19 h, then purified by VLC (0–40% AcOEt in heptane) to give the product (148 mg, 84% 2 steps) as a clear oil. ^{1}H NMR (300 MHz, $CDCl_3$) δ 5.60 (dt, *J* = 7.1, 6.5 Hz, 1H), 5.47 (dd, *J* = 15.5, 5.9 Hz, 1H), 5.15 (brs, 1H), 4.44 (brs, 1H), 3.66 (s, 3H), 2.62 (d, *J* = 5.1 Hz, 2H), 2.30 (dd, *J* = 16.6, 9.2 Hz, 3H), 2.06 (q, *J* = 7 Hz, 2H), 1.69 (dq, *J* = 14.3, 7.3 Hz, 2H), 1.44 (s, 9H); ^{13}C NMR (75 MHz, $CDCl_3$) δ 176, 174.3, 131.2, 129.8, 51.7, 39.6, 33.3, 31.5, 28.5, 24.3; HRMS calc'd for $C_{15}H_{25}NO_6H^+$ [M+H$^+$] = 316.1755, found 316.1760; $[\alpha]^{25}_D$ = –4°.

(R)-3-((tert-butoxycarbonyl)amino)-9-methoxy-9-oxononanoic acid (2.14).

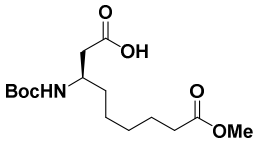

A solution of **2.13** (83 mg, 0.26 mmol) in THF (3 mL) was purged with argon. 10 wt. % Pd/C (10 mg, 10 wt. %) was then added and the mixture was purged with H_2 for 5 min then kept under H_2 atmosphere and stirred for 17h. The mixture was filtered on celite and evaporated to obtain the product (98%, 81 mg) as a clear oil. ^{1}H NMR (300 MHz, $CDCl_3$) δ 4.90 (brs, 1H), 3.88 (brs, 1H), 3.66 (s, 3H), 2.55 (brs, 2H), 2.30 (t, *J* = 7.4 Hz, 2H), 1.87 – 0.61 (m, 8H), 1.44 (s, 9H); ^{13}C NMR (75 MHz, $CDCl_3$) δ 176.7, 174.4, 155.6, 79.5, 51.6, 47.4, 39.2, 34.4, 34, 28.8, 28.4, 25.9, 24.8; HRMS calc'd for $C_{15}H_{27}NO_6H^+$ [M+H$^+$] = 318.1911, found 318.1912; $[\alpha]^{25}_D$ = +5.6°.

(E)-6-((2R,5R,8R,11S)-8-benzyl-2-isopropyl-5-methyl-3,6,9,13-tetraoxo-1,4,7,10-tetraazacyclotridecan-11-yl)hex-5-enoic acid (2.1a).

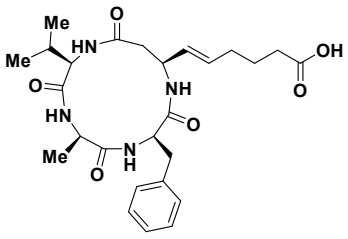

2.13 (31.3 mg, 0.1 mmol), HATU (38.8 mg, 0.1 mmol) and 2,6-lutidine (23 µL, 0.2 mmol) in DMF (1.5 mL) were preactivated for 5 min. and added to a tripeptide (Val-Ala-Phe) on solid support. After 18 h, the peptide was washed with DMF (x3), MeOH (x3) and CH_2Cl_2 (x3). The peptide was cleaved with 50% TFA in CH_2Cl_2 (2x 30 min) and evaporated. Precipitated in Et_2O (8 mL) obtained a crude tetrapeptide (88 mg), which was dissolved in DMF (130 mL). ^{i}Pr$_2$NEt (140 µL, 0.8 mmol) was added followed by HATU (78 mg, 0.2 mmol). The reaction was stirred for 65h and then evaporated. LiOH (32 mg, 1.3 mmol) in THF:H_2O (20 mL,1:1) was added to the crude compound and the mixture was stirred 7h. Preparative HPLC gave the desired product (3.8 mg, 7%, over 4 steps) as a white solid. ^{1}H NMR (500 MHz, DMSO) δ 12.03 (s, 1H), 7.87 (d, *J* = 6.8 Hz, 1H), 7.61 (d, *J* = 9.7 Hz, 1H), 7.40 (d, *J* = 7.5 Hz, 2H), 7.33 – 7.11 (m, 5H), 5.46 – 5.41 (m, 2H), 4.41 – 4.31 (m, 1H), 4.31 – 4.24 (m, 2H), 3.82 (t, *J* = 6.6 Hz, 1H),

3.06 – 2.81 (m, 2H), 2.62 – 2.48 (m, 2H), 2.20 (t, *J* = 7.4 Hz, 2H), 2.07 – 1.97 (m, 2H), 1.97 – 1.87 (m, 1H), 1.66 – 1.48 (m, 2H), 1.15 (d, *J* = 7.3 Hz, 3H), 0.92 (dd, *J* = 9.0, 7.0 Hz, 6H); HRMS calc'd for $C_{26}H_{36}N_4O_6H^+$ [M+H$^+$] = 501.2708, found 501.2716; Analytical HPLC: (gradient A; retention time: 11.6 min, purity: >99%, 230 nm)

(E)-6-((2R,5R,8R,11S)-8-(4-hydroxybenzyl)-2-isopropyl-5-methyl-3,6,9,13-tetraoxo-1,4,7,10-tetraazacyclotridecan-11-yl)hex-5-enoic acid (**2.1b**).

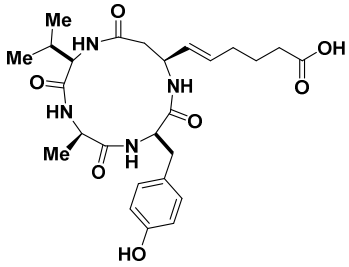

2.13 (31.3 mg, 0.1 mmol), HATU (38.8 mg, 0.1 mmol) and 2,6-lutidine (23 µL, 0.2 mmol) in DMF (1.5 mL) were preactivated for 5 min. and added to a tripeptide (Val-Ala-Tyr) on solid support. After 18 h, the peptide was washed with DMF (x3), MeOH (x3) and CH_2Cl_2 (x3). The peptide was cleaved with 50% TFA in CH_2Cl_2 (2x 30 min.) and evaporated. Precipitated in Et_2O (8 mL) obtained a crude tetrapeptide (89 mg), which was dissolved in DMF (130 mL). $^{i}Pr_2NEt$ (140 µL, 0.8 mmol) was added followed by HATU (78 mg, 0.2 mmol). The reaction was stirred for 65h and then evaporated. An unsuccessful purification gave 7 mg of impure compound. LiOH (1.3 mg, 0.054 mmol) in THF:H_2O (20 mL,1:1) was added to the mixture and stirred 18h. An additional amount of LiOH (4 mg, 0.15 mmol) was added an the mixture was stirred 7h, then 63h at 5°C. Preparative HPLC gave the desired product (4.2 mg, 8% over 4 steps) as a white solid. ^{1}H NMR (500 MHz, DMSO) δ 9.23 (s, 1H), 7.85 (d, *J* = 6.7 Hz, 1H), 7.52 (d, *J* = 9.7 Hz, 1H), 7.38 (d, *J* = 9.9 Hz, 1H), 7.31 (d, *J* = 7.3 Hz, 1H), 6.95 (d, *J* = 8.4 Hz, 2H), 6.66 (d, *J* = 8.4 Hz, 2H), 5.47 – 5.39 (m, 2H), 4.40 – 4.33 (m, 1H), 4.29 (dq, *J* = 14.9, 7.6 Hz, 1H), 4.19 (td, *J* = 9.3, 6.0 Hz, 1H), 3.81 (t, *J* = 6.5 Hz, 1H), 2.84 (dd, *J* = 13.9, 5.8 Hz, 1H), 2.75 (dd, *J* = 13.8, 9.1 Hz, 1H), 2.58 – 2.40 (m, 2H), 2.20 (t, *J* = 7.4 Hz, 2H), 2.11 – 1.98 (m, 2H), 1.98 – 1.90 (m, 1H), 1.65 – 1.48 (m, 2H), 1.16 (d, *J* = 7.4 Hz, 3H), 0.92 (dd, *J* = 8.3, 7.2 Hz, 6H); HRMS calc'd for $C_{26}H_{36}N_4O_7H^+$ [M+H$^+$] = 517.2657, found 517.2660; Analytical HPLC: (gradient A; retention time: 10.3 min, purity: >99%, 230 nm).

(E)-6-((2R,5R,8R,11S)-8-((1H-indol-2-yl)methyl)-2-isopropyl-5-methyl-3,6,9,13-tetraoxo-1,4,7,10-tetraazacyclotridecan-11-yl)hex-5-enoic acid (**2.1c**)

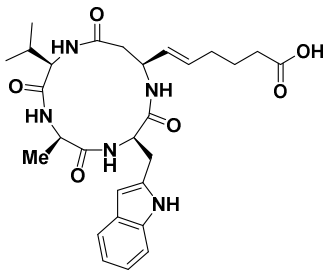

2.13 (31.3 mg, 0.1 mmol), HATU (38.8 mg, 0.1 mmol) and 2,6-lutidine (23 µL, 0.2 mmol) in DMF (1.5 mL) were preactivated for 5 min. and added to a tripeptide (Val-Ala-Trp) on solid support. After 18 h, the peptide was washed with DMF (x3), MeOH (x3) and CH_2Cl_2 (x3). The peptide was cleaved with 50% TFA in CH_2Cl_2 (2 times 30 min.) and evaporated. Precipitated in Et_2O (8 mL) obtained a crude tetrapeptide, which was dissolved in DMF (130 mL). $^{i}Pr_2NEt$ (140 µL, 0.8 mmol) was added followed by HATU (78 mg, 0.2 mmol). The reaction was stirred for 65h and then evaporated. An unsuccessful purification gave 3 mg of impure compound. LiOH (0.5 mg, 0.02 mmol) in THF:H_2O (20 mL,1:1) was added and the mixture was stirred 18h. An additional amount of LiOH (1 mg, 0.04 mmol) was added and the mixture was stirred 5h. Preparative HPLC gave the desired product (1.4 mg, 3% over 4 steps) as a white solid. ^{1}H NMR (500 MHz, DMSO) δ 7.82 (d, *J* = 6.8 Hz, 1H), 7.55 (d, *J* = 9.7 Hz, 1H), 7.50 (d, *J* = 7.8 Hz, 1H), 7.45 (d, *J* = 9.8 Hz, 1H), 7.37 (d, *J* = 7.3 Hz, 1H), 7.34 (d, *J* = 8.1 Hz, 1H), 7.16 – 7.04 (m, 2H), 6.98 (t, *J* = 7.5 Hz, 1H), 5.47 – 5.31 (m, 2H), 4.45 – 4.24 (m, 3H), 3.82 (t, *J* = 6.5 Hz, 1H), 3.09 – 3.00 (m, 2H), 2.48 – 2.37 (m, 2H), 2.19 (t, *J* = 7.3 Hz, 2H), 2.06 – 1.87 (m, 4H), 1.59 – 1.46 (m, 2H), 1.17 (d, *J* = 7.3 Hz, 3H), 0.92 (t, *J* = 6.4 Hz, 6H); HRMS calc'd for $C_{28}H_{37}N_5O_6H^+$ [M+H$^+$] = 540.2817, found 540.2807; Analytical HPLC: (gradient A; retention time: 11.66 min, purity: >99%, 230 nm)

6-((2R,5R,8R,11R)-8-benzyl-2-isopropyl-5-methyl-3,6,9,13-tetraoxo-1,4,7,10-tetraazacyclotridecan-11-yl)hexanoic acid (**2.2a**)

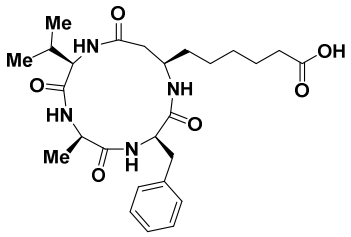

2.14 (25.4 mg, 0.08 mmol), HATU (36.5 mg, 0.1 mmol) and 2,6-lutidine (18 µL, 0.16 mmol) in DMF (1.5 mL) were preactivated for 5 min. and added to a tripeptide (Val-Ala-Phe) on solid support. After 18 h, the peptide was washed with DMF (x3), MeOH (x3) and CH_2Cl_2 (x3). The peptide was cleaved with 50% TFA in CH_2Cl_2 (2x 30 min.) and evaporated. Precipitated in Et_2O (8 mL) obtained a crude tetrapeptide, which was dissolved in DMF (170 mL). $^{i}Pr_2NEt$ (140 µL, 0.8 mmol) was added followed by HATU (61 mg, 0.16 mmol). The reaction was stirred for 24h and then evaporated. LiOH (34 mg, 1.5 mmol) in THF:H_2O (15 mL, 1:2) was added to the crude compound and stirred 4h, an additional amount of LiOH (19 mg, 0.8 mmol) was added and the reaction was stirred 5h. As the reaction had not finished, LiOH (35 mg, 0.8 mmol) was added and the reaction was stirred 17h. Preparative HPLC gave the desired product (4.2 mg, 10% over 4 steps) as a white solid. ^{1}H NMR (500 MHz, DMSO) δ 11.97 (s, 1H), 7.78 (d, *J* = 6.6 Hz, 1H), 7.55 (d, *J* = 8.7 Hz, 1H), 7.41 (d, *J* = 8.4 Hz, 1H), 7.34 – 7.10 (m, 6H), 4.31 – 4.20 (m, 2H), 3.81 (t, *J* = 7.0 Hz, 2H), 2.93 (dd, *J* = 13.7, 6.7 Hz, 1H), 2.84 (dd, *J* = 13.7, 8.5 Hz, 1H), 2.59 – 2.45 (m, 1H), 2.41 – 2.27 (m, 1H), 2.19 (t, *J* = 7.4 Hz, 2H), 1.94 (dq, *J* = 13.4, 6.7 Hz, 1H), 1.58 – 1.21 (m, 8H), 1.17 (d, *J* = 7.3 Hz, 3H), 0.92 (dd, *J* = 9.1, 7.0 Hz, 6H); HRMS calc'd for $C_{26}H_{38}N4O_6H^+$ [M+H$^+$] = 503.2864, found 503.2870, Analytical HPLC: (gradient B; retention time: 18.3 min, purity: >99%, 230 nm)

6-((2R,5R,8R,11R)-8-(4-hydroxybenzyl)-2-isopropyl-5-methyl-3,6,9,13-tetraoxo-1,4,7,10-tetraazacyclotridecan-11-yl)hexanoic acid (**2.2b**)

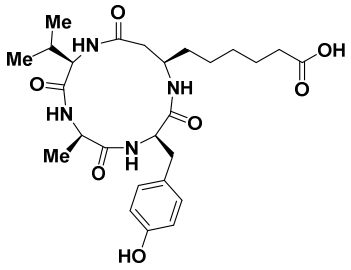

2.14 (25.4 mg, 0.08 mmol), HATU (36.5 mg, 0.1 mmol) and 2,6-lutidine (18 µL, 0.16 mmol) in DMF (1.5 mL) were preactivated for 5 min. and added to a tripeptide (Val-Ala-Tyr) on solid support. After 18 h, the peptide was washed with DMF (x3), MeOH (x3) and CH_2Cl_2 (x3). The peptide was cleaved with 50% TFA in CH_2Cl_2 (2x 30 min.) and evaporated. Precipitated in Et_2O (8 mL) obtained a crude tetrapeptide, which was dissolved in DMF (170 mL). $^{i}Pr_2NEt$ (140 µL, 0.8 mmol) was added followed by HATU (61 mg, 0.16 mmol). The reaction was stirred for 24h and then evaporated. LiOH (95 mg, 1.5 mmol) in THF:H_2O (15 mL, 1:2) was added to the crude compound and stirred 24h, an additional amount of LiOH (37 mg, 1.5 mmol) was added and the reaction was stirred 24h. Preparative HPLC gave the desired product (3.1 mg, 7% over 4 steps) as a white solid. ^{1}H NMR (500 MHz, DMSO) δ 9.21 (s, 1H), 7.77 (d, *J* = 7.0 Hz, 1H), 7.44 (d, *J* = 9.5 Hz, 1H), 7.37 (d, *J* = 9.8 Hz, 1H), 7.17 (d, *J* = 7.4 Hz, 1H), 6.94 (d, *J* = 8.4 Hz, 2H), 6.65 (d, *J* = 8.4 Hz, 2H), 4.26 (dq, *J* = 14.8, 7.3 Hz, 1H), 4.19 – 4.14 (m, 1H), 4.00 – 3.74 (m, 2H), 2.80 (dd, *J* = 13.8, 6.6 Hz, 1H), 2.72 (dd, *J* = 13.8, 8.4 Hz, 1H), 2.49 (dd, *J* = 8.5, 6.8 Hz, 1H), 2.32 (dd, *J* = 14.5, 3.2 Hz, 1H), 2.20 (t, *J* = 7.3 Hz, 2H), 1.99 – 1.90 (m, 1H), 1.67 – 1.21 (m, 8H), 1.18 (d, *J* = 7.4 Hz, 3H), 0.92 (dd, *J* = 8.5, 7.1 Hz, 6H); HRMS calc'd for $C_{26}H_{38}N4O7H^+$ [M+H$^+$] = 519.2813, found 519.2813; Analytical HPLC: (gradient A; retention time: 10.4 min, purity: >99%, 230 nm)

(R)-3-((((9H-fluoren-9-yl)methoxy)carbonyl)amino)-9-methoxy-9-oxononanoic acid (**2.19**)

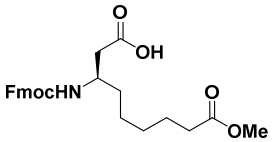

To **2.14** (171 mg, 0.54 mmol) in CH_2Cl_2 (20 mL) was added TFA (5 mL). After stirring at room temperature for 4.5h the compound was concentrated and used without further purification.

The crude compound was dissolved in H_2O (5 mL) at 0°C followed by addition of K_2CO_3 (127 mg, 0.92 mmol). FmocOSu (202 mg, 0.59 mmol) in 1,4-dioxane (5 mL) was added and the reaction was allowed to warm to rt. After stirring for 2.5h the reaction was diluted with H_2O (10 mL) and concentrated. The aqueous phase was washed with Et_2O (2 x 30 mL), acidified with 1M HCl (10 mL), then extracted with Et_2Cl_2 (4 X 30 mL) and concentrated. Purification by VLC (0 – 30% AcOEt/heptanes + 0.2% AcOH) gave the desired product (57% in 2 steps, 127 mg) as a white solid. ^{1}H NMR (300 MHz, cdcl$_3$) δ 7.75 (d, *J* = 7.4 Hz, 2H), 7.58 (d, *J* = 7.4 Hz, 2H), 7.38 (t, *J* = 7.4 Hz, 2H), 7.30 (t, *J* = 7.4 Hz, 2H), 5.22 (d, *J* = 9.1 Hz, 1H), 4.39 (d, *J* = 6.8 Hz, 2H), 4.21 (t, *J* = 6.8 Hz, 1H), 3.96 (d, *J* = 5.5 Hz, 1H), 3.65 (s, 3H), 2.70 – 2.48 (m, 2H), 2.29 (s, 2H), 1.58 (s, 4H), 1.33 (s, 4H); HRMS calc'd for $C_{25}H_{29}NO_6H^+$ [M+H$^+$] = 440.2068, found 440.2080; $[\alpha]^{25}_D$ = +8.5°.

6-((2R,5R,8R,11R)-8-((1H-indol-2-yl)methyl)-2-isopropyl-5-methyl-3,6,9,13-tetraoxo-1,4,7,10-tetraazacyclotridecan-11-yl)hexanoic acid (**2.2c**).

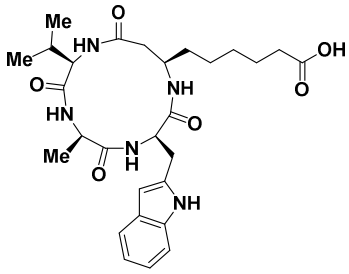

2.19 (95 mg, 0.22 mmol) was dissolved in anhydrous CH_2Cl_2 (5 mL) and ^{i}Pr$_2$NEt (75 µL, 0.43 mmol), then loaded to a trityl resin. The resin was washed with CH_2Cl_2 (x3), then capped with ^{i}Pr$_2$NEt:MeOH:CH_2Cl_2 (1:2:7). Loading of the resin was calculated to 0.7 mmol/g, corresponding to 96 µmol of **2.19**. Standard conditions for SPPS was used to attach D-Trp(Boc), D-Ala, and D-Val. The peptide was cleaved with CH_3CO_2H:CF_3CH_2OH:CH_2Cl_2 (1:1:3) for 2.5h, and evaporated. Precipitation in Et_2O (8 mL) obtained a crude tetrapeptide. Half of the crude compound was dissolved in DMF (170 mL) and ^{i}Pr$_2$NEt (100 µL, 0.6 mmol) was added followed by HATU (57 mg, 0.15 mmol). The reaction was stirred for 2h and then evaporated. LiOH (7 mg, 0.3 mmol) in THF:H_2O (5 mL, 1:1) was added to the crude compound and stirred 5h, where after additional LiOH (48 mg, 2 mmol) was added and the reaction was stirred 24h. The crude mixture was evaporated, then dissolved in CH_2Cl_2 (6 mL) followed by addition of TFA (6 mL). The reaction was stirred for 30 min, then evaporated. Preparative HPLC gave the desired product (12.4 mg, 48% over 12 steps) as a white solid. ^{1}H NMR (500 MHz, DMSO) δ 11.97 (s, 1H), 10.81 (d, *J* = 56.2 Hz, 1H), 7.75 (d, *J* = 6.8 Hz, 1H), 7.57 – 7.41 (m, 3H), 7.33 (d, *J* = 8.0 Hz, 1H), 7.22 (d, *J* = 7.2 Hz, 1H), 7.11 – 7.01 (m, 2H), 7.00 – 6.93 (m, 1H), 4.43 – 4.32 (m, 1H), 4.28 (dq, *J* = 15.1, 7.4 Hz, 1H), 3.87 – 3.77 (m, 2H), 3.04 (dd, *J* = 14.7, 6.8 Hz, 1H), 2.99 (dd, *J* = 14.8, 7.6 Hz, 1H), 2.55 – 2.45 (m, 1H), 2.31 (dd, *J* = 14.4, 3.3 Hz, 1H), 2.19 (t, *J* = 7.3 Hz, 2H), 2.03 – 1.85 (m, 1H), 1.54 – 1.10 (m, 8H), 1.18 (d, *J* = 7.4 Hz, 3H), 0.91 (t, *J* = 6.5 Hz, 6H); HRMS calc'd for $C_{28}H_{39}N_5O_6H^+$ [M+H$^+$] = 542.2973, found 542.2978; Analytical HPLC: (gradient A; retention time: 11.98 min, purity: >99%, 230 nm)

Biochemical profiling

Assay Materials

HDAC1 (Purity >45% by SDS-PAGE according to the supplier), HDAC4 (Purity >90% by SDS-PAGE according to the supplier), and HDAC 7 (Purity >90% by SDS-PAGE according to the supplier) were purchased from Millipore (Temecula, CA 92590). HDAC2 used for dose–response experiments (Full length, purity ≥94% by

SDS-PAGE according to the supplier) and HDAC 5 (Full length, purity ≥4% by SDS-PAGE according to the supplier) and HDAC8 used for dose-response experiments (Purity ≥90% by SDS-PAGE according to the supplier) were purchased from BPS Bioscience (San Diego, CA 92121). HDAC2 used for initial screening experiments (Full length, purity 50% by SDS-PAGE according to the supplier), HDAC3-NCoR1* complex (Purity 90% by SDS-PAGE according to supplier), HDAC6 (Purity >90% by SDS-PAGE according to the supplier), HDAC8 for initial screening experiments (Purity >50% by SDS-PAGE according to the supplier), HDAC10 (Purity >50% by SDS-PAGE according to the supplier), and HDAC11 (Purity >50% by SDS-PAGE according to the supplier) were purchased from Enzo Life Sciences (Postfach, Switzerland). HDAC9 (Full length, purity 12% by SDS-PAGE according to the supplier) was purchased from Abnova (Taipei, Taiwan). The HDAC assay buffer [50 mM tris/Cl, pH 8.0, 137 mM NaCl, 2.7 mM KCl, 1 mM $MgCl_2$, and bovine serum albumin (0.5 mg/mL)]. Trypsin (10,000 units/mg, TPCK treated from bovine pancreas) was from Sigma Aldrich (Steinheim, Germany). All peptides were purified to homogeneity (>95% purity by $HPLC_{230\ nm}$ using reversed-phase preparative HPLC), and the white fluffy materials obtained by lyophilization were kept at –20 °C. For assaying, peptide substrates were reconstituted in DMSO to give 5–10 mM stock solutions, the accurate concentrations of which were determined by co-injection on HPLC with a standard of known concentration.

In Vitro Histone Deacetylase Inhibition Assays

For inhibition of recombinant human HDACs the dose–response experiments with internal controls were performed in black low binding NUNC 96-well microtiter plates. Dilution series (3-fold dilution, 6 concentrations) were prepared in HDAC assay buffer from 5–10 mM DMSO stock solutions. The appropriate dilution of inhibitor (5 μL of 5 $\times$ the desired final concentration) was added to each well followed by HDAC assay buffer (10 μL) containing substrate [*Ac-Leu-Gly-Lys(Ac)-AMC* (50 μM) for HDAC1, 2, and 3; (80 μM) for HDAC6 and (100 μM) for HDAC11; (500 μM) for HDAC8; and *Ac-Arg-His-Lys(Ac)-Lys(Ac)-AMC* (125 μM) for HDAC10]. Finally, a solution of the appropriate HDAC (10 μL) was added and the plate was incubated at 37 °C for 30 min. Final HDAC concentrations: HDAC1: 6 ng/μL, HDAC2: 1 or 2 ng/μL, HDAC3: 0.2 ng/μL, HDAC6: 2.4 or 3.6 ng/μL, HDAC8: 0.1 or 0.2 ng/μL, HDAC10: 10 or 14 ng/μL and HDAC11: 10 ng/μL. Then trypsin (25 μL, 0.4 mg/mL) was added and the assay development was allowed to proceed for 15–30 min at room temperature, before the plate was read using a Perkin Elmer Enspire plate reader with excitation at 360 nm and detecting emission at 460 nm. Each assay was performed in duplicate. The data were analyzed as described in chapter 2.

Cheng–Prusoff K_i Calculations

Using the Cheng–Prusoff equation $K_i = IC_{50}/(1+[S]/Km)$ and assuming a standard fast-on–fast-off mechanism of inhibition, IC_{50} values were converted to K_i values using the substrate concentrations outlined above and the K_m values determined by Bradner, mazitschek and co-workers[169] for HDACs 1–9 and by Chou and co-workers[205] for HDAC11. For HDAC10, a K_m value for the applied substrate (Ac-RHKacKac-AMC) was obtained as described in ref [206].

3D-structure elucidation

NMR

NMR spectra were acquired using standard pulse sequences on a Unity Inova 500 by Varian (499.9 MHz for ^1H, 125.7 MHz for ^{13}C) or a Bruker Avance 800 MHz spectrometer (798.9 MHz for ^1H and 200.9 MHz for ^{13}C)

located at the Danish Instrument Centre for NMR Spectroscopy of Biological Macromolecules at Carlsberg Laboratory.

The deuterated solvent used for all compounds was DMSO-d_6. For homonuclear 2D experiments 4096 data points were recorded in the direct dimension and 512 in the indirect dimension. Typical d1 times were from 2 to 4 seconds, which were found to give almost identical results compared to 8 seconds for **2.10** and **2.27b**. The T1 times were investigated for a model compound (**2.10**) and all nuclei were found to have T1's up to approximately 1 second. All *J*-couplings were extracted from the 1D ^{1}H and DQF-COSY spectra. Distances were obtained from 2D NOESY or ROESY experiments using the isolated spin pair approximation (ISPA).[207] (The linear range was increased by the method suggested by Macur et al.[208] The used mixing time was 150 ms for all compounds. Prior different mixing times were used to construct buildup curves to ensure that only cross-peaks which fitted the ISPA were used. The *J*-couplings from angles were calculated by the Karplus equation for peptides.[209]

Simulations

Simulations were conducted using the program Maestro (Version 9.3.515, MMshare Version 2.1.515) from the Schrödinger suite. Conformational searches in implicit solvents (DMSO and H_2O) were run by MacroModel (version 9.9, Schrödinger, LLC, New York, NY, 2012) using the force fields OPLS2005 and MMFFs. Monte Carlo torsional sampling was used to generate the structures and the minimization method was PRCG. The number of steps was 30,000 and only conformations within 20 kJ/mol of the found minimum were considered. The solvent DMSO was treated as a constant dielectric constant of 47.0. The natural compound was altered to avoid very stable interactions with the ring amide functionalities, as this structure was not supported by the NMR data. The side chain amide (N-24) was thus exchanged with a methyl group. Both solvents and force fields gave similar results, and the distances and torsion angles were optimized by applying constraints on the side groups at C-6 and C-13 according to the observed *J*-couplings. The constraints were implemented by calculating the appropriate angles from *J*-couplings, using the structural knowledge obtained from NOE/ROEs. This angle was allowed to differ by 10 degrees and was governed by a force constant of 50 kJ/mol.

The structures obtained as well as structures from non-restricted minimizations were placed in the center of a cubic box of 45x45x45 Å^3, and explicit water was added using the program Desmond (Desmond Molecular Dynamics System, version 3.1, D. E. Shaw Research, New York, NY, 2012. Maestro-Desmond Interoperability Tools, version 3.1, Schrödinger, New York, NY, 2012) and the force field OPLS2005.[210] Berendsen coupling was used for temperature and pressure control.[211] The system was minimized by steepest decent to remove unwanted overlaps of atoms. The system was then heated from 30 K to 300 K in two steps; 30 to 100 K in 100 ps and 100 to 300 K in 200 ps. This was done with temperature coupling (tT=0.1 ps). The resulting system was held at 300 K and 1 bar with temperature and pressure couplings (tT=0.1 ps, tP=0.5 ps) and simulations of 10 ns was conducted. Structures were recorded every 20 ps. Again very similar simulated structures were observed.

Restricted simulations

Restricted simulations in implicit DMSO were conducted in MacroModel using the force field MMFFs. The minimization method was PRCG, and 30,000 steps were used to find conformations within 30 kJ/mol of the found minimum. The solvent DMSO was treated as a constant dielectric constant of 47.0. The distances were referenced to a diastereotopic methylene proton pair with a distance set to 1.78 Å using ISPA. The calculated

distances were applied to the structure and allowed to differ 20 %, governed by a force constant of 100 kJ/Å^2. Similar results to those of the unrestricted compounds were obtained. It should be noted that it was no longer needed to alter the side-chain of the natural compound, as the restrictions prevented the stable interactions with the ring amide functionalities.

Table 5. Distances used for restricted simulations. The values were allowed to differ 20 %.

2.27b

Nucleus1	**Nucleus2**	**Distance**
7	9a	2.94
7	9b	2.27
7	6	3.28
7	11	2.68
7	4	2.33
1	11	2.05
1	25a	2.94
1	25b	3.75
1	13	3.54
11	9b	2.57
11	25a	3.10
11	25b	3.42
11	10	3.12
19	9b	3.67
19	10	3.57
13	25a	2.83
13	25b	2.68
9b	9a	1.78

Azumamide A

7	Nucleus1	8	Nucleus2	9	Distances
10	1	11	25a	12	2.62
13	1	14	25b	15	2.80
16	1	17	11	18	2.23
19	1	20	3	21	2.10
22	4	23	3	24	2.66
25	4	26	7	27	2.26
28	7	29	9	30	2.82
31	11	32	18a	33	3.14
34	11	35	18b	36	2.90
37	11	38	25a	39	2.52
40	11	41	25b	42	2.42
43	10	44	9	45	2.04
46	9	47	18a	48	2.64
49	18b	50	18a	51	1.78

Distances and J-couplings from unrestricted simulations

Table 6. Distances of the conformation of **2.27b,** which fitted the NMR data the best. Based on NOESY data at 150 ms from 800 MHz. a: used as reference, b: some scalar coupling observed and thus not used as reference.

Nucleus1	Nucleus2	Meas	Calc	Lower bound	Violation	Upper bound	Violation
7	16/17	2.73	2.56	2.31		2.82	
7	15	2.53	2.70	2.43		2.97	
7	9a	3.41	2.86	2.57		3.14	0.27
7	9b	2.16	2.16[a]	1.94		2.37	
7	6	2.98	3.08	2.77		3.39	
7	11	2.63	2.58	2.32		2.84	
7	4	2.25	2.29	2.06		2.52	
1	14	2.62	2.60	2.34		2.86	
1	25b	3.56	3.52	3.17		3.87	
1	25a	2.36	2.81	2.53	0.17	3.09	
1	13	2.98	3.29	2.96		3.62	
1	11	2.06	1.98	1.78		2.17	
4	14	2.49	2.65	2.39		2.92	
4	16/17	3.99	3.91	3.52		4.30	
4	15	2.29	3.25	2.92	0.63	3.57	
11	18a/18b	3.27	2.72	2.45		2.99	0.28
11	9b	2.42	2.42	2.18		2.67	
11	25a	2.57	2.93	2.63	0.06	3.22	
11	10	2.93	2.84	2.55		3.12	
11	13	3.59	3.93	3.54		4.32	
27	14	2.92	3.76	3.39	0.47	4.14	
27	18a/18b	3.88	3.56	3.20		3.91	
27	25a	2.44	2.75	2.47	0.03	3.02	
27	25b	2.43	2.67	2.40		2.93	
27	13	2.99	3.15	2.84		3.47	
27	28	2.19	1.98[b]	1.78		2.17	0.02
20	18a/18b	2.36	2.59	2.33		2.85	
19	18a/18b	2.39	2.29	2.06		2.52	
19	9b	2.46	3.34	3.00	0.54	3.67	
19	10	3.91	3.15	2.83		3.46	0.45
3	14	2.33	2.26	2.03		2.49	
13	25a	2.74	2.58	2.33		2.84	
13	25b	3.06	2.41	2.17		2.65	0.41
10	18a/18b/9a	2.06	1.94	1.74		2.13	
6	16/17	2.33	2.41	2.17		2.65	
6	15	3.08	2.59	2.33		2.85	0.23
9b	9a	1.76	1.58[b]	1.43		1.74	0.02
15	16/17	2.06	2.29	2.06		2.52	

Table 7. *J*-couplings of the conformation of **2.27b,** which fitted the NMR data the best.

Nucleus1	Nucleus2	Meas	Calc	Diff
1	13	9.7	9.5	0.2
3	4	9.8	8.7	1.1
6	7	6.9	9.1	2.2
10	11	7	7.7	0.7
25a	13	9.2	10.5	1.3
15	6	6.8	12.9	6.1
25b	13	5.8	1.8	4.0
9b	10	12.6	12.6	0.0
9a	10	4.4	2.3	2.1

Table 8. Distances of the conformation of azumamide A, which fitted the NMR data the best. Based on ROESY data at 150 ms from 500 MHz. a: used as reference, b: some scalar coupling observed and thus not used as reference.

Nucleus1	Nucleus2	Meas	Calc	Lower bound	Violation	Upper bound	Violation
1	14	2.73	2.62	2.36		2.88	
1	25a	2.41	2.61	2.35		2.87	
1	25b	3.25	2.86	2.57		3.15	0.11
1	11	2.10	2.10[a]	1.89		2.31	
1	3	3.56	2.58	2.32		2.84	0.72
4	16/17	3.12	2.59	2.33		2.85	0.27
4	14	2.47	2.59	2.33		2.85	
4	15	2.17	2.42	2.18	0.01	2.67	
4	3	2.96	2.68	2.41		2.95	0.01
4	7	2.30	2.35	2.12		2.59	
7	16/17	2.97	2.62	2.35		2.88	0.10
7	31	2.23	2.20	1.98		2.42	
7	15	2.59	3.04	2.74	0.14	3.35	
7	9	3.58	3.21	2.89		3.53	0.05
7	6	2.99	2.92	2.63		3.22	
27	25a	2.44	2.47	2.22		2.72	
27	25b	2.43	2.45	2.20		2.69	
27	13	3.01	2.62	2.36		2.89	0.13
11	31	2.28	2.27	2.04		2.49	
11	18a	2.97	3.09	2.78		3.40	
11	18b	3.36	3.02	2.72		3.33	0.04
11	25a	2.94	2.46	2.21		2.71	0.24
11	25b	2.62	2.40	2.16		2.64	
11	10	2.93	2.59	2.33		2.85	0.08
20	22	2.54	3.03	2.73	0.19	3.34	
20	9	3.83	3.00	2.70		3.30	0.53

19	10	2.97	2.75	2.47		3.02	
19	9	2.59	2.71	2.44		2.98	
3	14	2.34	2.29	2.06		2.52	
10	9	2.47	2.11	1.90		2.32	0.15
6	15	3.08	2.95	2.65		3.24	
6	16/17	2.32	2.16	1.94		2.37	
9	31	2.28	2.13	1.92		2.35	
9	18a	3.18	2.73	2.46		3.00	0.18
18b	31	3.81	2.89	2.61		3.18	0.63
18b	18a	1.74	1.80	1.62		1.98	
18a	31	2.44	2.24	2.01		2.46	

Table 9. *J*-couplings of the conformation of azumamide A which fitted the NMR data the best.

Nucleus1	**Nucleus2**	**Meas**	**Calc**	**Diff**
1	13	9.1	9.6	0.5
4	3	8.7	8.3	0.4
7	6	8.35	9.7	1.3
11	10	8	7.7	0.3
13	25a	9.4	5.1	4.3
13	25b	6.7	5.3	1.4
10	9	3.8	3.1	0.7
6	15	10.1	12.9	2.8

Distances and J-couplings from restricted simulations

Table 10. Distances of the conformation of **2.27b** which fitted the NMR data the best. (NOESY data) at 150 ms from 800 MHz. a: used as reference, b: some scalar coupling observed and thus not used as reference.

Nucleus1	Nucleus2	Meas	Calc	Lower bound	Violation	Upper bound	Violation
7	17	2.920	2.851	2.566		3.136	
7	15	2.517	2.997	2.697	0.18	3.297	
7	9a	3.378	3.177	2.859		3.495	
7	9b	2.151	2.400	2.160	0.01	2.640	
7	6	2.974	3.421	3.079	0.105	3.763	
7	11	2.653	2.866	2.579		3.152	
7	4	2.228	2.551	2.296	0.07	2.806	
1	14	3.019	2.888	2.599		3.177	
1	25b	3.698	3.911	3.520		4.302	
1	25a	2.516	3.128	2.815	0.30	3.440	
1	13	2.989	3.655	3.290	0.30	4.021	
1	11	2.019	2.196	1.976		2.416	
4	14	2.882	2.952	2.656		3.247	
4	17	4.540	4.344	3.910		4.779	
4	15	2.350	3.609	3.248	0.90	3.969	
11	18a/18b	2.749	3.021	2.719		3.323	
11	9b	2.437	2.696	2.426		2.966	
11	25b	3.526	3.517	3.166		3.869	
11	25a	2.495	3.255	2.929	0.43	3.580	
11	10	2.932	3.155	2.839		3.470	
11	13	3.588	4.369	3.932	0.35	4.806	
27	14	3.607	4.182	3.764	0.16	4.600	
27	18a/18b	6.194	3.957	3.561		4.352	1.84
27	25a	2.402	3.055	2.750	0.35	3.361	
27	25b	2.505	2.964	2.668	0.16	3.261	
27	13	2.770	3.507	3.156	0.39	3.857	
27	28	2.194	2.198	1.978		2.418	
20	18a/18b	3.512	2.884	2.595		3.172	0.34
19	18a/18b	2.315	2.550	2.295		2.805	
19	9b	3.397	3.709	3.339		4.080	
19	10	3.451	3.500	3.150		3.850	
3	14	2.646	2.512	2.261		2.763	
13	25a	2.571	2.874	2.586	0.02	3.161	
13	25b	3.092	2.679	2.411		2.947	0.15
10	18a/18b/9a	2.218	2.153	1.938		2.369	
6	16	2.411	2.674	2.407		2.942	
6	15	3.083	2.880	2.592		3.168	
9b	9a	1.760	1.760	1.584		1.936	
15	17	2.086	2.547	2.292	0.21	2.802	

Table 11. *J*-couplings of the conformation of **2.27b** which fitted the NMR data the best.

Nucleus1	Nucleus2	Meas	Calc	Diff
1	13	9.7	9.5	0.2
3	4	9.8	8.7	1.1
6	7	6.9	8.9	2.0
10	11	7	7.8	0.8
25a	13	9.2	12.8	3.6
15	6	6.8	12.9	6.1
25b	13	5.8	2.5	3.3
9b	10	12.6	12.8	0.2
9a	10	4.4	2.6	1.8

Table 12. Distances of the conformation of azumamide A which fitted the NMR data the best. Based on ROESY data at 150 ms from 500 MHz. a: used as reference, b: some scalar coupling observed and thus not used as reference.

Nucleus1	Nucleus2	Meas	Calc	Lower bound	Violation	Upper bound	Violation
1	14	3.909	2.646	2.381		2.910	1.00
1	25a	3.153	2.885	0.268		2.597	
1	25b	3.278	2.637	0.641		2.373	
1	11	2.123	2.123	1.911		2.335	
4	16	2.978	2.610	2.349		2.871	0.11
4	14	2.693	2.612	2.351		2.874	
4	15	2.104	2.445	2.201	0.10	2.690	
4	3	2.980	2.704	2.434		2.975	0.01
4	7	2.586	2.373	2.136		2.610	
7	16	4.125	2.639	2.375		2.903	1.22
7	31	2.211	2.218	1.997		2.440	
7	15	2.545	3.069	2.762	0.22	3.376	
7	9	3.544	3.237	2.914		3.561	
7	6	2.977	2.951	2.656		3.246	
27	25a	2.322	2.494	2.245		2.744	
27	25b	2.669	2.470	2.223		2.717	
27	13	3.022	2.647	2.382		2.911	0.11
11	31	2.358	2.285	2.057		2.514	
11	18a	3.098	3.117	2.806		3.429	
11	18b	3.480	3.051	2.746		3.356	0.12
11	25a	3.122	2.417	0.704		2.176	
11	25b	2.151	2.482	0.330		2.234	0.08
11	10	2.900	2.615	2.353		2.876	0.02
20	22	2.517	3.060	2.754	0.24	3.366	
20	18b	3.822	2.771	2.494		3.048	0.77
20	9	3.656	3.027	2.725		3.330	0.33

20	10	3.871	3.116	2.804		3.428	0.44
19	10	3.478	2.770	2.493		3.047	0.43
19	9	2.566	2.738	2.464		3.012	
3	14	2.335	2.310	2.079		2.540	
10	9	2.423	2.129	1.917		2.342	0.08
6	15	3.076	2.975	2.677		3.272	
6	16	2.321	2.175	1.957		2.392	
9	31	2.278	2.154	1.939		2.369	
9	18a	3.206	2.753	2.478		3.029	0.18
18b	31	3.780	2.921	2.629		3.213	0.57
18b	18a	1.740	1.818	1.636		2.000	
18a	31	2.415	2.256	2.030		2.482	
15	16	2.061	2.072	1.864		2.279	
7	11	2.211	3.103	2.792	0.58	3.413	

Table 13. *J*-couplings of the conformation of azumamide A, which fitted the NMR data the best.

Nucleus1	**Nucleus2**	**Meas**	**Calc**	**Diff**
1	13	9.1	6.3	2.8
4	3	8.7	9.6	0.9
7	6	8.4	9.1	0.7
11	10	8	6.6	1.4
13	25a	6.7	2.0	4.7
13	25b	9.4	10.3	0.9
10	9	3.8	3.6	0.2
6	15	10.1	12.9	2.8

Azumamide A

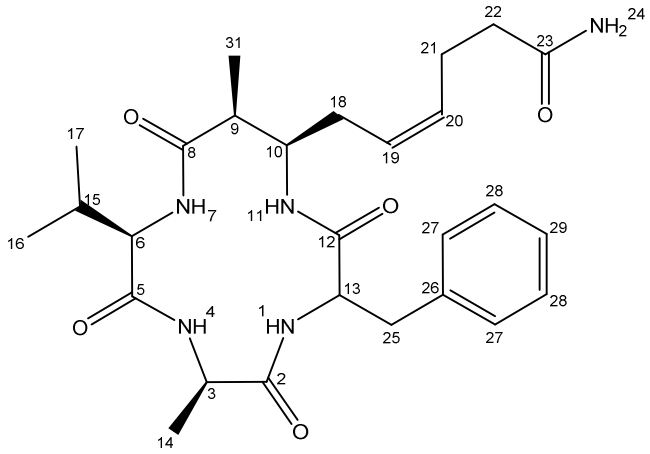

52	#	53	δ_H [ppm]/ 54 J coupling constants [Hz]	55	56	COSY 57	58	HMBC 59
60	1	61	7.71	62	63	13	64	
65	2	66	-	67	68	-	69	
70	3	71	4.13	72	73	4,14	74	
75	4	76	7.68	77	78	3	79	
80	5	81	-	82	83	-	84	
85	6	86	3.73	87	88	6,15	89	
90	7	91	7.41	92	93	6	94	
95	8	96	-	97	98	-	99	
100	9	101	2.53	102	103	10,31	104	
105	10	106	4.00	107	108	9,11,18a,18b	109	
110	11	111	7.10	112	113		114	
115	12	116	-	117	118	-	119	
120	13	121	4.14	122	123	1,25a,25b	124	
125	14	126	1.16	127	128	3	129	
130	15	131	2.11	132	133	6,16,17	134	
135	16	136	0.86	137	138	15	139	
140	17	141	0.88	142	143	15	144	
145	18a	146	2.21	147	148	19	149	
150	18b	151	2.40	152	153	19	154	
155	19	156	5.27	157	158	20,18a,18b	159	
160	20	161	5.40	162	163	19,21	164	
165	21	166	2.26	167	168	20	169	
170	22	171	2.09	172	173		174	
175	23	176	-	177	178		179	
180	24a	181	6.73	182	183		184	
185	24b	186	7.26	187	188		189	
190	25a	191	2.93	192	193	13,25b	194	
195	25b	196	3.01	197	198	13,25a	199	
200	26	201	-	202	203		204	

205	27	206	7.25	207	208	28	209	
210	28	211	7.18	212	213	27	214	
215	29	216	-	217	218		219	
220	31	221	1.30	222	223	9	224	

2.27b

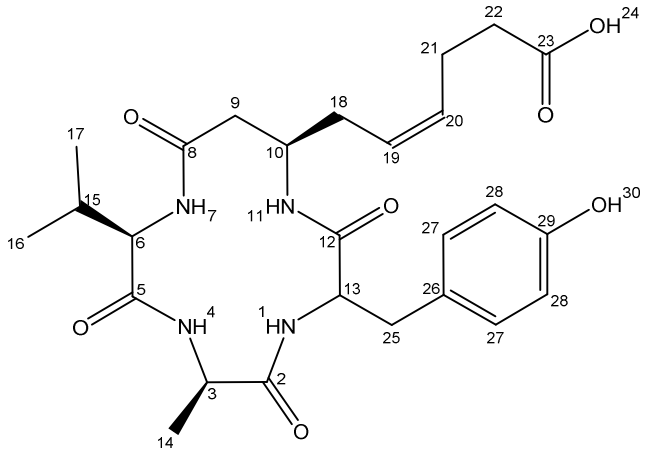

225	#	226	δ_H [ppm]/ 227 J coupling constants [Hz]	228	δ_C [ppm]	229	COSY 230	231	HMBC 232
233	1	234	7.54 (9.7)	235		236	13	237	
238	2	239	-	240		241	-	242	
243	3	244	4.26 (9.7,7.4)	245		246	4,14	247	
248	4	249	7.41 (9.8)	250		251	3	252	
253	5	254	-	255		256	-	257	
258	6	259	3.79 (6.6,6.6)	260		261	6,15	262	
263	7	264	7.85 (6.7)	265		266	6	267	
268	8	269	-	270		271	-	272	
273	9a	274	2.28 (11.3,3.8)	275		276	10,9b	277	
278	9b	279	2.46 (14.0,12.4)	280		281	10,9a	282	
283	10	284	3.92 (m)	285		286	11,18,9a,9b	287	
288	11	289	7.24 (7.1)	290		291		292	
293	12	294	-	295		296	-	297	
298	13	299	4.15 (9.4,9.4,5.9)	300		301	1,25a,25b	302	
303	14	304	1.15 (7.3)	305		306	3	307	
308	15	309	1.93 (oct: 6.8)	310		311	6,16,17	312	
313	16	314	0.90 (6.8)	315		316	15	317	
318	17	319	0.92 (6.8)	320		321	15	322	
323	18a	324	2.25 -	325		326	19/20	327	
328	18b	329	2.25 -	330		331	19/20	332	
333	19	334	5.36 -	335		336	20	337	
338	20	339	5.47 -	340		341	19	342	
343	21	344	2.25 -	345		346	19/20	347	
348	22	349	2.25 -	350		351	19/20	352	

353	23	354	-	355	356		357		
358	24	359	12.07	360	361		362		
363	25a	364	2.68 (13.9,9.3)	365	366	13,25b	367		
368	25b	369	2.81 (13.9,5.7)	370	371	13,25a	372		
373	26	374	-	375	376		377		
378	27	379	6.93 (8.4)	380	381	28	382		
383	28	384	6.63 (8.4)	385	386	27	387		
388	29	389	-	390	391		392		
393	30	394	9.22 s	395	396		397		

Experimentals for chapter 3

S-(but-3-en-1-yl) octanethioate (3.3).[172]

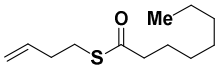

To thioacetamide (463 mg, 6.16 mmol) in anhydrous toluene (40 mL) was added octanoyl chloride (1.1 mL, 6.28 mmol) dropwise at 30°C. The reaction was stirred for 42h whereafter additional octanoyl chloride (0.84 mL, 4.93 mmol) was added. The reaction was stirred for 4h and the solvent evaporated. The crude product was hydrolyzed with 10% wt. NaOH (30 mL). The reaction was stirred for 30 min. and acidified with 1M HCl until pH = 2. The product was extracted with AcOEt (2 x 50 mL), dried ($MgSO_4$) and concentrated. The crude product (**3.4**) was used without further purification.

The thioacid was diluted with acetone (25 mL) whereafter K_2CO_3 (766 mg, 5.54 mmol) was added followed by 4-bromo-1-butene (0.56 mL, 5.54 mmol). The reaction was stirred at room temperaturefor 18h, then filtered and evaporated. Purification by VLC (1 – 10% CH_2Cl_2/heptane) gave the desired product (667 mg, 51% 2 steps) as a reddish oil. ^{1}H NMR (300 MHz, $CDCl_3$) δ 5.77 (ddt, 1H, *J* = 16.9, 10.2, 6.6 Hz), 5.11 – 4.99 (m, 2H), 2.92 (t, 2H, *J* = 7.3 Hz), 2.52 (t, 2H, *J* =7.54 Hz), 2.35 – 2.26 (m, 2H), 1.64 (p, 2H, *J* = 7.4 Hz), 1.36 – 1.18 (m, 8H), 0.96 – 0.81 (t, 3H, *J* = 6.9 Hz); ^{13}C NMR (300 MHz, $CDCl_3$) δ 199.6, 136.3, 116.5, 44.3, 33.8, 31.7, 29.03, 29.01, 28.1, 25.8, 22.7, 14.2.

(S,E)-tert-butyl 3-((tert-butoxycarbonyl)amino)-7-(octanoylthio)hept-4-enoate (3.5)

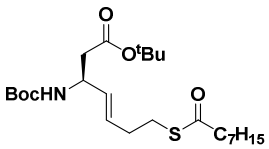

General methods for the cross methatesis.

To **2.7** in degassed, anhydrous solvent (c = ~0.1 M) was added **3.3** (2 equiv), followed by a catalyst. The reaction was heated for 17-23h, evaporated on silica and purified by VLC (0–10% AcOEt in heptane) to obtain the product (11–43%) as a dark oil.

Entry 1. The compound was synthesized according to the general procedure. After stirring in toluene at 60 °C using Grubbs catalyst 2nd generation (0.2 equiv) as the catalyst, the product was obtained in 38% yield (60% BRSM).

Entry 2. The compound was synthesized according to the general procedure. After stirring in toluene at 60 °C using Hoveyda-Grubbs catalyst 2nd generation (0.2 equiv) as the catalyst, the product was obtained in 26% yield (47% BRSM).

Entry 3 The compound was synthesized according to the general procedure. After stirring in DCE at 90 °C using Hoveyda-Grubbs catalyst 2nd generation (0.1 equiv) as the catalyst, the product was obtained in 15% yield (33% BRSM)

Entry 4. The compound was synthesized according to the general procedure. After stirring in toluene at 60 °C using Zhan catalyst 1B (0.2 equiv) as the catalyst, the product was obtained in 42% yield.

Entry 5. The compound was synthesized according to the general procedure. After stirring in toluene at 60 °C using **2.11** (0.2 equiv) as the catalyst, the product was obtained in 43% yield (66% BRSM).

Entry 6. The compound was synthesized according to the general procedure. After stirring in DCE at 90 °C using **2.11** (0.1 equiv + 0.05 equiv) as the catalyst, the product was obtained in 12% yield

^{1}H NMR (300 MHz, $CDCl_3$) δ 5.59 (dt, *J* = 15.5, 6.0 Hz, 1H), 5.49 (dd, *J* = 15.5, 5.4 Hz, 1H), 5.14 (brs, 1H), 4.41 (brs, 1H), 2.88 (t, *J* = 7.3 Hz, 2H), 2.63 – 2.49 (m, 2H), 2.47 (d, *J* = 5.3 Hz, 2H), 2.28 (dd, *J* = 13.7, 7.1 Hz, 2H), 1.72 – 1.55 (m, 2H), 1.44 (s, 18H), 1.37 – 1.12 (m, 8H), 0.87 (t, *J* = 6.7 Hz, 3H). ^{13}C NMR (75 MHz, $CDCl_3$) δ 199.7, 170.6, 155.1, 131.4, 129, 81.2, 79.5, 49.1, 44.3, 40.9, 32.4, 31.8, 29.9, 29.1, 28.5, 28.4, 28.2, 25.8, 22.7, 14.2. HRMS calc'd for $C_{24}H_{43}NO_5SH^+$ [M+H$^+$] = 458.2935, found 458.2940.

(S,E)-3-((tert-butoxycarbonyl)amino)-7-(octanoylthio)hept-4-enoic acid (3.6)

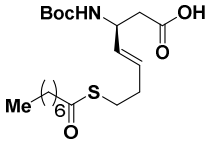

To the mixture of **3.5** and **2.7** in CH_2Cl_2 (25 mL) was added TFA (15 mL). The reaction was stirred for 2h, then evaporated and used without further purification. HRMS calc'd for $C_{15}H_{27}NO_3SH^+$ [M+H$^+$] = 302.1784, found 302.1809.

To the crude amino acid in anhydrous CH_2Cl_2 (20 mL) was added DIPEA (0.37 mL, 2.1 mmol), followed by Boc_2O (235 mg, 1.1 mmol). After stirring at rt for 24h, the organic phase was washed with 1M HCl (2 x 30 mL), brine (30 mL), dried and evaporated. The crude compound (**3.6**) was used without further purification. ^{1}H NMR (300 MHz, $CDCl_3$) δ 5.77 (ddt, *J* = 16.9, 10.2, 6.6 Hz, 1H), 5.11 – 4.99 (m, 2H), 2.92 (t, *J* = 7.3 Hz, 2H), 2.58 – 2.46 (m, 2H), 2.38 – 2.23 (m, 2H), 1.64 (p, *J* = 7.4 Hz, 2H), 1.39 – 1.11 (m, 8H), 0.96 – 0.81 (m, 3H). ^{13}C NMR (75 MHz, $CDCl_3$) δ 199.6, 136.3, 116.5, 44.3, 33.8, 31.7, 29.03, 29.01, 28.1, 25.8, 22.7, 14.2. HRMS calc'd for $C_{20}H_{35}NO_5SH^+$ [M+H$^+$] = 402.2309, found 402.2312.

((S,E)-3-amino-7-(octanoylthio)hept-4-enoyl)-D-valyl-D-alanyl-D-tyrosine (3.7).

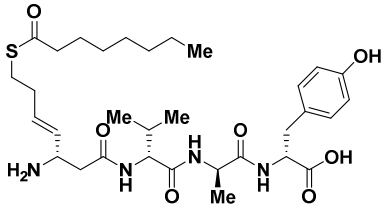

3.6 (81.5 mg (~1:1 mixture with the vinyl compound, equal to ~0.13 mmol)) was preactivated with HATU (90 mg, 0.24 mmol) and 2,6-lutidine (55.6 μL, 0.48 mmol) in DMF (5 mL) and added to a tripeptide (H-D-Val-D-Ala-D-Tyr(tBu)) bound to a polystyrene 2-chlorotrityl resin in a fritted syringe. The reaction was put on a tilting table for 15h, then washed with DMF (x3), MeOH (x3), CH_2Cl_2 (x3). The peptide was cleaved with 50% TFA in CH_2Cl_2, then triturated with Et_2O. Purification by preparative HPLC, provided the compound (8.7 mg, 10% yield) as a white solid. ^{1}H NMR (300 MHz, DMSO-d_6) δ 9.20 (s, 1H), 8.18 (d, *J* = 9.0 Hz, 1H), 8.08 (d, *J* = 7.5 Hz, 1H), 7.92 (d, *J* = 7.5 Hz, 1H), 6.98 (d, *J* = 8.4 Hz, 2H), 6.62 (d, *J* = 8.4 Hz, 2H), 5.74 (dt, *J* = 15.0, 6.6 Hz, 1H), 5.46 (dd, *J* = 15.6, 7.4 Hz, 1H), 4.42 – 4.11 (m, 3H), 3.94 (q, *J* = 6.8 Hz, 1H), 2.99 – 2.69 (m, 4H), 2.68 – 2.51 (m, 4H), 2.33 – 2.12 (m, 2H), 2.04 – 1.84 (m, 1H), 1.66 – 1.44 (m, 2H), 1.32 – 1.13 (m, 11H), 0.88 – 0.75 (m, 9H). HRMS calc'd for $C_{32}H_{50}N_4O_7SH^+$ [M+H$^+$] = 635.3473, found 635.3475.

(S)-but-3-en-1-yl 3-((tert-butoxycarbonyl)amino)pent-4-enoate (3.11)

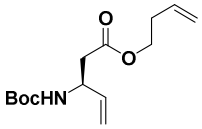

4-bromo-1-butene (0.32 ml, 3.19 mmol) was added to a solution of **2.8** (341.4 mg, 1.59 mmol) and K_2CO_3 (264.2 mg, 1.9 mmol) in anhydrous DMF (4 mL). The reaction was stirred for 3h and another portion of 4-bromo-1-butene was added (80 µL, 0.8 mmol). The reaction was stirred for 3h and diluted with H_2O (5 mL). The aqueous phase was extracted with AcOEt (2 x 10 mL) and the combined organic phases washed with 1M HCl (2 x 15 mL), $NaHCO_3$ (2 x 15 mL), brine (2 x 15 mL), dried (Na_2SO_4) and evaporated. The product (87%, 373.2 mg) was obtained as a clear oil. ^{1}H NMR (300 MHz, cdcl$_3$) δ 5.90 – 5.68 (m, 2H), 5.26 – 5.02 (m, 4H), 4.49 (s, 1H), 4.13 (t, *J* = 6.6 Hz, 2H), 2.60 (d, *J* = 5.7 Hz, 2H), 2.46 – 2.25 (m, 2H), 1.43 (s, 9H); ^{13}C NMR (75 MHz, $CDCl_3$) δ 171.2, 155.2, 137.3, 134, 117.5, 115.5, 79.7, 63.8, 49.4, 39.3, 33.1, 28.5; $[\alpha]^{25}_D$ = +23°.

tert-butyl (S,E)-(2-oxo-3,4,7,8-tetrahydro-2H-oxocin-4-yl)carbamate (3.12)

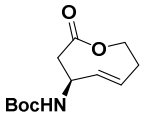

To **3.11** (156 mg, 0.58 mmol) in degassed anhydrous CH_2Cl_2 (3 mL) was added Grubbs 2nd generation catalyst and the reaction was heated to reflux for 18h. Purification by VLC (0–30% EtOAc in heptane), afforded an unclean product (59 mg, ~42%). ^{1}H NMR (300 MHz, $CDCl_3$) δ 5.84 – 5.32 (m, 2H), 4.48 (brs, 1H), 4.35 – 3.86 (m, 3H), 2.77 – 2.49 (m, 2H), 2.43 – 2.26 (m, 2H), 1.44 (s, 9H).

5-((3-((tert-butyldimethylsilyl)oxy)propyl)thio)-1-phenyl-1H-tetrazole (3.14a)[212]

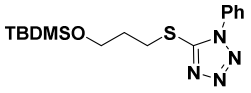

To a solution of PPh_3 (357 mg, 1.58 mmol) in anhydrous THF (8 mL) at 0 °C was added DIAD (282 µL, 1.43 mmol). The reaction was stirred for 5 min and **3.13a** (253 mg, 1.3 mmol) in anhydrous THF (2 mL) was added. The reaction mixture was stirred for 10 min and 1-phenyl-1H-tetrazole-5-thiol (281 mg, 1.58 mmol) was added. The reaction was allowed to warm to rt and stirred for 4h where after additional DIAD (26 mg, 0.13 mmol) was added at 0 °C. The reaction was allowed to warm to rt, stirred for 1h and evaporated. Purification by VLC (0 – 20% AcOEt/heptane) gave the product (81%, 369 mg) as a clear oil. ^{1}H NMR (300 MHz, $CDCl_3$) δ 7.74 – 7.40 (m, 5H), 3.73 (q, *J* = 5.8 Hz, 2H), 3.48 (q, *J* = 7.0 Hz, 2H), 2.04 (tt, *J* = 6.9, 5.8 Hz, 2H), 0.87 (s, 9H), 0.04 (s, 6H). ^{13}C NMR (75 MHz, $CDCl_3$) δ 154.6, 133.8, 130.2, 129.9, 124, 61.2, 32, 30.3, 26, 18.4, -5.3.

1-phenyl-5-((3-((triisopropylsilyl)oxy)propyl)thio)-1H-tetrazole (3.14b)

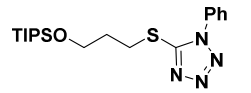

To a solution of PPh_3 (1.11 g, 4.9 mmol) in anhydrous THF (25 mL) at 0 °C was added DIAD (965 µL, 4.9 mmol). The reaction was stirred for 5 min and **3.13b** (956 mg, 4.1 mmol) in anhydrous THF (5 mL) was added. The reaction mixture was stirred for 20 min and 1-phenyl-1H-tetrazole-5-thiol (801 mg, 4.5 mmol) was added. The reaction was allowed to warm to rt, stirred for 2.5h and evaporated. Purification by VLC (0 – 20% AcOEt/heptane) gave the desired product as a clear oil (82%, 1.33 g). ^{1}H NMR (300 MHz, $CDCl_3$) δ 7.65 – 7.47 (m, 5H), 3.82 (t, *J* = 5.7 Hz, 2H), 3.52 (t, *J* = 7.0 Hz, 2H), 2.25 – 1.89 (m, 2H), 1.14 – 0.99 (m, 21H). ^{13}C NMR (75 MHz, $CDCl_3$) δ 154.7, 133.9, 130.2, 129.9, 124, 61.5, 32.2, 30.3, 18.1, 12.

5-((3-((tert-butyldimethylsilyl)oxy)propyl)sulfonyl)-1-phenyl-1H-tetrazole (3.15a)

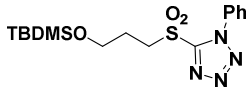

To a solution of **3.14a** (296 mg, 0.85 mmol) and $NaHCO_3$ (714 mg, 8.5 mmol) in CH_2Cl_2 (20 mL) was added ≤77% m-CPBA (1.42 g, 6.35 mmol). The reaction was stirred for 3h, then quenched with 1% aqueous NaOH (20 mL). The aqueous phase was extracted

with AcOEt (2 x 30 mL) and the combined organic phases were washed with 1% aqueous NaOH (50 mL), brine (2 x 50 mL), dried (Na_2SO_4) and evaporated. Purification by VLC (0 – 4% AcOEt/heptane) gave the product (85%, 275 mg) as white crystals. ^{1}H NMR (300 MHz, $CDCl_3$) δ 7.75 – 7.55 (m, 5H), 4.07 – 3.59 (m, 4H), 2.33 – 2.00 (m, 2H), 0.89 (s, 9H), 0.06 (s, 6H). ^{13}C NMR (75 MHz, $CDCl_3$) δ 131.6, 129.9, 125.2, 60.5, 53.5, 26, 25.7, 18.4, -5.3; Mp = 57 °C – 59 °C.

1-phenyl-5-((3-((triisopropylsilyl)oxy)propyl)sulfonyl)-1H-tetrazole (3.15b)

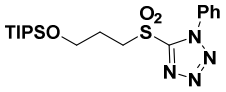

To a solution of **3.14b** (914 mg, 2.77 mmol) and $NaHCO_3$ (2.33 g, 27.7 mmol) in CH_2Cl_2 (50 mL) was added ≤77% m-CPBA (3.59 g, 20.8 mmol). The reaction was stirred for 3h, then quenched with 1% aqueous NaOH (25 mL). The aqueous phase was extracted with AcOEt (3 x 50 mL) and the combined organic phases were washed brine (2 x 50 mL), dried ($MgSO_4$) and evaporated. Purification by VLC (0 – 3% AcOEt/heptane) gave the product (66%, 656 mg) as a clear oil. 1H NMR (300 MHz, CDCl3) δ 7.79 – 7.49 (m, 5H), 4.00 – 3.68 (m, 4H), 2.26 – 2.09 (m, 2H), 1.21 – 0.89 (m, 21H). ^{13}C NMR (75 MHz, $CDCl_3$) δ 131.5, 129.8, 125.2, 60.8, 53.5, 25.8, 18.1, 12.

tert-butyl 3-((tert-butoxycarbonyl)amino)-7-((tert-butyldimethylsilyl)oxy)hept-4-enoate (3.18)

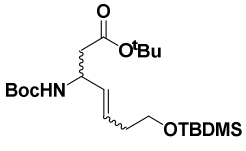

To **3.15b** (80 mg, 0.22 mmol) in anhydrous THF (2 mL) at –78 °C, was added KHMDS (0.5 M in toluene, 0.42 mL) dropwise. **3.16** (96 mg, 0.35 mmol) in anhydrous THF (0.5 mL) was added dropwise to the reaction. After 3h, an extra equivalent of KHMDS was added. After 10 min, the reaction was quenched with H_2O and purified by VLC (1–20% EtOAc in heptane). The product was obtained in 29% yield with impurities present. ^{1}H NMR (300 MHz, $CDCl_3$) δ 5.75 – 5.32 (m, 2H), 5.08 (s, 1H), 4.68 (s, 1H), 4.42 (s, 1H), 3.67 (t, J = 6.9 Hz, 2H), 2.60 – 2.33 (m, 2H), 2.26 (q, J = 6.8 Hz, 2H), 1.43 (s, 18H), 1.18 – 0.90 (m, 21H).

(S)-1-benzyl 4-tert-butyl 2-(tert-butoxycarbonylamino)succinate (3.19)

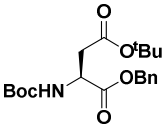

To Boc-L-Asp(^{t}Bu)-OH (397 mg, 1.37 mmol) in DMF (3 mL) was added K_2CO_3 (379 mg, 2.74 mmol) followed by benzylbromide (179 µL, 1.5 mmol). The reaction was stirred at rt for 2 h, then diluted with EtOAc (3 mL) and H_2O (5 mL).The aqueous phase was extracted with EtOAc (3 x 6 mL) and the combined organic phases were washed with 1M HCl (2x 20 mL), $NaHCO_3$ (2 x20 mL), brine (2 x 20 mL), dried ($MgSO_4$) and evaporated. The product was obtained as white crystals (97%, 505 mg). ^{1}H NMR (300 MHz, $CDCl_3$) δ 7.39 – 7.29 (m, 5H), 5.50 (d, *J* = 8.5 Hz, 1H), 5.17 (q, *J* = 12.3 Hz, 2H), 4.57 (dt, *J* = 8.8, 4.6 Hz, 1H), 2.92 (dd, *J* = 16.9, 4.8 Hz, 1H), 2.72 (dd, *J* = 16.8, 4.6 Hz, 1H), 1.41 (d, *J* = 11.7 Hz, 18H). ^{13}C NMR (75 MHz, $CDCl_3$) δ 171.3, 170.2, 155.6, 135.5, 128.7, 128.3, 81.8, 80.1, 67.4, 50.3, 38, 28.4, 28.1; $[\alpha]^{25}_D$ = +5.1°, Mp: 50.1 °C – 52.5 °C.

(S)-1-benzyl 4-tert-butyl 2-di(tert-butoxycarbonylamino)succinate (3.20).

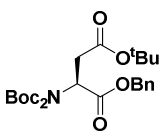

Boc_2O (235.7 mg, 0.11 mmol) in MeCN (0.5 mL) was added to **3.19** and DMAP (13.2 mg, 0.11 mmol) in MeCN (1 mL). The reaction was stirred at rt for 20h, then diluted with AcOEt (3 mL), washed with 1M $NaHSO_4$ (2 x 5 mL), $NaHCO_3$ (2 x 5 mL), brine (2 x 5 mL), dried ($MgSO_4$) and evaporated. Purification by VLC (0 – 10 % AcOEt/heptane) gave the desired product as white crystals (88%, 153.5 mg). ^{1}H NMR (300 MHz, $CDCl_3$) δ 7.49 – 7.21 (m, 5H), 5.46 (t, *J* = 6.9 Hz, 1H), 5.15 (s, 2H), 3.15 (dd, *J* = 16.0, 7.1 Hz, 1H), 2.65 (dd, *J* = 16.0, 6.8 Hz, 1H), 1.49 – 1.44 (m, 18H), 1.42 (s, 9H). ^{13}C NMR (75

MHz, $CDCl_3$) δ 170, 169.8, 151.9, 135.6, 128.6, 128.3, 128.2, 83.5, 81.2, 67.2, 55.3, 37.1, 28.1, 28.07. Mp: 61.4–62.4 °C; $[\alpha]^{25}_D$ = -40°.

(S)-4-(tert-butoxy)-2-(di(tert-butoxycarbonyl)amino)-4-oxobutanoic acid (**3.21**)

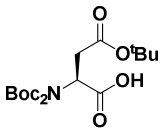

3.20 (244.8 mg, 0.51 mmol) in MeOH (2 mL) was purged with argon. 10 % Pd/C (25 mg) was added and the reaction purged with H_2 for 5 min. The reaction was stirred under H_2 atmosphere for 24h, filtered on celite and evaporated to obtain the product as white crystals (97%, 192.8 mg.) ^{1}H NMR (300 MHz, $CDCl_3$) δ 5.81 (dd, *J* = 7.1, 6.7 Hz, 1H), 3.43 (dd, *J* = 16.0, 7.3 Hz, 1H), 2.97 (dd, *J* = 16.0, 6.6 Hz, 1H), 1.83 (s, 18H), 1.77 (s, 9H). ^{13}C NMR (75 MHz, $CDCl_3$) δ 176.3, 169.7, 151.6, 83.8, 81.3, 55, 37, 28.1. Mp: 115.6–118.9°C; $[\alpha]^{25}_D$ = -51.8°.

(S)-tert-butyl 3-(di(tert-butoxycarbonyl)amino)-4-hydroxybutanoate (**3.22**)

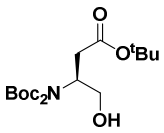

To a solution of **3.21** (150 mg, 0.385 mmol) in THF (2 mL) at –25°C was added NMM (43.3 µL, 0.393 mmol) followed by dropwise addition of iBuOCOCl (51 µL, 0.393 mmol). After 15 min., the reaction was heated to –10°C and stirred for 30 min before $NaBH_4$ (43.7 mg, 1.15 mmol) was added in one portion, followed by dropwise addition of MeOH (0.4 mL). After 30 min at –10°C, the reaction was warmed to rt and stirred for another 90 min. The reaction was quenched with NH4Cl (8 mL), washed with 1M HCl (2 x 10 mL), brine (2 x 10 mL), dried ($MgSO_4$) and evaporated. Purification by VLC (0 – 10% AcOEt/heptane) gave the desired product (29%, 41.4 mg) as a white solid. ^{1}H NMR (300 MHz, $CDCl_3$) δ 5.12 (d, *J* = 7.0 Hz, 1H), 4.26 – 3.99 (m, 3H), 2.49 (d, *J* = 5.9 Hz, 2H), 1.51 – 1.37 (m, 27H). ^{13}C NMR (75 MHz, $CDCl_3$) δ 170.3, 155.1, 153.4, 82.5, 81.4, 79.7, 67.6, 46.8, 37.2, 28.5, 28.2, 27.8; $[\alpha]^{25}_D$ = -5.3°.

(3-bromopropoxy)triisopropylsilane (**3.25**)

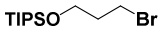

Imidazole (1.7 g, 25.18 mmol) was added to 3-bromopropanol (1.4 g, 10.07 mmol) in CH_2Cl_2 (20 mL). TIPSCl (2.14 mL, 10.07 mmol) was then added and the reaction was stirred for 17h at room temperature. The solution was diluted with H_2O (15 mL) and the aqueous phase was extracted with CH_2Cl_2 (3 x 15 mL). The combined organic phases were washed with $NaHCO_3$ (2 x 30 mL), brine (2 x 30 mL), dried ($MgSO_4$), and evaporated. Purification by VLC (heptane) gave the desired product (86%, 2.46 g) as a clear oil. ^{1}H NMR (300 MHz, $CDCl_3$) δ 3.82 (t, *J* = 5.7 Hz, 2H), 3.55 (t, *J* = 6.5 Hz, 2H), 2.06 (tt, *J* = 11.5, 5.7 Hz, 2H), 1.21 – 0.93 (m, 21H). ^{13}C NMR (75 MHz, $CDCl_3$) δ 60.9, 36.0, 31, 18.2, 12.1.

3-Triisopropylsilanyloxypropyltriphenylphosphonium bromide (**3.26**).[213]

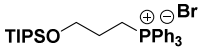

3.25 (1.16 g, 3.95 mmol) and PPh_3 in anhydrous toluene was heated to reflux for 4 days. The reaction was cooled to rt and diluted with heptane (25 mL). The product was filtered, washed with heptane (2 x 25 mL) and dried on high vacuum. The product was obtained as a white solid (69%, 1.52 g). ^{1}H NMR (300 MHz, $CDCl_3$) δ 7.81 – 7.53 (m, 15H), 3.90 – 3.47 (m, 4H), 1.99 – 1.60 (m, 2H), 0.92 (m, 21H). ^{13}C NMR (75 MHz, $CDCl_3$) δ 135.05 (t, *J* = 2.7 Hz), 133.41 (dd, *J* = 9.8, 8.5 Hz), 130.48 (dd, *J* = 12.5, 2.0 Hz), 118.11 (dd, *J* = 86.3, 8.8 Hz), 61.01 (dd, *J* = 125.5, 16.8 Hz), 25.93 (dd, *J* = 22.1, 3.9 Hz), 19.53 (dd, *J* = 86.7, 52.8 Hz), 17.78 (d, *J* = 20.7 Hz), 11.95 (d, *J* = 35.3 Hz).

(S,Z)-tert-butyl 3-((tert-butoxycarbonyl)amino)-7-((triisopropylsilyl)oxy)hept-4-enoate (**3.27**)

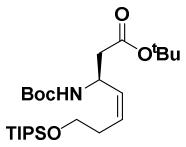

To oxalylchloride (0.21 mL, 2.39 mmol) in anhydrous CH_2Cl_2 (10 mL) at -78°C was added DMSO (0.34 mL, 4.78 mmol) dropwise. The reaction was stirred for 30 min and **3.16** (398.7 mg, 1.44 mmol) in anhydrous CH_2Cl_2 (2 mL) was added dropwise. After stirring for 20 min, Et_3N (1 mL, 7.24 mmol) was added dropwise and the reaction heated to -40°C. After stirring for 1h, the reaction was poured onto a 1:1 mixture of $NaHSO_4$/Et_2O (50 mL). The combined organic phases were washed with $NaHSO_4$, dried (Na_2SO_4), evaporated and put on high vacuum for 15 min while the Wittig reagent was prepared.

0.5 M KHMDS in toluene (4 mL, 2 mmol) was added dropwise to a solution of **3.26** in anhydrous THF (20 mL). After stirring for 30 min at rt, the reaction was cooled to -78°C and the above prepared aldehyde in THF (5 mL) was added dropwise. After stirring for 40 min, the reaction was allowed to warm to rt and stirred for 15h. The reaction mixture was diluted with Et_2O (25 mL), washed with 1M HCl (2 x 50 mL), $NaHCO_3$ (2x 50 mL), brine (50 mL), dried (Na_2SO_4) and evaporated. Purification by VLC (0 – 2% AcOEt/heptane) gave the desired product (41%, 281 mg 2 steps) as a clear oil. ^{1}H NMR (300 MHz, $CDCl_3$) δ 5.56 (dt, *J* = 11.0, 7.3 Hz, 1H), 5.42 (dd, *J* = 10.6, 9.0 Hz, 1H), 5.09 (s, 1H), 4.79 – 4.56 (m, 1H), 3.88 – 3.51 (m, 2H), 2.46 (d, *J* = 5.8 Hz, 2H), 2.43 – 2.30 (m, 2H), 1.42 (s, 9H), 1.41 (s, 9H), 1.12 – 0.98 (m, 21H). ^{13}C NMR (75 MHz, $CDCl_3$) δ 170.7, 155, 130.3, 129.4, 128.2, 81, 63, 41.4, 31.6, 28.5, 28.2, 18.1, 17.8, 12.5, 12.4, 12.1, HRMS calc'd for $C_{25}H_{49}NO_5SiH^+$ [M+H$^+$] = 472.3453, found 472.3460. $[\alpha]^{25}_D$ = +5.16°.

(R)-tert-butyl 3-((tert-butoxycarbonyl)amino)-7-hydroxyheptanoate (**3.28**)

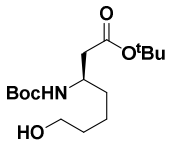

3.27 (404 mg, 0.856 mmol) was dissolved in anhydrous MeOH (10 mL) and purged with argon. 10% Pt/C (40 mg) was added and the reaction was purged with H_2. After stirring for 20h under H_2 atmosphere, the product was filtered on celite and evaporated to obtain the desired compound (98%, 396 mg) as a yellow oil, then used without further purification. ^{1}H NMR (300 MHz, $CDCl_3$) δ 4.91 (s, 1H), 3.95 – 3.80 (m, 1H), 3.66 (t, *J* = 6.2 Hz, 2H), 2.43 (dd, *J* = 15.1, 5.2 Hz, 1H), 2.36 (dd, *J* = 5.9, 15.1 Hz, 1H), 1.79 – 1.19 (m, 22H), 1.05 (s, 21H). ^{13}C NMR (75 MHz, cdcl$_3$) δ 171.2, 155.5, 80.9, 79.1, 63.3, 47.9, 40.7, 34.8, 32.9, 28.5, 28.2, 22.6, 18.2, 12.1. HRMS calc'd for $C_{25}H_{51}NO_5SiH^+$ [M+H$^+$] = 474.3609, found 474.3615. $[\alpha]^{25}_D$ = +3.8°.

The crude compound (351.3 mg, 0.74 mmol) in THF (2 mL) at 0°C were added AcOH (42 µL, 0.74 mmol) and TBAF (3 mL, 2.96 mmol). The reaction was allowed to warm to rt and stirred for 17h. The reaction was diluted with AcOEt (10 mL) and washed with 1M HCl (2 x 20 mL), $NaHCO_3$ (2 x 20 mL), brine (2 x 20 mL), dried (Na_2SO_4) and evaporated. Purification by flash chromatography (0–5% MeOH/CH_2Cl_2) gave the desired product (88%, 206 mg) as a clear oil. ^{1}H NMR (300 MHz, $CDCl_3$) δ 4.91 (d, *J* = 7.1 Hz, 1H), 4.02 – 3.72 (m, 1H), 2.42 (dd, J = 5.14, 14.8 Hz, 1H), 2.36 (dd, J = 5.85, 14.8 Hz, 2H), 1.68 (brs, 1H), 1.55 – 1.21 (m, 26H), 0.88 (t, *J* = 6.8 Hz, 3H). ^{13}C NMR (75 MHz, $CDCl_3$) δ 171.4, 155.5, 81, 48, 40.7, 34.6, 28.5, 28.4, 28.2, 22.6, 14.1; $[\alpha]^{25}_D$ = +3.6°.

(R)-tert-butyl 3-((tert-butoxycarbonyl)amino)-7-(tosyloxy)heptanoate (**3.30**)

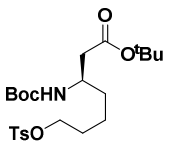

To **3.28** (213.7 mg, 0.67 mmol) in anhydrous CH_2Cl_2 was added TsCl (192.5 mg, 1 mmol) followed by Et_3N (281.5 μL, 2 mmol) and DMAP (8.2 mg, 0.07 mmol).The reaction was stirred for 5h at rt, then quenched with 1M HCl (12 mL). The aqueous phase was extracted with CH_2Cl_2 (2 x 20 mL) and the combined organic phases were washed with brine (20 mL), dried (Na_2SO_4) and evaporated. Purification by flash chromatography (5 – 15% AcOEt/hexane) gave the desired

product (83%, 263.5 mg) as a clear oil. ^{1}H NMR (300 MHz, $CDCl_3$) δ 7.77 (d, *J* = 8.4 Hz, 2H), 7.50 – 7.29 (m, 2H), 4.90 (d, *J* = 9.1 Hz, 1H), 4.00 (td, *J* = 6.3, 1.8 Hz, 2H), 3.91 – 3.67 (m, 1H), 2.44 (s, 3H), 2.39 (dd, *J* = 5.4, 15.3 Hz, 1H), 2.31 (dd, *J* = 15.3, 6.0 Hz, 1H), 1.77 – 1.58 (m, 2H), 1.43 (s, 9H), 1.41 (s, 9H). ^{13}C NMR (75 MHz, $CDCl_3$) δ 171, 155.4, 144.8, 133.2, 130.1, 130, 128, 81.1, 79.3, 70.5, 54.6, 47.5, 40.6, 34.2, 28.6, 28.5, 28.2, 22.2, 21.8. HRMS calc'd for $C_{23}H_{37}NO_7SH^+$ [M+H$^+$] = 472.2363, found 472.2379, $[\alpha]^{25}_D$ = +2.8°.

(R)-tert-butyl 3-((tert-butoxycarbonyl)amino)-7-(tritylthio)heptanoate (3.31)

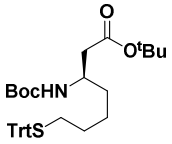

Ph_3CSH (313.6 mg, 1.125 mmol) and KO*t*Bu (180 mg, 1.58 mmol) was dissolved in anhydrous degassed THF (2 mL). The reaction was stirred for 5 min at rt, then cooled to 0°C where **3.30** (211 mg, 0.45 mmol) in anhydrous degassed THF (3 mL) was added dropwise to the solution. The reaction was slowly warmed to rt and stirred for 4h, then quenched with NH_4Cl (10 mL). The aqueous phase was extracted with Et_2O (3 x 10 mL) and the combined organic phases washed with brine (2 x 20 mL), dried (Na_2SO_4) and evaporated. ^{1}H NMR (300 MHz, $cdcl_3$) δ 7.44 – 7.34 (m, 5H), 7.30 – 7.14 (m, 10H), 4.86 (d, *J* = 7.9 Hz, 1H), 3.78 (brs, 1H), 2.37 (dd, *J* = 15.2, 5.4 Hz, 1H), 2.29 (dd, *J* = 15.2, 6.1 Hz, 1H), 2.12 (t, *J* = 7.1 Hz, 2H), 1.51 – 1.18 (m, 24H). ^{13}C NMR (75 MHz, $CDCl_3$) δ 171.1, 155.4, 145.1, 129.7, 127.9, 126.6, 81, 79.2, 66.5, 47.8, 40.6, 34.5, 31.9, 28.5, 28.2, 25.6. HRMS calc'd for $C_{35}H_{45}NO_4SNa^+$ [M+Na$^+$] = 598.2962, found 598.2962.

(R)-3-((((9H-fluoren-9-yl)methoxy)carbonyl)amino)-7-(tritylthio)heptanoic acid (3.32).

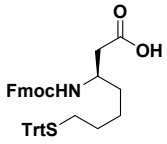

To **3.31** (48 mg, 0.08 mmol) in anhydrous CH_2Cl_2 (3 mL) at 0 °C was added TFA (0.87 mL) and the reaction was stirred for 4h. The solvent was evaporated and used without further purification. The crude compound was dissolved in a mixture of K_2CO_3 (19 mg, 0.14 mmol), H_2O (1 mL), and DMF (1.5 mL). FmocOSu (31 mg, 0.09 mmol) in DMF (0.5 mL) was added and the reaction was allowed to warm to room temperature. After 3h. the reaction was quenched with 1 M HCl (2 mL) and extracted with Et_2O (3x 5 mL). The combined organic phases were washed with brine (15 mL), dried and evaporated. Purification by VLC (5–15% EtOAc in heptane + 0.2% AcOH) afforded the product as a clear oil (56%, 30 mg, 2 steps). ^{1}H NMR (300 MHz, DMSO-d_6) δ 7.87 (d, *J* = 7.5 Hz, 2H), 7.65 (d, *J* = 7.8 Hz, 1H), 7.50 – 7.04 (m, 19H), 4.26 (d, *J* = 36.7 Hz, 3H), 3.90 – 3.54 (m, 1H), 2.39 – 2.20 (m, 1H), 2.04 (t, *J* = 6.9 Hz, 1H), 1.52 – 0.93 (m, 6H).

(R)-3-((R)-2-((R)-2-((R)-2-amino-3-methylbutanamido)propanamido)-3-(4-(tert-butoxy)phenyl)propanamido)-7-(tritylthio)heptanoic acid (3.33)

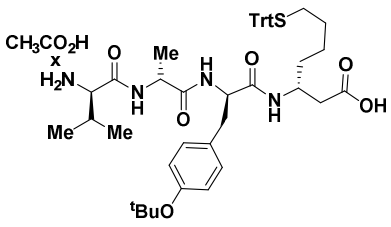

The linier peptide was synthesized using the standard conditions for SPPS. The peptide was cleaved with a mixture of CF_3CH_2OH:AcOH:CH_2Cl_2 (2:2:6) for 45 min. then cleavage was then repeated for 15 min. The solvent was evaporated and dried on high vacuum to afford the crude compound with some impurities present (64%, 68 mg, 9 steps). ^{1}H NMR (300 MHz, DMSO-d_6) δ 8.14 – 7.94 (m, 2H), 7.90 – 7.73 (m, 1H), 7.39 – 7.18 (m, 15H), 7.07 (d, *J* = 8.1 Hz, 2H), 6.81 (d, *J* = 8.3 Hz, 2H), 4.34 (s, 1H), 4.23 (s, 2H), 3.89 (s, 1H), 3.06 – 2.66 (m, 4H), 2.15 (t, *J* = 12.2 Hz, 2H), 2.02 (t, *J* = 7.0 Hz, 2H), 1.36 – 1.04 (m, 20H), 0.80 (dd, *J* = 29.6, 6.8 Hz, 6H).

(3R,6R,9R,13R)-3-(4-(tert-butoxy)benzyl)-9-isopropyl-6-methyl-13-(4-(tritylthio)butyl)-1,4,7,10-tetraazacyclotridecane-2,5,8,11-tetraone (**3.34**)

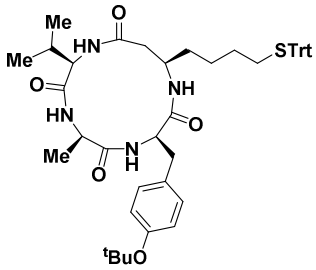

To **3.33** (63 mg, 0.072 mmol) and ^{i}PrEt$_2$N (0.1 mL, 0.58 mmol) in DMF (144 mL) was added HATU (56 mg, 0,144 mmol). The reaction was stirred at room temperature for 19h, then evaporated. The crude mixture was dissolved in EtOAc (100 mL), washed with 1M HCl (2x 10 mL) and purified by VLC (0–10% MeOH in CH_2Cl_2) to obtain the product (~18%, 10 mg) as a white solid with some impurities present.

(3R,6R,9R,13R)-3-(4-hydroxybenzyl)-9-isopropyl-13-(4-mercaptobutyl)-6-methyl-1,4,7,10-tetraazacyclotridecane-2,5,8,11-tetraone (**3.35**)

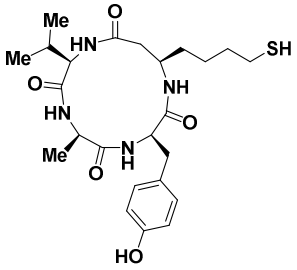

To **3.34** (10 mg, 0.013) in CH_2Cl_2 (2 mL) at 0 °C was added TFA (40 µL, 0.52 mmol) and ^{i}Pr$_3$SiH (3.2 µL, 0.026 mmol) and the reaction was then allowed to warm slowly to room temperature. After 2h the solvent was evaporated. ^{1}H NMR (400 MHz, DMSO-d_6) δ 9.12 (s, 1H), 7.91 (d, *J* = 8.0 Hz, 1H), 7.74 (d, *J* = 8.3 Hz, 1H), 7.56 (d, *J* = 8.1 Hz, 1H), 6.93 (d, *J* = 8.4 Hz, 2H), 6.86 (d, *J* = 9.1 Hz, 1H), 6.61 (d, *J* = 8.4 Hz, 2H), 4.25 (q, *J* = 8.0 Hz, 1H), 4.14 – 4.01 (m, 1H), 3.92 (brs, 1H), 3.79 (s, 1H), 3.06 (dd, *J* = 13.7, 6.7 Hz, 1H), 2.70 – 2.65 (m, 1H), 2.36 – 2.29 (m, 2H), 2.22 (d, *J* = 7.6 Hz, 2H), 2.01 – 1.87 (m, 1H), 1.50 (d, *J* = 3.8 Hz, 6H), 1.14 (d, *J* = 7.3 Hz, 3H), 0.88 (d, *J* = 6.4 Hz, 6H).

(S)-4-(tert-butoxy)-4-oxo-2-(((2-(trimethylsilyl)ethoxy)carbonyl)amino)butanoic acid (**3.40**)

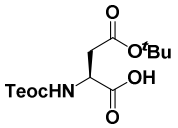

To L-Asp-OH (1 g, 5.3 mmol) and Et_3N (1.84 mL, 13.2 mmol) in H_2O (5 mL) and dioxane (5 mL) was added 4-Nitrophenyl 2-(trimethylsilyl)ethyl carbonate (1.5 g, 5.3 mmol). The reaction was stirred at room temperature for 24h, then diluted with H2O (5mL) and acidified with 1M $KHSO_4$ (10 mL). The mixture was extracted with Et_2O (4x 40 mL) and washed with brine (2x 60 mL). Purification by VLC (10–30% EtOAc in hexane + 2% AcOH) afforded the product (1.63 g, 93%) as white crystals. ^{1}H NMR (400 MHz, $CDCl_3$) δ 5.63 (d, *J* = 8.4 Hz, 1H), 4.65 – 4.56 (m, 1H), 4.18 (t, *J* = 8.5 Hz, 2H), 2.97 (dd, *J* = 17.1, 4.1 Hz, 1H), 2.75 (dd, *J* = 17.1, 5.1 Hz, 1H), 1.44 (s, 9H), 1.00 (t, *J* = 8.4 Hz, 2H), 0.04 (s, 9H). ^{13}C NMR (101 MHz, $CDCl_3$) δ 175.6, 170.5, 156.6, 82.4, 63.9, 50.4, 37.8, 28.2, 17.8, -1.36. Mp: 39.8–42.3 °C.

tert-butyl (S)-4-hydroxy-3-(((2-(trimethylsilyl)ethoxy)carbonyl)amino)butanoate (**3.39**)

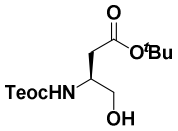

To **3.40** (275 mg, 0.82 mmol) and NMM (91 μL, 0.82 mmol) in 1,2-Dimethoxyethane (1 mL) at –15 °C was added ^{i}BuOCOCl (106 μL, 0.82 mmol). The reaction was stirred 20 min, then filtered and cooled to –20 °C followed by addition of $NaBH_4$ (47 mg, 1.23 mmol) in H_2O (0.5 mL). Additional H_2O (6 mL) was added, then stirred for 10 min, warmed to room temperature and stirred for 20 min. The mixture was extracted with EtOAc (3x 10 mL), washed with brine (2x 10 mL), dried ($MgSO_4$) and evaporated. Purification by VLC (30% EtOAC in hexane) afforded the product (204 mg, 77%) as a clear oil. ^{1}H NMR (400 MHz, $CDCl_3$) δ 5.33 (brs, 1H), 4.15 (d, *J* = 8.3 Hz, 2H), 4.05 – 3.92 (m, 1H), 3.71 (t, *J* = 5.1 Hz, 2H), 2.63 – 2.45 (m, 3H), 1.45 (d, *J* = 1.6 Hz, 9H), 0.98 (t, *J* = 8.4 Hz, 2H), 0.03 (s, 9H). ^{13}C NMR (101 MHz, $CDCl_3$) δ 171.2, 156.9, 81.6, 64.8, 63.4, 50, 37.5, 28.2, 17.8, -1.4.

4-(benzyloxy)butan-1-ol (**3.41a**).[214]

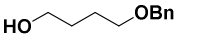

To 1,4-butanediol (2.42 mL, 27.3 mmol) and NaH (60% in mineral oil, 1.09 g, 27.3 mmol) in anhydrous THF (125 mL) was added BnBr (2.5 mL, 21 mmol) in anhydrous THF (7.5 mL) dropwise. The reaction was heated to reflux for 18h, then quenched with H_2O (50 mL). The aqueous phase was extracted with Et_2O (3x 50 mL) and the combined organic phases were washed with brine (2x75 mL, dried (MgSO4) and evaporated. Purification by VLC (0–40% EtOAc in hexane) afforded the product as a yellow oil (85%, 3.22 g). ^{1}H NMR (400 MHz, $CDCl_3$) δ 7.40 – 7.24 (m, 5H), 4.53 (s, 2H), 3.66 (q, *J* = 5.9 Hz, 2H), 3.53 (t, *J* = 5.8 Hz, 2H), 2.12 (t, *J* = 5.7 Hz, 1H), 1.79 – 1.62 (m, 4H); ^{13}C NMR (101 MHz, $CDCl_3$) δ 138.1, 128.4, 127.8, 127.7, 73.1, 70.4, 62.8, 30.2, 26.7

5-(benzyloxy)pentan-1-ol (**3.41b**).

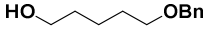

To 1,5-pentanediol (2.86 mL, 27.3 mmol) and NaH (60% in mineral oil, 1.09 g, 27.3 mmol) in anhydrous THF (125 mL) was added BnBr (2.5 mL, 21 mmol) in anhydrous THF (7.5 mL) dropwise. The reaction was heated to reflux for 18h, then quenched with H_2O (50 mL). The aqueous phase was extracted with Et_2O (3x 50 mL) and the combined organic phases were washed with brine (2x75 mL, dried (MgSO4) and evaporated. Purification by VLC (0–40% EtOAc in hexane) afforded the product as a yellow oil (68%, 2.76 g). ^{1}H NMR (400 MHz, $CDCl_3$) δ 7.32 – 7.16 (m, 5H), 4.43 (s, 2H), 3.62 – 3.52 (m, 2H), 3.41 (t, *J* = 6.5 Hz, 2H), 1.64 – 1.46 (m, 4H), 1.44 – 1.31 (m, 2H), 1.27 (s, 1H).

((4-bromobutoxy)methyl)benzene (**3.42a**).[214]

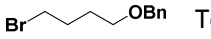

To PPh_3 (3.4 g, 13 mmol) in Et_2O (20 mL) at 0 °C was added CBr_4 (4.3 g, 13 mmol) in one portion and the reaction was stirred for 20 min. **3.41a** (1.02g, 5.65 mmol) in Et_2O (11 mL) was then added dropwise. The reaction was heated to reflux for 2h, then diluted with hexane and evaporated. The mixture was filtered on celite, diluted with hexane and evaporated again. This procedure was repeated four times. Purification by VLC (0–3% EtOAc in hexane) afforded the product as a clear oil (87%, 1.2 g). ^{1}H NMR (400 MHz, $CDCl_3$) δ 7.33 – 7.16 (m, 5H), 4.43 (s, 2H), 3.44 (t, *J* = 6.2 Hz, 2H), 3.37 (t, *J* = 6.7 Hz, 2H), 1.97 – 1.85 (m, 2H), 1.75 – 1.64 (m, 2H).

(((5-bromopentyl)oxy)methyl)benzene (**3.42b**).

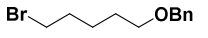

To PPh_3 (3.4 g, 13 mmol) in Et_2O (20 mL) at 0 °C was added CBr_4 (4.3 g, 13 mmol) in one portion and the reaction was stirred for 20 min. **3.41a** (1.02g, 5.65 mmol) in Et_2O (11 mL) was then added dropwise. The reaction was heated to reflux for 2h, then diluted with hexane and evaporated. The mixture was filtered on celite, diluted with hexane and evaporated again. This procedure was repeated three times. Purification by VLC (0–3% EtOAc in hexane) afforded the product as a clear oil (89%, 1.3 g). ^{1}H NMR (400 MHz, $CDCl_3$) δ 7.32 – 7.16 (m, 5H), 4.43 (s, 2H), 3.41 (t, *J* = 6.3 Hz, 2H), 3.33 (t, *J* = 6.8 Hz, 2H), 1.81 (p, *J* = 7.1 Hz, 2H), 1.62 – 1.53 (m, 2H), 1.50 – 1.41 (m, 2H).

(4-(benzyloxy)butyl)triphenylphosphonium bromide (**3.43a**)

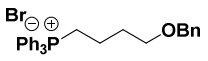

To PPh_3 (3.25 g, 12.4 mmol) in anhydrous toluene (40mL) was added **3.42a** (2.9 g, 11.8 mmol) and the reaction was heated to reflux for 24h. The crude product was dissolved in CH_2Cl_2 (4 mL) and triturated with Et_2O. The product was obtained as a white precipitate (45%, 2.7 g). ^{1}H NMR (400 MHz, $CDCl_3$) δ 7.89 – 7.59 (m, 15H), 7.38 – 7.08 (m, 5H), 4.46 (s, 2H), 3.88 – 3.73 (m, 2H), 3.66 – 3.56 (m, 2H), 2.09 – 1.96 (m, 2H), 1.85 – 1.73 (m, 2H).

Experimentals for chapter 4

benzyl 2-(1H-indol-3-yl)ethylcarbamate (**4.19**).[215]

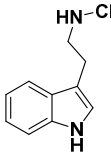

To a solution of tryptamine (13.67 mmol, 2.19 g) in 80 mL CH_2Cl_2 was added $NaHCO_3$ (68.3 mmol, 5.74 g) in 80 mL H_2O. Cbz-Cl (15.03 mmol, 2.2 mL) was then added slowly and stirred vigorously at rt for 40 min. The aqueous phase was extracted with CH_2Cl_2 (2 x 50 mL) and the combined organic phases were washed with brine (2 x 80 mL), dried (Na_2SO_4), and concentrated. Purification by silica gel chromatography (0–2% MeOH/DCM) afforded the product (3.57 g, 89%) as a white solid. ^{1}H NMR (500 MHz, $CDCl_3$) δ 8.07 (s, 1H), 7.61 (d, *J* = 7.8 Hz, 1H), 7.41 – 7.29 (m, 6H), 7.21 (t, *J* = 7.1 Hz, 1H), 7.13 (t, *J* = 7.4 Hz, 1H), 6.99 (s, 1H), 5.11 (s, 2H), 4.85 (s, 1H), 3.55 (dd, *J* = 12.8, 6.4 Hz, 2H), 2.99 (t, *J* = 6.7 Hz, 2H). ^{13}C NMR (126 MHz, $CDCl_3$) δ 156.5, 136.7, 136.5, 128.5, 128.2, 127.3, 122.23, 122.16, 119.5, 118.8, 112.7, 111.4, 66.7, 41.4, 25.8.

N-Cbz-*N*,1-dimethyltryptamine (**4.20**).

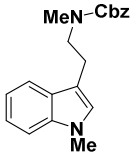

To a solution of **4.19** (3.16 mmol, 931 mg) in 20 mL anhydrous THF at 0 °C was added NaH (60% in mineral oil; 12.6 mmol, 504 mg). The reaction was stirred for 10 min where after MeI (14.2 mol, 0.9 mL) was added. After 10 min, the reaction was allowed to warm to rt. After stirring for 11 h, additional NaH (60% in mineral oil; 6.3 mmol, 202 mg) and MeI (8.2 mmol, 0.6 mL) was added and the reaction was stirred for 1.5 h. The reaction was quenched with NH_4Cl (10 mL) and the aqueous phase was extracted with EtOAc (2 x 10 mL). The combined organic phases were washed with $NaHCO_3$ (2 x 40 mL), brine (2 x 40 mL), dried (Na_2SO_4), and concentrated. Purified by silica gel chromatography (10–20% EtOAc in hexanes) afforded the product (954 mg, 93%) as a clear yellow oil. ^{1}H NMR (500 MHz, $CDCl_3$, compound exists as a 1.4:1 mixture of rotamers, the major rotamer is designated by *, minor rotamer designated by §) δ 7.65 (d, *J* = 7.9 Hz, 1H§), 7.45 (d, *J* = 7.9 Hz, 1H*), 7.42–7.26 (m, 6H*, 6H§), 7.25–7.18 (m, 1H*, 1H§), 7.11 (dd, *J* = 7.4, 7.4 Hz, 1H§), 7.02 (dd, *J* = 7.4, 7.4 Hz, 1H*), 6.89 (s, 1H§), 6.79 (s, 1H*), 5.17 (s, 2H§), 5.10 (s, 2H*), 3.73 (s, 3H§), 3.71 (s, 3H*), 3.59 (t, *J* = 7.9 Hz, 2H§), 3.54 (t, *J* = 7.7 Hz, 2H*), 3.01 (t, *J* = 7.9 Hz, 2H§), 2.96 (t, *J* = 7.8 Hz, 2H*), 2.95 (s, 3H*), 2.92 (s, 3H§).; ^{13}C NMR (125 MHz, $CDCl_3$; compound exists as a 1.4:1 mixture of rotamers) δ 156.3, 156.2, 136.9, 136.8, 128.4, 128.0, 127.9, 127.86, 127.8, 127.7, 126.7, 121.5, 118.83, 118.78, 118.7, 111.5, 111.4, 109.2, 67.1, 66.9, 50.2, 49.8, 35.0, 34.5, 24.1, 23.4.; FTIR (NaCl/thin film): 3056, 3030, 1703, 1699, 1484, 1475, 1403, 1211, 1192, 1134 cm^{-1}; HRMS (MM) calc'd for $C_{20}H_{23}N_2O_2$ $[M+H]^+$323.1754, found 323.1758.

benzyl methyl(2-(1-methyl-2-phenyl-1H-indol-3-yl)ethyl)carbamate (**4.21**).[195]

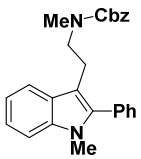

Four oven-dried microwave vials were each charged with **4.20** (231 mg, 0.72 mmol), 2-NO_2Bz (288 mg, 1.1 mmol), $Pd(OAc)_2$ (6.25 mg, 37.4 μmol), $AgBF_4$ (228 mg, 1.2 mmol, weighed into small vials in a glovebox then removed from the glovebox and transferred quickly to the microwave vials), PhI (0.33 mL, 3.0 mmol), and 4.5 mL DMF. The microwave vials were sealed under argon and the orange reaction mixtures were stirred at room temperature for 30 minutes, then heated in the microwave for 4 min at 150 °C. The four reaction mixtures were then combined and filtered through celite with 60 mL EtOAc, washed (3 x 40 mL saturated aqueous NH_4Cl, 3 x 40 mL saturated aqueous $NaHCO_3$,

3 x 40 mL brine), dried (Na_2SO_4), filtered, and concentrated. Purification by silica gel column chromatography (8% EtOAc in hexanes) afforded the product (921 mg, 81%) as a yellow solid. ^{1}H NMR (500 MHz, $CDCl_3$, compound exists as a 1.7:1 mixture of rotamers, the major rotamer is designated by *, minor rotamer designated by §) δ 7.74 (d, *J* = 7.9 Hz, 1H§), 7.53-7.22 (m, 13H*, 12H§), 7.17 (dd, *J* = 7.5, 7.5 Hz, 1H§), 7.06 (dd, *J* = 7.6, 7.6 Hz, 1H*), 5.09 (s, 2H§), 4.98 (s, 2H*), 3.59 (s, 3H§), 3.57 (s, 3H*), 3.50 (t, *J* = 8.2 Hz, 2H§), 3.45 (t, *J* = 7.8 Hz, 2H*), 2.97 (t, *J* = 7.5 Hz, 2H§), 2.91 (t, *J* = 7.8 Hz, 2H*), 2.78 (s, 3H*), 2.76 (s, 3H§).; ^{13}C NMR (125 MHz, $CDCl_3$; compound exists as a 1.7:1 mixture of rotamers) δ 156.1, 156.0, 138.6, 138.4, 137.1, 136.8, 131.8, 131.7, 130.4, 128.4, 128.14, 128.10, 128.0, 127.84, 127.81, 127.7, 127.5, 121.8, 119.42, 119.37, 119.0, 118.6, 109.7, 109.6, 109.4, 109.3, 67.0, 66.8, 50.5, 49.7, 34.8, 34.6, 30.81, 30.76, 23.5, 23.0; FTIR (NaCl/thin film): 3055, 3030, 2939, 1703, 1699, 1695, 1471, 1403, 1362, 1197, 1138 cm^{-1}; HRMS (MM) calc'd for $C_{26}H_{27}N_2O_2$ $[M+H]^+$ 399.2067, found 399.2087.

N,1-dimethyl-2-phenyltryptamine (4.22).[216]

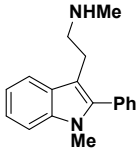

A solution of **4.21** (574 mg, 1.44 mmol) in CH_2Cl_2 (15 mL) was prepared in a flame-dried flask under argon. Et_3SiH (9.2 mL, 57.7 mmol) and Et_3N (0.4 mL, 2.87 mmol) were then added, followed by $Pd_2(dba)_3$•$CHCl_3$ (298 mg, 0.288 mmol). The dark red reaction solution was stirred for 16 hours and the resultant dark brown mixture was filtered through celite with 50 mL EtOAc, washed (2 x 40 mL saturated aqueous $NaHCO_3$, 2 x 40 mL brine), dried (Na_2SO_4), filtered, and concentrated. The crude residue was purified by silica gel column chromatography (0–8% MeOH in DCM) to afford the product (332 mg, 87%) as a yellow oil. ^{1}H NMR (500 MHz, $CDCl_3$) δ 7.68 (d, *J* = 7.8 Hz, 1H), 7.53–7.38 (m, 5H), 7.35 (ddd, *J* = 8.2, 0.8, 0.8 Hz, 1H), 7.26 (ddd, *J* = 8.1, 6.9, 1.0 Hz, 1H), 7.16 (ddd, *J* = 8.1, 7.0, 1.0 Hz, 1H), 3.59 (s, 3H), 2.92 (t, *J* = 7.2 Hz, 2H), 2.82 (t, *J* = 7.1 Hz, 2H), 2.34 (s, 3H), 1.37 (s, 1H).; ^{13}C NMR (125 MHz, $CDCl_3$) δ 138.7, 137.0, 131.1, 130.3, 128.8, 128.5, 127.0, 122.0, 119.8, 118.7, 109.46, 107.0, 49.3, 32.4, 30.8, 21.3.; FTIR (NaCl/thin film): 3051, 2934, 2840, 2789, 1468, 1442, 1430, 1364, 1333, 1236, 1131, 1013 cm^{-1}; HRMS (MM) calc'd for $C_{18}H_{21}N_2$ $[M+H]^+$ 265.1699, found 265.1707.

3a-hydroxy-1,1a-dimethyl-2a-phenylpyrroloindoline (4.16)

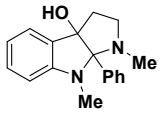

A 15 mL flame-dried flask containing **4.22** (59.5 mg, 0.23 mmol) was charged with flame-dried 4Å molecular sieves and MeCN (1.3 mL). NCS (recrystallized from toluene, 30.2 mg, 0.225 mmol) was then added as a solution in 2 mL MeCN dropwise and the reaction was stirred in the dark at room temperature for 4 hours, followed by addition of more NCS (15.4 mg, 0.115 mmol) as a solution in 1 mL MeCN. After 1.5 hours, the dark green reaction solution was quenched with 5 mL aqueous $Na_2S_2O_3$ (10 wt %) and extracted with EtOAc (3 x 5 mL). The combined organic layers were washed with 30 mL brine, dried (Na_2SO_4), filtered, and concentrated. The crude oil was combined with MeCN (5 mL), H_2O (5 mL) and SiO_2 (5 mL), then vigorously stirred open to air at room temperature for 30 minutes, filtered and washed with EtOAc, dried (Na_2SO_4), filtered and concentrated. The crude was subjected to silica gel column chromatography (0–1% MeOH/DCM) and then to reverse phase preparative HPLC (0.01:18:82 to 0.01:80:20 TFA:MeCN:H_2O) using an Agilent 1200 Series HPLC with an Agilent XDB-C18 5 μM column (9.4 x 250 mm). The combined product-containing eluent was diluted with 20 mL saturated aqueous $NaHCO_3$ and extracted with EtOAc (3 x 30 mL). The combined organic layers were dried (Na_2SO_4), filtered, and concentrated to afford the product (21.0 mg, 33%) as a yellow solid. ^{1}H NMR (500 MHz, $CDCl_3$) δ 7.75 – 6.90 (m, 6H), 7.32 (ddd, *J* = 8.6, 7.3, 1.4 Hz, 1H), 6.71 (ddd, *J* = 7.4, 7.4, 1.0 Hz, 1H), 6.44 (d, *J* = 7.8 Hz, 1H), 3.07 – 3.01 (m, 1H), 2.77 (s, 3H), 2.62 – 2.55 (m, 1H), 2.49 (s, 3H), 2.29 – 2.23 (m, 2H), 1.44 (br s, 1H).; ^{13}C NMR (125

MHz, $CDCl_3$) δ 152.5, 137.1, 130.7, 129.9, 128.7, 128.0, 123.9, 116.9, 104.0, 98.3, 90.6, 51.4, 40.5, 36.6, 34.4.; FTIR (NaCl/thin film): 3540, 3435, 3051, 2931, 2791, 1608, 1492, 1473, 1445, 1370, 1308, 1106, 1028 cm^{-1}; HRMS (MM) calc'd for $C_{18}H_{21}N_2O$ $[M+H]^+$ 281.1648, found 281.1655.

3a-amino-1,1a-dimethyl-2a-phenylpyrroloindoline (**4.24**)

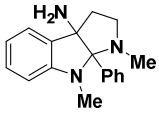

A 15 mL oven-dried flask containing **4.22** (39.6 mg, 0.15 mmol) was charged with flame-dried 4Å molecular sieves and MeCN (0.9 mL). NCS (recrystallized from toluene, 20.1 mg, 0.15 mmol) was then added as a solution in MeCN (1.75 mL) dropwise. After stirring in the dark at room temperature for 3 hours, the off-white reaction solution was quenched with 2.8 mL aqueous ammonia and stirred vigorously open to air for 20 minutes. The mixture was then diluted with H_2O (10 mL) and extracted with EtOAc (3 x 5 mL). The combined organic layers were washed with brine (15 mL), dried (Na_2SO_4), filtered, and concentrated. The crude oil was purified by silica gel column chromatography (0–1% MeOH in DCM) to afford the product (24.0 mg, 57% yield) as a yellow oil. ^{1}H NMR (500 MHz, $CDCl_3$) δ 7.73 (br s, 1H), 7.54 – 7.27 (m, 3H), 7.24 (dd, *J* = 7.2, 1.3 Hz, 1H), 7.19 (ddd, *J* = 7.7, 7.7, 1.4 Hz, 1H), 6.83 (br s, 1H), 6.68 (ddd, *J* = 7.4, 7.4, 1.0 Hz, 1H), 6.40 (d, *J* = 7.8 Hz, 1H), 2.96 (dd, *J* = 9.1, 7.0 Hz, 1H), 2.79 (s, 3H), 2.58 (ddd, *J* = 12.0, 9.1, 5.1 Hz, 1H), 2.47 (s, 3H), 2.20 (dd, *J* = 12.2, 5.1 Hz, 1H), 1.95 (ddd, *J* = 12.1, 12.1, 7.1 Hz, 1H), 1.12 (br s, 2H).; ^{13}C NMR (125 MHz, $CDCl_3$) δ 152.5, 138.6, 132.0, 129.1, 128.9, 128.5, 127.8, 127.7, 123.9, 116.6, 103.6, 99.0, 74.8, 51.2, 42.0, 36.8, 34.6.; FTIR (NaCl/thin film): 3051, 2930, 2861, 2791, 2254, 1606, 1495, 1473, 1445, 1372, 1308, 1035 cm^{-1}; HRMS (MM) calc'd for $C_{18}H_{22}N_3$ $[M+H]^+$ 280.1808, found 280.1818.

N-Cbz-1-methyltryptamine (**4.25**).[217]

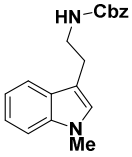

To **4.19** (212 mg, 0.721 mmol) in acetone (3 mL) was added KOH (202 mg, 3.60 mmol). After 10 min, MeI (49 µL, 0.787 mmol) was added and the orange reaction solution was stirred 1 hour at room temperature, followed by addition of more KOH (202 mg, 3.60 mmol) and MeI (49 µL, 0.787 mmol). After stirring for 3.5 hours at room temperature, the reaction was diluted with toluene, filtered, and concentrated. Purification by silica gel column chromatography (5–20% EtOAc in hexanes) afforded the product (151 mg, 68%). ^{1}H NMR (500 MHz, $CDCl_3$) δ 7.59 (d, *J* = 7.9 Hz, 1H), 7.43 – 7.29 (m, 6H), 7.24 (ddd, *J* = 8.2, 7.0, 1.1 Hz, 1H), 7.11 (t, *J* = 7.4 Hz, 1H), 6.86 (s, 1H), 5.11 (s, 2H), 4.83 (brs, 1H), 3.74 (s, 3H), 3.54 (dd, *J* = 12.8, 6.5 Hz, 2H), 2.97 (t, *J* = 6.7 Hz, 2H).

N-Cbz-1-methyl-2-phenyltryptamine (**4.26**).[195]

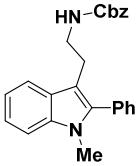

An oven-dried microwave vial was charged with **4.25** (134 mg, 0.435 mmol), 2-NO_2Bz (147 mg, 0.653 mmol), $Pd(OAc)_2$ (3.3 mg, 20 µmol), $AgBF_4$ (131 mg, 0.672 mmol), weighed into a small vial in a glovebox then removed from the glovebox and transferred quickly to the microwave vial), PhI (0.19 mL, 1.70 mmol), and 4.3 mL DMF. The microwave vial was sealed under argon and the orange solution was stirred at room temperature for 30 minutes, then heated in the microwave for 4 min at 150 °C. The resultant brown reaction mixture was filtered through celite with EtOAc, washed (2 x 10 mL saturated aqueous NH_4Cl, 2 x 10 mL saturated aqueous $NaHCO_3$, 2 x 10 mL brine), dried (Na_2SO_4), filtered, and concentrated. Purification by silica gel column chromatography (6–12% EtOAc in hexanes) afforded the product (142 mg, 85%) as an orange oil. ^{1}H NMR (500 MHz, $CDCl_3$, compound exists as a 5.6:1 mixture of rotamers, the major rotamer is designated by *, minor rotamer designated by §) δ 7.67 (d, *J* = 7.9 Hz, 1H*), 7.54 (br s, 1H§), 7.50 – 7.41 (m, 3H*, 3H§), 7.40 – 7.26 (m, 9H*, 9H§), 7.17 (dd, *J* = 7.4 Hz, 1H*), 7.12 (br s, 1H§), 5.04 (s, 2H*, 2H§), 4.73 (t, *J* = 6.8 Hz, 1H*), 4.51 (br s, 1H§), 3.58 (s, 3H*, 3H§), 3.44 (td, *J* = 6.7, 6.7 Hz, 2H*),

3.38 (br s, 1H[§]), 2.94 (t, *J* = 6.9 Hz, 2H*), 2.90 (br s, 1H[§]).; ^{13}C NMR (125 MHz, $CDCl_3$; compound exists as a 5.6:1 mixture of rotamers, only the major rotamer is reported) δ 156.2, 138.8, 137.1, 131.7, 130.6, 128.5, 128.4, 128.2, 128.0, 121.9, 119.5, 118.9, 109.6, 109.4, 66.4, 41.7, 30.8, 25.1.; FTIR (NaCl/thin film): 3413, 3339, 3055, 3030, 2940, 1718, 1701, 1511, 1368, 1361, 1334, 1233, 1132 cm^{-1}; HRMS (MM) calc'd for $C_{25}H_{25}N_2O_2$ $[M+H]^+$ 385.1911, found 385.1924.

3a-hydroxy-1a-methyl-2a-phenylpyrroloindoline (**4.27**).

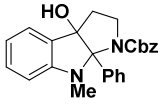

A 5 mL oven-dried flask containing **4.26** (24.0 mg, 62.5 μmol) was charged with flame-dried 4Å molecular sieves and MeCN (0.5 mL). NCS (recrystallized from toluene, 8.4 mg, 0.225 mmol) was then added as a solution in MeCN (1.25 mL) dropwise. After stirring in the dark at room temperature for 6 hours, the light yellow reaction solution was quenched with aqueous $Na_2S_2O_3$ (10 wt %, 5 mL) and extracted with EtOAc (4 x 5 mL). The combined organic layers were washed with brine (15 mL), dried (Na_2SO_4), filtered, and concentrated. The crude residue was combined with MeCN (1.5 mL), H_2O (1.5 mL) and SiO_2 (1.5 mL), then vigorously stirred open to air at room temperature for 30 minutes, filtered through a 1.5 mL silica plug with EtOAc, and concentrated. Purification by reverse phase preparative HPLC (60:40 to 90:10 MeCN:H_2O) using an Agilent 1200 Series HPLC with an Agilent XDB-C18 5 μM column (9.4 x 250 mm) afforded the product (13.7 mg, 55%) as a light yellow-green oil. ^{1}H NMR (500 MHz, $CDCl_3$, compound exists as a 1.1:1 mixture of rotamers, the major rotamer is designated by *, minor rotamer designated by [§]; due to overlap in the NMR, the rotamer shifts were confirmed by HSQC 2D NMR) δ 7.48 – 7.09 (m, 11H*, 11H[§]), 6.83 – 6.75 (m, 2H*), 6.75 – 6.68 (m, 2H[§]), 6.58 (d, *J* = 7.8 Hz, 1H*), 6.50 (d, *J* = 7.9 Hz, 1H[§]), 5.12 (d, *J* = 12.4 Hz, 1H*), 5.07 – 5.01 (m, 1H*, 1H[§]), 4.85 (d, *J* = 12.3 Hz, 1H[§]), 4.05 (dd, *J* = 9.7 Hz, 1H[§]), 3.98 (dd, *J* = 9.5 Hz, 1H*), 3.30 (ddd, *J* = 11.1, 11.1, 6.2 Hz, 1H*), 3.21 (ddd, *J* = 11.5, 11.5, 5.9 Hz, 1H[§]), 3.04 (s, 3H*), 2.75 (s, 3H[§]), 2.50 – 2.39 (m, 1H*, 1H[§]), 2.31 – 2.19 (m, 1H*, 1H[§]), 1.50 (br s, 1H*, 1H[§]).; ^{13}C NMR (125 MHz, $CDCl_3$, compound exists as a 1.1:1 mixture of rotamers) δ 155.0, 154.5, 151.1, 151.0, 136.7, 135.6, 130.8, 128.6, 128.4, 128.2, 128.1, 128.0, 127.8, 127.7, 127.6, 127.4, 127.3, 123.62, 123.59, 118.1, 117.8, 106.53, 106.45, 89.6, 88.6, 67.0, 66.7, 46.3, 46.2, 34.1, 33.6, 31.9, 31.3.; FTIR (NaCl/thin film): 3049, 3056, 3032, 2945, 2891, 1695, 1684, 1675, 1609, 1491, 1401, 1348, 1186, 1117, 1004 cm^{-1}; HRMS (MM) calc'd for $C_{25}H_{25}N_2O_3$ $[M+H]^+$401.1860, found 401.1877.

3a-hydroxy-1a-methyl-2a-phenylpyrroloindoline (**4.17**)

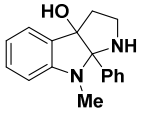

A solution of **4.27** (10.1 mg, 25.2 μmol) in THF (1.0 mL) was prepared in a flame-dried flask. Et_3SiH (0.16 mL, 1.0 mmol) and Et_3N (7.0 μL, 50 μmol) were then added, followed by $Pd_2(dba)_3$•$CHCl_3$ (5.0 mg, 4.8 μmol). The dark red reaction solution was stirred for 19 hours at room temperature, then filtered through celite with THF, combined with an equal volume of saturated aqueous $NaHCO_3$, and stirred at room temperature for 5 hours. The aqueous layer was then extracted with EtOAc (3 x 15 mL) and the combined organic layers were dried (Na_2SO_4), filtered and concentrated. The crude residue was purified by silica gel column chromatography (0–2% MeOH in DCM) to afford the product (6.1 mg, 91% yield) as a yellow solid. ^{1}H NMR (300 MHz, $CDCl_3$) δ 7.50 – 7.27 (m, 5H), 7.25 (ddd, *J* = 7.2, 1.4, 0.5 Hz, 1H), 7.20 (ddd, *J* = 7.7, 7.7, 1.3 Hz, 1H), 6.68 (ddd, *J* = 7.4, 7.4, 1.0 Hz, 1H), 6.42 (d, *J* = 7.9 Hz, 1H), 3.25 (ddd, *J* = 9.4, 5.1, 3.8 Hz, 1H), 2.94 – 2.83 (m, 1H), 2.63 (s, 3H), 2.32 – 2.25 (m, 2H), 1.03 – 0.89 (br m, 1H), 0.65 – 0.51 (br m, 1H).;^{13}C NMR (125 MHz, $CDCl_3$) δ 151.2, 138.2, 130.7, 130.1, 128.6, 128.2, 127.4, 123.9, 117.1, 104.3, 95.2, 89.6, 43.3, 41.9, 28.5.; FTIR (NaCl/thin film): 3340, 3051, 2931, 2874, 1609, 1495, 1446, 1375, 1307, 1121, 1062 cm^{-1}; HRMS (MM) calc'd for $C_{17}H_{19}N_2O$ $[M+H]^+$ 267.1492, found 267.1502.

(L)-N_α-Cbz-tryptophan (**4.29**).[218]

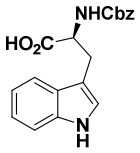

A solution of L-tryptophan (896 mg, 4.39 mmol) and K_2CO_3 (1.52 g, 10.97 mmol) in H_2O (25 mL) was cooled to 0 °C in an ice bath. *N*-(Benzyloxycarbonyloxy)succinimide (988 mg, 3.97 mmol) was then added as a solution in wet DMF (25 mL) and the reaction was allowed to warm to room temperature. After stirring 40 minutes, the mixture was diluted with 300 mL H_2O and washed with EtOAc (2 x 10 mL). The aqueous layer was then cooled to 0 °C, acifidied with 6 mL concentrated HCl, and extracted with EtOAc (3 x 100 mL). The combined organic layers were washed with brine (2 x 150 mL), dried (Na_2SO_4), filtered, and concentrated (coevaporated with DCM and MeOH) to afford the product (1.07 g, 80%) as a white foam. ^{1}H NMR spectral data were in agreement with the literature.[219]

(L)-N_α-Cbz-N_α,1-dimethyltryptophan (**4.30**).

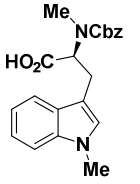

A solution of **4.29** (875 mg, 2.59 mmol) in THF (5 mL) was cooled to 0 °C in an ice bath. NaH (60% dispersion in oil, 516 mg, 12.9 mmol) was then added, followed by MeI (0.96 mL, 15.4 mmol). The yellow reaction mixture was allowed to warm to room temperature and stirred for 29 hours, then diluted with H_2O (10 mL) and acidified with 1 mL concentrated HCl. The aqueous layer was extracted with EtOAc (3 x 10 mL) and the combined organic layers were washed with brine (3 x 30 mL), dried (Na_2SO_4), filtered, and concentrated. Purified by silica gel column chromatography (5–50% EtOAc in hexanes with 2–4% AcOH) afforded the product (600 mg, 63%) as a yellow-brown foam. ^{1}H NMR (500 MHz, $CDCl_3$, compound exists as a 1.3:1 mixture of rotamers, the major rotamer is designated by *, minor rotamer designated by §) δ 10.54 (br s, 1H*, 1H§), 7.60 (d, *J* = 7.9 Hz, 1H*), 7.55 (d, *J* = 7.9 Hz, 1H§), 7.38 – 7.21 (m, 6H*, 6H§), 7.16 – 7.07 (m, 2H*, 2H§), 6.85 (s, 1H*), 6.76 (s, 1H§), 5.17 (s, 2H*), 5.09 – 4.99 (m, 1H*, 3H§), 3.684 (s, 3H*), 3.677 (s, 3H§), 3.50 (d, *J* = 5.0 Hz, 1H§), 3.47 (d, *J* = 4.9 Hz, 1H*), 3.32 (dd, *J* = 15.5, 10.6 Hz, 1H*), 3.18 (dd, *J* = 15.3, 10.5 Hz, 1H§), 2.92 (s, 3H§), 2.83 (s, 3H*).; ^{13}C NMR (125 MHz, $CDCl_3$; compound exists as a 1.3:1 mixture of rotamers, the major rotamer is designated by *, minor rotamer designated by §)) δ 176.5§, 176.4*, 157.0*, 156.3§, 136.93§, 136.88*, 136.6*, 136.2§, 128.5*, 128.4§, 128.01*, 127.96§, 127.9§, 127.7*, 127.3§, 127.1*, 121.8§, 121.7*, 119.1§, 119.0*, 118.5*, 118.4§, 109.5§, 109.4*, 109.32§, 109.27*, 67.6§, 67.5*, 59.9*, 59.4§, 32.67*, 32.66§, 32.0*, 31.7§, 25.0§, 24.4*.; FTIR (NaCl/thin film): 3034, 2939, 1741, 1701, 1664, 1475, 1455, 1403, 1326, 1214, 1141 cm^{-1}; $[\alpha]_D^{25}$ = –40.6º (*c* = 0.68, $CHCl_3$). HRMS (MM) calc'd for $C_{21}H_{23}N_2O_4$ $[M+H]^+$ 367.1652, found 367.1667.

(L)-N_α-Cbz-N_α,1-dimethyl-2-phenyltryptophan (**4.31**).[195]

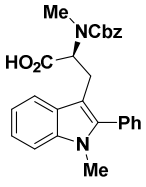

Two oven-dried microwave vials were each charged with 2-NO_2Bz (255 mg, 1.13 mmol), $Pd(OAc)_2$ (6.25 mg, 37.4 μmol), $AgBF_4$ (240 mg, 1.23 mmol, weighed into small vials in a glovebox then removed from the glovebox and transferred quickly to the microwave vials), and PhI (0.34 mL, 3.04 mmol). A solution of **4.30** (276 mg, 0.754 mmol) in DMF (4 mL) was then added to each vial. The microwave vials were sealed under argon and the reaction mixtures were stirred at room temperature for 30 minutes, then heated in the microwave for 4 min at 150 °C. The two reaction mixtures were then combined and filtered through celite with 15 mL EtOAc, washed with saturated aqueous NH_4Cl (2 x 20 mL), brine (2 x 20 mL), dried (Na_2SO_4), filtered, and concentrated. Purification by silica gel column chromatography (5–20% EtOAc in hexanes, with 4% AcOH) followed by washing with saturated aqueous $NaHCO_3$ afforded the product (366 mg, 55%) as a light yellow foam. The enantiomeric excess was

determined to be 94% by chiral SFC analysis (AD-H, 2.5 mL/min, 25% IPA in CO_2, λ = 254 nm): t_R(major) = 4.6 min t_R(minor) = 7.2 min. ^{1}H NMR (300 MHz, $CDCl_3$, compound exists as a 2.6:1 mixture of rotamers, the major rotamer is designated by *, minor rotamer designated by §) δ 7.55 (d, *J* = 7.9 Hz, 1H*), 7.46 (d, *J* = 7.9 Hz, 1H§), 7.32 – 6.85 (m, 13H*, 12H§), 6.57 (d, *J* = 7.4 Hz, 1H§), 4.87 (br d, *J* = 11.6 Hz, 1H§), 4.78 (d, *J* = 12.6 Hz, 1H*), 4.64 (d, *J* = 12.6 Hz, 1H*), 4.51 (d, *J* = 12.6 Hz, 1H§), 4.35 (d, *J* = 12.5 Hz, 1H§), 4.04 (br d, *J* = 10.3 Hz, 1H*), 3.53 – 3.25 (m, 5H*, 4H§), 3.03 – 2.88 (m, 1H§), 2.28 (s, 3H*), 2.11 (s, 3H§).; ^{13}C NMR (125 MHz, $CDCl_3$; compound exists as a 2.6:1 mixture of rotamers) δ 176.5, 176.3, 156.3, 155.6, 139.4, 139.0, 137.1, 136.5, 136.1, 131.6, 131.4, 130.6, 130.5, 128.5, 128.4, 128.3, 128.2, 127.8, 127.6, 127.4, 127.1, 121.9, 121.8, 119.6, 118.6, 118.4, 109.6, 109.4, 108.2, 107.8, 67.18, 67.15, 61.1, 59.7, 33.0, 32.2, 30.8, 30.7, 24.4, 23.9.; FTIR (NaCl/thin film): 3056, 3031, 2936, 1699, 1695, 1683, 1605, 1469, 1401, 1363, 1328, 1137 cm^{-1}; $[\alpha]_D^{25}$ = –133.3° (*c* = 0.84, $CHCl_3$). HRMS (MM) calc'd for $C_{27}H_{27}N_2O_4$ $[M+H]^+$ 443.1965, found 443.1984.

(S)-2-(((benzyloxy)carbonyl)(methyl)amino)-3-(1-methyl-2-phenyl-1H-indol-3-yl)propanoic acid (**4.32**)

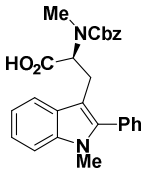

To a solution of **4.31** (90 mg, 0.2 mmol) in anhydrous CH_2Cl_2 (2.0 mL) was added Et_3SiH (1.2 mL, 8 mmol) and Et_3N (56 µL, 0.4 mmol) followed by $Pd_2(dba)_3$•$CHCl_3$ (30 mg, 0.04 mol). The dark red reaction solution was stirred for 24 hours at room temperature, then filtered through celite with CH_2Cl_2 and MeOH. Purification by silica gel column chromatography (2–5% MeOH in CH_2Cl_2) afforded an impure product (38 mg) and attempts to purify the product further lead to loss of the product. Purification was achieved after several fractions from different reaction was combined. ^{1}H NMR (500 MHz, CD_3OD) δ 7.78 (d, *J* = 7.6 Hz, 1H), 7.56 (t, *J* = 7.1 Hz, 2H), 7.50 (t, *J* = 6.7 Hz, 3H), 7.41 (d, *J* = 8.1 Hz, 1H), 7.24 (t, *J* = 7.5 Hz, 1H), 7.14 (t, *J* = 7.2 Hz, 1H), 3.72 (brs, 1H), 3.59 (s, 3H), 3.54 – 3.40 (m, 1H), 3.23 – 2.99 (m, 1H), 2.38 (s, 3H).

(*S*)-N_α-Cbz-N_α,1-dimethyl-2-phenyltryptophan methyl ester (**4.33**).

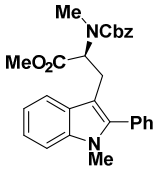

A solution of **4.31** (104 mg, 0.235 mmol) in wet MeOH (3 mL) was charged with $SOCl_2$ (34 µL, 0.47 mmol), then heated to 40 °C. After stirring for 5 hours, the reaction was diluted with 10 mL H_2O and extracted with EtOAc (3 x 10 mL). The combined organic layers were dried (Na_2SO_4) and concentrated. Purification by silica gel column chromatography (15% EtOAc in hexanes) afforded the product (92.6 mg, 86%) as a yellow oil. ^{1}H NMR (500 MHz, $CDCl_3$, compound exists as a 1.5:1 mixture of rotamers, the major rotamer is designated by *, minor rotamer designated by §) δ 7.67 (d, *J* = 7.9 Hz, 1H§), 7.59 (d, *J* = 7.9 Hz, 1H*), 7.49 – 7.19 (m, 11H§, 11H*), 7.17 – 7.10 (m, 1H§, 1H*), 6.97 – 6.90 (m, 1H§, 1H*), 5.02 (d, *J* = 12.5 Hz, 1H§), 4.89 (d, *J* = 12.6 Hz, 1H§), 4.82 – 4.71 (m, 2H*, 1H§), 4.62 (d, *J* = 12.3 Hz, 1H*), 3.65 (s, 3H§), 3.55 (s, 3H*), 3.531 (s, 3H§), 3.527 (s, 3H*), 3.51 – 3.45 (m, 1H*, 1H§), 3.27 (dd, *J* = 14.9, 10.3 Hz, 1H§), 3.21 (dd, *J* = 14.9, 10.8 Hz, 1H*), 2.49 (s, 3H§), 2.40 (s, 3H*).; ^{13}C NMR (125 MHz, $CDCl_3$; compound exists as a 1.5:1 mixture of rotamers) δ 171.6, 171.4, 156.0, 155.5, 139.4, 139.0, 137.0, 136.7, 136.2, 131.6, 131.5, 130.6, 130.5, 128.5, 128.4, 128.3, 128.17, 128.15, 128.1, 127.71, 127.68, 127.6, 127.54, 127.46, 127.2, 121.8, 121.7, 119.49, 119.47, 118.6, 118.4, 109.5, 109.3, 108.3, 108.0, 66.92, 66.86, 60.5, 59.9, 52.03, 51.98, 32.4, 32.3, 30.70, 30.67, 24.5, 24.1.; FTIR (NaCl/thin film): 3033, 2946, 1743, 1740, 1734, 1704, 1700, 1696, 1468, 1399, 1363, 1314, 1270, 1214, 1139 cm^{-1}; $[\alpha]_D^{25}$ = –82.8º (*c* = 0.22, $CHCl_3$). HRMS (MM) calc'd for $C_{28}H_{29}N_2O_4$ $[M+H]^+$ 457.2122, found 457.2128.

(L)-N_α,1-dimethyl-2-phenyltryptophan methyl ester (**4.34**).

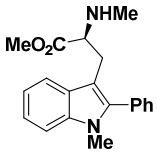

A solution of **4.33** (91.0 mg, 0.199 mmol) in DCM (2 mL) was prepared in a flame-dried flask under nitrogen. Et_3SiH (1.3 mL, 8.1 mmol) and Et_3N (55 μL, 0.40 mmol) were then added, followed by $Pd_2(dba)_3$ (41.0 mg, 44.8 μmol). The dark red reaction solution was stirred for 20 hours and the resultant dark brown mixture was filtered through celite with EtOAc (15 mL), washed with saturated aqueous $NaHCO_3$ (2 x 15 mL), brine (2 x 15 mL), dried (Na_2SO_4), filtered, and concentrated. Purification by silica gel column chromatography (5–15% EtOAc in hexanes, then 15% EtOAc in hexanes with 4% NH_4OH, then 5% MeOH in DCM with NH_4OH) afforded the product (26.4 mg, 41%) as a colorless oil. ^{1}H NMR (500 MHz, $CDCl_3$) δ 7.69 (d, *J* = 7.9 Hz, 1H), 7.59 – 7.38 (m, 5H), 7.34 (d, *J* = 8.2 Hz, 1H), 7.26 (ddd, *J* = 8.2, 7.1, 1.2 Hz, 1H), 7.17 (ddd, *J* = 8.0, 7.0, 1.0 Hz, 1H), 3.57 (s, 3H), 3.51 (s, 3H), 3.48 (dd, *J* = 7.7, 6.4 Hz, 1H), 3.15 (dd, *J* = 14.3, 6.4 Hz, 1H), 3.05 (dd, *J* = 14.3, 7.7 Hz, 1H), 2.24 (s, 3H). $[\alpha]_D^{25}$ = +16.1° (*c* = 0.19, $CHCl_3$). ^{13}C NMR (126 MHz, $CDCl_3$) δ 175.2, 139.4, 137.2, 131.8, 130.86, 130.85, 128.63, 128.62, 128.4, 127.8, 121.9, 119.6, 119.2, 109.5, 108.3, 64.3, 51.7, 35, 31, 28.8.

3a-hydroxypyrroloindoline methyl ester (**4.35**, **4.36**).

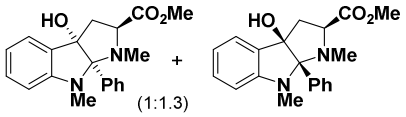

A flame-dried flask containing **4.34** (24.1 mg, 0.748 mmol) was charged with flame-dried 4Å molecular sieves and MeCN (1 mL). NCS (recrystallized from toluene, 10.0 mg, 0.746 mmol) was then added as a solution in MeCN (1 mL) dropwise. After stirring in the dark at room temperature for 5.5 hours, more NCS (5.0 mg, 0.37 mmol, 0.50 equiv) was added as a solution in MeCN (0.5 mL). After stirring an additional 40 minutes, the reaction was quenched with aqueous $Na_2S_2O_3$ (10 wt %,1 mL) and the organic layer was washed with brine (2 x 3 mL), dried (Na_2SO_4), filtered, and concentrated. The residue was combined with MeCN (2 mL), H_2O (2 mL) and SiO_2 (2 mL), then stirred open to air at room temperature for 30 minutes. The mixture was then filtered with EtOAc (20 mL) and the aqueous layer was extracted with EtOAc (2 x 2 mL). The combined organic layers were concentrated and purification by silica gel column chromatography (10–15% EtOAc in hexanes) afforded the product (10.3 mg, 41%) as a yellow oil (note: by then exchanging the column solvent to 2% MeOH in DCM, 6.0 mg (25%) of the starting material, **4.34** could be recovered). **4.35**, **436** was isolated as a 1.3:1 mixture favoring the *exo* diastereomer as determined by ^{1}H NMR. Optical rotation, HRMS, and spectral data are reported for the mixture of diastereomers. The relative stereochemistry and respective ^{1}H and ^{13}C NMR data for each diastereomer was determined by 2D NMR analysis and by comparison to the ^{1}H NMR spectrum of re-isolated *endo* diastereomer (**4.35**) in the subsequent saponification step generating *exo*-3a-hydroxypyrroloindoline carboxylic acid (**4.13**). ^{1}H NMR (500 MHz, $CDCl_3$) δ 7.47 – 7.28 (m, 4H^{exo}, 4H^{endo}), 7.26 – 7.08 (m, 3H^{exo}, 3H^{endo}), 6.73 (ddd, *J* = 7.4, 7.4, 1.0 Hz, 1H^{exo}), 6.64 (ddd, *J* = 7.4, 7.4, 1.0 Hz, 1H^{endo}), 6.46 (dd, *J* = 8.3, 0.8 Hz, 1H^{exo}), 6.43 (d, *J* = 7.9 Hz, 1H^{endo}), 3.97 (d, *J* = 8.3 Hz, 1H^{endo}), 3.76 (s, 3H^{exo}), 3.42 (dd, *J* = 11.2, 5.4 Hz, 1H^{exo}), 3.24 (s, 3H^{endo}), 2.91 (s, 3H^{endo}), 2.80 (s, 3H^{exo}), 2.79 (s, 3H^{endo}), 2.73 (dd, *J* = 12.4, 1.0 Hz, 1H^{endo}), 2.59 (dd, *J* = 11.9, 5.4 Hz, 1H^{exo}), 2.53 (dd, *J* = 12.3, 8.5 Hz, 1H^{endo}), 2.41 (s, 3H^{exo}), 2.31 (dd, *J* = 11.6, 11.6 Hz, 1H^{exo}), 1.43 (s, 1H^{exo}), 1.31 (s, 1H^{endo}).; ^{13}C NMR (125 MHz, $CDCl_3$) δ 173.9^{endo}, 173.3^{exo}, 151.7^{exo}, 151.5^{endo}, 137.6^{endo}, 136.9^{exo}, 130.6^{endo}, 130.3^{exo}, 129.5^{exo}, 128.8^{endo,exo}, 128.5^{endo}, 128.4^{exo}, 128.2^{endo}, 124.3^{endo}, 124.0^{exo}, 117.2^{exo}, 116.6^{endo}, 104.9^{endo}, 104.6^{exo}, 98.2^{exo}, 95.9^{endo}, 88.9^{endo}, 88.0^{exo}, 64.2^{endo}, 63.4^{exo}, 52.0^{exo}, 51.2^{endo}, 43.7^{exo}, 41.3^{endo}, 34.9^{exo}, 34.8^{endo}, 33.9^{exo}, 31.6^{endo}.; FTIR (NaCl/thin film): 3467, 2920, 2850, 1750, 1734, 1609, 1494, 1447, 1375, 1311, 1202, 1101 cm^{-1}; $[\alpha]_D^{25}$ = +33.2º (*c* = 0.55, $CHCl_3$). HRMS (MM) calc'd for $C_{20}H_{23}N_2O_3$ $[M+H]^+$ 339.1703, found 339.1715.

exo-hydroxypyrroloindoline carboxylic acid (**4.13**).

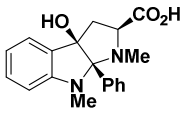

A solution of the 1.3:1 mixture of hydroxypyrroloindoline methyl esters **4.35**, **4.36** (5.5 mg, 16 μmol, 1.0 equiv) in THF (0.5 mL) was cooled to 0 °C in an ice bath. LiOH (3.9 mg, 0.16 mmol, 10 equiv) was then added as a solution in H_2O (0.5 mL). After stirring 2.5 hours at 0 °C, the reaction was quenched with 3 drops 3 M HCl, diluted with H_2O (3 mL), and extracted with EtOAc (3 x 4 mL). The combined organic layers were washed with brine (10 mL), dried (Na_2SO_4), filtered, and concentrated. Purified by silica gel column chromatography (10% EtOAc:hexanes then 2–10% MeOH in CH_2Cl_2) afforded the product (1.4 mg, 47% based on **4.36**) as a yellow oil and 1.2 mg (50% recovery) of **4.35**. The enantiomeric excess of **4.13** was determined to be 82% by chiral SFC analysis (OJ-H, 2.5 mL/min, 20% IPA in CO_2, λ = 254 nm): t_R(major) = 2.4 min t_R(minor) = 3.3 min. $[\alpha]_D^{25}$ = -99.0° (*c* = 0.14, MeCN). ^{1}H NMR (500 MHz, $CDCl_3$) δ 7.66 – 7.26 (m, 7H), 6.77 (ddd, *J* = 7.4, 7.4, 0.9 Hz, 1H), 6.50 (ddd, *J* = 7.6, 0.8, 0.8 Hz, 1H), 3.44 (dd, *J* = 10.9, 6.0 Hz, 1H), 2.80 (s, 3H), 2.70 (dd, *J* =12.4, 6.0 Hz, 1H), 2.48 (s, 3H), 2.34 (dd, *J* = 12.4, 10.9 Hz, 1H), 1.51 (br s, 1H).

N-Cbz-*N*-methyltryptophol (**4.37**).

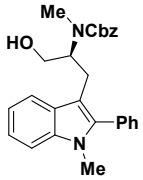

A solution of **4.31** (305 mg, 0.69 mmol) in THF (11 mL) was prepared in a flame-dried flask and cooled to –30 °C using a Neslab CC 100 cryocool. The flask was then charged with 4-methylmorpholine (111 μL, 1.01 mmol), followed by methyl chloroformate (59 μL, 0.69 mmol). The reaction solution was then warmed to –10 °C and stirred for 30 minutes, then cooled to -30 °C. $NaBH_4$ (78 mg, 2.07 mmol) was then added, followed by dropwise addition of wet MeOH (0.7 mL) over 10 minutes and subsequent warming to –20 °C. After stirring for 1 hour at –20 °C, the reaction mixture was allowed to warm to room temperature and quenched with saturated aqueous NH_4Cl (5 mL). The aqueous layer was extracted with EtOAc (2 x 5 mL) and the combined organic layers were washed with saturated aqueous $NaHCO_3$ (2 x 4 mL), brine (2 x 5 mL), dried (Na_2SO_4), filtered and concentrated. Purified by silica gel column chromatography (0–1% MeOH in DCM) afforded the product (222 mg, 75%) as a light yellow oil. ^{1}H NMR (500 MHz, $CDCl_3$, compound exists as a 1:1 mixture of rotamers) δ 7.73 (d, *J* = 7.9 Hz, 0.5H), 7.54 (d, *J* = 8.0 Hz, 0.5H), 7.51 – 7.26 (m, 11H), 7.22 – 7.15 (m, 0.5H), 7.14 – 7.02 (m, 1.5H), 5.08 (d, *J* = 12.5 Hz, 0.5H), 5.00 (d, *J* = 12.5 Hz, 0.5H), 4.90 (d, *J* = 12.2 Hz, 0.5H), 4.85 (d, *J* = 12.3 Hz, 0.5H), 4.54 – 4.43 (m, 0.5H), 4.29 – 4.18 (m, 0.5H), 3.66 (dd, *J* = 11.8, 3.5 Hz, 0.5H), 3.60 – 3.44 (m, 5.5H), 3.08 (dd, *J* = 14.4, 7.1 Hz, 0.5H), 2.97 (dd, *J* = 14.4, 7.5 Hz, 0.5H), 2.88 (d, *J* = 7.2 Hz, 1H), 2.61 (s, 1.5H), 2.58 (s, 1.5H).; ^{13}C NMR (125 MHz, $CDCl_3$; compound exists as a 1:1 mixture of rotamers) δ 157.0, 156.7, 138.7, 138.6, 137.0, 136.7, 136.5, 131.7, 131.6, 130.6, 130.5, 128.8, 128.6, 128.5, 128.44, 128.38, 128.36, 128.29, 128.25, 128.2, 127.9, 127.81, 127.80, 127.7, 127.5, 127.3, 121.8, 119.53, 119.45, 118.9, 118.7, 109.40, 109.36, 109.3, 109.2, 108.7, 67.1, 66.9, 63.2, 62.52, 60.50, 58.3, 31.5, 30.8, 30.7, 28.8, 24.3, 23.9.; FTIR (NaCl/thin film): 3436, 3056, 2936, 1699, 1694, 1683, 1470, 1455, 1443, 1404, 1366, 1339, 1237, 1216, 1143 cm^{-1}; $[\alpha]_D^{25}$ = –39.6° (*c* = 2.02, $CHCl_3$). HRMS (ESI) calc'd for $C_{27}H_{29}N_2O_3$ $[M+H]^+$ 429.2173, found 429.2175.

(S)-3-(1-methyl-2-phenyl-1H-indol-3-yl)-2-(methylamino)propan-1-ol (**4.38**).

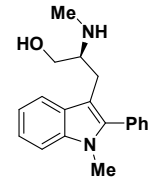

A solution of **4.37** (174 mg, 0.4 mmol) in DCM (8 mL) was prepared in a flame-dried flask. Et_3SiH (2.6 mL, 16.3 mmol) and Et_3N (0.11 mL, 0.8 mmol) were then added, followed by $Pd_2(dba)_3 \bullet CHCl_3$ (84 mg, 81 μmol). The dark red reaction solution was stirred for 17.5 hours at room temperature, then filtered through celite with EtOAc (60 mL), washed with saturated aqueous $NaHCO_3$ (2 x 20 mL), brine (2 x 15 mL), dried (Na_2SO_4), filtered and concentrated. Purification by silica gel column chromatography (0–1% MeOH in DCM) afforded the product (110 mg, 92%) as white crystals. ^{1}H NMR (300 MHz, $CDCl_3$) δ 7.65 (dddd, *J* = 7.9, 1.2, 0.8, 0.3 Hz, 1H), 7.54 – 7.36 (m, 5H), 7.36 (ddd, *J* = 8.1, 0.9, 0.9 Hz, 1H), 7.27 (ddd, *J* = 8.2, 6.9, 1.2 Hz, 1H), 7.17 (ddd, *J* = 8.0, 6.9, 1.2 Hz, 1H), 3.58 (s, 3H), 3.55 (dd, *J* = 10.7, 3.5 Hz, 1H), 3.21 (dd, *J* = 10.8, 4.9 Hz, 1H), 2.99 (dd, *J* = 16.4, 9.3 Hz, 1H), 2.84 – 2.74 (m, 2H), 2.25 (s, 3H), 1.93 (br s, 2H).; ^{13}C NMR (125 MHz, $CDCl_3$) δ 139.0, 137.0, 131.8, 130.63, 130.61, 128.60, 128.59, 128.3, 127.8, 121.8, 119.5, 118.9, 109.4, 109.2, 62.3, 61.3, 33.6, 30.8, 26.1.; FTIR (NaCl/thin film): 3306, 3054, 2920, 2852, 2799, 1468, 1442, 1365, 1334, 1237, 1066, 1013 cm^{-1}; $[\alpha]_D^{25}$ = +13.3° (*c* = 1.10, $CHCl_3$). HRMS (ESI) calc'd for $C_{19}H_{23}N_2O$ $[M+H]^+$ 295.1805, found 295.1810.

(S)-N-methyl-1-(1-methyl-2-phenyl-1H-indol-3-yl)-3-((triethylsilyl)oxy)propan-2-amine (**4.39**).

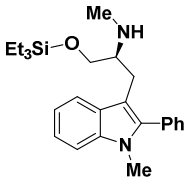

To a solution of **4.38** (52 mg, 0.177 mmol) in THF (2.5 mL) at 0 °C was added was added Et_3N (49 μL, 0.35 mmol), DMAP (4.3 mg, 35 μmol) followed by dropwise addition of TESCl (59 μL, 0.35 mmol). The reaction was allowed to warm to room temperature over 1 hour, then stirred an additional 2 hours. The reaction was quenched with saturated aqueous $NaHCO_3$ (3 mL). The aqueous layer was extracted with EtOAc (2 x 3 mL) and the combined organic phases were washed with brine (2 x 6 mL), dried (Na_2SO_4) and concentrated. Purification by silica gel column chromatography (0–4% MeOH in DCM) afforded the product (52 mg, 71%) as a yellow oil. ^{1}H NMR (500 MHz, $CDCl_3$) δ 7.68 (d, *J* = 7.9 Hz, 1H), 7.51 – 7.44 (m, 3H), 7.44 – 7.35 (m, 2H), 7.33 (d, *J* = 8.2 Hz, 1H), 7.25 (ddd, *J* = 8.2, 7.0, 1.3 Hz, 1H), 7.15 (ddd, *J* = 7.9, 7.0, 1.0 Hz, 1H), 3.57 (s, 3H), 3.43 (dd, *J* = 10.0, 4.4 Hz, 1H), 3.34 (dd, *J* = 10.0, 6.3 Hz, 1H), 2.93 (dd, *J* = 13.5, 5.1 Hz, 1H), 2.85 – 2.71 (m, 2H), 2.33 (s, 3H), 0.86 (t, *J* = 8.0 Hz, 9H), 0.49 (q, *J* = 8.0 Hz, 5H); ^{13}C NMR (126 MHz, $CDCl_3$) δ 138.8, 137.0, 131.9, 130.6, 130.6, 128.4, 128.1, 127.9, 121.7, 119.2, 119.1, 109.8, 109.2, 64.6, 62.4, 34.1, 30.8, 25.8, 6.7, 4.3; FTIR (NaCl/thin film): 3057, 2952, 2908, 2873, 2799, 1602, 1466, 1362, 1332, 1238, 1095, 1014, 972, 819 cm^{-1}; $[\alpha]_D^{25}$ = +16.7° (*c* = 2.59, $CHCl_3$).

(3S,4R)-4-(sec-butyl)-3-methyloxetan-2-one (**4.51**). [202]

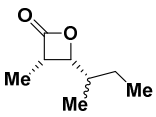

General procedure for 2+2 cycloaddition

A flame dried 25 mL flask was charged with $LiClO_4$ (492 mg, 4.62 mmol) (transferred in a glovebox), then dissolved in Et_2O (1.4 mL) under vigorous stirring. TMS protected quinidine (55.5 mg, 0.14 mmol) in 2.8 DCM was added and the reaction was cooled to – 40 °C where after anhydrous DIPEA (0.61 mL, 3.5 mmol) was added followed by 2-methylbutyraldehyde (0.15 mL, 1.4 mmol). Propionyl chloride (0.24 mL, 2.8 mmol) in 0.7 mL DCM was then added over 6 hours and the reaction was stirred for another 6 hours. The reaction was then quenched with Et_2O (10 mL) and the reaction allowed to warm to room temperature. The mixture was filtered on SiO_2 (5mL) with Et_2O (3 x 20 mL). The crude residue was purified by silica gel chromatography (gradient elution, 8 –15% EtOAc in hexanes) to give the product as a clear oil.

methyl (tert-butoxycarbonyl)-L-phenylalaninate (4.60).[220]

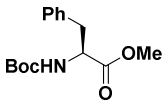

To a solution of L-Phe-OMe (1.52 g, 7.03 mmol) in DCM (50 mL) at 0 °C was added anhydrous DIPEA (1.59 mL, 9.14 mmol) followed by di-tert-butyl dicarbonate (2.1 mL, 9.14 mmol). The reaction was allowed to warm to room temperature overnight, then washed with 1M HCl (2 x 50 mL), $NaHCO_3$,(2 x 50 mL), brine (2 x 50 mL), dried (Na_2SO_4) and concentrated. Purification by silica gel chromatography (0–10% EtOAc in hexanes) afforded the product (1.96 g, >99% yield) as a clear oil. ^{1}H NMR (300 MHz, $CDCl_3$) δ 7.37 – 7.19 (m, 3H), 7.19 – 7.06 (m, 2H), 4.99 (d, *J* = 7.6 Hz, 1H), 4.59 (dd, *J* = 13.7, 6.7 Hz, 1H), 3.72 (s, 3H), 3.09 (qd, *J* = 13.9, 6.0 Hz, 2H), 1.42 (s, 9H).

(S)-tert-butyl (3-hydroxy-3-methyl-1-phenylbutan-2-yl)carbamate (4.61).[221]

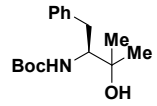

To a solution of **4.60** (477 mg, 1.7 mmol) in THF (2 mL) at 0 °C was added MeMgBr (3 M in Et_2O, 2.3 mL, 6.8 mmol) over 30 min then stirred overnight. The reaction was diluted with 7 mL THF, then quenched by dropwise addition of MeOH (1 mL) followed by H_2O (1 mL). The reaction mixture was diluted with EtOAc (10 mL) and the organic phase was filtered on Celite with EtOAc (2 x 10 mL). The combined filtrates were evaporated and redissolved in Et_2O (10 mL), filtered on Celite and concentrated again to give the product (448 mg, 94%) of as white crystals. ^{1}H NMR (300 MHz, $CDCl_3$) δ 7.34 – 7.12 (m, 5H), 4.58 (d, *J* = 9.4 Hz, 1H), 3.76 – 3.62 (m, 1H), 3.09 (dd, *J* = 14.2, 3.6 Hz, 1H), 2.60 (dd, *J* = 14.2, 11.1 Hz, 1H), 2.34 (brs, 1H), 1.31 (s, 6H), 1.30 (s, 9H).

(S)-4-benzyl-5,5-dimethyloxazolidin-2-one (4.62).[221]

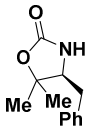

To a solution of **4.61** (905 mg, 3.24 mmol) in THF (20 mL) at 0 °C was added potassium t-butoxide (440 mg, 3.92 mmol) in one portion. The yellow reaction was stirred for 30 min, then quenched with saturated aqueous NH_4Cl (15 mL). The aqueous phases were extracted with EtOAc (3 x 15 mL) and the combined organic phases were washed with brine (2 x 15 mL), dried (Na_2SO_4) and concentrated. Purification by silica gel chromatography (0–1% MeOH/DCM with 2% NH_4OH) afforded the product (539 mg, 81%) as white needle crystals. ^{1}H NMR (300 MHz, $CDCl_3$) δ 7.40 – 7.13 (m, 5H), 4.73 (brs, 1H), 3.68 (ddd, *J* = 10.9, 3.7, 0.7 Hz, 1H), 2.84 (dd, *J* = 13.3, 3.7 Hz, 1H), 2.66 (dd, *J* = 13.3, 10.9 Hz, 1H), 1.49 (s, 3H), 1.46 (s, 3H).

(S)-4-benzyl-5,5-dimethyl-3-propionyloxazolidin-2-one (4.55). [222]

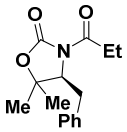

To **4.62** (102 mg, 0.496 mmol) in THF (5 mL) at –78 °C was added n-BuLi (2.5 M, 208 µL, 0.52 mmol) dropwise. The reaction was stirred for 30 min where after propionyl chloride (46 µl, 0.52 mmol) was added dropwise. After stirring for 10 min at -78 °C, the reaction was allowed to warm to room temperature and stirred for another 3 hours. The reaction was quenched with saturated aqueous NH_4Cl (2 mL) and extracted with EtOAc (3x 2 mL). The combined organic phases were washed with $NaHCO_3$ (2 x 6 mL), brine (2x6 mL), dried (Na_2SO_4) and concentrated. Purification by silica gel chromatography (6% EtOAc in hexanes) afforded the product (105 mg, 81% yield) as white needle crystals. ^{1}H NMR (300 MHz, $CDCl_3$) δ 7.39 – 7.16 (m, 5H), 4.51 (dd, *J* = 9.5, 3.9 Hz, 1H), 3.15 (dd, *J* = 14.3, 3.9 Hz, 1H), 3.01 – 2.79 (m, 3H), 1.37 (s, 3H), 1.36 (s, 3H), 1.14 (t, *J* = 7.4 Hz, 3H).

(S)-4-benzyl-3-((2S,3S)-3-hydroxy-2-methyl-4-methylenehexanoyl)-5,5-dimethyloxazolidin-2-one (**4.54**).[223]

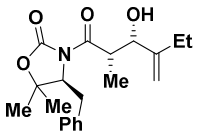

To a solution of **4.55** (49 mg, 0.19 mmol) in CH_2Cl_2 (4 mL) at 0 °C was added n-Bu_2BOTf (1M in CH_2Cl_2, 210 µL, 0.21 mmol) dropwise. After 30 min, freshly distilled DIPEA (58 µL, 0.33 mmol) was added dropwise and the reaction was stirred for another 30 min. The reaction was then cooled to –78 °C, stirred for 30 min where after 2-ethyl acrolein was added dropwise. The reaction was allowed to warm to room temperature overnight. The reaction was quenched with a pH=7 buffer (2 mL) and a mixture of H_2O_2/MeOH (1:2, 2 mL). After stirring for 1 hour, the mixture was concentrated, then dissolved in CH_2Cl_2 (8 mL). The aqueous phase was extracted with CH_2Cl_2 (2x2 mL) and the combined organic phases were washed with $NaHCO_3$ (2x10 mL), brine (2x10mL), dried (Na_2SO_4) and concentrated. Purification by silica gel chromatography (0–1% MeOH in CH_2Cl_2) afforded the product (43 mg, 67%) as a clear oil. ^{1}H NMR (500 MHz, $CDCl_3$) δ 7.38 – 7.17 (m, 5H), 5.17 – 5.14 (m, 1H), 4.99 – 4.97 (m, 1H), 4.54 (dd, *J* = 9.1, 4.4 Hz, 1H), 4.40 (brs, 1H), 3.96 (dtd, *J* = 10.6, 7.0, 3.5 Hz, 1H), 3.08 (dd, *J* = 14.3, 4.4 Hz, 1H), 2.91 (dd, *J* = 14.3, 9.1 Hz, 1H), 2.77 (brs, 1H), 2.14 – 1.92 (m, 2H), 1.40 (s, 3H), 1.38 (s, 3H), 1.11 (d, *J* = 7.0 Hz, 3H), 1.07 (t, *J* = 7.4 Hz, 3H). dr (94:6) determined by NMR.

(S)-4-benzyl-3-((2S,3R,4R)-3-hydroxy-2,4-dimethylhexanoyl)-5,5-dimethyloxazolidin-2-one (**4.53**).[203]

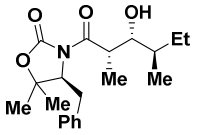

To a solution of **4.54** (94 mg, 0.27 mmol) in degassed CH_2Cl_2 (4.5 mL) (in a glass inlet in the glovebox) was added [Rh(NBD)(DIPHOS-4)BF_4]. The reaction was then sealed in a pressure chamber and removed from the glovebox. The reaction was pressurized to 100 psi H_2 then flushed to replace any O_2 leftovers. The reaction was then pressurized to 460 psi and stirred for 1 hour. The crude mixture was filtered on a short SiO_2 column with a 50:50 mixture of EtOAc/hexanes to give the product (76 mg, 80%) as a clear oil. ^{1}H NMR (500 MHz, $CDCl_3$) δ 7.41 – 7.14 (m, 5H), 4.54 (dd, *J* = 9.0, 4.6 Hz, 1H), 3.92 (qd, *J* = 7.0, 2.5 Hz, 1H), 3.58 (dd, *J* = 8.9, 2.5 Hz, 1H), 3.06 (dd, *J* = 14.3, 4.6 Hz, 1H), 2.91 (dd, *J* = 14.3, 9.0 Hz, 1H), 1.86 – 1.70 (m, 1H), 1.54 – 1.45 (m, 2H), 1.40 (s, 3H), 1.38 (s, 3H), 1.15 (d, *J* = 7.1 Hz, 3H), 0.90 (t, *J* = 7.4 Hz, 3H), 0.86 (d, *J* = 6.8 Hz, 3H). ^{13}C NMR (126 MHz, $CDCl_3$) δ 178.4, 152.2, 136.7, 129.2, 128.8, 127, 82.4, 75, 63.4, 39.8, 37, 35.6, 28.6, 25.2, 22.4, 14.9, 11, 10.2. dr (83:11:6).

7 References

[1] C. H. Arrowsmith, C. Bountra, P. V. Fish, K. Lee, M. Schapira, *Nature Reviews Drug Discovery* **2012**, *11*, 384-400.
[2] K. Luger, A. W. Mader, R. K. Richmond, D. F. Sargent, T. J. Richmond, *Nature* **1997**, *389*, 251-260.
[3] S. Pepenella, K. J. Murphy, J. J. Hayes, *Chromosoma* **2013**, 1-11.
[4] B. D. Strahl, C. D. Allis, *Nature* **2000**, *403*, 41-45.
[5] A. De Ruijter, A. Van Gennip, H. Caron, S. Kemp, A. van Kuilenburg, *Biochem. J* **2003**, *370*, 737-749.
[6] E. L. Greer, Y. Shi, *Nature reviews genetics* **2012**, *13*, 343-357.
[7] D. Rossetto, N. Avvakumov, J. Côté, *epigenetics* **2012**, *7*, 1098-1108.
[8] I. Hammond-Martel, H. Yu, E. Affar, *Cell. Signal.* **2012**, *24*, 410-421.
[9] M. Shogren-Knaak, H. Ishii, J.-M. Sun, M. J. Pazin, J. R. Davie, C. L. Peterson, *Science (New York, N.Y.)* **2006**, *311*, 844-847.
[10] B. Fierz, C. Chatterjee, R. K. McGinty, M. Bar-Dagan, D. P. Raleigh, T. W. Muir, *Nature Chemical Biology* **2011**, *7*, 113-119.
[11] G. Lagger, D. O'Carroll, M. Rembold, H. Khier, J. Tischler, G. Weitzer, B. Schuettengruber, C. Hauser, R. Brunmeir, T. Jenuwein, C. Seiser, *The EMBO journal* **2002**, *21*, 2672-2681.
[12] J.-i. Nakayama, J. C. Rice, B. D. Strahl, C. D. Allis, S. I. S. Grewal, *Science (New York, N.Y.)* **2001**, *292*, 110-113.
[13] F. Winston, C. D. Allis, *Nature structural biology* **1999**, *6*, 601-604.
[14] M. Grunstein, *Nature* **1997**, *389*, 349-352.
[15] M. D. Shahbazian, M. Grunstein, *Annu. Rev. Biochem.* **2007**, *76*, 75-100.
[16] M. Li, J. Luo, C. L. Brooks, W. Gu, *Journal of Biological Chemistry* **2002**, *277*, 50607-50611.
[17] C. Choudhary, C. Kumar, F. Gnad, M. L. Nielsen, M. Rehman, T. C. Walther, J. V. Olsen, M. Mann, *Science (New York, N.Y.)* **2009**, *325*, 834-840.
[18] M. Haberland, R. L. Montgomery, E. N. Olson, *Nat Rev Genet* **2009**, *10*, 32-42.
[19] F. Thaler, C. Mercurio, *ChemMedChem* **2013**.
[20] Y. Zhang, H.-H. Ng, H. Erdjument-Bromage, P. Tempst, A. Bird, D. Reinberg, *Genes & development* **1999**, *13*, 1924-1935.
[21] aS. C. Galasinski, K. A. Resing, J. A. Goodrich, N. G. Ahn, *Journal of Biological Chemistry* **2002**, *277*, 19618-19626; bM. K. Pflum, J. K. Tong, W. S. Lane, S. L. Schreiber, *The Journal of biological chemistry* **2001**, *276*, 47733-47741.
[22] I. M. Adcock, P. Ford, K. Ito, P. Barnes, *Respiratory research* **2006**, *7*, 21.
[23] P. Karagianni, J. Wong, *Oncogene* **2007**, *26*, 5439-5449.
[24] M. G. Guenther, O. Barak, M. A. Lazar, *Molecular and cellular biology* **2001**, *21*, 6091-6101.
[25] P. J. Watson, L. Fairall, G. M. Santos, J. W. Schwabe, *Nature* **2012**, *481*, 335-340.
[26] C. J. Millard, P. J. Watson, I. Celardo, Y. Gordiyenko, S. M. Cowley, C. V. Robinson, L. Fairall, J. W. Schwabe, *Molecular Cell* **2013**.
[27] S. L. Gantt, C. G. Joseph, C. A. Fierke, *Journal of Biological Chemistry* **2010**, *285*, 6036-6043.
[28] R. L. Montgomery, C. A. Davis, M. J. Potthoff, M. Haberland, J. Fielitz, X. Qi, J. A. Hill, J. A. Richardson, E. N. Olson, *Genes & development* **2007**, *21*, 1790-1802.
[29] R. L. Montgomery, M. J. Potthoff, M. Haberland, X. Qi, S. Matsuzaki, K. M. Humphries, J. A. Richardson, R. Bassel-Duby, E. N. Olson, *The Journal of clinical investigation* **2008**, *118*, 3588.
[30] S. K. Knutson, B. J. Chyla, J. M. Amann, S. Bhaskara, S. S. Huppert, S. W. Hiebert, *The EMBO journal* **2008**, *27*, 1017-1028.
[31] S. Bhaskara, B. J. Chyla, J. M. Amann, S. K. Knutson, D. Cortez, Z.-W. Sun, S. W. Hiebert, *Molecular Cell* **2008**, *30*, 61-72.

[32] C. M. Grozinger, S. L. Schreiber, *Proceedings of the National Academy of Sciences* **2000**, *97*, 7835-7840.
[33] W. Fischle, F. Dequiedt, M. J. Hendzel, M. G. Guenther, M. A. Lazar, W. Voelter, E. Verdin, *Mol Cell* **2002**, *9*, 45-57.
[34] E. Verdin, F. Dequiedt, H. G. Kasler, *Trends Genet* **2003**, *19*, 286-293.
[35] T. A. McKinsey, C. L. Zhang, E. N. Olson, *Current opinion in genetics & development* **2001**, *11*, 497-504.
[36] R. B. Vega, K. Matsuda, J. Oh, A. C. Barbosa, X. Yang, E. Meadows, J. McAnally, C. Pomajzl, J. M. Shelton, J. A. Richardson, G. Karsenty, E. N. Olson, *Cell* **2004**, *119*, 555-566.
[37] A. R. Guardiola, T.-P. Yao, *Journal of Biological Chemistry* **2002**, *277*, 3350-3356.
[38] H. Zou, Y. Wu, M. Navre, B.-C. Sang, *Biochemical and Biophysical Research Communications* **2006**, *341*, 45-50.
[39] aJ. J. Tong, J. Liu, N. R. Bertos, X.-J. Yang, *Nucleic Acids Research* **2002**, *30*, 1114-1123; bD. D. Fischer, R. Cai, U. Bhatia, F. A. Asselbergs, C. Song, R. Terry, N. Trogani, R. Widmer, P. Atadja, D. Cohen, *Journal of Biological Chemistry* **2002**, *277*, 6656-6666.
[40] C. Hubbert, A. Guardiola, R. Shao, Y. Kawaguchi, A. Ito, A. Nixon, M. Yoshida, X. F. Wang, T. P. Yao, *Nature* **2002**, *417*, 455-458.
[41] J. J. Kovacs, P. J. M. Murphy, S. Gaillard, X. A. Zhao, J. T. Wu, C. V. Nicchitta, M. Yoshida, D. O. Toft, W. B. Pratt, T. P. Yao, *Molecular Cell* **2005**, *18*, 601-607.
[42] O. Witt, H. E. Deubzer, T. Milde, I. Oehme, *Cancer letters* **2009**, *277*, 8-21.
[43] Y. Zhang, S. Kwon, T. Yamaguchi, F. Cubizolles, S. Rousseaux, M. Kneissel, C. Cao, N. Li, H.-L. Cheng, K. Chua, *Molecular and cellular biology* **2008**, *28*, 1688-1701.
[44] A. Villagra, F. Cheng, H.-W. Wang, I. Suarez, M. Glozak, M. Maurin, D. Nguyen, K. L. Wright, P. W. Atadja, K. Bhalla, *Nature immunology* **2008**, *10*, 92-100.
[45] X. Lai, J. Li, Z. Lian, B. Niu, Y. Chen, W. Liao, Z. Liu, J. Gong, in *Transplantation proceedings, Vol. 43*, Elsevier, **2011**, pp. 2728-2732.
[46] P. A. Jones, S. B. Baylin, *Nature reviews genetics* **2002**, *3*, 415-428.
[47] M. New, H. Olzscha, N. B. La Thangue, *Molecular oncology* **2012**, *6*, 637-656.
[48] A. Burgess, A. Ruefli, H. Beamish, R. Warrener, N. Saunders, R. Johnstone, B. Gabrielli, *Oncogene* **2004**, *23*, 6693-6701.
[49] C. B. Yoo, P. A. Jones, *Nature Reviews Drug Discovery* **2006**, *5*, 37-50.
[50] K. Watanabe, K. Okamoto, S. Yonehara, *Cell Death & Differentiation* **2004**, *12*, 10-18.
[51] A. Ashkenazi, V. M. Dixit, *Science (New York, N.Y.)* **1998**, *281*, 1305-1308.
[52] R. W. Johnstone, *Nature Reviews Drug Discovery* **2002**, *1*, 287-299.
[53] L. M. Dejean, S. Martinez-Caballero, S. Manon, K. W. Kinnally, *Biochimica et Biophysica Acta (BBA) - Molecular Basis of Disease* **2006**, *1762*, 191-201.
[54] M. J. Smyth, E. Krasovskis, V. R. Sutton, R. W. Johnstone, *Proceedings of the National Academy of Sciences* **1998**, *95*, 7024-7029.
[55] aA. A. Ruefli, D. Bernhard, K. M. Tainton, R. Kofler, M. J. Smyth, R. W. Johnstone, *International journal of cancer* **2002**, *99*, 292-298; bA. A. Ruefli, M. J. Ausserlechner, D. Bernhard, V. R. Sutton, K. M. Tainton, R. Kofler, M. J. Smyth, R. W. Johnstone, *Proceedings of the National Academy of Sciences* **2001**, *98*, 10833-10838.
[56] H. Y. Cohen, S. Lavu, K. J. Bitterman, B. Hekking, T. A. Imahiyerobo, C. Miller, R. Frye, H. Ploegh, B. M. Kessler, D. A. Sinclair, *Molecular Cell* **2004**, *13*, 627-638.
[57] C. Subramanian, J. A. Jarzembowski, A. W. Opipari Jr, V. P. Castle, R. P. Kwok, *Neoplasia (New York, NY)* **2011**, *13*, 726.
[58] L. Qiu, A. Burgess, D. P. Fairlie, H. Leonard, P. G. Parsons, B. G. Gabrielli, *Molecular biology of the cell* **2000**, *11*, 2069-2083.
[59] T. Yamaguchi, F. Cubizolles, Y. Zhang, N. Reichert, H. Kohler, C. Seiser, P. Matthias, *Genes & development* **2010**, *24*, 455-469.

[60] J. K. Ryu, W. J. Lee, K. H. Lee, J.-H. Hwang, Y.-T. Kim, Y. B. Yoon, C. Y. Kim, *Cancer Letters* **2006**, *237*, 143-154.
[61] M. A. Jordan, L. Wilson, *Nature Reviews Cancer* **2004**, *4*, 253-265.
[62] A. R. Robbins, S. A. Jablonski, T. J. Yen, K. Yoda, R. Robey, S. E. Bates, D. L. Sackett, *Cell Cycle* **2005**, *4*, 717-726.
[63] J.-W. Lee, S.-H. Bae, J.-W. Jeong, S.-H. Kim, K.-W. Kim, *Experimental & molecular medicine* **2004**, *36*, 1-12.
[64] M. S. Kim, H. J. Kwon, Y. M. Lee, J. H. Baek, J.-E. Jang, S.-W. Lee, E.-J. Moon, H.-S. Kim, S.-K. Lee, H. Y. Chung, *Nature medicine* **2001**, *7*, 437-443.
[65] X. Kong, Z. Lin, D. Liang, D. Fath, N. Sang, J. Caro, *Molecular and cellular biology* **2006**, *26*, 2019-2028.
[66] aB. Mann, J. Johnson, M. Cohen, R. Justice, R. Pazdur, *The oncologist* **2007**, *12*, 1247-1252; bK. M. VanderMolen, W. McCulloch, C. J. Pearce, N. H. Oberlies, *The Journal of antibiotics* **2011**, *64*, 525-531.
[67] S. Stockwell, *Oncology Times* **2011**.
[68] P. A. Marks, *Expert opinion on investigational drugs* **2010**, *19*, 1049-1066.
[69] M. Finnin, J. Donigian, A. Cohen, V. Richon, R. Rifkind, P. Marks, R. Breslow, N. Pavletich, *Nature* **1999**, *401*, 188-193.
[70] P. Bertrand, *Eur J Med Chem*, *45*, 2095-2116.
[71] C. Corminboeuf, P. Hu, M. E. Tuckerman, Y. Zhang, *Journal of the American Chemical Society* **2006**, *128*, 4530-4531.
[72] K. Vanommeslaeghe, F. D. Proft, S. Loverix, D. Tourwe, P. Geerlings, *Bioorgan Med Chem* **2005**, *13*, 3987-3992.
[73] P. A. Marks, R. Breslow, *Nat Biotechnol* **2007**, *25*, 84-90.
[74] N. Tsuji, M. Kobayashi, K. Nagashima, Y. Wakisaka, K. Koizumi, *The Journal of antibiotics* **1976**, *29*, 1-6.
[75] M. Yoshida, M. Kijima, M. Akita, T. Beppu, *The Journal of biological chemistry* **1990**, *265*, 17174-17179.
[76] F. Wagner, M. Weïwer, M. Lewis, E. Holson, *Neurotherapeutics : the journal of the American Society for Experimental NeuroTherapeutics* **2013**, *10*, 589-604.
[77] J. A. Day, S. M. Cohen, *Journal of Medicinal Chemistry* **2013**, *56*, 7997-8007.
[78] A. Vannini, C. Volpari, G. Filocamo, E. C. Casavola, M. Brunetti, D. Renzoni, P. Chakravarty, C. Paolini, R. De Francesco, P. Gallinari, C. Steinkuhler, S. Di Marco, *Proc Natl Acad Sci U S A* **2004**, *101*, 15064-15069.
[79] M. Boissinot, M. Inman, A. Hempshall, S. R. James, J. H. Gill, P. Selby, D. T. Bowen, R. Grigg, P. N. Cockerill, *Leukemia research* **2012**.
[80] D. J. Witter, P. Harrington, K. J. Wilson, M. Chenard, J. C. Fleming, B. Haines, A. M. Kral, J. P. Secrist, T. A. Miller, *Bioorganic & medicinal chemistry letters* **2008**, *18*, 726-731.
[81] T. Beckers, C. Burkhardt, H. Wieland, P. Gimmnich, T. Ciossek, T. Maier, K. Sanders, *International journal of cancer* **2007**, *121*, 1138-1148.
[82] J. C. Bressi, A. J. Jennings, R. Skene, Y. Q. Wu, R. Melkus, R. De Jong, S. O'Connell, C. E. Grimshaw, M. Navre, A. R. Gangloff, *Bioorganic & medicinal chemistry letters* **2010**, *20*, 3142-3145.
[83] L. Whitehead, M. R. Dobler, B. Radetich, Y. Zhu, P. W. Atadja, T. Claiborne, J. E. Grob, A. McRiner, M. R. Pancost, A. Patnaik, W. Shao, M. Shultz, R. Tichkule, R. A. Tommasi, B. Vash, P. Wang, T. Stams, *Bioorgan Med Chem* **2011**, *19*, 4626-4634.
[84] O. M. Moradei, T. C. Mallais, S. Frechette, I. Paquin, P. E. Tessier, S. M. Leit, M. Fournel, C. Bonfils, M. C. Trachy-Bourget, J. Liu, T. P. Yan, A. H. Lu, J. Rahil, J. Wang, S. Lefebvre, Z. Li, A. F. Vaisburg, J. M. Besterman, *J Med Chem* **2007**, *50*, 5543-5546.
[85] C. J. Phiel, F. Zhang, E. Y. Huang, M. G. Guenther, M. A. Lazar, P. S. Klein, *Journal of Biological Chemistry* **2001**, *276*, 36734-36741.
[86] N. Gurvich, O. M. Tsygankova, J. L. Meinkoth, P. S. Klein, *Cancer Research* **2004**, *64*, 1079-1086.

[87] G. Rosenberg, *Cell Mol Life Sci* **2007**, *64*, 2090-2103.
[88] K. Krennhrubec, B. L. Marshall, M. Hedglin, E. Verdin, S. M. Ulrich, *Bioorganic & medicinal chemistry letters* **2007**, *17*, 2874-2878.
[89] F. F. Wagner, D. E. Olson, J. P. Gale, T. Kaya, M. Weïwer, N. Aidoud, M. r. Thomas, E. L. Davoine, B. r. n. C. Lemercier, Y.-L. Zhang, *Journal of Medicinal Chemistry* **2013**, *56*, 1772-1776.
[90] G. Estiu, E. Greenberg, C. B. Harrison, N. P. Kwiatkowski, R. Mazitschek, J. E. Bradner, O. Wiest, *J Med Chem* **2008**, *51*, 2898-2906.
[91] K. V. Butler, J. Kalin, C. Brochier, G. Vistoli, B. Langley, A. P. Kozikowski, *Journal of the American Chemical Society* **2010**, *132*, 10842-10846.
[92] J. H. Kalin, J. A. Bergman, *Journal of Medicinal Chemistry* **2013**.
[93] S. Balasubramanian, J. Ramos, W. Luo, M. Sirisawad, E. Verner, J. Buggy, *Leukemia* **2008**, *22*, 1026-1034.
[94] G. Estiu, N. West, R. Mazitschek, E. Greenberg, J. E. Bradner, O. Wiest, *Bioorg Med Chem* **2010**, *18*, 4103-4110.
[95] T. Suzuki, Y. Ota, M. Ri, M. Bando, A. Gotoh, Y. Itoh, H. Tsumoto, P. R. Tatum, T. Mizukami, H. Nakagawa, *Journal of Medicinal Chemistry* **2012**, *55*, 9562-9575.
[96] M. Lobera, K. P. Madauss, D. T. Pohlhaus, Q. G. Wright, M. Trocha, D. R. Schmidt, E. Baloglu, R. P. Trump, M. S. Head, G. A. Hofmann, *Nature Chemical Biology* **2013**.
[97] K. J. Jensen, *Peptide and protein design for biopharmaceutical applications*, Wiley Online Library, **2009**.
[98] J. Taunton, C. A. Hassig, S. L. Schreiber, *Science (New York, N.Y.)* **1996**, *272*, 408-411.
[99] K. Umehara, K. Nakahara, S. Kiyoto, M. Iwami, M. Okamoto, H. Tanaka, M. Kohsaka, H. Aoki, H. Imanaka, *J. Antibiot.* **1983**, *36*, 478-483.
[100] A. Closse, R. Huguenin, *Helvetica chimica acta* **1974**, *57*, 533.
[101] J. M. Liesch, C. C. Sweeley, G. D. Staffeld, M. S. Anderson, D. J. Weber, R. P. Scheffer, *Tetrahedron* **1982**, *38*, 45-48.
[102] H. Itazaki, K. Nagashima, K. Sugita, H. Yoshida, Y. Kawamura, Y. Yasuda, K. Matsumoto, K. Ishii, N. Uotani, H. Nakai, A. Terui, S. Yoshimatsu, Y. Ikenishi, Y. Nakagawa, *J. Antibiot.* **1990**, *43*, 1524-1532.
[103] aA. Hirota, A. Suzuki, H. Suzuki, S. Tamura, *Agricultural and Biological Chemistry* **1973**, *37*, 643-647; bS. Takayama, A. Isogai, M. Nakata, H. Suzuki, A. Suzuki, *Agricultural and Biological Chemistry* **1984**, *48*, 839-842.
[104] M. Kijima, M. Yoshida, K. Sugita, S. Horinouchi, T. Beppu, *The Journal of biological chemistry* **1993**, *268*, 22429-22435.
[105] J. Taunton, J. L. Collins, S. L. Schreiber, *Journal of the American Chemical Society* **1996**, *118*, 10412-10422.
[106] R. Furumai, Y. Komatsu, N. Nishino, S. Khochbin, M. Yoshida, S. Horinouchi, *Proc Natl Acad Sci U S A* **2001**, *98*, 87-92.
[107] H. Stähelin, A. Trippmacher, *European Journal of Cancer (1965)* **1974**, *10*, 801-808.
[108] S. Wang, X. Li, Y. Wei, Z. Xiu, N. Nishino, *ChemMedChem* **2013**.
[109] S. B. Singh, D. L. Zink, J. D. Polishook, A. W. Dombrowski, S. J. DarkinRattray, D. M. Schmatz, M. A. Goetz, *Tetrahedron Letters* **1996**, *37*, 8077-8080.
[110] S. Singh, D. Zink, J. Liesch, R. Mosley, A. Dombrowski, G. Bills, S. Darkin-Rattray, D. Schmatz, M. Goetz, *The Journal of organic chemistry* **2002**, *67*, 815-825.
[111] aJ.-M. Jin, S. Lee, J. Lee, S.-R. Baek, J.-C. Kim, S.-H. Yun, S.-Y. Park, S. Kang, Y.-W. Lee, *Molecular Microbiology* **2010**, *76*, 456-466; bK. W. von Bargen, E.-M. Niehaus, K. Bergander, R. Brun, B. Tudzynski, H.-U. Humpf, *Journal of Natural Products* **2013**, *76*, 2136-2140.
[112] L. Mou, G. Singh, *Tetrahedron Letters* **2001**, *42*, 6603-6606.
[113] U. Schmidt, J. Langner, *J Pept Res* **1997**, *49*, 67-73.
[114] F. Berst, M. Ladlow, A. B. Holmes, *Chemical Communications* **2002**, 508-509.

[115] S. L. Colletti, R. W. Myers, S. J. Darkin-Rattray, A. M. Gurnett, P. M. Dulski, S. Galuska, J. J. Allocco, M. B. Ayer, C. Li, J. Lim, T. M. Crumley, C. Cannova, D. M. Schmatz, M. J. Wyvratt, M. H. Fisher, P. T. Meinke, *Bioorganic & medicinal chemistry letters* **2001**, *11*, 107-111.
[116] M. Kranz, P. J. Murray, S. Taylor, R. J. Upton, W. Clegg, M. R. Elsegood, *J Pept Sci* **2006**, *12*, 383-388.
[117] W. S. Horne, C. A. Olsen, J. M. Beierle, A. Montero, M. R. Ghadiri, *Angewandte Chemie-International Edition* **2009**, *48*, 4718-4724.
[118] A. Montero, J. M. Beierle, C. A. Olsen, M. R. Ghadiri, *J Am Chem Soc* **2009**, *131*, 3033-3041.
[119] C. A. Olsen, A. Montero, L. J. Leman, M. R. Ghadiri, *ACS Medicinal Chemistry Letters* **2012**, *3*, 749-753.
[120] K. Taori, V. J. Paul, H. Luesch, *J Am Chem Soc* **2008**, *130*, 1806-1807.
[121] Y. Ying, K. Taori, H. Kim, J. Hong, H. Luesch, *J Am Chem Soc* **2008**, *130*, 8455-8459.
[122] M. B. Hodge, H. F. Olivo, *Tetrahedron* **2004**, *60*, 9397-9403.
[123] T. Seiser, F. Kamena, N. Cramer, *Angew Chem Int Ed Engl* **2008**, *47*, 6483-6485.
[124] C. G. Nasveschuk, D. Ungermannova, X. Liu, A. J. Phillips, *Org Lett* **2008**, *10*, 3595-3598.
[125] A. Bowers, N. West, J. Taunton, S. L. Schreiber, J. E. Bradner, R. M. Williams, *J Am Chem Soc* **2008**, *130*, 11219-11222.
[126] aH. Benelkebir, S. Marie, A. L. Hayden, J. Lyle, P. M. Loadman, S. J. Crabb, G. Packham, A. Ganesan, *Bioorg Med Chem* **2011**, *19*, 3650-3658; bS. Wen, G. Packham, A. Ganesan, *The Journal of organic chemistry* **2008**, *73*, 9353-9361.
[127] Q. Xiao, L.-P. Wang, X.-Z. Jiao, X.-Y. Liu, Q. Wu, P. Xie, *Journal of Asian natural products research* **2010**, *12*, 940-949.
[128] A. K. Ghosh, S. Kulkarni, *Org Lett* **2008**, *10*, 3907-3909.
[129] X. Zeng, B. Yin, Z. Hu, C. Liao, J. Liu, S. Li, Z. Li, M. C. Nicklaus, G. Zhou, S. Jiang, *Organic Letters* **2010**, *12*, 1368-1371.
[130] J. Hong, H. Luesch, *Natural Product Reports* **2012**, *29*, 449-456.
[131] K. E. Cole, D. P. Dowling, M. A. Boone, A. J. Phillips, D. W. Christianson, *J Am Chem Soc* **2011**, *133*, 12474-12477.
[132] aY. Ying, Y. Liu, S. R. Byeon, H. Kim, H. Luesch, J. Hong, *Org Lett* **2008**, *10*, 4021-4024; bF. Chen, A.-H. Gao, J. Li, F.-J. Nan, *ChemMedChem* **2009**, *4*, 1269-1272; cJ. A. Souto, E. Vaz, I. Lepore, A.-C. Pöppler, G. Franci, R. Álvarez, L. Altucci, A. n. R. de Lera, *Journal of Medicinal Chemistry* **2010**, *53*, 4654-4667.
[133] A. A. Bowers, N. West, T. L. Newkirk, A. E. Troutman-Youngman, S. L. Schreiber, O. Wiest, J. E. Bradner, R. M. Williams, *Org Lett* **2009**, *11*, 1301-1304.
[134] N. Nishino, B. Jose, S. Okamura, S. Ebisusaki, Y. T. Kato, Y. Sumida, M. Yoshida, *Organic Letters* **2003**, *5*, 5079-5082.
[135] A. A. Bowers, T. J. Greshock, N. West, G. Estiu, S. L. Schreiber, O. Wiest, R. M. Williams, J. E. Bradner, *J Am Chem Soc* **2009**.
[136] H. Ueda, H. Nakajima, Y. Hori, T. Fujita, M. Nishimura, T. Goto, M. Okuhara, *The Journal of antibiotics* **1994**, *47*, 301-310.
[137] R. Furumai, A. Matsuyama, N. Kobashi, K. H. Lee, M. Nishiyama, H. Nakajima, A. Tanaka, Y. Komatsu, N. Nishino, M. Yoshida, S. Horinouchi, *Cancer Res* **2002**, *62*, 4916-4921.
[138] K. W. Li, J. Wu, W. Xing, J. A. Simon, *Journal of the American Chemical Society* **1996**, *118*, 7237-7238.
[139] T. J. Greshock, D. M. Johns, Y. Noguchi, R. M. Williams, *Organic Letters* **2008**, *10*, 613-616.
[140] aC. Wang, C. J. Flemming, Y.-Q. Cheng, *MedChemComm* **2012**, *3*, 976-981; bK. Narita, T. Kikuchi, K. Watanabe, T. Takizawa, T. Oguchi, K. Kudo, K. Matsuhara, H. Abe, T. Yamori, M. Yoshida, *Chemistry-A European Journal* **2009**, *15*, 11174-11186.
[141] Y. Nakao, S. Yoshida, S. Matsunaga, N. Shindoh, Y. Terada, K. Nagai, J. K. Yamashita, A. Ganesan, R. W. van Soest, N. Fusetani, *Angew Chem Int Ed Engl* **2006**, *45*, 7553-7557.
[142] H. C. Brown, K. S. Bhat, *Journal of the American Chemical Society* **1986**, *108*, 5919-5923.
[143] I. Izzo, N. Maulucci, G. Bifulco, F. De Riccardis, *Angew Chem Int Ed Engl* **2006**, *45*, 7557-7560.
[144] S. Wen, K. L. Carey, Y. Nakao, N. Fusetani, G. Packham, A. Ganesan, *Org Lett* **2007**, *9*, 1105-1108.
[145] J. A. Ellman, *Pure and applied chemistry* **2003**, *75*, 39-46.

[146] S. Chandrasekhar, C. L. Rao, M. Seenaiah, P. Naresh, B. Jagadeesh, D. Manjeera, A. Sarkar, M. P. Bhadra, *The Journal of organic chemistry* **2008**, *74*, 401-404.
[147] N. Maulucci, M. G. Chini, S. D. Micco, I. Izzo, E. Cafaro, A. Russo, P. Gallinari, C. Paolini, M. C. Nardi, A. Casapullo, R. Riccio, G. Bifulco, F. De Riccardis, *J Am Chem Soc* **2007**, *129*, 3007-3012.
[148] J. S. Villadsen, H. M. Stephansen, A. R. Maolanon, P. Harris, C. A. Olsen, *Journal of Medicinal Chemistry* **2013**, *56*, 6512-6520.
[149] L. Auzzas, A. Larsson, R. Matera, A. Baraldi, B. t. Deschênes-Simard, G. Giannini, W. Cabri, G. Battistuzzi, G. Gallo, A. Ciacci, *Journal of Medicinal Chemistry* **2010**, *53*, 8387-8399.
[150] J. T. Randolph, P. Waid, C. Nichols, D. Sauer, F. Haviv, G. Diaz, G. Bammert, L. M. Besecke, J. A. Segreti, K. M. Mohning, *Journal of Medicinal Chemistry* **2004**, *47*, 1085-1097.
[151] S. C. Mwakwari, W. Guerrant, V. Patil, S. I. Khan, B. L. Tekwani, Z. A. Gurard-Levin, M. Mrksich, A. K. Oyelere, *Journal of Medicinal Chemistry* **2010**, *53*, 6100-6111.
[152] T. Liu, G. Kapustin, F. A. Etzkorn, *Journal of Medicinal Chemistry* **2007**, *50*, 2003-2006.
[153] L. A. Marcaurelle, E. Comer, S. Dandapani, J. R. Duvall, B. Gerard, S. Kesavan, M. D. Lee IV, H. Liu, J. T. Lowe, J.-C. Marie, *Journal of the American Chemical Society* **2010**, *132*, 16962-16976.
[154] C. J. Vickers, C. A. Olsen, L. J. Leman, M. R. Ghadiri, *ACS Medicinal Chemistry Letters* **2012**, *3*, 505-508.
[155] aS. J. Crabb, M. Howell, H. Rogers, M. Ishfaq, A. Yurek-George, K. Carey, B. M. Pickering, P. East, R. Mitter, S. Maeda, *Biochemical Pharmacology* **2008**, *76*, 463-475; bT. L. Newkirk, A. A. Bowers, R. M. Williams, *Nat Prod Rep* **2009**, *26*, 1293-1320.
[156] S. M. Sternson, J. C. Wong, C. M. Grozinger, S. L. Schreiber, *Organic Letters* **2001**, *3*, 4239-4242.
[157] S. Terracciano, S. Di Micco, G. Bifulco, P. Gallinari, R. Riccio, I. Bruno, *Bioorgan Med Chem* **2010**, *18*, 3252-3260.
[158] R. H. Grubbs, S. J. Miller, G. C. Fu, *Accounts of chemical research* **1995**, *28*, 446-452.
[159] C. W. Bielawski, R. H. Grubbs, *Prog. Polym. Sci.* **2007**, *32*, 1-29.
[160] S. J. Connon, S. Blechert, *Angewandte Chemie International Edition* **2003**, *42*, 1900-1923.
[161] aS. S. Zhu, D. R. Cefalo, D. S. La, J. Y. Jamieson, W. M. Davis, A. H. Hoveyda, R. R. Schrock, *Journal of the American Chemical Society* **1999**, *121*, 8251-8259; bT. M. Trnka, R. H. Grubbs, *Accounts of chemical research* **2001**, *34*, 18-29.
[162] J. Hérisson, Y. Chauvin, *Makromol. Chem* **1971**, *141*, 161-176.
[163] M. S. Sanford, J. A. Love, R. H. Grubbs, *Journal of the American Chemical Society* **2001**, *123*, 6543-6554.
[164] P. E. Romero, W. E. Piers, *Journal of the American Chemical Society* **2005**, *127*, 5032-5033.
[165] M. S. Sanford, M. Ulman, R. H. Grubbs, *Journal of the American Chemical Society* **2001**, *123*, 749-750.
[166] C. Samojłowicz, M. Bieniek, K. Grela, *Chemical Reviews* **2009**, *109*, 3708-3742.
[167] A. K. Chatterjee, T.-L. Choi, D. P. Sanders, R. H. Grubbs, *Journal of the American Chemical Society* **2003**, *125*, 11360-11370.
[168] aA. Michrowska, R. Bujok, S. Harutyunyan, V. Sashuk, G. Dolgonos, K. Grela, *Journal of the American Chemical Society* **2004**, *126*, 9318-9325; bK. Grela, S. Harutyunyan, A. Michrowska, *Angewandte Chemie* **2002**, *114*, 4210-4212.
[169] J. E. Bradner, N. West, M. L. Grachan, E. F. Greenberg, S. J. Haggarty, T. Warnow, R. Mazitschek, *Nat Chem Biol* **2010**, *6*, 238-243.
[170] C. Yung-Chi, W. H. Prusoff, *Biochemical Pharmacology* **1973**, *22*, 3099-3108.
[171] H. Kessler, R. Gratias, G. Hessler, M. Gurrath, G. Müller, *Pure and applied chemistry* **1996**, *68*, 1201-1206.
[172] T. Masaharu, K. Haruo, M. Shigeyasu, T. Toshio, I. Kunio, *Phosphorus, Sulfur, and Silicon and the Related Elements* **2003**, *178*.
[173] E. N. Prilezhaeva, *Russian Chemical Reviews* **2000**, *69*, 367-408.
[174] J. B. Baudin, G. Hareau, S. A. Julia, O. Ruel, *Tetrahedron letters* **1991**, *32*, 1175-1178.
[175] L. A. Warren, S. Smiles, *Journal of the Chemical Society (Resumed)* **1930**, 1327-1331.

[176] aJ. B. Baudin, G. Hareau, S. A. Julia, R. Lorne, O. Ruel, *B Soc Chim Fr* **1993**, *130*, 856-878; bP. R. Blakemore, *Journal of the Chemical Society, Perkin Transactions 1* **2002**, 2563-2585.
[177] P. R. Blakemore, W. J. Cole, P. J. Kocieński, A. Morley, *Synlett* **1998**, *1998*, 26-28.
[178] P. J. Kocienski, A. Bell, P. R. Blakemore, *Synlett* **2000**, *2000*, 365-366.
[179] G. Wittig, G. Geissler, *Annalen Der Chemie-Justus Liebig* **1953**, *580*, 44-57.
[180] W. S. Wadsworth, W. D. Emmons, *Journal of the American Chemical Society* **1961**, *83*, 1733-1738.
[181] M. Schlosser, K. F. Christmann, *Angewandte Chemie International Edition in English* **1966**, *5*, 126-126.
[182] E. Vedejs, C. Marth, *Tetrahedron Letters* **1987**, *28*, 3445-3448.
[183] P. A. Byrne, D. G. Gilheany, *Chemical Society Reviews* **2013**.
[184] E. Vedejs, M. J. Peterson, in *Topics in Stereochemistry*, John Wiley & Sons, Inc., **1994**, pp. 1-157.
[185] L. Kurti, B. Czakó, *Strategic applications of named reactions in organic synthesis*, Elsevier Academic Press Burlington, MA, **2005**.
[186] M. J. Gresser, P. A. Keller, S. M. Wales, *Tetrahedron Letters* **2009**, *50*, 4899-4902.
[187] C.-J. Zheng, C.-J. Kim, K. S. Bae, Y.-H. Kim, W.-G. Kim, *Journal of Natural Products* **2006**, *69*, 1816-1819.
[188] M. Varoglu, T. H. Corbett, F. A. Valeriote, P. Crews, *The Journal of organic chemistry* **1997**, *62*, 7078-7079.
[189] K. Shaw, Y. Aracava, A. Akaike, J. Daly, D. Rickett, E. Albuquerque, *Molecular pharmacology* **1985**, *28*, 527-538.
[190] L. M. Repka, J. Ni, S. E. Reisman, *Journal of the American Chemical Society* **2010**, *132*, 14418-14420.
[191] M. E. Kieffer, L. M. Repka, S. E. Reisman, *Journal of the American Chemical Society* **2012**, *134*, 5131-5137.
[192] L. M. Repka, Ph.D. Thesis, California Institute of Technology **2013**.
[193] A. L. Hodgkin, A. Huxley, B. Katz, *The Journal of physiology* **1952**, *116*, 424.
[194] N. Dascal, *Critical Reviews in Biochemistry and Molecular Biology* **1987**, *22*, 317-387.
[195] J. Ruiz-Rodriguez, F. Albericio, R. Lavilla, *Chemistry* **2010**, *16*, 1124-1127.
[196] C.-S. Jiang, Y.-W. Guo, *Mini Reviews in Medicinal Chemistry* **2011**, *11*, 728-745.
[197] V. R. Hegde, P. Dai, M. Patel, P. R. Das, M. S. Puar, *Tetrahedron letters* **1997**, *38*, 911-914.
[198] R. Nagarajan, L. Huckstep, D. Lively, D. DeLong, M. Marsh, N. Neuss, *Journal of the American Chemical Society* **1968**, *90*, 2980-2982.
[199] P. A. Miller, P. W. Trown, W. Fulmor, G. O. Morton, J. Karliner, *Biochemical and Biophysical Research Communications* **1968**, *33*, 219-221.
[200] N. Kawahara, K. Nozawa, M. Yamazaki, S. Nakajima, K. Kawai, *Chemical & pharmaceutical bulletin* **1990**, *38*, 73-78.
[201] J. A. Codelli, A. L. Puchlopek, S. E. Reisman, *Journal of the American Chemical Society* **2011**, *134*, 1930-1933.
[202] C. Zhu, X. Q. Shen, S. G. Nelson, *Journal of the American Chemical Society* **2004**, *126*, 5352-5353.
[203] D. A. Evans, M. M. Morrissey, *Journal of the American Chemical Society* **1984**, *106*, 3866-3868.
[204] J. A. Love, J. P. Morgan, T. M. Trnka, R. H. Grubbs, *Angewandte Chemie International Edition* **2002**, *41*, 4035-4037.
[205] E. S. Inks, B. J. Josey, S. R. Jesinkey, C. J. Chou, *ACS chemical biology* **2011**.
[206] A. S. Madsen, C. A. Olsen, *Angewandte Chemie International Edition* **2012**, *51*, 9083-9087.
[207] aA. A. Bothner-By, R. Stephens, J. Lee, C. D. Warren, R. Jeanloz, *Journal of the American Chemical Society* **1984**, *106*, 811-813; bH. Kessler, C. Griesinger, K. Wagner, *Journal of the American Chemical Society* **1987**, *109*, 6927-6933.
[208] aS. Macur, B. Farmer II, L. Brown, *Journal of Magnetic Resonance (1969)* **1986**, *70*, 493-499; bH. Hu, K. Krishnamurthy, *Journal of Magnetic Resonance* **2006**, *182*, 173-177.
[209] A. Pardi, M. Billeter, K. Wüthrich, *Journal of Molecular Biology* **1984**, *180*, 741-751.
[210] aD. Shivakumar, J. Williams, Y. Wu, W. Damm, J. Shelley, W. Sherman, *Journal of Chemical Theory and Computation* **2010**, *6*, 1509-1519; bK. Bowers, E. Chow, H. Xu, R. Dror, M. Eastwood, B.

Gregersen, J. Klepeis, I. Kolossvary, M. Moraes, F. Sacerdoti, in *ACM/IEEE SC 2006 Conference (SC'06). IEEE*, **2006**, pp. 43-43.
[211] H. J. Berendsen, J. P. M. Postma, W. F. van Gunsteren, A. DiNola, J. Haak, *The Journal of chemical physics* **1984**, *81*, 3684.
[212] R. Sedrani, J. Kallen, L. M. Martin Cabrejas, C. D. Papageorgiou, F. Senia, S. Rohrbach, D. Wagner, B. Thai, A.-M. Jutzi Eme, J. France, L. Oberer, G. Rihs, G. Zenke, J. Wagner, *Journal of the American Chemical Society* **2003**, *125*, 3849-3859.
[213] E. G. Bowen, D. J. Wardrop, *Organic Letters* **2010**, *12*, 5330-5333.
[214] A. B. Charette, M. Grenon, A. Lemire, M. Pourashraf, J. Martel, *Journal of the American Chemical Society* **2001**, *123*, 11829-11830.
[215] S. R. Kandukuri, J. A. Schiffner, M. Oestreich, *Angew Chem Int Ed Engl* **2012**, *51*, 1265-1269.
[216] P. S. Baran, C. A. Guerrero, N. B. Ambhaikar, B. D. Hafensteiner, *Angew Chem Int Ed Engl* **2005**, *44*, 606-609.
[217] Y. Yang, X. Jiang, F. L. Qing, *J Org Chem* **2012**, *77*, 7538-7547.
[218] L. Lapatsanis, G. Milias, K. Froussios, M. Kolovos, *Synthesis* **1983**, *1983*, 671-673.
[219] L. H. J. Kleijn, F. M. Müskens, S. F. Oppedijk, G. de Bruin, N. I. Martin, *Tetrahedron Letters* **2012**, *53*, 6430-6432.
[220] M. Camplo, V. Niddam, P. Barthélémy, P. Faury, N. Mourier, V. Simon, A. S. Charvet, C. Trabaud, J. C. Graciet, J. C. Chermann, J. L. Kraus, *European Journal of Medicinal Chemistry* **1995**, *30*, 789-800.
[221] S. D. Bull, S. G. Davies, S. Jones, M. E. C. Polywka, R. Shyam Prasad, H. J. Sanganee, *Synlett* **1998**, *1998*, 519-521.
[222] S. Beaumont, E. A. Ilardi, L. R. Monroe, A. Zakarian, *Journal of the American Chemical Society* **2010**, *132*, 1482-1483.
[223] I. R. Davies, M. Cheeseman, R. Green, M. F. Mahon, A. Merritt, S. D. Bull, *Organic Letters* **2009**, *11*, 2896-2899.

Journal of Medicinal Chemistry

Article

pubs.acs.org/jmc

Total Synthesis and Full Histone Deacetylase Inhibitory Profiling of Azumamides A−E as Well as β^2- *epi*-Azumamide E and β^3-*epi*-Azumamide E

Jesper S. Villadsen, Helle M. Stephansen, Alex R. Maolanon, Pernille Harris, and Christian A. Olsen*

Department of Chemistry, Technical University of Denmark, Kemitorvet 207, Kongens Lyngby DK-2800, Denmark

Supporting Information

ABSTRACT: Cyclic tetrapeptide and depsipeptide natural products have proven useful as biological probes and drug candidates due to their potent activities as histone deacetylase (HDAC) inhibitors. Here, we present the syntheses of a class of cyclic tetrapeptide HDAC inhibitors, the azumamides, by a concise route in which the key step in preparation of the noncanonical disubstituted β-amino acid building block was an Ellman-type Mannich reaction. By tweaking the reaction conditions during this transformation, we gained access to the natural products as well as two epimeric homologues. Thus, the first total syntheses of azumamides B−D corroborated the originally assigned structures, and the synthetic efforts enabled the first full profiling of HDAC inhibitory properties of the entire selection of azumamides A−E. This revealed unexpected differences in the relative potencies within the class and showed that azumamides C and E are both potent inhibitors of HDAC10 and HDAC11.

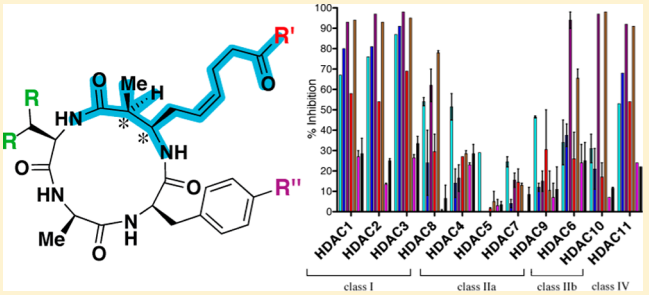

INTRODUCTION

Macrocyclic peptides have played important roles in the field of epigenetics due to their potent activities as inhibitors of histone deacetylase (HDAC) enzymes. One of the two HDAC targeting drugs (**1**[1] and **3**) that are approved by the U.S. Food and Drug Administration (FDA) for clinical treatment of cutaneous T-cell lymphoma is the macrocyclic natural product romidepsin (**3**).[2] Furthermore, a cyclic tetrapeptide, trapoxin,[3] played an instrumental role in the first isolation of a mammalian HDAC enzyme.[4,5] Thus, this class of inhibitors holds promise as tool compounds as well as potential drug candidates targeting HDACs.[6−9]

Though clearly bearing an overall resemblence to the classical cyclic tetrapeptide HDAC inhibitors [including, for example, apicidin (**4**)],[10] the azumamides (**5**−**9**) are structurally unique in that their extended Zn^{2+}-coordinating amino acid (shown in yellow in Figure 1) is a disubstituted β-amino acid.[11] Furthermore, we found the azumamides interesting due to the relatively strong potencies reported for azumamide E against class I HDACs[12] in spite of its weak Zn^{2+}-coordinating carboxylic acid functionality.[13] Previously, azumamide A[14,15] and azumamide E[12,14−16] have been prepared by multistep chemical syntheses, but only azumamide E was tested against recombinant HDAC isoforms 1−9.[12] Furthermore, in vitro profiling with recombinant HDACs has witnessed important new developments since the publication of those results.[17,18] We therefore found it relevant to explore the properties of these macrocycles in more detail by preparing the complete selection of natural products (**5**−**9**), and profiling their activities against the full panel of recombinant human Zn^{2+}-dependent HDAC enzymes, HDAC1−11.

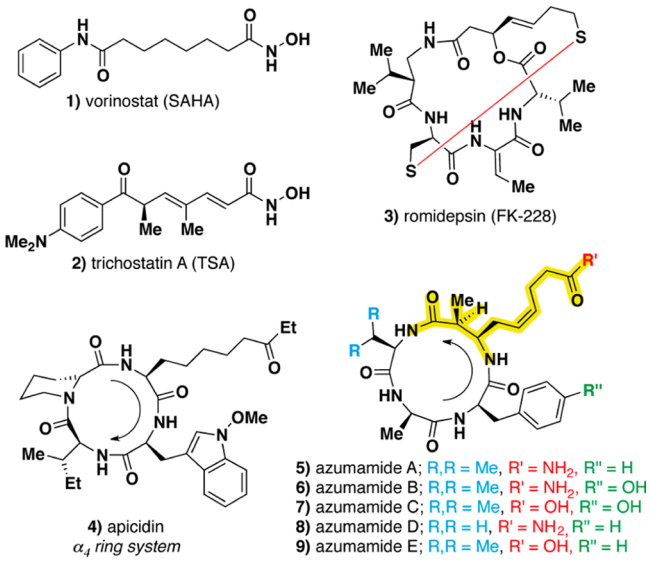

Figure 1. Structures of archetypical HDAC inhibitors (**1**−**4**) and target azumamides **5**−**9**.

As total syntheses of azumamides B−D had not been reported previously, this work would also allow unequivocal validation of the proposed structures.[11]

For syntheses of the azumamides, we envisaged two significant challenges: first, efficient stereoselective synthesis

Received: June 6, 2013
Published: July 18, 2013

of the disubstituted β-amino acid, and second, the macrocyclization step, which is known to be difficult for small cyclic peptides in general[19] and furthermore proved challenging in previously reported syntheses of azumamide analogues.[12]

RESULTS AND DISCUSSION

Building Block Synthesis. For our synthesis of the β-amino acid building block, we chose a diastereoselective Ellman-type Mannich reaction to set the stereochemistry, as also previously reported by Ganesan and co-workers.[15] However, to avoid having this important transformation at a late stage in our synthetic route, we decided to optimize this reaction between a propionate ester and a simple imine as shown in eq 1.

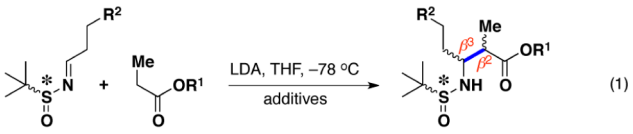

R1 and R2 are defined in Table 1.

This should give an intermediate with the correct stereochemistry (2*S*,3*R*), which could be readily elaborated to give the desired β-amino acid by robust organic synthetic transformations (vide infra). Mannich reactions between ester enolates and chiral sulfinylimines have been studied extensively,[20,21] and using previously reported conditions as our starting point we conducted an optimization study as outlined in Table 1. The *tert*-butyl ester showed superior selectivity (entry 5) compared to the less bulky methyl, ethyl, allyl, and PMB esters (entries 1−4), and furthermore, the methyl ester did not proceed to completion in our hands. Somewhat surprisingly, however, the major diastereoisomer in entry 5 proved to have (2*S*,3*S*) configuration as determined by X-ray crystallography upon desilylation (Figure 2).

This indicates that the pathway leading to our major isomer did not proceed through the six-membered Zimmerman−Traxler-type transition state,[22] which has been proposed to be responsible for the diastereoselectivity with similar substrates.[20,23] By using HMPA as an additive instead of a Lewis acid, this reaction has previously been shown to proceed through a different transition state,[20] and indeed we saw the same product distribution when using HMPA and $TiCl(O^iPr)_3$ as additives with our substrates (entries 5 and 6). This indicates that the six-membered transition state, where coordination of

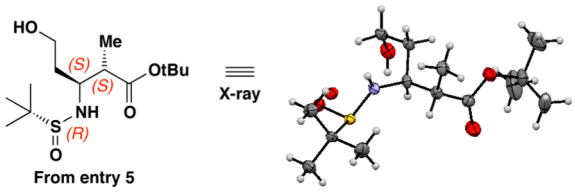

Figure 2. X-ray crystal structure of the (2*S*,3*S*) precursor obtained by desilylation of the major product in entry 5 of Table 1.

titanium is crucial, is highly unlikely to play a significant role in the formation of our major isomer. This is not in agreement with the diastereoselectivities observed with the substrates reported by Ganesan and co-workers.[15] Thus, to address whether the steric bulk of the triisopropylsilyl ether was responsible for interrupting the six-membered transition state, we performed the reaction with different means of protecting the alcohol (entries 7−9). No significant effect was observed, however, indicating instead that the steric bulk of the *tert*-butyl ester caused the predominance of a different transition state when using our substrates. This is also in agreement with the original study by Tang and Ellman[20] where the level of selectivity decreased for 2,3-disubstituted β-amino acids when the bulk of the ester increased from methyl to *tert*-butyl.

Because we were interested in taking advantage of solid-phase synthesis methods to prepare the linear tetrapeptide azumamide precursors with a minimum of chromatographic purification steps, we were keen on keeping the acid-labile *tert*-butyl ester protecting group, which would allow easy protecting group manipulation to give an Fmoc-protected β-amino acid building block. Hence, instead of substituting this protecting group, we decided to optimize the Mannich reaction conditions to deliver the desired stereochemistry. First, we changed the stereochemistry of the sulfinylimine to the *R*-enantiomer, which expectedly furnished the enantiomer of entries 5−9 (2*R*,3*R*) as the major isomer (entry 10). We then hypothesized that the configuration of the 2-position would be sensitive to the *E*/*Z* configuration of the enolate. Using Ireland's conditions for forming the enolate in the presence of HMPA,[24,25] we achieved >80% *Z*-isomer, which gratifyingly afforded the (2*S*,3*R*) product as major isomer (entry 11). Under the developed conditions, we prepared compound **12**, which was further elaborated to give Fmoc-protected β-amino acid **16** in 15% overall yield with just four column chromatographic purification steps from compound **10** (Scheme 1).

Table 1. Optimization of Stereochemical Outcome of the Mannich Reaction Shown in Equation 1

entry	auxiliary*	R^1	R^2	additive	enolate[a]	dr[b]	major isomer
1	*R*	Me	$OSi(^iPr)_3$	$TiCl(O^iPr)_3$	*E*	47:39:10:4	ND[c]
2	*R*	Et	$OSi(^iPr)_3$	$TiCl(O^iPr)_3$	*E*	49:29:11:11	ND
3	*R*	allyl	$OSi(^iPr)_3$	$TiCl(O^iPr)_3$	*E*	46:34:10:10	ND
4	*R*	PMB	$OSi(^iPr)_3$	$TiCl(O^iPr)_3$	*E*	46:33:11:10	ND
5	*R*	^{t}Bu	$OSi(^iPr)_3$	$TiCl(O^iPr)_3$	*E*	60:26:8:6	(2*S*,3*S*)[d]
6	*R*	^{t}Bu	$OSi(^iPr)_3$	HMPA	*E*	71:15:14:0	(2*S*,3*S*)
7	*R*	^{t}Bu	OBn	$TiCl(O^iPr)_3$	*E*	70:18:12:0	ND
8	*R*	^{t}Bu	OPMB	$TiCl(O^iPr)_3$	*E*	77:13:10:0	(2*S*,3*S*)
9	*R*	^{t}Bu	$OSi(Et)_3$	$TiCl(O^iPr)_3$	*E*	75:21:4:0	(2*S*,3*S*)[d]
10	*S*	^{t}Bu	$OSi(^iPr)_3$	HMPA	*E*	77:18:5:0	(2*R*,3*R*)[e]
11	*S*	^{t}Bu	$OSi(^iPr)_3$	HMPA[f]	*Z*	64:25:8:2	(2*S*,3*R*)[g]

[a]Major configuration of the enolate as determined by NMR and by trapping with ^{t}BuMe$_2$SiCl. [b]Diastereomeric ratio determined by ^{1}H NMR. [c]ND = not determined. [d]Determined by X-ray crystallography on its desilylated homologue. [e]Determined spectroscopically by comparison with its enantiomer from entries 5 and 9. [f]HMPA (5.4 equiv) was added prior to the substrate to obtain the (*Z*)-enolate (>80%). [g]Determined by comparison of spectroscopic data of the fully elaborated Boc-protected β-amino acid with previously reported data.[12]

dx.doi.org/10.1021/jm4008449 | J. Med. Chem. 2013, 56, 6512−6520

Scheme 1. Synthesis of β-Amino Acid Building Block 16.[a]

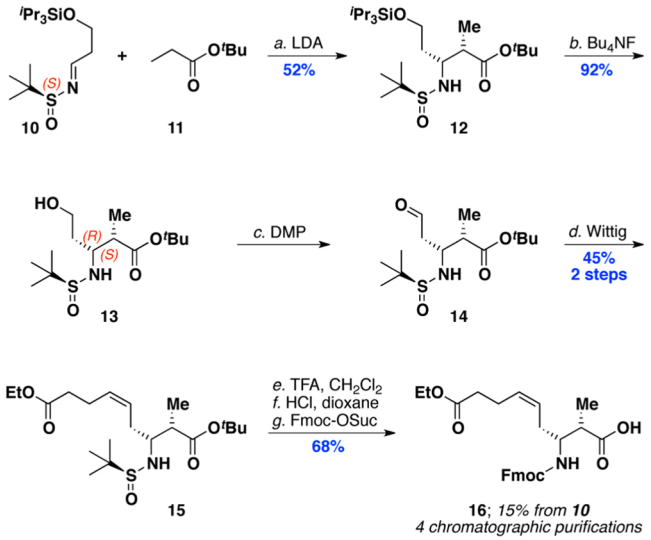

[a]Reagents and conditions: (a) HMPA (6.4 equiv), LDA (2.6 equiv), **11** (2.5 equiv), THF, −78 °C, 30 min; then **10**, −78 °C, 30 min. (b) AcOH (1.0 equiv), Bu_4NF (2.0 equiv), THF, 0 °C → rt, 1.5 h. (c) $NaHCO_3$ (1.5 equiv), Dess−Martin periodinane (1.4 equiv), dry CH_2Cl_2, 0 °C → rt, 1.5 h. (d) KHMDS (1.9 equiv), Ph_3PBr-$(CH_2)_3COOEt$ (2.0 equiv), THF, −78 °C → rt, 18 h. (e) TFA−CH_2Cl_2 (1:1, 10 mL, 80 equiv), 0 °C → rt, 3 h. (f) HCl (4.0 M in dioxane, 3.0 equiv), dioxane, 3 h. (g) Na_2CO_3 (4.0 equiv), Fmoc-OSuc (1.2 equiv), dioxane−H_2O, 0 °C → rt, 2 h.

The Boc-protected homologue of **16** was also prepared to confirm the (2*S*,3*R*) stereochemistry by comparison of spectroscopic data (optical rotation and NMR) with those previously reported (Figure S1 in Supporting Information).[12] Furthermore, the β^2- and β^3-epimeric building blocks were prepared by elaboration of the major isomers from entries 10 and 5, respectively (see Supporting Information for details). Although the achieved diastereomeric ratios were not particularly impressive, this strategy very nicely provided the correct stereochemistry along with two novel β-amino acids, enabling investigation of the biochemical effect of stereochemical configuration at these two chiral centers.

Cyclic Peptide Synthesis. Because three different points of cyclization had been reported for azumamide E and since these were all performed with different coupling reagents,[12,14,15] we performed cyclization experiments using a simplified model peptide to address the issue. Not too surprisingly, this showed that macrolactamizations with the most sterically hindered amino acids at the C-terminal were particularly poor, resulting in significant amounts of N-terminal guanidinylation, incomplete cyclization, epimerization, and/or dimerization (Table S1 in Supporting Information). Thus, we prepared the linear tetrapeptides **17**, **19**, and **21** on solid support by standard Fmoc solid-phase synthesis using β-amino acid **16** and commercially available Fmoc-D-amino acids.

In Scheme 2A, the cyclization was then performed at the β-amino acid position and in Scheme 2B at the alanine residue, whereas the preparation of azumamide D (**8**) was achieved by cyclization between the two least sterically challenging alanine residues (Scheme 2C). After cleavage from the 2-chlorotrityl polystyrene resin with dilute TFA, the linear tetramers were ring-closed by use of HATU under dilute conditions (0.4−0.5 mM),[26−29] and furthermore slow addition of the linear peptide by syringe pump to a solution of Hünig's base and HATU, as described by Ganesan and co-workers,[15] was tested. Judging from LC−MS analyses of the reaction mixtures, we could not observe any significant differences between the cyclization yields obtained with the different methods. Although all the couplings proceeded satisfactorily, with full conversion of linear peptides and minor amounts of the corresponding dimers as the only observed byproducts, the resulting overall isolated yields were relatively low (~10%). We ascribe this to difficulties during purification of the macrocyclic products by preparative reversed-phase HPLC caused by poor water solubility, as we were able to recover more material by purifying the macrocycles by column chromatography. Unfortunately, however, this did not provide the final compounds in satisfyingly high purity for the bioassays, and thus the final compounds were all subjected to preparative reversed-phase HPLC purification although this resulted in a loss of material. Carbodiimide-mediated amidation of the side chain was attempted for conversion of **7** to **6** and **23** to **8**, but the reaction was slow and gave varying yields (**6** vs **8**, Scheme 2). Instead, HATU-mediated coupling was attempted for conversion of **9** to **5**, and this proved faster and gave an acceptable yield (**5**). Spectral data of all the natural products **5**−**9** were in excellent agreement with those originally reported for the azumamides isolated from natural sources,[5] thus corroborating the original structural assignment (Figures S2−S6 in Supporting Information). Finally, the two epimeric β-amino acid building blocks were applied in analogous syntheses of β^3-*epi*-azumamide E (**26**) and β^2-*epi*-azumamide E (**29**) as shown in Scheme 3.

HDAC Screening. As an initial test of the HDAC inhibitory potency of all seven compounds, we first screened against the full panel of recombinant human HDACs at two compound concentrations (50 μM and 5 μM). Protocols for HDAC1−9 were adapted from Bradner et al.,[18] using the fluorogenic Ac-LeuGlyLys(Ac)-AMC substrate for HDAC1−3 and 6 while using the Ac-LeuGlyLys(tfa)-AMC substrate for HDAC4, 5, and 7−9. For HDAC10 we used the tetrapeptide Ac-ArgThr-Lys(Ac)Lys(Ac)-AMC,[30] which was recently reported to perform well with this enzyme.[31] Finally, for HDAC11, we also used Ac-LeuGlyLys(Ac)-AMC as substrate.[32]

The site-specifically epimerized compounds exhibited no activity as previously reported for an analogue having both stereocenters inverted.[7] It was not surprising that **26** was inactive, but it is noteworthy that the subtle change of inverting the stereochemistry of a single methyl group in **29** had such a detrimental effect across the entire selection of enzymes (Figure 3). Furthermore, none of the compounds **5**−**9** were able to inhibit class IIa HDAC activity against a trifluoroacetylated substrate (Figure 3).

Inhibitor K_i Values. Next, we performed dose−response experiments for all compound−HDAC combinations that gave above 50% inhibition in the initial assay (Figure S7 and Table S2 in Supporting Information). The obtained IC_{50} values were converted to K_i values by use of the Cheng−Prusoff equation $[K_i = IC_{50}/(1 + [S]/K_m)]$ with the assumption of a standard fast-on−fast-off mechanism of inhibition. Reported K_m values were applied for the calculations except HDAC10, where we determined the K_m for the used substrate to be 1.5 ± 0.2 μM (Figure 4).

Low potencies were recorded against HDACs 6 and 8, which is in accordance with previous data for azumamide E (Table 2);[6] however, compounds **7** and **9** were both potent inhibitors of HDACs 10 and 11. Although they are classified together

dx.doi.org/10.1021/jm4008449 | J. Med. Chem. 2013, 56, 6512−6520

Scheme 2. Synthesis of Azumamides A–E by Solid-Phase Synthesis Followed by Head-to-Tail Macrolactamization in Solution[a]

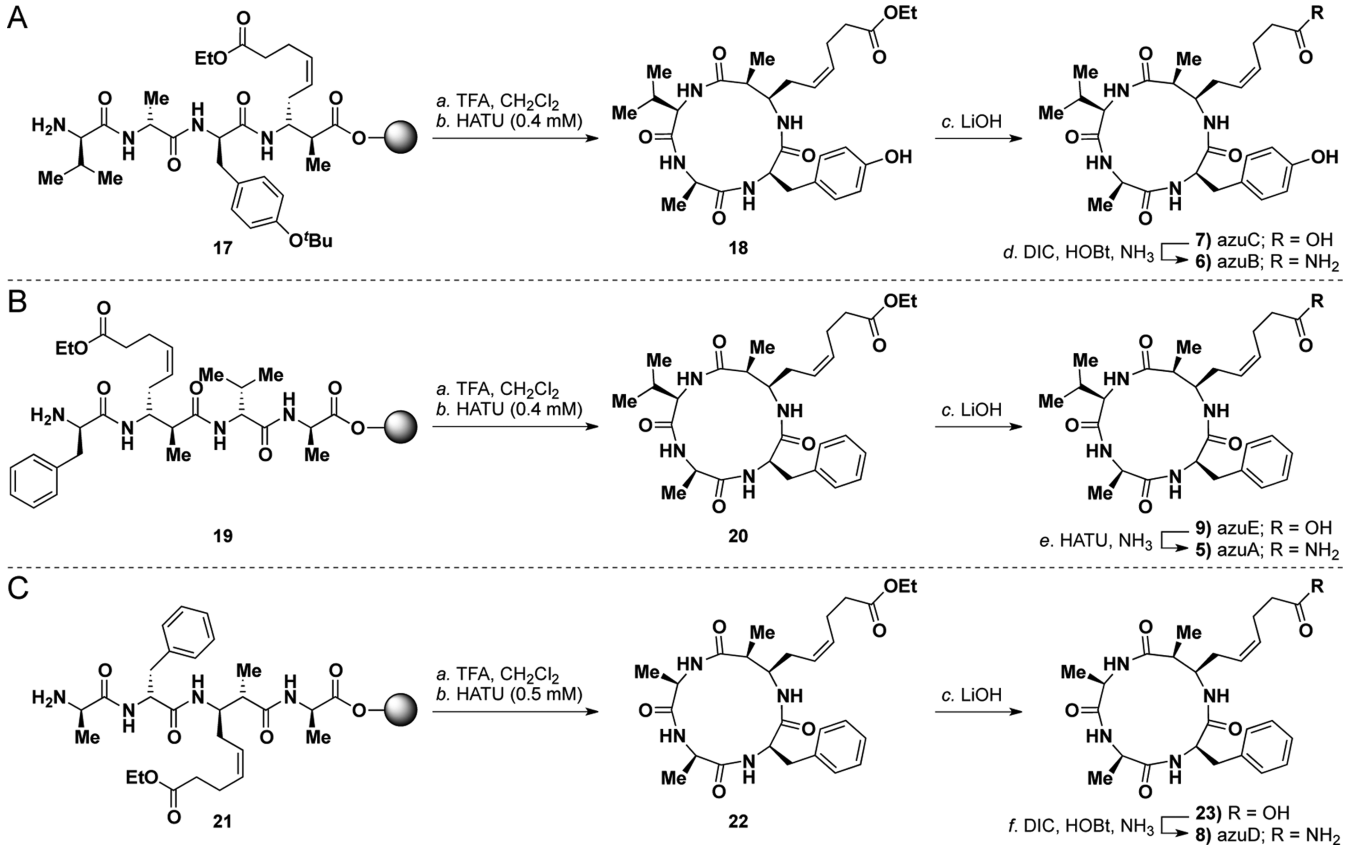

[a]Reagents and conditions: (a) TFA–CH_2Cl_2 (1:1), 2 × 30 min. (b) HATU, $^iPr_2NEt$ (8.0 equiv), DMF (0.4–0.5 mM peptide concn), 17–21 h; then HATU (0.5 equiv), 1–3 h [A, 11% **18** after preparative HPLC; B, 25% **20** after column chromatography; C, 19% **22** after column chromatography]. (c) LiOH, THF–H_2O (1:1). (d) DIC (11 equiv), HOBt (3.0 equiv), $^iPr_2NEt$ (4.0 equiv), NH_3–dioxane (25 equiv), DMF–CH_2Cl_2 (2:1), 5 days, 67%. (e) HATU (2.0 equiv), $^iPr_2NEt$ (5.5 equiv), NH_3–dioxane (25 equiv), DMF, 5.5 h, 40% (for steps c and e). (f) DIC (6.0 equiv), HOBt (3.0 equiv), $^iPr_2NEt$ (4.0 equiv), NH_3–dioxane and NH_3–MeOH (30 equiv), CH_2Cl_2–DMF (2:1), 13 days, 11% (for steps c and f).

Scheme 3. Synthesis of the Two Epimers 26 and 29 of Azumamide E by Solid-Phase Synthesis Followed by Head-to-Tail Macrolactamization in Solution[a]

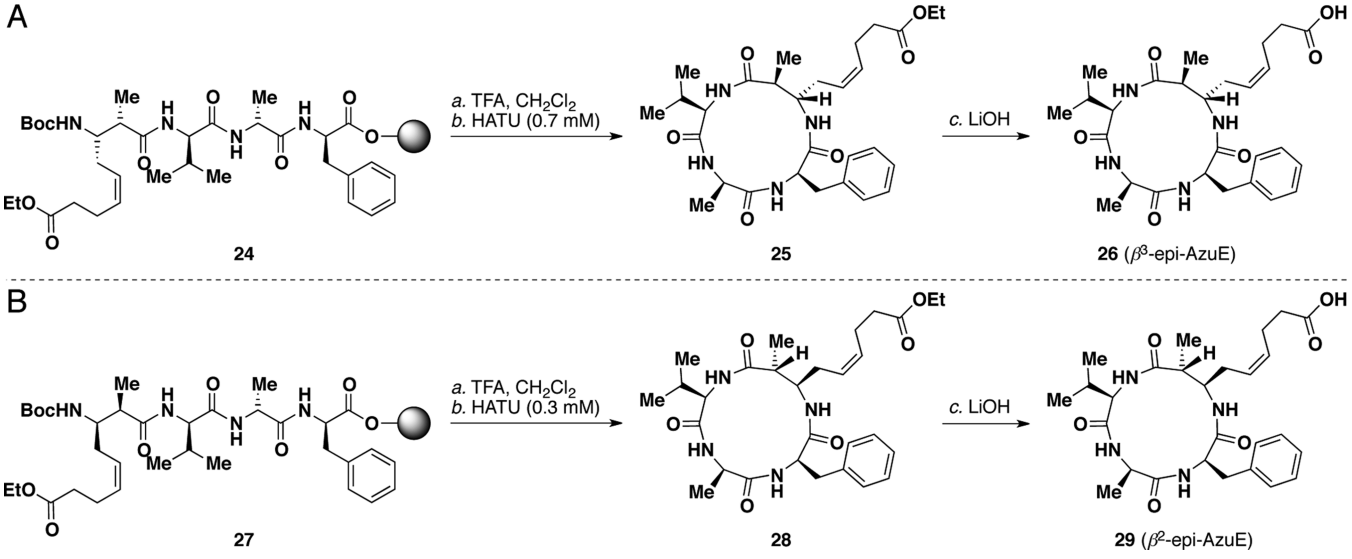

[a]Reagents and conditions: (a) TFA–CH_2Cl_2 (1:1), 2 × 30 min. (b) HATU, $^iPr_2NEt$ (8.0 equiv), DMF (0.3–0.7 mM peptide concn), 17–21 h. (c) LiOH, THF–H_2O (1:1).

(class IIb), HDACs 6 and 10 clearly interact very differently with these inhibitors.

Generally, we found the compounds with a carboxylic acid Zn^{2+}-binding group (**7** and **9**) to be more potent than the

dx.doi.org/10.1021/jm4008449 | J. Med. Chem. 2013, 56, 6512–6520

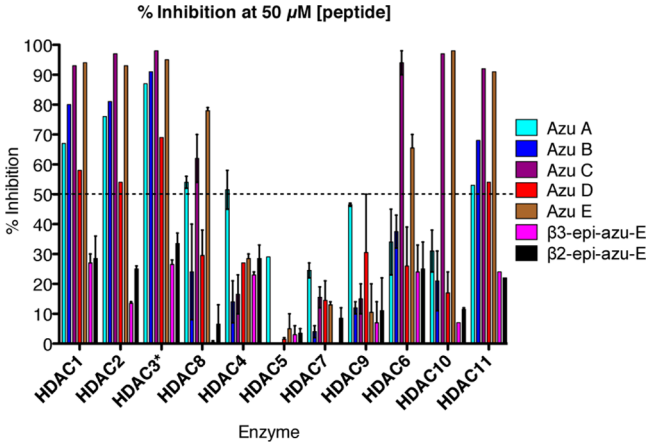

Figure 3. Single-dose HDAC inhibitory screening. Assays were performed at 50 μM (shown) and 5 μM (not shown) peptide concentrations. We chose <50% inhibition at 50 μM as our cutoff to sort away inactive compounds before performing full dose−response experiments. All compound−enzyme combinations that were discarded at this stage were tested in at least two individual assays performed in duplicate. Error bars represent the standard deviation. (*) Fusion protein of GST-tagged HDAC3 with the deacetylase activation domain (DAD) of nuclear receptor corepressor (NCoR1).

carboxamides (**5**, **6**, and **8**), which is in contrast to the originally reported HDAC inhibition data obtained for the natural products against an HDAC-containing cell extract.[5] However, the data presented herein agree with subsequent work from Ganesan and co-workers[15] on azumamide A (**5**) and azumamide E (**9**). We thus show that this applies to all the azumamides, which also confirms that a carboxylate Zn^{2+}-binding group renders HDAC inhibitors significantly more potent than a corresponding carboxamide, as would be expected from literature precendents.[19,26,27] Furthermore, compound **7** was more potent than **9** against HDACs 1−3, 6, 10, and 11, which is also in contrast to the original evaluation that found azuE (**9**) more potent than azuC (**7**) against crude enzymes from K562 cell extract.[5] The tyrosine-containing compound (**7**) exhibited ∼2-fold higher potency against HDACs 1, 3, 6, 10, and 11, whereas the phenylalanine-containing azumamide E (**9**) was only more potent against HDAC8, albeit at micromolar K_i values.

Finally, the inhibition of HDAC11 by azumamides C (**7**) and E (**9**) is, to the best of our knowledge, the first demonstration of potent cyclic peptide inhibitors of this isozyme.[33] Notably, these binding affinities were achieved without the presence of a strong Zn^{2+} chelator, such as hydroxamic acid.

CONCLUSIONS

In summary, we report total syntheses of all five azumamides, including for the first time azumamides B−D, which corroborate the originally proposed structures. Our synthetic route furthermore enabled preparation of site-specifically edited analogues for exploration of structure−activity relationships (SAR).[34−36] The HDAC profiling results show that the β-amino acid residue, present in all the azumamides, is sensitive to even slight modifications. In addition, the original HDAC testing using cell extract indicated that azumamide E was the most

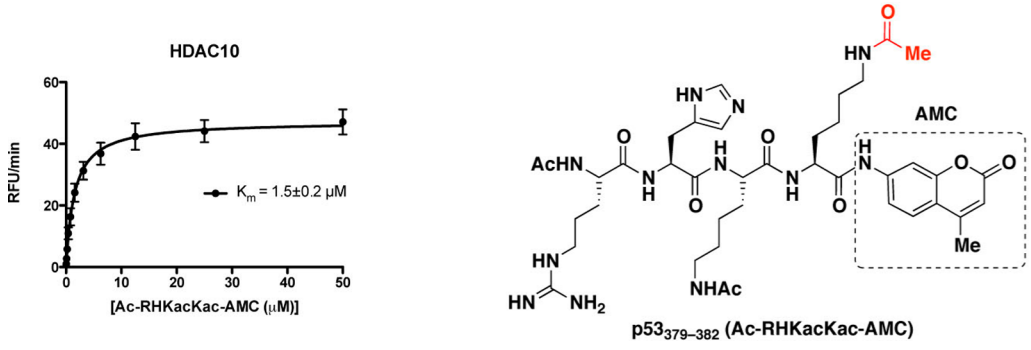

Figure 4. Michaelis−Menten plot for HDAC10.

Table 2. Potencies of Azumamides against Zn^{2+}-Dependent Histone Deacetylases[a]

	K_i values (nM)										
	class I				class IIa				class IIb		class IV
compd	HDAC1	HDAC2	HDAC3[b]	HDAC8	HDAC4	HDAC5	HDAC7	HDAC9	HDAC6	HDAC10	HDAC11
5 (azuA)	>5000	>5000	3200	>5000	52%[c]	IA[d]	IA	IA	IA	IA	>5000
6 (azuB)	5000	3000	3000	IA	IA	IA	IA	IA	IA	IA	>5000
7 (azuC)	32 ± 1	40 ± 20	14 ± 1	>5000	IA	IA	IA	IA	2000	10 ± 4	35 ± 3
8 (azuD)	>5000	>5000	3700	IA	IA	IA	IA	IA	IA	IA	>5000
9 (azuE)	67 ± 7	50 ± 30	25 ± 5	4400	IA	IA	IA	IA	>5000	20 ± 12	60 ± 16
26 (β^3-*epi*-azuE)	IA	IA	IA	IA	IA	IA	IA	IA	IA	IA	IA
29 (β^2-*epi*-azuE)	IA	IA	IA	IA	IA	IA	IA	IA	IA	IA	IA
1 (SAHA)	8 ± 1.5	7 ± 1.5	12 ± 4	700 ± 20	IA	IA	IA	IA	22 ± 9	NT[e]	13 ± 2
3 (FK-228)[f]	0.002	0.038	0.15	0.15	20.5	550	1250	1100	10	NT	NT

[a] IC_{50} values were determined from at least two individual dose−response experiments performed in duplicate (Figure S7 in Supporting Information), and K_i values were calculated from the Cheng−Prusoff equation. [b] Fusion protein of GST-tagged HDAC3 with deacetylase activation domain NCoR1. [c] Percent inhibition at 50 μM inhibitor concentration. [d] IA = inactive (<50% inhibition at 50 μM [inhibitor], Figure 3). [e] NT = not tested. [f] Data from Bradner et al.[18]

dx.doi.org/10.1021/jm4008449 | J. Med. Chem. 2013, 56, 6512−6520

potent of the series, but the comprehensive profiling presented herein shows that azumamide C is in fact ~2-fold more potent than azumamide E against the majority of the isozymes.

By taking advantage of the modular methodologies described in this article and building on the gained SAR information, we are currently investigating collections of azumamide analogues in search of more potent and selective ligands based on this promising scaffold.

EXPERIMENTAL SECTION

General. All chemicals and solvents were analytical-grade and were used without further purification. Vacuum liquid chromatography (VLC) was performed on silica gel 60 (particle size 0.015−0.040 μm). UPLC−MS analyses were performed on a Phenomenex Kinetex column (1.7 μm, 50 × 2.10 mm) by use of a Waters Acquity ultra-high-performance liquid chromatography system. A gradient with eluent I (0.1% HCOOH in water) and eluent II (0.1% HCOOH in acetonitrile) rising linearly from 0% to 95% II during t = 0.00−2.50 min was applied at a flow rate of 1 mL/min (gradient A) or during t = 0.00−5.20 min (gradient B). Analytical HPLC was performed on a Phenomenex Luna column [150 mm × 4.6 mm, C_{18} (3 μm)] by use of an Agilent 1100 LC system equipped with a UV detector. Gradient C, with eluent III (0.1% TFA in water) and eluent IV (0.1% TFA in acetonitrile) rising linearly from 0% to 95% IV during t = 2−20 min, was applied at a flow rate of 1 mL/min. Preparative reversed-phase HPLC was performed on a Phenomenex Luna column [250 mm × 20 mm, C_{18} (5 μm, 100 Å)] by use of an Agilent 1260 LC system equipped with a diode-array UV detector and an evaporative light scattering detector (ELSD). A gradient, with eluent V (95:5:0.1, water−MeCN−TFA) and eluent VI (0.1% TFA in acetonitrile) rising linearly from 0% to 95% IV during t = 5−45 min, was applied at a flow rate of 20 mL/min. All tested compounds were purified to homogeneity and shown by both analytical HPLC (gradient C) and LC−MS (gradient A) to be of more than 95% purity. One- and two-dimensional NMR spectra were recorded on a Varian Mercury 300 instrument or a Varian INOVA 500 MHz instrument. All spectra were recorded at 298 K. Correlation spectroscopy (COSY) spectra were recorded with a relaxation delay of 1.5 s before each scan, a spectral width of 6k × 6k, and eight FIDs and 1k × 512 data points collected. Heteronuclear single quantum coherence (HSQC) spectra were recorded with a relaxation delay of 1.5 s before each scan, a spectral width of 6k × 25k, and 16 FIDs and 1k × 128 data points collected. Heteronuclear two-bond correlation (H2BC) spectra were recorded with a relaxation delay of 1.5 s before each scan, a spectral width of 4k × 35k, and 16 FIDs at 295 K and 1k × 256 data points collected. Heteronuclear multiple-bond correlation (HMBC) spectra were recorded with a relaxation delay of 1.5 s before each scan, a spectral width of 6k × 35k, and 32 FIDs and 1k × 256 data points collected. Chemical shifts are reported in parts per million (ppm) relative to deuterated solvent peaks as internal standards (δH, DMSO-d_6 2.50 ppm; δC, DMSO-d_6 39.52 ppm, δH, CD_3OH 3.30 ppm; δH, $CDCl_3$ 7.26 ppm; δC, $CDCl_3$ 77.16 ppm). Coupling constants (J) are given in hertz (Hz). Multiplicities of ^{1}H NMR signals are reported as follows: s, singlet; d, doublet; t, triplet; q, quartet; m, multiplet.

General Procedure for Mannich Reactions. A solution of LDA (2.1 equiv) was added dropwise to a solution of the ester (2.0 equiv) in dry THF at −78 °C. After the mixture was stirred for 30 min, $Ti(O\text{-}iPr)_3Cl$ (4.2 equiv) in dry THF was added dropwise. The orange solution was stirred for 30 min and the imine (1.0 equiv) in dry THF was added dropwise. The mixture was stirred for 3 h or until thin-layer chromatography (TLC) showed full conversion of the imine. The mixture was quenched with saturated aqueous NH_4Cl and allowed to reach room temperature. Water was added and the mixture was decanted into a separatory funnel. EtOAc−water (1:1) was added to the remaining Ti precipitate, and the mixture was stirred vigorously for 5 min before being added to the separatory funnel. The aqueous phase was extracted with EtOAc and the combined organic phases were washed again with water, dried ($MgSO_4$), filtered, and concentrated in vacuo.

Azumamide A, (*Z*)-6-[(2*R*,5*R*,8*R*,11*R*,12*S*)-8-Benzyl-2-isopropyl-5,12-dimethyl-3,6,9,13-tetraoxo-1,4,7,10-tetraazacyclotridecan-11-yl]hex-4-enamide (5). LiOH (89 mg, 3.72 mmol, 85 equiv) in water (4.0 mL) was added to a stirred solution of the impure cyclic peptide **20** (24.2 mg, approximately 0.045 mmol) in THF (4 mL). After 2.5 h of stirring, the organic solvent was removed in vacuo. The aqueous phase was acidified with 1 M HCl to pH 2 and extracted with EtOAc (4 × 30 mL) and CH_2Cl_2 (40 mL). The organic phases were dried (Na_2SO_4), filtered, and concentrated to afford crude azumamide E, which was used without further purification. Analytical UPLC−MS gradient A, t_R = 1.47 min. To a solution of the above crude azumamide E (≈0.045 mmol) in DMF (3.0 mL) were added HATU (34 mg, 0.09 mmol, 2 equiv), iPr_2NEt (43 μL, 0.25 mmol, 5.5 equiv), and, after 5 min, NH_3−dioxane (0.9 mL, 0.45 mmol, 10 equiv). After 1 h, NH_3−dioxane (0.45 mL, 0.23 mmol, 5 equiv) was added. UPLC−MS analysis showed 50% conversion after 3 h, and HATU (34 mg, 0.09 mmol, 2 equiv) and NH_3−dioxane (0.45 mL, 0.23 mmol, 5 equiv) were added. After an additional 1 h, DMF (1.0 mL) followed by HATU (17 mg, 0.045 mmol, 1 equiv) and NH_3−dioxane (0.45 mL, 0.23 mmol, 5 equiv) were added, and stirring was continued for 1 h before concentration in vacuo. The residue was dissolved in MeCN−H_2O and purified by preperative HPLC to give azumamide A (**5**) (4.8 mg, 12% overall). $[\alpha]_D$ +56° (c = 0.2, MeOH); previously reported[11] $[\alpha]_D$ +33° (c = 0.1, MeOH). ^{1}H NMR (500 MHz, CD_3OH) δ 8.18 (d, J = 8.6 Hz, 1H), 8.16 (d, J = 9.0 Hz, 1H), 7.72 (d, J = 8.2 Hz, 1H), 7.59 (m, 2H), 7.20 (m, 5H), 6.74 (br s, 1H), 5.48 (m, 1H), 5.37 (m, 1H), 4.33 (dt, J = 9.0, 7.0 Hz, 1H), 4.24 (m, 2H), 3.81 (dd, J = 10.4 Hz and 8.4 Hz, 1H), 3.10 (m, 2H), 2.72 (m, 1H), 2.57 (dt, J = 14.1, 6.9 Hz, 1H), 2.41 (m, 2H), 2.27 (m, 4H), 1.30 (d, J = 7.5 Hz, 3H), 1.23 (d, J = 7.3 Hz, 3H), 0.96 (d, J = 6.5 Hz, 3H), 0.94 (d, J = 6.7 Hz, 3H). HRMS (ESI-TOF) m/z calcd for $C_{27}H_{38}N_4O_7H^+$ 514.3029; found 514.3032 $[M + H]^+$. HPLC gradient C, t_R = 11.62 min (>95%).

Azumamide B, (*Z*)-6-[(2*R*,5*R*,8*R*,11*R*,12*S*)-8-(4-Hydroxybenzyl)-2-isopropyl-5,12-dimethyl-3,6,9,13-tetraoxo-1,4,7,10-tetraazacyclotridecan-11-yl]hex-4-enamide (6). An aqueous solution of LiOH (0.5 M, 55 μL, 2.0 mmol, 2.5 equiv) was added to the cyclic peptide **18** (6.1 mg) in THF−H_2O (1:1, 2 mL) at 0 °C. After 30 min the ice bath was removed. Additional portions of LiOH solution (55 μL, 2.0 mmol, 2.5 equiv) were added after 2, 4, and 6 h, and stirring was continued for an additional 19 h to ensure full conversion. Then water (0.5 mL) was added and the organic solvent was removed in vacuo. The aqueous phase was acidified with 1 M HCl and extracted with EtOAc (5 × 20 mL). The organic phase was dried (Na_2SO_4), filtered, and concentrated in vacuo to afford the crude azumamide C, which was used without further purification. To a solution of crude azumamide C (5.8 mg, 10.9 μmol) in DMF (2 mL) were added HOBt (4.4 mg, 33 μmol, 3 equiv), DIC (5.1 μL, 34 μmol, 3 equiv), and iPr_2NEt (7.6 μL, 44 μmol, 4 equiv). After 10 min, NH_3−dioxane (0.5 M, 0.11 mL, 55 μmol, 5 equiv) was added. After 1.5 h, DIC (5 μL, 34 μmol, 3 equiv) was added, followed by NH_3−dioxane (0.5 M, 0.11 mL, 55 μmol, 5 equiv). After the mixture was stirred for 16 h, additional DIC (2 equiv) and NH_3−dioxane (5 equiv) were added, and this procedure was repeated once more after 18 h. Finally, CH_2Cl_2 (1 mL) was added, followed by DIC (3 equiv) and NH_3−dioxane (10 equiv), and after 2 days of stirring at room temperature, the reaction mixture was concentrated, dissolved in MeCN−H_2O (2:1), and purified by preparative HPLC to give azumamide B (**6**) (3.6 mg, 62%, two steps) as a white solid. $[\alpha]_D$ +65° (c = 0.15, MeOH); previously reported[11] $[\alpha]_D$ +45° (c = 0.1, MeOH). ^{1}H NMR (500 MHz, CD_3OH) δ 8.13 (d, J = 7.9 Hz, 1H), 8.00 (d, J = 8.9 Hz, 1H), 7.85 (d, J = 7.2 Hz, 1H), 7.61 (d, J = 8.2 Hz, 1H), 7.01 (d, J = 8.4 Hz, 3H), 6.67 (d, J = 8.4 Hz, 3H), 5.49 (m, 1H), 5.37 (dd, J = 18.0 and 7.3 Hz, 2H), 4.29 (pentet, J = 7.2 Hz, 1H), 4.15 (m, 1H), 4.05 (m, 1H), 3.60 (m, 1H), 3.13 (dd, J = 13.7, 10.1 Hz, 1H), 3.00 (dd, J = 13.8, 6.3 Hz, 1H), 2.70 (m, 2H), 2.36 (ddd, J = 22.3, 21.5, 7.1 Hz, 11H), 1.29 (d, J = 7.2 Hz, 3H), 1.27 (d, J = 7.4 Hz, 3H), 0.95 (d, J = 5.7 Hz, 3H), 0.93 (d, J = 6.0 Hz, 3H). HRMS (ESI-TOF) m/z calcd for $C_{27}H_{39}N_5O_6H^+$ 530.2978; found 530.2973 $[M + H]^+$. HPLC gradient C, t_R = 10.31 min (>95%).

dx.doi.org/10.1021/jm4008449 | J. Med. Chem. 2013, 56, 6512−6520

Azumamide C, (*Z*)-6-[(2*R*,5*R*,8*R*,11*R*,12*S*)-8-(4-Hydroxybenzyl)-2-isopropyl-5,12-dimethyl-3,6,9,13-tetraoxo-1,4,7,10-tetraazacyclotridecan-11-yl]hex-4-enoic Acid (7). LiOH (49 mg, 2.0 mmol, 35 equiv) in water (5.0 mL) was added to the crude cyclic peptide **18** (61 mg) in THF (5.0 mL). The solution was stirred for 16 h and concentrated in vacuo. The resulting residue was dissolved in THF−H_2O (1:1, 10 mL) by adding a few drops of TFA, and then purification by preparative HPLC afforded azumamide C (**7**) (2.2 mg, 9% overall) as a white solid. $[\alpha]_D$ +49° (*c* = 0.14, MeOH); previously reported[11] $[\alpha]_D$ +21° (*c* = 0.1, MeOH). ^{1}H NMR (500 MHz, CD_3OH) δ 8.08 (d, *J* = 7.7 Hz, 1H), 7.99 (d, *J* = 8.4 Hz, 1H), 7.84 (s, 1H), 7.62 (d, *J* = 8.1 Hz, 1H), 7.01 (d, *J* = 8.4 Hz, 2H), 6.67 (d, *J* = 8.4 Hz, 2H), 5.48 (t, *J* = 8.8 Hz, 1H), 5.38 (dt, *J* = 10.7, 7.0 Hz, 1H), 4.29 (pentet, *J* = 7.3 Hz 1H), 4.16 (m, 1H), 4.01 (m, 1H), 3.58 (m, 1H), 3.15 (dd, *J* = 13.7, 10.2 Hz 1H), 3.00 (dd, *J* = 13.7, 6.0 Hz, 1H), 2.72 (m, 1H), 2.67 (m, 1H) 2.39 (m, 5H), 1.29 (d, *J* = 7.2 Hz, 3H), 1.27 (d, *J* = 7.3 Hz, 3H), 0.95 (d, *J* = 6.0 Hz, 3H), 0.93 (d, *J* = 6.0 Hz, 3H). HRMS (ESI-TOF) *m*/*z* calcd for $C_{27}H_{38}N_4O_7H^+$ 531.2819; found 531.2815 $[M + H]^+$. HPLC gradient C, t_R = 11.04 min (>95%).

Azumamide D, (*Z*)-6-[(2*R*,5*R*,8*R*,11*R*,12*S*)-8-Benzyl-2,5,12-trimethyl-3,6,9,13-tetraoxo-1,4,7,10-tetraazacyclotridecan-11-yl]hex-4-enamide (8). LiOH (53 mg, 2.21 mmol) in water (5.0 mL) was added to a stirred solution of the impure cyclic peptide **22** (22.7 mg, approximately 0.044 mmol) in THF (3 mL). After 4 h the organic solvent was removed in vacuo and the water (0.5 mL) was added to the aqueous phase, which was then acidified with 1 M HCl (2 mL) and extracted with EtOAc (4 × 20 mL). The organic phases were dried ($MgSO_4$), filtered, and concentrated to give the crude acid **23**, which was used without further purification. To a solution of the crude acid **23** (≈23 μmol) in CH_2Cl_2−DMF (8:1, 2.3 mL) were added HOBt (10 mg, 66 μmol, 3.0 equiv), DIC (10 μL, 66 μmol, 3 equiv), and iPr$_2$NEt (15 μL, 88 μmol, 4 equiv). After 5 min, NH_3−dioxane (0.5 M, 0.22 mL, 110 μmol, 5 equiv) was added. After 1 h, NH_3−dioxane (0.5 M, 0.22 mL, 110 μmol, 5 equiv) was added. After the mixture was stirred for 18 h, additional DMF (0.5 mL) was added, followed by NH_3−MeOH (2.0 M, 0.11 mL, 230 μmol, 10 equiv). After an additional 5 h, DIC (7 μL, 46 μmol, 2 equiv) was added. The next day NH_3−MeOH (2.0 M, 0.06 mL, 111 μmol, 5 equiv) was added and the mixture was stirred for 10 days. Finally, DIC (3.4 μL, 23 μmol, 1 equiv) was added, followed by NH_3−MeOH (2.0 M, 0.055 mL, 210 μmol, 5 equiv), and after 2 days the mixture was concentrated, dissolved in MeCN−H_2O (2:1), and purified by preparative HPLC to afford azumamide D (**8**) (1.2 mg, 4% overall) as a white solid. $[\alpha]_D$ +32° (*c* = 0.08, MeOH); previously reported[11] $[\alpha]_D$ +25° (*c* = 0.1, MeOH). ^{1}H NMR (500 MHz, CD_3OH) δ 8.03 (d, *J* = 7.8 Hz, 1H), 8.01 (d, *J* = 8.8 Hz, 1H) 7.94 (d, *J* = 6.8 Hz, 1H), 7.58 (s, 1H), 7.32 (d, *J* = 7.5 Hz, 1H), 7.25−7.14 (m, 5H), 6.75 (s, 1H), 5.47 (m, 1H), 5.39 (m, 1H), 4.35 (m, 1H), 4.19 (m, 1H) 4.17− 4.11 (m, 2H), 3.09 (m, 2H), 2.69 (m, 1H), 2.62 (m, 1H), 2.41 (m, 2H), 2.28 (m, 1H), 1.47 (d, *J* = 7.4 Hz, 3H), 1.28 (d, *J* = 7.4 Hz, 3H), 1.22 (d, *J* = 7.3 Hz, 3H). HRMS (ESI-TOF) *m*/*z* calcd for $C_{25}H_{35}N_5O_5H^+$ 486.2716; found 486.2710 $[M + H]^+$. HPLC gradient C, t_R = 10.55 min (>95%).

Azumamide E, (*Z*)-6-[(2*R*,5*R*,8*R*,11*R*,12*S*)-8-Benzyl-2-isopropyl-5,12-dimethyl-3,6,9,13-tetraoxo-1,4,7,10-tetraazacyclotridecan-11-yl]hex-4-enoic Acid (9). LiOH (18.5 mg, 0.77 mmol, 40 equiv) in water (4 mL) was added to a stirred solution of the impure cyclic peptide **20** (10.5 mg, approximately 0.02 mmol) in THF (4 mL). After 1 h, LiOH (10 mg, 0.42 mmol, 20 equiv) in water (1 mL) was added, and after 2 h, LiOH (5.0 mg, 0.21 mmol, 1 equiv) in water (0.5 mL) was added. The solution was stirred for 16 h and another portion of LiOH (6.0 mg, 0.25 mmol, 1.3 equiv) in water (0.5 mL) was added. After an additional 2.5 h of stirring, the organic solvent was removed in vacuo. The aqueous phase was acidified with 1 M HCl and extracted with EtOAc (4 × 25 mL). The combined organic phases were dried (Na_2SO_4), filtered, and concentrated. The resulting residue was dissolved in MeCN−water [(3:2), 2.5 mL] and purified by preparative HPLC to afford azumamide E (**9**) (4.3 mg, 15% overall) as a white solid. $[\alpha]_D$ +66° (*c* = 0.2, MeOH); previously reported[11] $[\alpha]_D$ +53° (*c* = 0.1, MeOH). ^{1}H NMR (500 MHz, CD_3OH) δ 8.10 (d, *J* = 7.7 Hz, 1H), 7.95 (d, *J* = 8.8 Hz, 1H), 7.84 (br s, 1H), 7.63 (d, *J* = 8.4 Hz, 1H), 7.28−7.16 (m, 5H), 5.48 (m, 1H), 5.37 (m, 1H), 4.28 (pentet, *J* = 7.5 Hz, 1H), 4.16 (m, 1H), 4.08 (m, 1H), 3.59 (m, 1H), 3.25 (dd, *J* = 13.6, 10.4 Hz, 1H), 3.11 (dd, *J* = 13.6, 6.1 Hz, 1H), 2.72 (m, 1H), 2.68 (m, 1H), 2.39 (d, *J* = 1.7 Hz, 6H), 2.39 (m, 6H), 1.28 (d, *J* = 7.1 Hz, 3H), 1.27 (d, *J* = 7.4 Hz, 3H), 0.94 (m, 6H). HRMS (ESI-TOF) *m*/*z* calcd for $C_{27}H_{38}N_4O_6H^+$ 515.2869; found 515.2869 $[M + H]^+$. HPLC gradient C, t_R = 12.53 min (>95%).

Assay Materials. HDAC1 (purity >45% by SDS−PAGE according to the supplier), HDAC4 (purity >90% by SDS−PAGE according to the supplier), and HDAC7 (purity >90% by SDS−PAGE according to the supplier) were purchased from Millipore (Temecula, CA). HDAC2 used for dose−response experiments (full length, purity ≥94% by SDS−PAGE according to the supplier), HDAC5 (full length, purity ≥4% by SDS−PAGE according to the supplier), and HDAC8 used for dose−response experiments (purity ≥90% by SDS−PAGE according to the supplier) were purchased from BPS Bioscience (San Diego, CA). HDAC2 used for initial screening experiments (full length, purity 50% by SDS−PAGE according to the supplier), HDAC3−"NCoR1" complex [(purity 90% by SDS−PAGE according to supplier; fusion protein of GST-tagged HDAC3 with the deacetylase activation domain (DAD) of NCoR1 (nuclear receptor corepressor)], HDAC6 (purity >90% by SDS−PAGE according to the supplier), HDAC8 for initial screening experiments (purity >50% by SDS−PAGE according to the supplier), HDAC10 (purity >50% by SDS−PAGE according to the supplier), and HDAC11 (purity >50% by SDS−PAGE according to the supplier) were purchased from Enzo Life Sciences (Postfach, Switzerland). HDAC9 (full length, purity 12% by SDS−PAGE according to the supplier) was purchased from Abnova (Taipei, Taiwan). The HDAC assay buffer consisted of 50 mM Tris-HCl, pH 8.0, 137 mM NaCl, 2.7 mM KCl, 1 mM $MgCl_2$, and bovine serum albumin (0.5 mg/mL). Trypsin [10 000 units/mg;, from bovine pancreas, treated with L-(tosylamido-2-phenyl)ethyl chloromethyl ketone (TPCK)] was from Sigma Aldrich (Steinheim, Germany). All peptides were purified to homogeneity (>95% purity by $HPLC_{230nm}$ via reversed-phase preparative HPLC), and the white fluffy materials obtained by lyophilization were kept at −20 °C. For assaying, peptides were reconstituted in DMSO to give 5−10 mM stock solutions, the accurate concentrations of which were determined by coinjection on HPLC with a standard of known concentration.

In Vitro Histone Deacetylase Inhibition Assays. For inhibition of recombinant human HDACs, dose−response experiments with internal controls were performed in black low-binding Nunc 96-well microtiter plates. Dilution series (3-fold dilution, 10 concentrations) were prepared in HDAC assay buffer from 5−10 mM DMSO stock solutions. The appropriate dilution of inhibitor (10 μL of 5× the desired final concentration) was added to each well followed by HDAC assay buffer (25 μL) containing substrate [Ac-Leu-Gly-Lys(Ac)-AMC, 40 μM for HDAC1−3 and 80 μM for HDAC6 and 11; Ac-Leu-Gly-Lys(Tfa)-AMC, 40 μM for HDAC4, 240 μM for HDAC5, 80 μM for HDAC7, 400 μM for HDAC8, and 160 μM for HDAC9; Ac-Arg-His-Lys(Ac)-Lys(Ac)-AMC, 100 μM for HDAC10]. Finally, a solution of the appropriate HDAC (15 μL) was added and the plate was incubated at 37 °C for 30 min [HDAC1, 150 ng/well; HDAC2, 100 ng/well; HDAC3, 10 ng/well; HDAC4, 2 ng/well; HDAC5, 40 ng/well; HDAC6, 60 ng/well; HDAC7, 2 ng/well; HDAC8, 5 ng/well; HDAC9, 40 ng/well; HDAC10, 500 ng/well; HDAC11, 500 ng/well]. Then trypsin (50 μL, 0.4 mg/mL) was added and the assay development was allowed to proceed for 15−30 min at room temperature, before the plate was read on a Perkin-Elmer Enspire plate reader with excitation at 360 nm and detecting emission at 460 nm. Each assay was performed in duplicate. The data were analyzed by nonlinear regression with GraphPad Prism to afford IC_{50} values from the dose−response experiments, and K_i values were determined from the Cheng−Prusoff equation [$K_i = IC_{50}/(1 + [S]/K_m)$] with the assumption of a standard fast-on−fast-off mechanism of inhibition.

■ ASSOCIATED CONTENT

Supporting Information

Two tables showing cyclization experiments performed on a simplified model peptide and IC_{50} values from dose−response experiments; seven figures showing comparison of ^{1}H and ^{13}C chemical shifts for **S18** with previously reported values, ^{1}H NMR data comparisons for azumamides A−E, and dose−response curves for determination of IC_{50} values for "active" inhibitors; two schemes illustrating synthesis of β^3-epi building block (**S6**) and β^2-epi building block (**S11**); additional text with full experimental details and compound characterization data; and ^{1}H and ^{13}C NMR spectra. A CIF file for the X-ray crystal structures is available (CCDC 933151).This material is available free of charge via the Internet at http://pubs.acs.org.

■ AUTHOR INFORMATION

Corresponding Author

*E-mail cao@kemi.dtu.dk; phone +45-45252105.

Notes

The authors declare no competing financial interest.

■ ACKNOWLEDGMENTS

This work was supported by the Lundbeck Foundation (Young Group Leader Fellowship, C.A.O.), the Danish Independent Research Council−Natural Sciences (Steno Grant 10-080907, C.A.O.), and the Carlsberg Foundation. Novo Nordisk A/S is thanked for a generous donation of peptide coupling reagents used in this work. We thank Ms. Anne Hector and Dr. Charlotte H. Gotfredsen for assistance with NMR spectroscopy and Ms. Tina Gustafsson for technical assistance with UPLC−MS and HRMS. Dr. A. S. Madsen is gratefully acknowledged for assistance with the biochemical assays.

■ ABBREVIATIONS USED

AMC, 7-amino-4-methylcoumarin; Boc, *tert*-butoxycarbonyl; DAD, deacetylase activation domain; DIC, *N*,*N*′-diisopropylcarbodiimide; DMF, *N*,*N*-dimethylformamide; DMSO, dimethyl sulfoxide; ESI, electrospray ionization; FID, free induction decay; Fmoc, fluorenylmethyloxycarbonyl; H3, histone 3 protein; H4, histone 4 protein; HATU, *O*-(7-azabenzotriazol-1-yl)-*N*,*N*,*N*′,*N*′-tetramethyluronium hexafluorophosphate; HDAC, histone deacetylase; HMPA, hexamethylphosphoramide; HOBt, hydroxybenzotriazole; HPLC, high-performance liquid chromatography; KHMDS, potassium hexamethyldisilazide; LDA, lithium diisopropylamide; MS, mass spectrometry; NCoR, nuclear receptor corepressor; NMR, nuclear magnetic resonance; PMB, *p*-methoxybenzyl; rt, room temperature; SDS−PAGE, sodium dodecyl sulfate−polyacrylamide gel electrophoresis; TFA, trifluoroacetic acid; THF, tetrahydrofuran; TOF, time-of-flight; t_R, retention time; UPLC, ultra-high-performance liquid chromatography

■ REFERENCES

(1) Marks, P. A.; Breslow, R. Dimethyl sulfoxide to vorinostat: development of this histone deacetylase inhibitor as an anticancer drug. *Nat. Biotechnol.* **2007**, *25*, 84−90.

(2) Furumai, R.; Matsuyama, A.; Kobashi, N.; Lee, K. H.; Nishiyama, M.; Nakajima, H.; Tanaka, A.; Komatsu, Y.; Nishino, N.; Yoshida, M.; Horinouchi, S. FK228 (depsipeptide) as a natural prodrug that inhibits class I histone deacetylases. *Cancer Res.* **2002**, *62*, 4916−4921.

(3) Kijima, M.; Yoshida, M.; Sugita, K.; Horinouchi, S.; Beppu, T. Trapoxin, an antitumor cyclic tetrapeptide, is an irreversible inhibitor of mammalian histone deacetylase. *J. Biol. Chem.* **1993**, *268*, 22429−22435.

(4) Taunton, J.; Hassig, C. A.; Schreiber, S. L. A mammalian histone deacetylase related to the yeast transcriptional regulator Rpd3p. *Science* **1996**, *272*, 408−411.

(5) Taunton, J.; Collins, J. L.; Schreiber, S. L. Synthesis of natural and modified trapoxins, useful reagents for exploring histone deacetylase function. *J. Am. Chem. Soc.* **1996**, *118*, 10412−10422.

(6) Beumer, J. H.; Tawbi, H. Role of histone deacetylases and their inhibitors in cancer biology and treatment. *Curr. Clin. Pharmacol.* **2010**, *5*, 196−208.

(7) Haberland, M.; Montgomery, R. L.; Olson, E. N. The many roles of histone deacetylases in development and physiology: implications for disease and therapy. *Nat. Rev. Genet.* **2009**, *10*, 32−42.

(8) Kazantsev, A. G.; Thompson, L. M. Therapeutic application of histone deacetylase inhibitors for central nervous system disorders. *Nat. Rev. Drug Discovery* **2008**, *7*, 854−868.

(9) Minucci, S.; Pelicci, P. G. Histone deacetylase inhibitors and the promise of epigenetic (and more) treatments for cancer. *Nat. Rev. Cancer* **2006**, *6*, 38−51.

(10) Darkin-Rattray, S. J.; Gurnett, A. M.; Myers, R. W.; Dulski, P. M.; Crumley, T. M.; Allocco, J. J.; Cannova, C.; Meinke, P. T.; Colletti, S. L.; Bednarek, M. A.; Singh, S. B.; Goetz, M. A.; Dombrowski, A. W.; Polishook, J. D.; Schmatz, D. M. Apicidin: a novel antiprotozoal agent that inhibits parasite histone deacetylase. *Proc. Natl. Acad. Sci. U.S.A.* **1996**, *93*, 13143−13147.

(11) Nakao, Y.; Yoshida, S.; Matsunaga, S.; Shindoh, N.; Terada, Y.; Nagai, K.; Yamashita, J. K.; Ganesan, A.; van Soest, R. W.; Fusetani, N. Azumamides A-E: histone deacetylase inhibitory cyclic tetrapeptides from the marine sponge *Mycale izuensis*. *Angew. Chem., Int. Ed.* **2006**, *45*, 7553−7557.

(12) Maulucci, N.; Chini, M. G.; Micco, S. D.; Izzo, I.; Cafaro, E.; Russo, A.; Gallinari, P.; Paolini, C.; Nardi, M. C.; Casapullo, A.; Riccio, R.; Bifulco, G.; De Riccardis, F. Molecular insights into azumamide E histone deacetylases inhibitory activity. *J. Am. Chem. Soc.* **2007**, *129*, 3007−3012.

(13) Wang, D.; Helquist, P.; Wiest, O. Zinc binding in HDAC inhibitors: a DFT study. *J. Org. Chem.* **2007**, *72*, 5446−5449.

(14) Izzo, I.; Maulucci, N.; Bifulco, G.; De Riccardis, F. Total synthesis of azumamides A and E. *Angew. Chem., Int. Ed.* **2006**, *45*, 7557−7560.

(15) Wen, S.; Carey, K. L.; Nakao, Y.; Fusetani, N.; Packham, G.; Ganesan, A. Total synthesis of azumamide A and azumamide E, evaluation as histone deacetylase inhibitors, and design of a more potent analogue. *Org. Lett.* **2007**, *9*, 1105−1108.

(16) Chandrasekhar, S.; Rao, C. L.; Seenaiah, M.; Naresh, P.; Jagadeesh, B.; Manjeera, D.; Sarkar, A.; Bhadra, M. P. Total synthesis of azumamide E and sugar amino acid-containing analogue. *J. Org. Chem.* **2009**, *74*, 401−404.

(17) Lahm, A.; Paolini, C.; Pallaoro, M.; Nardi, M. C.; Jones, P.; Neddermann, P.; Sambucini, S.; Bottomley, M. J.; Lo Surdo, P.; Carfi, A.; Koch, U.; De Francesco, R.; Steinkuhler, C.; Gallinari, P. Unraveling the hidden catalytic activity of vertebrate class IIa histone deacetylases. *Proc. Natl. Acad. Sci. U.S.A.* **2007**, *104*, 17335−17340.

(18) Bradner, J. E.; West, N.; Grachan, M. L.; Greenberg, E. F.; Haggarty, S. J.; Warnow, T.; Mazitschek, R. Chemical phylogenetics of histone deacetylases. *Nat. Chem. Biol.* **2010**, *6*, 238−243.

(19) White, C. J.; Yudin, A. K. Contemporary strategies for peptide macrocyclization. *Nat. Chem.* **2011**, *3*, 509−524.

(20) Tang, T. P.; Ellman, J. A. Asymmetric synthesis of β-amino acid derivatives incorporating a broad range of substitution patterns by enolate additions to *tert*-butanesulfinyl imines. *J. Org. Chem.* **2002**, *67*, 7819−7832.

(21) Robak, M. T.; Herbage, M. A.; Ellman, J. A. Synthesis and applications of *tert*-butanesulfinamide. *Chem. Rev.* **2010**, *110*, 3600−3740.

(22) Zimmerman, H. E.; Traxler, M. D. The stereochemistry of the Ivanov and Reformatsky reactions. 1. *J. Am. Chem. Soc.* **1957**, *79*, 1920−1923.

(23) Cutter, A. C.; Miller, I. R.; Keily, J. F.; Bellingham, R. K.; Light, M. E.; Brown, R. C. D. Total syntheses of (−)-epilupinine and (−)-tashiromine using imino-aldol reactions. *Org. Lett.* **2011**, *13*, 3988−3991.
(24) Ireland, R. E.; Mueller, R. H.; Willard, A. K. Ester enolate Claisen rearrangement: Stereochemical control through stereoselective enolate formation. *J. Am. Chem. Soc.* **1976**, *98*, 2868−2877.
(25) Oare, D. A.; Heathcock, C. H. Acyclic stereoselection. 47. Stereochemistry of the Michael addition of ester and ketone enolates to α,β-unsaturated ketones. *J. Org. Chem.* **1990**, *55*, 157−172.
(26) Montero, A.; Beierle, J. M.; Olsen, C. A.; Ghadiri, M. R. Design, synthesis, biological evaluation, and structural characterization of potent histone deacetylase inhibitors based on cyclic α/β-tetrapeptide architectures. *J. Am. Chem. Soc.* **2009**, *131*, 3033−3041.
(27) Olsen, C. A.; Ghadiri, M. R. Discovery of potent and selective histone deacetylase inhibitors via focused combinatorial libraries of cyclic $\alpha3\beta$-tetrapeptides. *J. Med. Chem.* **2009**, *52*, 7836−7846.
(28) Vickers, C. J.; Olsen, C. A.; Leman, L. J.; Ghadiri, M. R. Discovery of HDAC inhibitors that lack an active site Zn^{2+}-binding functional group. *ACS Med. Chem. Lett.* **2012**, *3*, 505−508.
(29) Olsen, C. A.; Montero, A.; Leman, L. J.; Ghadiri, M. R. Macrocyclic peptoid-peptide hybrids as inhibitors of class I histone deacetylases. *ACS Med. Chem. Lett.* **2012**, *3*, 749−753.
(30) Madsen, A. S.; Olsen, C. A. Substrates for efficient fluorometric screening employing the NAD-dependent sirtuin 5 lysine deacylase (KDAC) enzyme. *J. Med. Chem.* **2012**, *55*, 5582−5590.
(31) Madsen, A. S.; Olsen, C. A. Profiling of substrates for zinc-dependent lysine deacylase enzymes: HDAC3 exhibits decrotonylase activity in vitro. *Angew. Chem., Int. Ed.* **2012**, *51*, 9083−9087.
(32) Inks, E. S.; Josey, B. J.; Jesinkey, S. R.; Chou, C. J. A novel class of small molecule inhibitors of HDAC6. *ACS Chem. Biol.* **2012**, *7*, 331−337.
(33) Auzzas, L.; Larsson, A.; Matera, R.; Baraldi, A.; Deschenes-Simard, B.; Gianni, G.; Cabri, W.; Bayyistuzzi, G.; Gallo, G.; Ciacci, A.; Vesci, L.; Pisano, C.; Hanessian, S. *J. Med. Chem.* **2010**, *53*, 8387−8399.
(34) Szpilman, A. M.; Carreira, E. M. Probing the biology of natural products: Molecular editing by diverted total synthesis. *Angew. Chem., Int. Ed.* **2010**, *49*, 9592−9628.
(35) Wender, P. A.; Buschmann, N.; Cardin, N. B.; Jones, L. R.; Kan, C.; Kee, J. M.; Kowalski, J. A.; Longcore, K. E. Gateway synthesis of daphnane congeners and their protein kinase C affinities and cell-growth activities. *Nat. Chem.* **2011**, *3*, 615−619.
(36) Wilson, R. M.; Danishefsky, S. J. On the reach of chemical synthesis: creation of a mini-pipeline from an academic laboratory. *Angew. Chem., Int. Ed.* **2010**, *49*, 6032−6056.

Chemical Science

Dynamic Article Links ►

Cite this: DOI: 10.1039/c0xx00000x

www.rsc.org/xxxxxx

EDGE ARTICLE

Structural editing of the azumamide scaffold: Synthesis and structure–activity relationships†

Alex R. Maolanon,[a] Jesper S. Villadsen,[a] Pernille Harris[a] and Christian A. Olsen*[,a]

Received (in XXX, XXX) Xth XXXXXXXXX 20XX, Accepted Xth XXXXXXXXX 20XX

DOI: 10.1039/b000000x

In our pursuit for potent and selective HDAC inhibitors, we designed four series of cyclic tetra peptide compounds, based on the azumamide scaffold. We have probed different modifications in the unique β-amino acid moiety and synthesized tryptophan-containing analogs. The biochemical profiling of the azumamide analogs was combined with high-resolution NMR solution structures to correlate the biological activity to specific structural features. We hypothesize that the β^2-methyl group, found in the azumamides, has an important side chain directing function, which guides the zinc-binding side chain towards the active site.

Introduction

Histone deacetylases (HDACs) are a group of epigenetic modulators, which catalyze the removal of ε-*N*-acetylated lysine residues, found in the N-terminal tails of histone proteins. An aberrant HDAC expression has been associated with various types of cancer, the enzymes have therefore been a target in the development of anticancer drugs.[1] So far, two HDAC inhibitors have been approved by the FDA (**1**[2] and **4**[3]) for clinical treatment of cutaneous T-cell lymphoma and several compounds are in clinical trials.[4]

A pharmacophore model has been used to describe most HDAC inhibitors. The model consists of a cap group that interacts with motifs on the surface of the protein, a linker region, and a zinc-binding group (ZBG), which reaches into the active site. HDAC inhibitors bearing a hydroxamic acid ZBG (**1**, **2**), have proven to be potent HDAC inhibitors.[5] However, macrocyclic tetra peptides as apicidin (**3**), azumamide C (**5a**), and azumamide E (**5b**) also demonstrate high activity, in spite of their weak Zn^{2+}-coordinating side chain functionality.[6] The azumamides are structurally related to apicidin (**3**), but the macrocyclic scaffold has a disubstituted β-amino acid. Furthermore the azumamides are unique in having a retro-enantio arrangement.

Macrocycles have been proposed to possess a scaffold with a higher potential for selectivity.[7] This suggestion has been based on less conserved amino acids in the rim of the active site, across the HDAC isozymes.[8] The combination of a large cap group and a poor ZBG, could be an advantage for obtaining selective HDAC inhibitors, as a strong ZBG might be too dominant an interaction to confer high selectivity.

The structural changes reported for the azumamides are primarily limited to modification of the Zn^{2+}-binding group[9] and manipulation of the stereochemistry.[6b, 10]

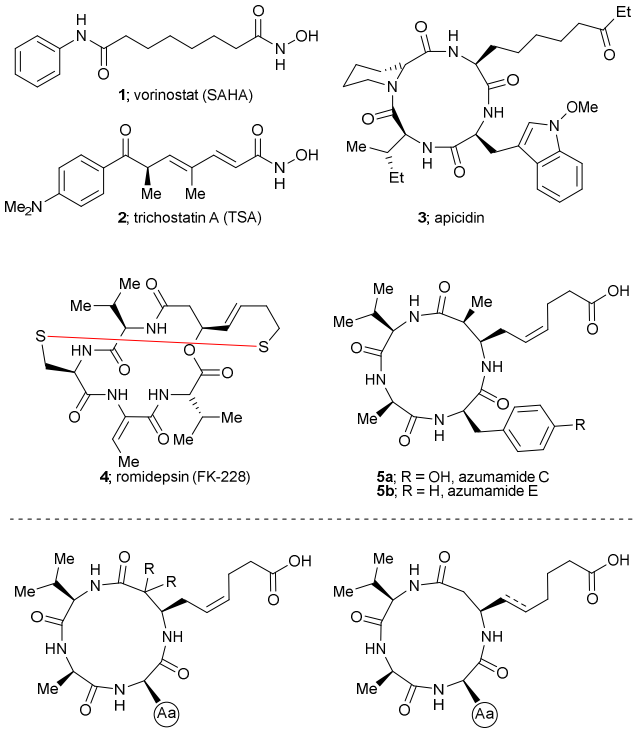

Figure 1. Known HDAC inhibitors (top) and target compounds (bottom)

Interactions between the cyclic peptide core and the surface of the protein seem to be important for isoform selectivity.[10-11] Isoform selective HDAC inhibitors could provide a powerful new tool for understanding the function of HDAC enzymes and be the basis for developing new drug candidates.[12]

Results and discussion

Design and synthesis

In pursuit of isoform selective compounds we conducted a structure-activity relationship (SAR) study, where we synthesized a variety of structurally edited azumamides. Our previous work have shown that changes in the stereochemistry of the β-amino acid substituents in azumamide E had a detrimental impact on activity.[6b] We therefore set out to explore modifications at the β^2-position, without altering the stereochemistry. Instead we incorporated a dimethylated as well as a desmethylated β-amino acid in the cyclic peptide, **6a-c** and **7a-c**, respectively.

Considering the saturated side chain of **3** and the *trans* olefin in **4**, we speculated that the *cis* olefin in the azumamides would not be essential for activity. To explore this hypothesis, we prepared **8** and **9**, as it could easily be obtained from commercially available Boc-L-Asp-O^{t}Bu. We recently found that the nature of the aromatic amino acid effects the biological activity.[6b] Hence, an indole motif, also present in **3**, was incorporated in our target compounds in addition to Phe and Tyr, which are found in the azumamides.

Building block synthesis

The building block, employed for the synthesis of the dimethylated analogs **6a–c**, was prepared by a method recently developed in our laboratory. The diastereoselective Ellman-type Mannich reaction between the enolate of tert -butyl isobutyrate and the enantiomer of 30 sulfinyl imine **10** afforded the desired Mannich product in 58% yield and with a diastereoselectivity of (77:23) in favour of the R-isomer.

Table 1 Screening of acetates for the Ellman-type Mannich reaction

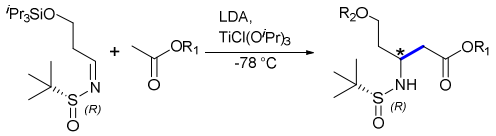

entry	R[1]	additive	d.r.	major isomer, total yield (%)[d]
1	Et	TiCl(O^{i}Pr)$_3$	>99:1	*3R*[a] (94)[b]
2	^{t}Bu	TiCl(O^{i}Pr)$_3$	74:16	*3R*[c] (68)
3	^{t}Bu	HMPA	18:72	*3S*[c] (61)
4	PMB	TiCl(O^{i}Pr)$_3$	82:18	ND

[a] Determined by X-ray crystallography from the desilylated and re-esterified *tert*-butyl ester **19**. [b] Crude yield. [c] Determined spectroscopically by comparison with the crystallized compound from entry 1. (supplementary figure S1). [d] Total yield of all diastereoisomers.

The absolute stereochemistry of the Mannich product was determined by X-ray crystallography upon desilylation with Bu$_4$NF. The alcohol was elaborated to give the Boc-protected β-amino acid **22** (scheme 3) in 16% overall yield from the sulfinyl imine (Supplementary scheme S1). The desmethylated β-amino acid building blocks **15** (Boc protected) and **16** (Fmoc-protected) were prepared by a similar route (scheme 1). The Boc-derivative only allows one cyclization site, whereas the introduction of the Fmoc group would allow macrolactamization at all four positions. Initially, an optimization study was conducted, where various acetate enolates were investigated to produce the best diastereomeric ratio and yield in the Mannich reaction (table 1).

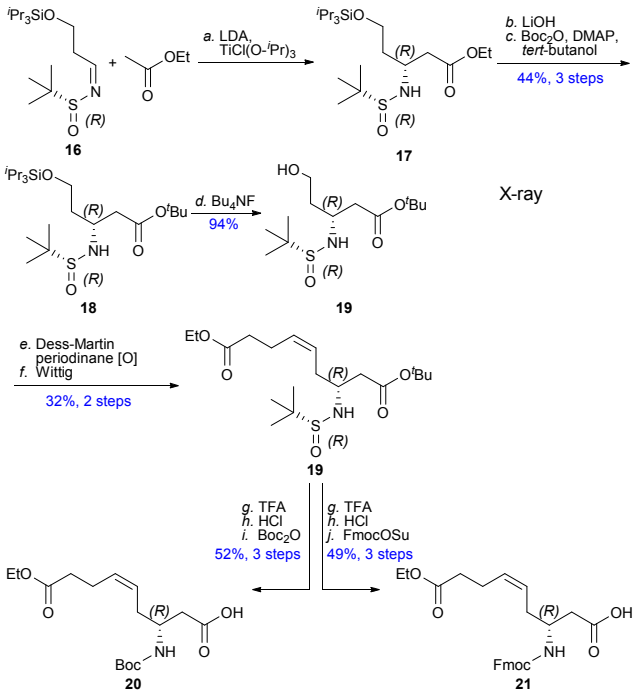

Scheme 1. Reagents and conditions: (a) LDA (2.1 equiv), EtOAc (2.0 equiv), TiCl(O-^{i}Pr)$_3$ (4.2 equiv), THF, –78 ºC, 30 min; then **16**, –78 ºC, 20 min. (b) LiOH (4.5 equiv), THF–water, 17h. (c) Boc$_2$O (1.4 equiv), DMAP (0.3 equiv), *tert*-butanol, 16 h, then Boc$_2$O (0.3 equiv), 15 h (d) AcOH (1.0 equiv), Bu$_4$NF (2.0 equiv), THF, 0 ºC → rt, 75 min. (e) NaHCO$_3$ (1.5 equiv), Dess-Martin periodinane (1.5 equiv), dry CH$_2$Cl$_2$, 0 ºC → rt, 40 min. (f) KHMDS (1.9 equiv), Ph$_3$PBr(CH$_2$)$_3$COOEt, (2.0 equiv), THF, –78 ºC → rt, 40 min. (g) TFA–CH$_2$Cl$_2$ (1:1, 10 mL, 117–192 equiv), 0 ºC → rt, 2–3 h. (h) HCl (4.0 M in dioxane, 1.8–2.5 equiv), dioxane, 1–3 h. (i) ^{i}Pr$_2$Net (3.0 equiv), Boc$_2$O (2.0 equiv), dry CH$_2$Cl$_2$, 6 h, then Boc$_2$O (1.0 equiv), 16 h. (j) Na$_2$CO (4.0 equiv), FmocOSu (1.2 equiv) water–dioxane (5:1, 6 mL), 0 ºC → rt, 45 min.

It is interesting, that the desired (3*R*) configuration is obtained from the (*R*)-auxillary in the case of *tert*-butyl acetates, whereas the equivalent *tert*-butyl isobutyrate reaction yields the (3*S*) configuration as the major diastereomer. The high dr obtained with ethyl acetate and the switchover in diastereoselectivity induced by the addition of HMPA confirms the hypothesis that the acetate mediated reaction proceeds through a six-membered Zimmerman–Traxler-type transition state, where coordination to titanium is essential for the high diastereoselectivity.

To establish the stereochemistry of the product from entry 1, the compound was re-esterified to the tert -butyl ester, since the *tert*-butyl ester alcohols in most cases were crystalline. Gratifyingly, the alcohol crystallized and the stereochemistry was determined by X-ray crystallography. Furthermore, an acid labile protection group for the carboxylic acid was required to obtain orthogonality. This strategy nicely provided the Fmoc- and Boc-protected β-amino acids **15** and **16** (Scheme 1).

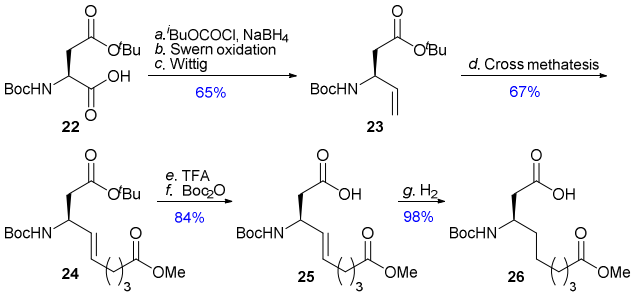

Scheme 2. (a) N-methylmorpholine (1.0 equiv), isobutyl chloroformate (1.0 equiv), $NaBH_4$ (3.0 equiv), MeOH, THF, –30 ºC → rt, 160 min. (b) oxalyl chloride (1.7 equiv), DMSO (3.3 equiv), Et_3N (5.0 equiv.), CH_2Cl_2, –78 ºC → –40 ºC → rt, 2h. (c) PPh_3CH_3Br (2.2 equiv), KHMDS (0.5 M in toluene) (2.1 equiv), THF, –78 ºC → rt, 4 h. (d) methyl 5-hexenoate (3 equiv), Hoveyda Grubbs 2nd gen. catalyst (0.1 equiv), CH_2Cl_2, 40 ºC, 24h. (e) TFA–CH_2Cl_2 (1:3), 2h. (f) Boc_2O (1.3 equiv.), $^iPr_2NEt$ (2.6 equiv.), CH_2Cl_2. (g) H_2, Pd/C (1% w/w), THF, 19h.

The building blocks used to synthesize compound **8a-c** and **9a-c** were prepared from the readily available Boc-L-Asp-O^{t}Bu **22**. Using a slightly modified procedure from Bradner *et al*[13], acid **22** was reduced to the corresponding alcohol and a subsequent Swern oxidation yielded the aldehyde, which was used immediately in a Wittig reaction to produce the terminal alkene **23**.

Table 2 Catalyst screening for cross-methatesis

entry	catalyst	yield (%)[a]
1	Grubbs cat. 1st gen., 0.1 equiv	11
2	Grubbs cat. 2nd gen., 0.05 equiv	54
3	Grubbs cat. 2nd gen., 0.1 equiv	62
4	Hoveyda Grubbs cat. 1st gen., 0.1 equiv	12
5	Hoveyda Grubbs cat. 2nd gen., 0.1 equiv	67
6	cat. (A)	62
7	cat. (B)	52

[a] Isolated trans isomer.

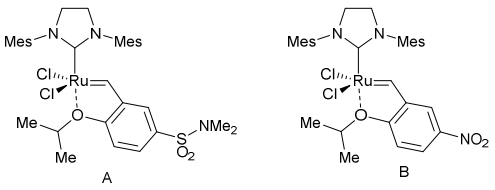

The optimal conditions for the succeeding cross methathesis was found using Hoveyda-Grubbs 2nd generation catalyst (see table 2), which afforded the *trans* olefin in a good yield. Acidic deprotection followed by reprotection of the amino functionality gave the final building block for **8** whereas hydrogenation of **25** gave the desired *β*-amino acid **26** for the synthesis of **9** (Scheme 2).

All the synthesized building blocks were coupled to a tripeptide on solid support, which after deprotection and cleavage were cyclized using HATU under dilute conditions (0.3–0.8 mM). Saponification of the cyclic peptides gave the final compounds albeit in poor yield. The synthesis of the tryptophan analogues proved particularly challenging, revealed by an unsuccessful synthesis of **9c** by the original synthetic route. Changing the point of cyclization had previous shown to have an effect on a simplified linear tetrapeptide. The Boc protection group of **27** was therefore substituted for an Fmoc group allowing the building block to be loaded directly on to the resin. Even though we expected a better cyclization reaction, using the less hindered and more flexible *β*-amino acid at the C-terminal, we were surprised to find the dramatic effect this alteration had, when we isolated **9c** with a yield of 48% (12 steps) from the Fmoc building block. (supplementary scheme S2).

Biochemical profiling

An initial screen against HDAC4 and 7 at concentrations between 10–100 μM, indicated that the analogs were poor inhibitors of class IIa. All desmethylated compounds were therefore characterized with dose–response experiments on recombinant human HDACs on class I, class IIb, and class IV.

Preliminary testing of the dimethylated series (**6a–c**) indicated low activity. With this in mind, these compounds were only screened at two concentrations (10 μM and 20 μM, see SI, table S1). The Phe- and Tyr-containing analogs (**6a** and **6b**) were poor inhibitors of HDAC1–3 and no inhibition was observed on HDAC6, HDAC8, HDAC10, and HDAC11 at 20 μM. However, **6c**, containing a tryptophan as the aromatic residue, displayed activity against HDAC1–3 (~50% inhibition at 10 µM). **6c** also showed activity against HDAC6, HDAC8, HDAC10, and HDAC11, although none of the isoforms were inhibited more than 50% at 20 µM. The positive effect of tryptophan indicates that this aromatic amino acid is superior to Phe and Tyr in establishing favorable interactions with the surface of the HDAC enzymes. The low activity of **6a–6c** emphasize the sensitivity of modifications to the β^2-position.

The IC_{50} values obtained from dose-response experiments on the six cyclic peptides (**7a–7c**, **8a–8c,** and **9a–9c**) were converted to K_i values, using Cheng-Prusoff's equation [$K_i = IC_{50}/(1 + [S]/K_m)$], assuming a fast-on–fast-off mechanism. The results are shown in table 3.

The compounds showed the highest activity against HDAC10, followed by HDAC1-3. Activity was also found against HDAC11, while poor inhibition was observed against HDAC6 and 8.

Compared to HDAC6 and 8, removal of the methyl group seem to have a minor effect compared to the azumamides. However, azumamide C and E are relatively weak inhibitors of these isozymes, so the small difference is also an expression of the general poor activity against the enzymes.

When the other HDAC isoforms are compared, it is evident that the methyl group has an important function, as **7a** and **7b** show a 5 to 36-fold decrease in potency.

Compounds with a *trans* olefin in the side chain shows the weakest inhibitory activity, while analogs containing a cis olefin and a saturated side chain are equally potent. Regarding the aromatic residue, phenylalanine-containing compounds are the weakest inhibitors, while differences between compounds containing a tyrosine relative to a tryptophane is insignificant. These data are in agreement with the activity of azumamide C, which is the most potent inhibitor for all HDAC enzymes. The negative effect of incorporating a phenylalanine and a *trans* olefin is evident from compound **8a**, which portray the weakest inhibition for HDAC1–3, 10 and 11.

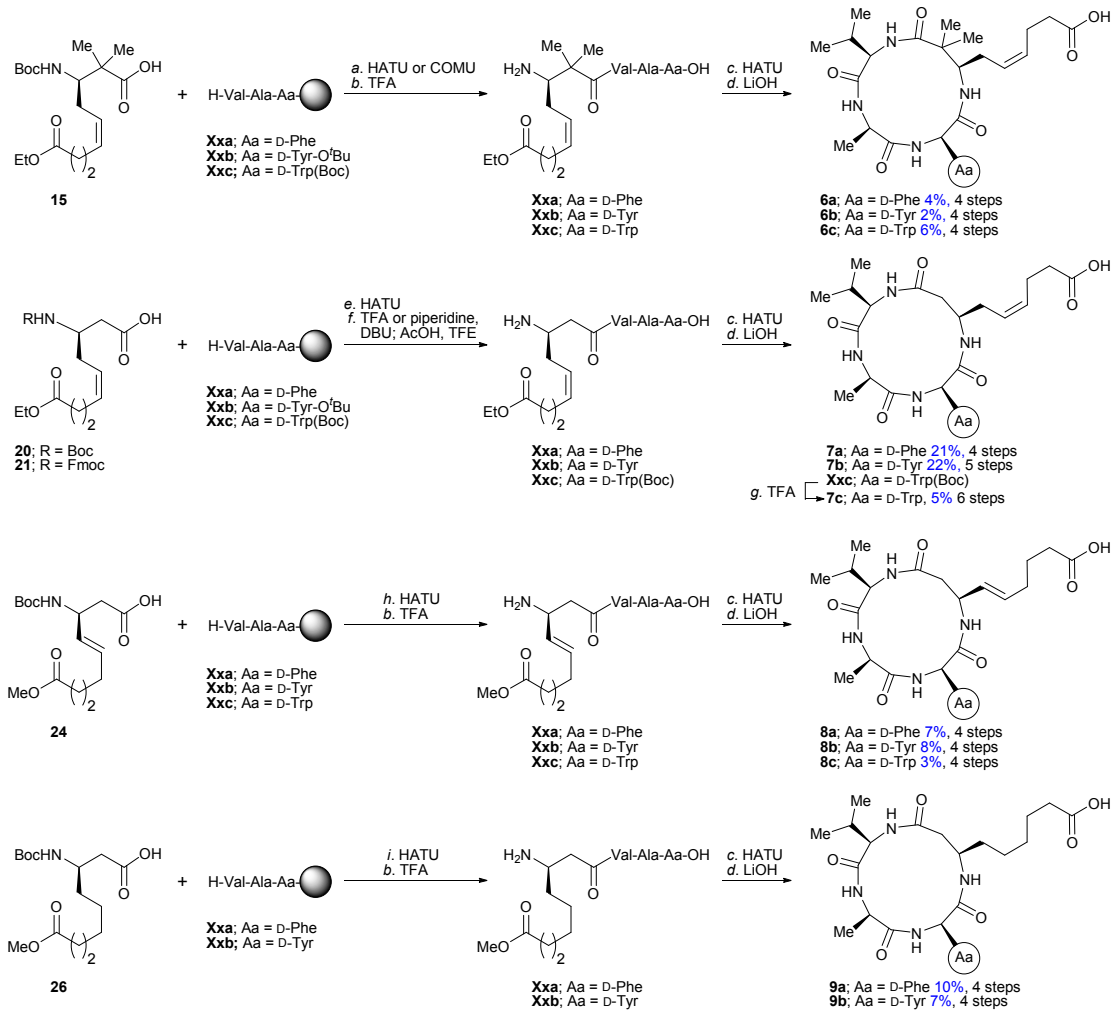

Scheme 4. Reagents and conditions: (*a*) Resin (1.5 equiv), **x** (1.0 equiv), HATU or COMU (1.5 equiv), *i*Pr_2Net (3.0 equiv), DMF, 16 h or **x** (1.1 equiv), resin (1.0 equiv), HATU (1.5 equiv), *i*Pr_2Net (3.0 equiv), DMF, 17 h (*b*) TFA–CH_2Cl_2 (1:1), 2 × 30 min. (*c*) HATU (1.5–2.2 equiv), $^i Pr_2$NEt (5–10 equiv), DMF (0.4 mM peptide concentration), 16 h. 17–21 h (*d*) LiOH (36–50 equiv), THF–water (1:1), 16–17 h. (*e*) Resin (1.0 or 1.5 equiv), HATU (1.5 equiv), 2,6-lutidine (3.0 equiv), **x** (1.1 or 1.0 equiv), DMF, 16 h. (*f*) TFA–CH_2Cl_2 (1:1), 2 × 30 min or piperidine–DMF (1:4, 2 × 30 min); DBU–piperidine–DMF (2:2:96, 30 min); AcOH–TFE–CH_2Cl_2 (6:2:2, 1.5 mL), 2 × 2 h. (*g*) TFA–CH_2Cl_2 (1:1), 1 h.

NMR Studies

All amide bonds in azumamide A-E exhibit *trans* conformations,[10] we therefore analyzed the NMR spectra of the azumamide analogs, to see if any cis amides were present. NOESY/ROESY interactions between H^{α} on adjacent amino acids would indicate a *cis* amide, but no correlations were found.

We hoped to solve the 3D-solution structure in water, as this conformation would resemble the assay conditions best. Unfortunately, the azumamide analogs were insoluble in H_2O. Up to 15% DMSO-d_6 was added, but an insufficient amount of compound was dissolved to obtain a useful NMR spectrum. All samples were therefore analyzed in DMSO-d_6.

NOESY/ROESY data were used to set constraints to the cyclic structure when the simulations were performed in the program 'Maestro'. This was done by adding a penalty to the system if the distance between two protons changed more than 20%, compared to the data from the NMR spectra.

An amide NH between the aromatic residue and alanine from the natural compound points to the middle of the structure. This conformation originates from the NOESY correlation between the NH and H^{α}-Ala. However, in this conformation, the distance between the NH and the methyl group in alanine does not correlate with the NMR data; so even though the cyclic peptide can be viewed as a rigid structure, the 3-D conformation is an ensample of closely related structures with a certain flexibility. Overall, the structural difference in the backbone between the azumamides and the des-methylated compounds were small. Similar NOESY/ROESY correlations were found and the J-couplings were comparable (SI).

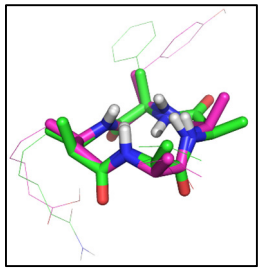

	K_i (μM)						
	Class I				Class IIb		Class IV
Compound	HDAC1	HDAC2	HDAC3	HDAC8	HDAC6	HDAC10	HDAC11
8a	1.41±0.37	1.86±0.04	1.62±0.31	8.57±3.61	IA[a]	IA	3.60±0.61
8b	0.83±0.26	0.66±0.28	0.55±0.26	IA	2.60±0.96	0.30±0.004	1.43±0.42
8c	0.57±0.08	0.45±0.31	0.65±0.44	3.35±2.06	4.44±0.36	0.26±0.005	1.24±0.61
9a	1.02±0.39	0.85±0.11	0.78±0.23	IA	IA	0.53±0.163	2.43±1.27
9b	0.78±0.68	0.32±0.20	0.26±0.16	IA	3.96±2.24	0.15±0.074	0.98±0.82
9c[b]	1.15±0.13	1.58±0.38	2.35±0.91	12.17±0.77	IA	0.38±0.068	3.20±1.80
7a	0.65±0.26	0.98±0.14	0.91±0.16	IA	IA	0.27±0.034	1.72±0.26
7b	0.34±0.23	0.21±0.07	0.37±0.29	IA	7.08±0.72	0.15±0.007	0.87±0.40
7c	0.23±0.13	0.17±0.01	0.57±0.16	5.93±0.71	IA	0.13±0.036	0.95±0.71

NMR Studies

The docking simulations on **7a–7c**, **8a–8c,** and **9a–9c** were performed in HDAC3 (PDB: 4A69).[14] It should be noted that these preliminary docking results were performed on a rigid enzyme and thus neglects potential induced fit effects. Optimized structures will be obtained by allowing the enzyme to minimize after the docking.

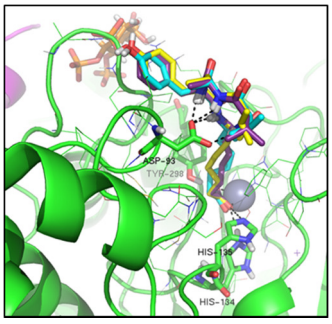

Each analog bind in a similar fashion to HDAC3, compound **7b**, **8b**, **9b** is shown as representative examples in figure 1.

Asp93 has a particularly important interaction by coordinating with all the amide nitrogens in the cyclic core. Besides from coordination with the zinc atom, the carboxylic acid ZBG forms favorable interactions with His 134, His135, and Tyr298 (Figure 2.11). It is not clear from the docking results why the natural products possess a higher HDAC inhibitory activity relative to the analogs. However, favorable lipophilic interactions could occur between Phe200 and the methyl group in the azumamides.

The phenylalanine containing compounds (including azumamide E), show a lower activity towards HDAC1–3. Since tyrosine and tryptophan can form hydrogen bonds, these interactions would be an obvious explanation for the higher activity. However, the phenylalanine containing compounds are only 2-fold less potent. The change in activity might therefore be a combination of the negative effect from removing a water molecule from the binding site and the positive effect from obtaining favorable hydrogen bond interactions. No hydrophilic interactions can be seen from the docking results, but since a rigid enzyme has been used for the simulations, amino acids near the cavity might move to interact with the ligand. His22 and Asp92 are located close to the aromatic substituent and might have a role in the binding.

Cytotoxicity tests

The work is ongoing.

Notes and references

Department of Chemistry, Technical University of Denmark, Kemitorvet 207, Kgs. Lyngby, DK-2800, Denmark. Fax: +45 XXXX XXXX; Tel: +45 4525 2105; E-mail: cao@kemi.dtu.dk

† Electronic Supplementary Information (ESI) available: Experimental materials and methods, charaterisation data, ^{1}H NMR and ^{13}C NMR spectra for all synthesised compounds, selected COSY, HSQC and ROESY spectra, and crystallographic data (CIF) as well as Supplementary Figures??. See DOI: 10.1039/b000000x/

‡ Footnotes should appear here. These might include comments relevant to but not central to the matter under discussion, limited experimental and spectral data, and crystallographic data.

1. Bolden, J. E.; Peart, M. J.; Johnstone, R. W., Anticancer activities of histone deacetylase inhibitors. *Nat Rev Drug Discov* **2006,** *5* (9), 769-84.

2. Marks, P. A., The clinical development of histone deacetylase inhibitors as targeted anticancer drugs. *Expert opinion on investigational drugs* **2010,** *19* (9), 1049-1066.

3. VanderMolen, K. M.; McCulloch, W.; Pearce, C. J.; Oberlies, N. H., Romidepsin (Istodax, NSC 630176, FR901228, FK228, depsipeptide): a natural product recently approved for cutaneous T-cell lymphoma. *The Journal of antibiotics* **2011,** *64* (8), 525-531.

4. Arrowsmith, C. H.; Bountra, C.; Fish, P. V.; Lee, K.; Schapira, M., Epigenetic protein families: a new frontier for drug discovery. *Nature Reviews Drug Discovery* **2012,** *11* (5), 384-400.

5. Wagner, F.; Weïwer, M.; Lewis, M.; Holson, E., Small Molecule Inhibitors of Zinc-dependent Histone Deacetylases. *Neurotherapeutics : the journal of the American Society for Experimental NeuroTherapeutics* **2013,** *10* (4), 589-604.

6. (a) Singh, S. B.; Zink, D. L.; Polishook, J. D.; Dombrowski, A. W.; DarkinRattray, S. J.; Schmatz, D. M.; Goetz, M. A., Apicidins: Novel cyclic tetrapeptides as coccidiostats and antimalarial agents from Fusarium pallidoroseum. *Tetrahedron Letters* **1996,** *37* (45), 8077-8080; (b) Villadsen, J. S.; Stephansen, H. M.; Maolanon, A. R.; Harris, P.; Olsen, C. A., Total Synthesis and Full Histone Deacetylase Inhibitory Profiling of

Azumamides A–E as Well as β2- epi-Azumamide E and β3-epi-Azumamide E. *Journal of Medicinal Chemistry* **2013,** *56* (16), 6512-6520.

7. Newkirk, T. L.; Bowers, A. A.; Williams, R. M., Discovery, biological activity, synthesis and potential therapeutic utility of naturally occurring histone deacetylase inhibitors. *Nat Prod Rep* **2009,** *26* (10), 1293-320.

8. Sternson, S. M.; Wong, J. C.; Grozinger, C. M.; Schreiber, S. L., Synthesis of 7200 small molecules based on a substructural analysis of the histone deacetylase inhibitors trichostatin and trapoxin. *Organic Letters* **2001,** *3* (26), 4239-4242.

9. Wen, S.; Carey, K. L.; Nakao, Y.; Fusetani, N.; Packham, G.; Ganesan, A., Total synthesis of azumamide A and azumamide E, evaluation as histone deacetylase inhibitors, and design of a more potent analogue. *Org Lett* **2007,** *9* (6), 1105-8.

10. Maulucci, N.; Chini, M. G.; Micco, S. D.; Izzo, I.; Cafaro, E.; Russo, A.; Gallinari, P.; Paolini, C.; Nardi, M. C.; Casapullo, A.; Riccio, R.; Bifulco, G.; De Riccardis, F., Molecular insights into azumamide e histone deacetylases inhibitory activity. *J Am Chem Soc* **2007,** *129* (10), 3007-12.

11. Furumai, R.; Komatsu, Y.; Nishino, N.; Khochbin, S.; Yoshida, M.; Horinouchi, S., Potent histone deacetylase inhibitors built from trichostatin A and cyclic tetrapeptide antibiotics including trapoxin. *Proc Natl Acad Sci U S A* **2001,** *98* (1), 87-92.

12. (a) Beumer, J. H.; Tawbi, H., Role of histone deacetylases and their inhibitors in cancer biology and treatment. *Current Clinical Pharmacology* **2010,** *5* (3), 196-208; (b) Haberland, M.; Montgomery, R. L.; Olson, E. N., The many roles of histone deacetylases in development and physiology: implications for disease and therapy. *Nat Rev Genet* **2009,** *10* (1), 32-42.

13. Bowers, A. A.; Greshock, T. J.; West, N.; Estiu, G.; Schreiber, S. L.; Wiest, O.; Williams, R. M.; Bradner, J. E., Synthesis and Conformation-Activity Relationships of the Peptide Isosteres of FK228 and Largazole. *J Am Chem Soc* **2009**.

14. Watson, P. J.; Fairall, L.; Santos, G. M.; Schwabe, J. W., Structure of HDAC3 bound to co-repressor and inositol tetraphosphate. *Nature* **2012,** *481* (7381), 335-340.